Behavioural Neurology

Applications of Theranostics for Detecting and Targeting CNS Injuries and Diseases

Lead Guest Editor: Muh-Shi Lin
Guest Editors: Yu-Yo Sun, Horacio Soto, Chung-Feng Kao, and Cui Mei

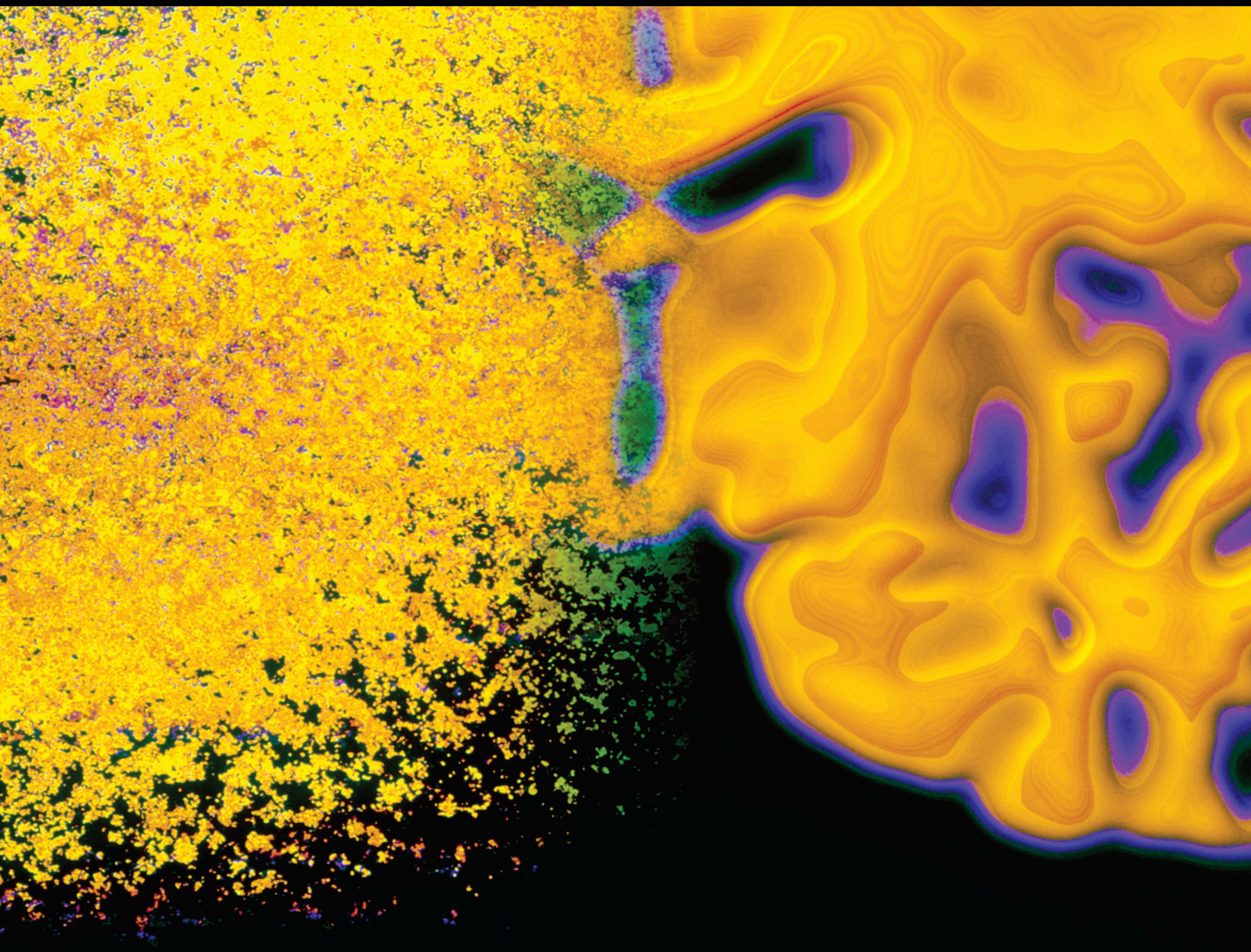

Applications of Theranostics for Detecting and Targeting CNS Injuries and Diseases

Behavioural Neurology

Applications of Theranostics for Detecting and Targeting CNS Injuries and Diseases

Lead Guest Editor: Muh-Shi Lin
Guest Editors: Yu-Yo Sun, Horacio Soto, Chung-Feng Kao, and Cui Mei

Contents

Applications of Theranostics for Detecting and Targeting CNS Injuries and Diseases
Yu-Yo Sun, Horacio Soto, Chung-Feng Kao, Cui Mei, and Muh-Shi Lin
Editorial (2 pages), Article ID 9891859, Volume 2022 (2022)

Corrigendum to "Does the Personality of Patients with Parkinson's Disease Affect the Decision to Perform Deep Brain Stimulation Surgery? A Cross-Sectional Study in a Chinese Cohort"
Wei Lin, Dan Wang, Likun Yang, Jie Zhu, Jingjie Ge, Chuantao Zuo, and Yuhai Wang
Corrigendum (1 page), Article ID 9781803, Volume 2021 (2021)

Mild Gait Impairment and Its Potential Diagnostic Value in Patients with Early-Stage Parkinson's Disease
Zhuang Wu, Xu Jiang, Min Zhong, Bo Shen, Jun Zhu, Yang Pan, Jingde Dong, Pingyi Xu, Wenbin Zhang, Jun Yan, and Li Zhang
Research Article (8 pages), Article ID 6696454, Volume 2021 (2021)

BDNF Protein and BDNF mRNA Expression of the Medial Prefrontal Cortex, Amygdala, and Hippocampus during Situational Reminder in the PTSD Animal Model
Shao-Han Chang, Ying Hao Yu, Alan He, Chen Yin Ou, Bai Chuang Shyu, and Andrew Chih Wei Huang
Research Article (13 pages), Article ID 6657716, Volume 2021 (2021)

Does the Personality of Patients with Parkinson's Disease Affect the Decision to Perform Deep Brain Stimulation Surgery? A Cross-Sectional Study in a Chinese Cohort
Wei Lin, Dan Wang, Likun Yang, Jie Zhu, Jingjie Ge, Chuantao Zuo, and Yuhai Wang
Research Article (6 pages), Article ID 6639255, Volume 2021 (2021)

Ultrarapid Endoscopic-Aided Hematoma Evacuation in Patients with Thalamic Hemorrhage
Kuan-Yu Chen, Woon-Man Kung, Lu-Ting Kuo, and Abel Po-Hao Huang
Research Article (8 pages), Article ID 8886004, Volume 2021 (2021)

Efficacy of a Smart Antisnore Pillow in Patients with Obstructive Sleep Apnea Syndrome
Tsung-Te Chung, Ming-Tsung Lee, Ming-Chou Ku, Kai-Chieh Yang, and Cheng-Yu Wei
Research Article (6 pages), Article ID 8824011, Volume 2021 (2021)

Prevalence and Associated Factors of Visual Hallucinations in Patients with Vascular Cognitive Impairment
Chih-Lin Chen, Min-Hsien Hsu, Chao-Hsien Hung, Pai-Yi Chiu, and Chung-Hsiang Liu
Research Article (7 pages), Article ID 8866763, Volume 2021 (2021)

Basolateral Amygdala but Not Medial Prefrontal Cortex Contributes to Chronic Fluoxetine Treatments for PTSD Symptoms in Mice
Ying Hao Yu, Chen Yin Ou, Bai Chuang Shyu, and Andrew Chih Wei Huang
Research Article (8 pages), Article ID 8875087, Volume 2020 (2020)

Machine Learning Based on a Multiparametric and Multiregional Radiomics Signature Predicts Radiotherapeutic Response in Patients with Glioblastoma
Zi-Qi Pan, Shu-Jun Zhang, Xiang-Lian Wang, Yu-Xin Jiao, and Jian-Jian Qiu
Research Article (12 pages), Article ID 1712604, Volume 2020 (2020)

Wild Bitter Melon Exerts Anti-Inflammatory Effects by Upregulating Injury-Attenuated CISD2 Expression following Spinal Cord Injury
Woon-Man Kung, Chai-Ching Lin, Chan-Yen Kuo, Yu-Ching Juin, Po-Ching Wu, and Muh-Shi Lin
Research Article (12 pages), Article ID 1080521, Volume 2020 (2020)

Retinal Levels of Amyloid Beta Correlate with Cerebral Levels of Amyloid Beta in Young APPswe/PS1dE9 Transgenic Mice before Onset of Alzheimer's Disease
Xi Mei, Mengxiang Yang, Lina Zhu, Qi Zhou, Xingxing Li, Zhongming Chen, and Chenjun Zou
Research Article (8 pages), Article ID 1574816, Volume 2020 (2020)

Abnormal Homocysteine Metabolism: An Insight of Alzheimer's Disease from DNA Methylation
Tingting Pi, Bo Liu, and Jingshan Shi
Review Article (11 pages), Article ID 8438602, Volume 2020 (2020)

A Novel Metabolic Connectome Method to Predict Progression to Mild Cognitive Impairment
Min Wang, Zhuangzhi Yan, Shu-yun Xiao, Chuantao Zuo, and Jiehui Jiang
Research Article (9 pages), Article ID 2825037, Volume 2020 (2020)

Hindawi
Behavioural Neurology
Volume 2022, Article ID 9891859, 2 pages
https://doi.org/10.1155/2022/9891859

Editorial

Applications of Theranostics for Detecting and Targeting CNS Injuries and Diseases

Yu-Yo Sun,[1,2] **Horacio Soto**,[3] **Chung-Feng Kao**,[4,5] **Cui Mei**,[6] **and Muh-Shi Lin**[7,8,9,10]

[1]*Institute of Biopharmaceutical Sciences, National Sun Yat-sen University, Kaohsiung 804201, Taiwan*
[2]*Department of Neuroscience, Center for Brain Immunology and Glia (BIG), University of Virginia, School of Medicine, Charlottesville, VA, USA*
[3]*Cancer Clinical Trials Access Program, Kaiser Permanente, Bellflower, USA*
[4]*Department of Agronomy, College of Agriculture and Natural Resources, National Chung Hsing University, Taichung, Taiwan*
[5]*Advanced Plant Biotechnology Center, National Chung Hsing University, Taichung, Taiwan*
[6]*Department of Neurology, Huashan Hospital, Fudan University, Shanghai, China*
[7]*Division of Neurosurgery, Department of Surgery, Kuang Tien General Hospital, Taichung, Taiwan*
[8]*Department of Biotechnology and Animal Science, College of Bioresources, National Ilan University, Yilan, Taiwan*
[9]*Department of Biotechnology, College of Medical and Health Care, Hung Kuang University, Taichung, Taiwan*
[10]*Department of Health Business Administration, College of Medical and Health Care, Hung Kuang University, Taichung, Taiwan*

Correspondence should be addressed to Muh-Shi Lin; neurosurgery2005@yahoo.com

Received 22 February 2022; Accepted 22 February 2022; Published 15 April 2022

As of today, the limit of medical science is the inability to efficiently and completely eliminate neuronal damage caused by secondary insult from neurological trauma and neurodegenerative diseases. In general, the primary insult occurs at the time of impact; it involves contusions, lacerations, and axonal injury as a result of shearing, tearing, or stretching with consequent impairment of the neural architecture. Initial traumatic injuries or pathogen-associated molecular patterns (PAMPs) from misfolded proteins evoke secondary insult by virtue of dynamic interactions among ischemic, inflammatory, cytotoxic processes, and mitochondrial dysfunction [1]. These types of molecular-level elements that may contribute to the holistic scale are implicated in the pathogenesis of neuro-oncology. Impaired immune competence, such as dysregulation of macrophages and microglia, and mitochondrial dysfunction reciprocally impact the microenvironment of glioblastoma and its prognosis [2]. As such, the future perspectives are to ensure the detection of disease at an extremely early stage through advanced diagnostic methods or to salvage primary lesions via advanced surgical interventions and, most fundamentally, to prevent widespread secondary injuries by exploring the microscopic pathogenesis or through interventions on a molecular level, which will be the objective and mission of the scientific community in the coming years.

Following a meticulous peer review process, we have decided to include 12 manuscripts in this special issue, composed of 11 research and 1 review article. In the clinical context, olfactory impairment is being recognized as a marker for the early detection of cognitive decline and Alzheimer's disease (AD) dementia. The transport pathways of olfactory signals superimpose substantially with those of dopamine and 5-hydroxytryptamine. Structural and physical dysfunction between the brain areas involved leads to dysregulated neurotransmission and accordingly to impaired olfaction [3]. Beyond olfactory dysfunction, X. Mei et al. indicated that amyloid β (Aβ) levels in the mouse retina corresponded to Aβ amounts in the brain; the appropriate time to measure retinal Aβ deserves emphasis. Moreover, Professor A. C. W. Huang et al. found in posttraumatic stress disorder (PTSD) animals a subtle affiliation of brain-derived neurotrophic factor (BDNF) expression in the medial prefrontal cortex (mPFC), amygdala, and hippocampus during situational reminders, whereas fluoxetine, a class of specific 5-hydroxytryptamine

reuptake inhibitor drugs, was effective only on the basal amygdale, but not on the mPFC. The interconnections and pathogenesis of these complex neural structures need to be further understood in the setting of neurodegenerative diseases.

Early and nuanced clinical neurological symptoms can facilitate detection of disease, and subsequent remission of these neurological manifestations may even lead to greater postoperative benefit. Z. Wu et al. showed gait profile can aid in the diagnosis of early Parkinson's disease (PD). C.-L. Chen et al. reported that vascular cognitive impairment (VCI) with visual hallucinations frequently exhibited more severe dementia and neuropsychiatric symptoms. W. Lin et al. highlighted that more advantage can be gained through deep brain stimulation (DBS) under the proper treatment of neurological presentations during PD.

The tendency towards minimally invasive approaches or milder modalities has contributed to an improved quality of treatment. K.-Y. Chen et al. suggested that minimally invasive endoscopic-assisted surgery can be employed safely and effectively in the treatment of thalamic hemorrhage. T.-T. Chung et al. demonstrated that the smart antisnore pillow can be a useful device for patients with obstructive sleep apnea syndrome, rather than uncomfortable continuous positive airway pressure.

The implementation of artificial intelligence technology assists in early detection, shortens the period of diagnosis, and forecasts the outcome of the disease. Z.-Q. Pan et al. display that machine learning-based radiomic features (tumour shape, intensity, and texture) can predict the response to radiotherapy in patients with glioblastomas. Professor J. Jiang et al. introduced a metabolic connectome-based predictive model for ^{18}F-fluorodeoxyglucose- (FDG-) PET images to facilitate the identification of brain metabolic dysfunction and established a clinically applicable biomarker to predict the progression of mild cognitive impairment to AD.

Upstream blockage of molecular pathogenic mechanisms contributes to the repression of disease advancement. In their review, T. Pi et al. underlined that the environmental factor, homocysteine, has mediated DNA methylation and contributes to the development of AD. CDGSH iron-sulfur structural domain 2 (CISD2) exerted anti-inflammatory effects by functioning as an upstream regulatory constituent of the PPAR-β/NF-κB signal through the findings of M.-S. Lin et al. The anti-inflammatory natural compound wild bitter melon (WBM) showed a modulatory effect on CISD2 expression in injured animals and cells. This protective protein, CISD2, holds high potential as a target for the treatment of injury and disease in the central nervous system (CNS) [4].

Ultimately, we expect the endeavors of the authors to generate multidisciplinary viewpoints and novel insights that will achieve further advances in the domain of CNS injury and disease.

Yu-Yo Sun
Horacio Soto
Chung-Feng Kao
Cui Mei
Muh-Shi Lin

Conflicts of Interest

I declare that we have no conflict of interest or private agreements with companies concerning the manuscripts in this special issue.

References

[1] S. Lee, S. Park, J. Won, S. R. Lee, K. T. Chang, and Y. Hong, "The incremental induction of neuroprotective properties by multiple therapeutic strategies for primary and secondary neural injury," *International Journal of Molecular Sciences*, vol. 16, no. 8, pp. 19657–19670, 2015.

[2] R. O. Lu and W. S. Ho, "Mitochondrial dysfunction, macrophage, and microglia in brain cancer," *Frontiers in Cell and Development Biology*, vol. 8, p. 620788, 2020.

[3] M. S. Lin, I. H. Chiu, and C. C. Lin, "Ultrarapid inflammation of the olfactory bulb after spinal cord injury: protective effects of the granulocyte colony-stimulating factor on early neurodegeneration in the brain," *Frontiers in Aging Neuroscience*, vol. 13, 2021.

[4] M. S. Lin, "CISD2 attenuates inflammation and regulates microglia polarization in EOC microglial cells-as a potential therapeutic target for neurodegenerative dementia," *Frontiers in Aging Neuroscience*, vol. 12, p. 260, 2020.

Hindawi
Behavioural Neurology
Volume 2021, Article ID 9781803, 1 page
https://doi.org/10.1155/2021/9781803

Corrigendum

Corrigendum to "Does the Personality of Patients with Parkinson's Disease Affect the Decision to Perform Deep Brain Stimulation Surgery? A Cross-Sectional Study in a Chinese Cohort"

Wei Lin,[1] Dan Wang,[1] Likun Yang,[1] Jie Zhu,[1] Jingjie Ge,[2] Chuantao Zuo,[2] and Yuhai Wang[1]

[1]*Department of Neurosurgery, Joint Logistics Support Unit No. 904 Hospital, School of Medicine, Anhui Medical University, Wuxi, China*
[2]*PET Center, Huashan Hospital, Fudan University, Shanghai, China*

Correspondence should be addressed to Yuhai Wang; wangyuhai67@126.com

Received 17 April 2021; Accepted 17 April 2021; Published 29 May 2021

In the article titled "Does the Personality of Patients with Parkinson's Disease Affect the Decision to Perform Deep Brain Stimulation Surgery? A Cross-Sectional Study in a Chinese Cohort" [1], the authors identified an error in the Discussion that was introduced during the preparation of the manuscript. Statistical differences were not reported between PD-DBS and PD-MED, and the article should be corrected as follows:

"Statistically significant differences were reported between the PD-DBS and PD-MED patients with regard to the H&Y stage, disease duration, and UPDRS III scores. These data indicated that PD was more severe in the PD-DBS group and that these patients required surgical intervention because medication was not sufficiently effective."

Should be corrected to

"Statistically significant differences were not reported between the PD-DBS and PD-MED patients with regard to H&Y stage, disease duration, and UPDRS III scores."

References

[1] W. Lin, D. Wang, L. Yang et al., "Does the Personality of Patients with Parkinson's Disease Affect the Decision to Perform Deep Brain Stimulation Surgery? A Cross-Sectional Study in a Chinese Cohort," *Behavioural Neurology*, vol. 2021, Article ID 6639255, 6 pages, 2021.

Hindawi
Behavioural Neurology
Volume 2021, Article ID 6696454, 8 pages
https://doi.org/10.1155/2021/6696454

Research Article

Mild Gait Impairment and Its Potential Diagnostic Value in Patients with Early-Stage Parkinson's Disease

Zhuang Wu,[1] **Xu Jiang**,[1] **Min Zhong**,[1] **Bo Shen**,[1] **Jun Zhu**,[1] **Yang Pan**,[1] **Jingde Dong**,[1] **Pingyi Xu**,[2] **Wenbin Zhang**,[3] **Jun Yan**,[1] **and Li Zhang**[1]

[1]*Department of Geriatric Neurology, Affiliated Brain Hospital of Nanjing Medical University, Nanjing, China*
[2]*Department of Neurology, First Affiliated Hospital of Guangzhou Medical University, Guangzhou, China*
[3]*Department of Neurosurgery, Affiliated Brain Hospital of Nanjing Medical University, Nanjing, China*

Correspondence should be addressed to Li Zhang; neuro_zhangli@163.com

Received 13 November 2020; Accepted 20 March 2021; Published 5 April 2021

Academic Editor: Horacio Soto

Background and Purpose. Patients with early-stage Parkinson's disease (PD) have gait impairments, and gait parameters may act as diagnostic biomarkers. We aimed to (1) comprehensively quantify gait impairments in early-stage PD and (2) evaluate the diagnostic value of gait parameters for early-stage PD. *Methods*. 32 patients with early-stage PD and 30 healthy control subjects (HC) were enrolled. All participants completed the instrumented stand and walk test, and gait data was collected using wearable sensors. *Results*. We observed increased variability of stride length (SL) ($P < 0.001$), stance phase time (StPT) ($P = 0.004$), and swing phase time (SwPT) ($P = 0.011$) in PD. There were decreased heel strike (HS) ($P = 0.001$), range of motion of knee ($P = 0.036$), and hip joints ($P < 0.001$) in PD. In symmetry analysis, no difference was found in any of the assessed gait parameters between HC and PD. Only total steps (AUC = 0.763, $P < 0.001$), SL (AUC = 0.701, $P = 0.007$), SL variability (AUC = 0.769, $P < 0.001$), StPT variability (AUC = 0.712, $P = 0.004$), and SwPT variability (AUC = 0.688, $P = 0.011$) had potential diagnostic value. When these five gait parameters were combined, the predictive power was found to increase, with the highest AUC of 0.802 ($P < 0.001$). *Conclusions*. Patients with early-stage PD presented increased variability but still symmetrical gait pattern. Some specific gait parameters can be applied to diagnose early-stage PD which may increase diagnosis accuracy. Our findings are helpful to improve patient's quality of life.

1. Introduction

Gait damage is a common feature in patients with Parkinson's disease (PD). The gait characteristics of PD are decreased pace, step length, and arm swing [1–3]. As the disease progresses, some patients may suffer from the festination and freezing of gait [4, 5]. These disorders may induce falls and fractures, which increase mortality [6]. Thus, in the gait analysis of PD, identifying changes in the gait characteristics is a priority. With the rapid development of technology, wearable sensors can be used to quantify gait parameters. However, few studies about quantitative gait analysis in early-stage PD have been published. In early-stage PD, affected individuals walk at a slower pace and with a more variable and asymmetric gait pattern than normal [7]. Foot heights during heel strike are significantly decreased which are reflective of dragging the foot in early-stage PD [8]. A reduction in physical activity and gait speed is also associated with prodromal PD [9]. During a long-term follow-up of patients with early-stage PD, stride length and step time variability increased when patients walked at a normal pace [10]. All these studies suggest that patients with early-stage PD already have gait damage. However, gait characteristics extensively vary with no consistency across studies [7, 11]. Previous studies also have some limitations. First, most of them have focused on spatiotemporal gait parameters. These spatiotemporal gait parameters distantly reflect the gait changes of patients with PD as they lack disease specificity [12–14]. Clinical gait analysis mainly includes spatiotemporal and kinematic gait parameters [15]. Further studies validating changes in kinematic gait parameters

in early-stage PD are needed. Second, appropriate technological solutions, such as wearable sensors, can improve PD diagnosis [16]. For example, previous studies have demonstrated that postural control is compromised in early-stage PD and may thus act as a diagnostic biomarker [17, 18]. However, similar articles are rare, and only five papers dealing the early diagnosis have been summarized in a recent review [19]. Accordingly, the present study is aimed at (1) comparing the differences in spatiotemporal gait parameters, kinematic gait parameters, and variability and symmetry analyses of gait performance between patients with early-stage PD and normal people and (2) evaluating the diagnostic value of gait parameters for patients with early-stage PD. We hypothesized that patients with early-stage PD present an asymmetrical and variable gait pattern. Some spatiotemporal and kinematic gait parameters can be applied to diagnose early-stage PD. Our results may aid the diagnosis of early-stage PD. Early identification of gait damage in patients with PD is beneficial to the choice of treatment methods such as drugs and rehabilitation. Targeted improvement of the patient's gait will help improve the patient's quality of life.

2. Methods

2.1. Participants. A total of 32 patients with early-stage PD (22 men, and 10 women; mean duration of disease 2.41 ± 1.30 years) were recruited from the Department of Geriatrics, Affiliated Brain Hospital of Nanjing Medical University, between October 2018 and November 2019. We also recruited 30 HC from the caregivers of the patients with PD. Inclusion criteria for early-stage PD were as follows: (1) diagnosis of PD according to the Movement Disorder Society (MDS) criteria [20], (2) Hoehn-Yahr (H-Y) stage of 1-2, and (3) disease duration of <4 years [21]. Exclusion criteria for PD were as follows: (1) other diseases that could affect gait, including cerebrovascular disease, orthopedic disease, and spinal column diseases; (2) inability to follow doctor's instructions; (3) have received other PD therapies, i.e., rehabilitation therapy. Inclusion criteria for HC were as follows: (1) no medical history of PD, cerebrovascular disease, orthopedic disease, and spinal column diseases; (2) ability to follow doctor's instructions. Ethical approval was obtained from the Medical Ethics Committee of the Affiliated Brain Hospital of Nanjing Medical University. After a complete explanation of the study to all participants, they signed a written informed consent before the experiment. All above-mentioned procedures were performed according to the declaration of Helsinki.

2.2. Demographic and Clinical Measures. For all participants, we collected the following demographic characteristics: age, height, weight, gender, and degree of education. Cognition was assessed with the Montreal Cognitive Assessment (MoCA). All participants were tested in the morning. The Unified Parkinson's Disease Rating Scale (UPDRS) and H-Y scale were used to assess the severity of PD motor symptoms. For patients with PD, their antiparkinsonian medication was stopped for at least 24 h (72 h for controlled-release antiparkinsonian medication).

2.3. Quantitative Gait Evaluation. All participants completed the instrumented stand and walk test (ISAW), a reliable and sensitive method of measuring gait [22]. All participants were asked to stand quietly for 30 seconds with their arms at their sides and look straight ahead, then walking 7 meters at a self-select and comfortable speed, turning 180° and returned to their initial place. We explained the steps of ISAW in detail to all participants before the test. Also, all participants walked twice in advance to be familiar with the test. After that, we started to collect gait data. When all subjects underwent this test, gait data was collected at the same time.

2.4. Equipment. We used the JiBuEn gait-analysis system to collect gait data. This gait-analysis system comprised shoes and modules with Micro-Electro-Mechanical System sensors fixed behind the upper and lower limbs, under the shoe heel bottom. The system gathered motion information and transmitted it to a computer. The hexahedral calibration technique, high-order low-pass filter, and zero-correction algorithm were used in data preprocessing. The accuracy of this system has been tested before [23]. Through the latest JiBuEn gait-analysis system, we can obtain spatiotemporal gait parameters (total steps of ISAW, stride length, gait velocity, cadence, stride time, stance phase time, swing phase time, variability of stride length, variability of stride time, variability of stance phase time, and variability of swing phase time) and kinematic gait parameters (heel strike angle, toe-off angle, and range of motion of ankle, knee, and hip joints).

2.5. Statistical Analysis. Data are expressed as the mean ± standard deviation. The significance level was set at 0.05. Count data were given as percentages. For both groups, measurement data were initially analyzed with the Kolmogorov-Smirnov test. For normally distributed data, the independent t-test was used to perform intergroup comparison of measurement data. For nonnormally distributed data of intergroup gait characteristics, the Mann-Whitney U Test was used. The χ^2 test was used for count data. Variability of gait parameters from the left and right sides were calculated separately (Equation (1)) and then combined (Equation (2)). This method can avoid confusion due to step changes caused by the asymmetry between the left and right sides in PD [24]. The symmetry of gait parameters was assessed through the asymmetry index (AI) (Equation (3)) [25–27].

$$CV_{separate} = standard\ deviation \div mean, \tag{1}$$

$$\%CV_{combined} = \sqrt{\frac{CV_L + CV_R}{2}} * 100. \tag{2}$$

The subscripts R and L represent the right and left sides of participants, respectively. CV means coefficient of variation.

$$\%AI = \frac{\max\ (X_L, X_R) - \min\ (X_L, X_R)}{\max\ (X_L, X_R)} * 100, \tag{3}$$

where X = [SL, ST, StPT, SwPT, HS, TO, ROM − AJ, ROM − KJ, ROM − HJ], the subscripts R and L represent the right and left sides of participants, respectively. SL: stride length; ST: stride time; StPT: stance phase time; SwPT: swing phase time; HS: heel strike angle; TO: toe-off angle; ROM: range of motion; AJ: ankle joint; KJ: knee joint; and HJ: hip joint.

The predictive performance of gait parameters was evaluated by receiver operating characteristic (ROC) curve analysis. The logistic regression model was used to evaluate different predictive parameters and calculate predictive probability. Predictive probability was then used for ROC analysis. The optimum cut-off values to predict PD were calculated with Youden Index. IBM SPSS software version 23 was used for data analyses. Figures were configured using Graph Pad Prism Software version 8.0.1.

3. Results

3.1. Clinical Characteristics of Participants. Sixty-two participants were included in this study, and their demographic, cognitive, and clinical characteristics are shown in Table 1. Among the 32 PD patients, 22 (68.8%) were male and 20 (62.5%) started with the left side, the mean age was 65.66 ± 10.16 years, the mean height was 165.78 ± 6.74 cm, and the mean weight was 65.94 ± 10.05 kg. Moreover, 4 (12.5%), 7(21.9%), 17 (53.1%), and 4 (12.5%) cases received education of illiteracy, primary school, middle school, and college, respectively. The mean duration of PD was 2.41 ± 1.30 years, and the mean Hoehn-Yahr (H-Y) stage of the disease was 1.73 ± 0.44. The total UPDRS III score was 22.91 ± 9.32.

3.2. Changes in Spatiotemporal Gait Parameters. We measured spatiotemporal gait parameters, including total steps (TS) of ISAW, stride length (SL), gait velocity (GV), cadence (CA), stride time (ST), stance phase time (StPT), and swing phase time (SwPT). Moreover, we calculated the variabilities of SL (CV-SL), ST (CV-ST), StPT (CV-StPT), and SwPT (CV-SwPT). We observed only slight differences between the HC and early-stage PD in these spatiotemporal gait parameters (Table 2). For patients with early-stage PD, the TS of ISAW was 12.81 ± 3.42 steps, which was a significant increase of ~24.01% compared with that of the HC. Compared with the HC, SL decreased by ~9.32% in early-stage PD. We also observed increased variability of SL ($P < 0.001$), StPT ($P = 0.004$), and SwPT ($P = 0.011$) in early-stage PD.

3.3. Changes in Kinematic Gait Parameters. Kinematic gait parameters were evaluated based on the range of motion (ROM) of the ankle, knee, and hip joints. ROM was defined as the difference between the minimum and maximum angles of the above three joints in the sagittal plane. Moreover, toe-off (TO) and heel strike (HS) angles were included in our study (Figure 1). We observed significant differences in HS, ROM-knee joints (ROM-KJ), and ROM-hip joints (ROM-HJ) between two groups but none in TO and ROM-ankle joints (ROM-AJ) between two groups.

3.4. Symmetry Analysis of Gait Parameters. We included the spatiotemporal and kinematic gait parameters in the symmetry analysis. In the analysis of gait symmetry, there was no difference in any of the assessed gait parameters between the HC and PD (Table 3).

Table 1: Clinical characteristics of participants.

	HC	PD	P
N	30	32	
Age (years)	62.43 ± 6.43	65.66 ± 10.16	0.139
Height (cm)	163.23 ± 4.72	165.78 ± 6.74	0.106
Weight (kg)	63.23 ± 8.61	65.94 ± 10.05	0.261
Male (%)	17 (56.7)	22 (68.8)	0.325
MoCA	25.40 ± 1.16	25.00 ± 2.58	0.618
Education (%)			0.094
Illiteracy	1 (3.3)	4 (12.5)	
Primary school	7 (23.4)	7 (21.9)	
Middle school	22 (73.3)	17 (53.1)	
College	0	4 (12.5)	
Duration of PD (years)		2.41 ± 1.30	
H-Y stage		1.73 ± 0.44	
Onset side (%)		Left (62.5)	
UPDRS III total scores		22.91 ± 9.32	

Data is shown as Mean ± SD. MoCA: Montreal Cognitive Assessment; H-Y stage: Hoehn-Yahr stage; UPDRS III: Unified Parkinson's Disease Rating Scale part 3.

Table 2: Spatiotemporal gait parameters of participants.

	HC	PD	P
TS (steps)	10.33 ± 2.09	12.81 ± 3.42	0.001**
SL (m)	1.18 ± 0.10	1.07 ± 0.16	0.003*
GV (m/s)	0.91 ± 0.14	0.85 ± 0.20	0.204
CA (steps/min)	93.27 ± 9.21	95.20 ± 16.99	0.576
ST (s)	1.30 ± 0.14	1.31 ± 0.28	0.899
StPT (%)	64.88 ± 2.21	64.75 ± 5.22	0.312
SwPT (%)	35.12 ± 2.21	35.25 ± 5.22	0.396
CV-SL (%)	20.92 ± 2.82	24.88 ± 4.65	<0.001**
CV-ST (%)	21.38 ± 5.10	23.25 ± 6.90	0.229
CV-StPT (%)	14.80 ± 3.07	17.23 ± 4.56	0.004*
CV-SwPT (%)	19.67 ± 4.57	23.14 ± 6.80	0.011*

Data is shown as Mean ± SD. TS: total steps; SL: stride length; GV: gait velocity; CA: cadence; ST: stride time; StPT: stance phase time; SwPT: swing phase time; CV: coefficient of variation; *$P < 0.05$; **$P \leq 0.001$.

3.5. ROC Analysis of Gait Parameters. We used the ROC curve to evaluate the value of gait parameters in predicting early-stage PD to HC. We found only a few gait parameters with potential diagnostic value (Figure 2). TS, SL, and SL variability showed significant value in predicting early-stage PD with AUCs of 0.763 (95%CI = 0.645 − 0.882; $P < 0.001$), 0.701 (95%CI = 0.570 − 0.832; $P = 0.007$), and 0.769 (95%CI = 0.653 − 0.885; $P < 0.001$), respectively. At a cut-off of 10 steps, TS offered the best accuracy in predicting early-stage PD with the sensitivity and specificity of 78.12%

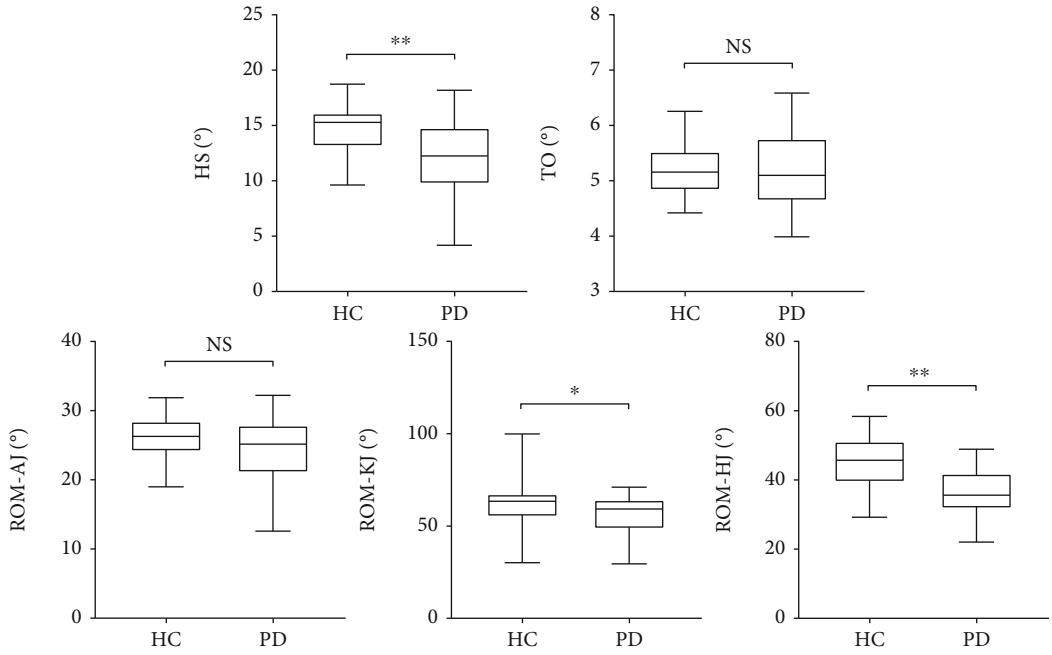

Figure 1: Changes in kinematic gait parameters. HS: heel strike angle; TO: toe-off angle; ROM: range of motion; AJ: ankle joint; KJ: knee joint; HJ: hip joint. "ns" means no significance, $^{*}P < 0.05$, $^{**}P \leq 0.001$.

Table 3: Symmetry analysis of gait parameters.

	HC	PD	P
AI-SL (%)	2.47 ± 0.88	2.27 ± 0.86	0.406
AI-ST (%)	6.64 ± 8.43	9.99 ± 10.76	0.083
AI-StPT (%)	4.75 ± 5.80	5.53 ± 5.47	0.434
AI-SwPT (%)	8.09 ± 8.71	9.56 ± 8.49	0.451
AI-HS (%)	16.41 ± 8.83	19.84 ± 13.70	0.250
AI-TO (%)	9.75 ± 6.19	10.92 ± 9.01	0.554
AI-ROM-AJ (%)	9.83 ± 7.36	12.11 ± 10.84	0.693
AI-ROM-KJ (%)	15.02 ± 15.16	16.92 ± 15.80	0.612
AI-ROM-HJ (%)	7.04 ± 5.44	12.61 ± 11.62	0.061

Data is shown as Mean ± SD. AI: asymmetry index; SL: stride length; ST: stride time; StPT: stance phase time; SwPT: swing phase time; HS: heel strike angle; TO: toe-off angle; ROM: range of motion; AJ: ankle joint; KJ: knee joint; HJ: hip joint.

and 63.33%, respectively. 1.045 was the optimum cut-off of SL. The sensitivity and specificity were 43.75% and 100%, respectively. With the cut-off value at 20.820 of SL variability, the sensitivity and specificity were 90.62% and 56.67%, respectively. No significant value for ST variability was observed in predicting early-stage PD with an AUC of 0.554 (95%CI = 0.406 – 0.702; $P = 0.468$). However, either StPT variability or SwPT variability can effectively predict early-stage PD, with AUCs of 0.712 (95%CI = 0.581 – 0.842; $P = 0.004$) and 0.688 (95%CI = 0.556 – 0.821; $P = 0.011$), respectively. The optimum cut-off of StPT variability was 16.125, clearly distinguishing between early-stage PD and HC. Sensitivity and specificity were 53.13% and 83.33%, respectively. At a cut-off of 21.794, SwPT variability offered the highest accuracy in predicting PD with sensitivity and specificity of 50.00% and 83.33%, respectively. We further explored the predictive value of kinematic gait parameters and found that HS, TO, ROM-AJ, ROM-KJ, and ROM-HJ all cannot predict early-stage PD (figures not shown in this article).

To explore the predictive value of the combination of TS, SL, SL variability, StPT variability, and SwPT variability, we combined these five gait parameters in a logistical analysis model to calculate probability. We then used ROC analysis to calculate the AUC (Figure 3). When the five gait parameters were combined, the predictive power was found to increase, with the highest AUC of 0.802 (95%CI = 0.695 – 0.906; $P < 0.001$). At a cut-off value of 0.388, the sensitivity and specificity of the association to predict early-stage PD were 90.62% and 60.00%, respectively.

4. Discussion

This study was a cross-sectional, single-center, observational one that was conducted to (1) quantify gait impairments in early-stage PD using wearable sensors from spatiotemporal gait parameters, kinematic gait parameters, and variability and symmetry analyses of gait parameters and (2) evaluate the predictive value of gait parameters for early-stage PD. Our finding may aid the diagnosis of early-stage PD and improve personalized care in patients with early-stage PD.

A previous study has demonstrated that SL was the most prominent parameter of altered gait in initial stages of PD patients [28]. During a long-term follow-up of patients with early-stage PD, SL and ST variability increased when patients walked at a normal pace [10]. These passages were consistent with our study. For spatiotemporal parameters, we found

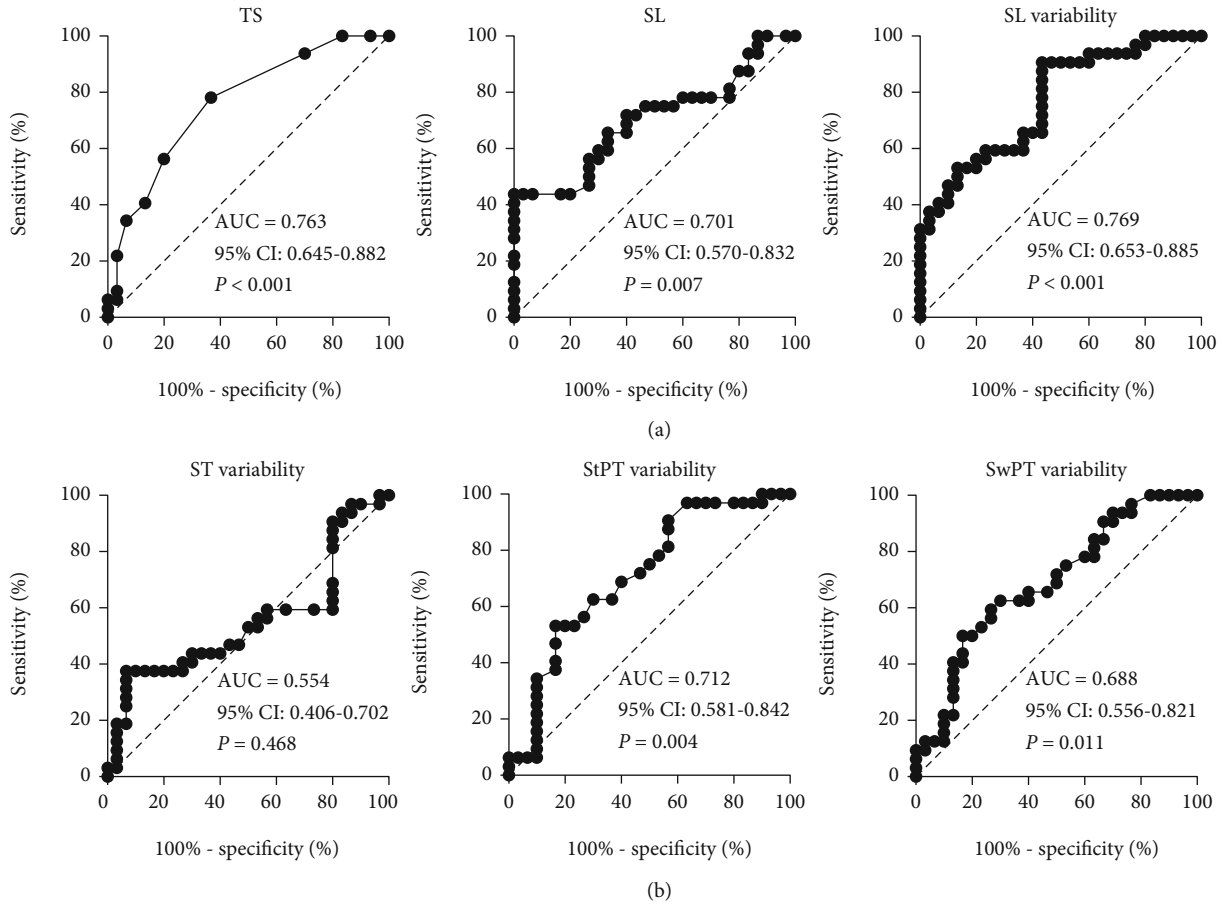

Figure 2: Receiver operating characteristics (ROC) analysis for gait parameters. TS: total steps; SL: stride length; SL variability: stride length variability; ST variability: stride time variability; StPT variability: stance phase time variability; SwPT variability: swing phase time variability; AUC: area under the curve; CI: confidence interval.

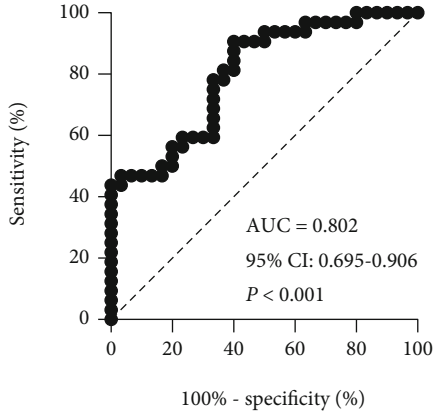

Figure 3: Receiver operating characteristics (ROC) analysis for the combination of TS, SL, SL variability, StPT variability, and SwPT variability. The combination of those five gait parameters increased the predictive power with the highest AUC of 0.802 (95% CI 0.695–0.906, $P < 0.001$). TS: total steps; SL: stride length; SL variability: stride length variability; StPT variability: stance phase time variability; SwPT variability: swing phase time variability; AUC: area under the curve; CI: confidence interval.

impairment only in the TS of ISAW, SL, SL variability, StPT, and SwPT variability in patients with early-stage PD. This finding suggested that gait impairment in patients with PD stems from a short SL and a more variable gait pattern. This is noteworthy because previous research has demonstrated that variability in gait predicted falls in older adults and PD [29]. Although patients with early-stage PD have minor gait impairments, their potential risk of falling cannot be ignored. Another study has used mean step length and mean step length variability to accurately classify PD [7]. Based on previous research and the present one, we used ROC curves to evaluate the predictive value of gait parameters for early-stage PD. We found that TS, SL, SL variability, StPT variability, and SwPT variability can predict PD alone. However, we did not find statistically significant values in other gait parameters predicting PD. Particularly for TS and SL variability, the AUC of these two parameters can reach 0.763 and 0.769, respectively, suggesting that these two parameters had relatively high predictive value. Moreover, when TS, SL, SL variability, StPT variability, and SwPT variability were combined, the predictive power increased and showed the highest AUC of 0.802. This finding is important because diagnosing early-stage PD is a clinical challenge. Overall, our study demonstrated the feasibility of applying gait

parameters to diagnose early-stage PD. Quantifying gait parameters using wearable devices, combined with the patient's clinical performance and auxiliary examination, can increase diagnosis accuracy.

The onset of PD is mostly unilateral and it may be attributed to the degeneration of dopaminergic cells starting with an asymmetrical pattern. The consistency of activities on both lower limbs is defined as symmetry [30]. In our study, PD patients with an onset of left and right sides accounted for 62.5% and 37.5%, respectively. We did not find statistical differences in the symmetry analysis of gait parameters. This is inconsistent with our hypothesis and the clinical performance of patients with PD. Previous studies have demonstrated that patients with PD walked in a more asymmetric gait pattern compared to HC [3, 7, 26, 27]. We tentatively attribute this to more advanced stage patients with PD were enrolled in previous studies. These studies all have included patients with H-Y stage 3. It means that the presence of postural instability in some patients of previous studies [31]. However, only patients with H-Y stage 1-2 were included in our research. In addition, the loss of dopamine markers occurred rapidly and virtually completed by 4-year disease duration [21]. Therefore, the disease duration of all patients with PD in our study was less than 4 years. To our best knowledge, this inclusion criterion was not admitted to any previous studies. A study involving patients with H-Y stage 1-1.5 and a mean disease duration of 1.38 years has shown that the gait variables are significantly altered but gait symmetry remains preserved during early-stage PD [28]. Last but not least, in our study, gait speed of HC and early-stage PD were 0.91 ± 0.14 m/s and 0.85 ± 0.20 m/s, respectively. There was no difference in gait speed performance between two groups. This is noteworthy, because many gait parameters are speed-dependent [27]. The comparisons between the other gait parameters can be biased by the different gait speed. This may result in different conclusions because of previous studies failing to control speed. Our study showed that patients with a mean H-Y stage of 1.73 and a mean disease duration of 2.41 years retained their symmetrical gait pattern. A symmetrical gait pattern in patients with early-stage PD might be attributed to that the preserved symmetric gait function in both the motor cortex and supplementary motor cortex which may compensate for an asymmetrical dopaminergic cells distributed pattern in basal ganglia [28]. Based on these studies and our results, we hypothesized that although the onset of PD was mostly unilateral, the gait pattern of early-stage PD remained symmetrical. We found that up to a mean H-Y stage of 1.73, patients with PD retained a symmetrical gait pattern. As the disease progressed, an asymmetrical gait pattern gradually appeared. However, further study is needed to verify our hypothesis.

Previous studies have rarely analyzed kinematic parameters in early-stage PD. We observed significant differences in HS, ROM-KJ, and ROM-HJ between two groups. A smaller HS angle indicated a decreased foot height which reflected foot dragging. A study has demonstrated decreased foot height in early-stage PD [8] which is consistent with our study. Patients with PD showed reduced ROM-AJ, ROM-KJ, and ROM-HJ on both sides [27]. This finding slightly differs from ours because no impairment of ROM-AJ was found in early-stage PD. We attribute the discrepancy to the different methods of calculation. Our ROM calculation method was based on the average value of the left and right sides, and the aforementioned study has calculated them independently which may magnify the difference. Moreover, they have also included patients with H-Y stage 3. From the distribution of damaged joints, we speculated that gait damage started from the proximal joints and affected the distal joint as the disease progressed. Our research extended previous findings in showing that the gait damage of patients with early-stage PD was mild and primarily focused on kinematic parameters. However, it is the spatiotemporal gait parameters that had potential value for early PD diagnosis.

The strengths of our study are as follows. First, gait impairments in early-stage PD were comprehensively analyzed by using wearable sensors from spatiotemporal gait parameters, kinematic gait parameters, and variability and symmetry analyses of gait parameters. Second, we extended previous studies by exploring the predictive value of gait parameters in early-stage PD. Third, the disease duration of all patients with PD in our study was less than 4 years. This inclusion criterion was not admitted to previous studies since the loss of dopamine markers occurred rapidly and virtually completed by 4 years disease duration. However, our study also has several limitations. First, our study had a small sample size and was conducted at a single center. Therefore, clinical inspection can have a selection bias. Second, this was not a de novo group. Some of these patients had already taken anti-PD drugs. However, their antiparkinsonian medication was stopped for at least 24 h (72 h for controlled-release antiparkinsonian medication) to minimize the impact of drugs on gait performance. Third, PD is a kind of heterogeneous disease, and the possible influence of nonmotor symptoms on gait performance was not accounted for in our study.

5. Conclusion

In conclusion, gait damage of patients with early-stage PD was mild and mostly focuses on kinematic gait parameters. Patients with early-stage PD presented increased variability but still symmetrical gait pattern. Some spatiotemporal gait parameters, e.g., TS of ISAW, SL, SL variability, StPT, and SwPT variability, can be applied to help diagnose early-stage PD. Quantifying gait parameters using wearable devices, combined with the patient's clinical performance and auxiliary examination, may increase diagnosis accuracy. Our findings are helpful to reveal gait impairments in patients with early-stage PD. Choosing the corresponding treatment methods based on the revealed gait damage is essential to improve the patient's quality of life. Further research, especially longitudinal cohort and de novo group ones, is needed to evaluate the evolution of PD gait pattern. This is a dynamic process.

Data Availability

The data used to support the findings of this study are available from the corresponding author upon request.

Conflicts of Interest

The authors declare that there is no conflict of interest regarding the publication of this paper.

Authors' Contributions

ZW and XJ performed the research, collected and analysed the data, and drafted and revised the manuscript. LZ and JY designed the study and revised the manuscript critically. MZ, BS, and JZ helped in collection of data and analysis of data. YP and JD helped in clinical data analyses. PX and WZ revised the manuscript. All authors approved the publication of this final version. Zhuang Wu and Xu Jiang contributed equally to this work.

Acknowledgments

We acknowledge all participants in this research for their understanding and participation. We thank all the researchers of JiBuEn gait analysis system for their timely technical support. In addition, we would like to thank Dr. Dong Yan, for her suggestions and help in this research. This study was funded by the (1) Key Research and Development Project of the Ministry of Science and Technology (grant no. 2016YFC1306600), (2) Special Funds of the Jiangsu Provincial Key Research and Development Projects (grant nos. BE2018610 and BE2019612), (3) Jiangsu Provincial Cadre Health Research Projects (grant no. BJ16001), and (4) Nanjing Medical Science and Technique Development Foundation (grant no. ZKX17031).

References

[1] X. Huang, J. M. Mahoney, M. M. Lewis, G. Du, S. J. Piazza, and J. P. Cusumano, "Both coordination and symmetry of arm swing are reduced in Parkinson's disease," *Gait & Posture*, vol. 35, no. 3, pp. 373–377, 2012.

[2] M. Pistacchi, M. Gioulis, F. Sanson et al., "Gait analysis and clinical correlations in early Parkinson's disease," *Functional Neurology*, vol. 32, no. 1, pp. 28–34, 2017.

[3] S. B. Koh, Y. M. Park, M. J. Kim, and W. S. Kim, "Influences of elbow, shoulder, trunk motion and temporospatial parameters on arm swing asymmetry of Parkinson's disease during walking," *Human Movement Science*, vol. 68, p. 102527, 2019.

[4] E. B. Forsaa, J. P. Larsen, T. Wentzel-Larsen, and G. Alves, "A 12-year population-based study of freezing of gait in Parkinson's disease," *Parkinsonism & Related Disorders*, vol. 21, no. 3, pp. 254–258, 2015.

[5] C. Curtze, J. G. Nutt, P. Carlson-Kuhta, M. Mancini, and F. B. Horak, "Objective gait and balance impairments relate to balance confidence and perceived mobility in people with Parkinson disease," *Journal of Neurophysiology*, vol. 96, no. 11, pp. 1734–1743, 2016.

[6] P. Martinez-Martin, "An introduction to the concept of "quality of life in Parkinson's disease"," *Journal of Neurology*, vol. 245, Supplement 1, pp. S2–S6, 1998.

[7] R. Z. U. Rehman, S. Del Din, Y. Guan, A. J. Yarnall, J. Q. Shi, and L. Rochester, "Selecting clinically relevant gait characteristics for classification of early Parkinson's disease: a comprehensive machine learning approach," *Scientific Reports*, vol. 9, no. 1, p. 17269, 2019.

[8] K. J. Shin, J. Park, S. Ha et al., "Decreased foot height may be a subclinical shuffling gait in early stage of Parkinson's disease: a study of three-dimensional motion analysis," *Gait & Posture*, vol. 76, pp. 64–67, 2020.

[9] M. I. Maraki, L. Stefanis, M. Yannakoulia et al., "Motor function and the probability of prodromal Parkinson's disease in older adults," *Movement Disorders : Official Journal of the Movement Disorder Society*, vol. 34, no. 9, pp. 1345–1353, 2019.

[10] M. A. Hobert, S. Nussbaum, T. Heger, D. Berg, W. Maetzler, and S. Heinzel, "Progressive gait deficits in Parkinson's disease: a wearable-based biannual 5-year prospective study," *Frontiers in Aging Neuroscience*, vol. 11, p. 22, 2019.

[11] M. Djuric-Jovicic, M. Belic, I. Stankovic, S. Radovanovic, and V. S. Kostic, "Selection of gait parameters for differential diagnostics of patients with de novo Parkinson's disease," *Neurological Research*, vol. 39, no. 10, pp. 853–861, 2017.

[12] K. M. Beavers, D. P. Beavers, D. K. Houston et al., "Associations between body composition and gait-speed decline: results from the health, aging, and body composition study," *The American Journal of Clinical Nutrition*, vol. 97, no. 3, pp. 552–560, 2013.

[13] S. Lord, B. Galna, and L. Rochester, "Moving forward on gait measurement: toward a more refined approach," *Movement Disorders : Official Journal of the Movement Disorder Society*, vol. 28, no. 11, pp. 1534–1543, 2013.

[14] F. Cuzzolin, M. Sapienza, P. Esser et al., "Metric learning for Parkinsonian identification from IMU gait measurements," *Gait & Posture*, vol. 54, pp. 127–132, 2017.

[15] D. TarniŢă, "Wearable sensors used for human gait analysis," *Romanian Journal of Morphology and Embryology = Revue roumaine de morphologie et embryologie*, vol. 57, no. 2, pp. 373–382, 2016.

[16] A. H. Butt, E. Rovini, D. Esposito, G. Rossi, C. Maremmani, and F. Cavallo, "Biomechanical parameter assessment for classification of Parkinson's disease on clinical scale," *International Journal of Distributed Sensor Networks*, vol. 13, no. 5, 2017.

[17] M. Mancini, F. B. Horak, C. Zampieri, P. Carlson-Kuhta, J. G. Nutt, and L. Chiari, "Trunk accelerometry reveals postural instability in untreated Parkinson's disease," *Parkinsonism & Related Disorders*, vol. 17, no. 7, pp. 557–562, 2011.

[18] N. Chastan and L. M. Decker, "Posturo-locomotor markers of preclinical Parkinson's disease," *Clinical Neurophysiology*, vol. 49, no. 2, pp. 173–180, 2019.

[19] E. Rovini, C. Maremmani, and F. Cavallo, "How wearable sensors can support Parkinson's disease diagnosis and treatment: a systematic review," *Frontiers in Neuroscience*, vol. 11, p. 555, 2017.

[20] R. B. Postuma, D. Berg, M. Stern et al., "MDS clinical diagnostic criteria for Parkinson's disease," *Movement Disorders : Official Journal of the Movement Disorder Society*, vol. 30, no. 12, pp. 1591–1601, 2015.

[21] J. H. Kordower, C. W. Olanow, H. B. Dodiya et al., "Disease duration and the integrity of the nigrostriatal system in Parkinson's disease," *Brain : a Journal of Neurology*, vol. 136, no. 8, pp. 2419–2431, 2013.

[22] M. Mancini, L. King, A. Salarian, L. Holmstrom, J. McNames, and F. B. Horak, "Mobility lab to assess balance and gait with

synchronized body-worn sensors," *Journal of Bioengineering & Biomedical Science*, vol. 7, Supplement 1, 2011.

[23] S. Tao, X. Zhang, H. Cai, Z. Lv, C. Hu, and H. Xie, "Gait based biometric personal authentication by using MEMS inertial sensors," *Journal of Ambient Intelligence and Humanized Computing*, vol. 9, no. 5, pp. 1705–1712, 2018.

[24] B. Galna, S. Lord, and L. Rochester, "Is gait variability reliable in older adults and Parkinson's disease? Towards an optimal testing protocol," *Gait & Posture*, vol. 37, no. 4, pp. 580–585, 2013.

[25] K. K. Patterson, W. H. Gage, D. Brooks, S. E. Black, and W. E. McIlroy, "Evaluation of gait symmetry after stroke: a comparison of current methods and recommendations for standardization," *Gait & Posture*, vol. 31, no. 2, pp. 241–246, 2010.

[26] M. Zhang, N. S. Artan, H. Gu et al., "Gait study of Parkinson's disease subjects using haptic cues with a motorized walker," *Sensors*, vol. 18, no. 10, 2018.

[27] M. Serrao, G. Chini, G. Caramanico et al., "Prediction of responsiveness of gait variables to rehabilitation training in Parkinson's disease," *Frontiers in Neurology*, vol. 10, p. 826, 2019.

[28] M. Grajic, I. Stankovic, S. Radovanovic, and V. Kostic, "Gait in drug naïve patients with de novo Parkinson's disease – altered but symmetric," *Neurological Research*, vol. 37, no. 8, pp. 712–716, 2015.

[29] J. M. Hausdorff, "Gait dynamics, fractals and falls: finding meaning in the stride-to-stride fluctuations of human walking," *Human Movement Science*, vol. 26, no. 4, pp. 555–589, 2007.

[30] W. Herzog, B. M. Nigg, L. J. Read, and E. Olsson, "Asymmetries in ground reaction force patterns in normal human gait," *Medicine and Science in Sports and Exercise*, vol. 21, no. 1, pp. 110–114, 1989.

[31] C. G. Goetz, W. Poewe, O. Rascol et al., "Movement Disorder Society Task Force report on the Hoehn and Yahr staging scale: status and recommendations," *Movement Disorders*, vol. 19, no. 9, pp. 1020–1028, 2004.

Hindawi
Behavioural Neurology
Volume 2021, Article ID 6657716, 13 pages
https://doi.org/10.1155/2021/6657716

Research Article

BDNF Protein and BDNF mRNA Expression of the Medial Prefrontal Cortex, Amygdala, and Hippocampus during Situational Reminder in the PTSD Animal Model

Shao-Han Chang,[1,2] Ying Hao Yu,[3,4] Alan He,[3] Chen Yin Ou,[3] Bai Chuang Shyu,[2] and Andrew Chih Wei Huang[3]

[1]*Taiwan International Graduate Program in Interdisciplinary Neuroscience, National Cheng Kung University and Academia Sinica, Taipei, Taiwan*
[2]*Institute of Biomedical Sciences, Academia Sinica, Taipei, Taiwan*
[3]*Department of Psychology, Fo Guang University, Yilan County 26247, Taiwan*
[4]*Department of Biotechnology and Animal Science, National Ilan University, Yilan 26047, Taiwan*

Correspondence should be addressed to Bai Chuang Shyu; bmbai@gate.sinica.edu.tw
and Andrew Chih Wei Huang; chweihuang@mail.fgu.edu.tw

Received 10 November 2020; Revised 9 February 2021; Accepted 22 February 2021; Published 9 March 2021

Academic Editor: Yu Yo Sun

Whether BDNF protein and BDNF mRNA expression of the medial prefrontal cortex (mPFC; cingulated cortex area 1 (Cg1), prelimbic cortex (PrL), and infralimbic cortex (IL)), amygdala, and hippocampus (CA1, CA2, CA3, and dentate gyrus (DG)) was involved in fear of posttraumatic stress disorder (PTSD) during the situational reminder of traumatic memory remains uncertain. Footshock rats experienced an inescapable footshock (3 mA, 10 s), and later we have measured fear behavior for 2 min in the footshock environment on the situational reminder phase. In the final retrieval of situational reminder, BDNF protein and mRNA levels were measured. The results showed that higher BDNF expression occurred in the Cg1, PrL, and amygdala. Lower BDNF expression occurred in the IL, CA1, CA2, CA3, and DG. BDNF mRNA levels were higher in the mPFC and amygdala but lower in the hippocampus. The neural connection analysis showed that BDNF protein and BDNF mRNA exhibited weak connections among the mPFC, amygdala, and hippocampus during situational reminders. The present data did not support the previous viewpoint in neuroimaging research that the mPFC and hippocampus revealed hypoactivity and the amygdala exhibited hyperactivity for PTSD symptoms. These findings should be discussed with the previous evidence and provide clinical implications for PTSD.

1. Introduction

Posttraumatic stress disorder (PTSD) is a severe and chronic mental illness. PTSD symptoms can be caused by severe traumatic events, including illness (e.g., cancer [1, 2]), situations of conflict (e.g., war [3]), and natural disasters (e.g., earthquakes [4]). According to the *Diagnostic and Statistical Manual of Mental Disorders* (DSM-5), PTSD has numerous critical symptoms [5]. For example, patients may persistently suppress stimuli associated with the traumatic stimulus and induce emotional numbing [6] by reexposing the environmental stimulus (i.e., the conditioned stimulus (CS)) associated with previous traumatic events (i.e., the unconditioned stimulus (US)) [7]. Patients with PTSD often experience persistent traumatic events as well as feelings of fear, helplessness, and horror [8, 9]. In the animal model of PTSD, growing studies employed the procedure of the situational reminder to imitate PTSD patients who continuously experience traumatic events [10–14]. Therefore, the present study used the procedure of situational reminder to test fear for PTSD symptoms.

Brain-derived neurotrophic factor (BDNF) is a signal that regulates axon and dendrite growth [15]. The intracellular signaling cascade of BDNF is associated with tropomyosin-related kinase B (TrkB) receptors to govern neuronal survival, axonal growth, and synaptic plasticity [16, 17]. Previous studies have reported that BDNF expression in the medial prefrontal cortex (mPFC), amygdala, and hippocampus was likely associated with stress-related events and PTSD symptoms [16]. For example, the early-weaned mice showed increased freezing behavior following fear conditioning, and these mice exhibited decreases in BDNF expression and mRNA transcripts for BDNF exon III in the mPFC [18]. Using the single prolonged-stress footshock procedure of the PTSD model indicated that the prefrontal cortex has lower BDNF levels [19]. BDNF secretions in the ventral hippocampus-infralimbic cortex (IL) pathway could alter the fear contextual conditioning [20]. Under long-term restraint stress, the basolateral amygdala (BLA) exhibited higher levels in BDNF protein and BDNF mRNA expression; moreover, the CA3 of the hippocampus has lower BDNF protein and BDNF mRNA expression [21]. A study of predator scent stress in animals suggested that neuropeptide S microinjections in the BLA reduced stress-related behavior and ameliorated low levels of BDNF in the BLA [22]. As animals with early footshock experiences and then receiving a cue fear conditioning, the footshock decreased BDNF expression in the dentate gyrus (DG) of the hippocampus in the PTSD animal model [23]. Recently, the inhibition of the hyperpolarization-activated cyclic nucleotide-gated channel 1 (HCN1) was revealed to reduce stress-related immobility behavior and escaped time in the water maze test; moreover, BDNF-mTOR signaling in the prefrontal cortex and the hippocampus was facilitated by the inhibition of the HCN1 [24]. Sleep deprivation after contextual conditioning was shown to reduce BNDF and p-ERK levels in the hippocampus and amygdala and attenuated memory retrieval [25]. Nevertheless, fewer studies provided conflict data related to the BDNF involvements of the mPFC, amygdala, and hippocampus in stress or PTSD [26, 27]. For example, chronic stress treatments were negatively associated with BDNF mRNA expression and positively linked with *TrkB* mRNA expression in the CA1 of the hippocampus [26]. Recently, a research study found that acute treatment with ketamine reduced freezing behavior, but this treatment did not affect BDNF expression or glucose metabolism in the hippocampus, frontal cortex, or amygdala in the PTSD animal model [27]. Therefore, whether BDNF expression of the frontal cortex, amygdala, and hippocampus regulated PTSD symptoms should be scrutinized in the present study.

On the other hand, the review paper suggested that the mPFC as well as the hippocampus was negatively connected to the amygdala; moreover, the mPFC was positively connected with the hippocampus [28]. In this study, the mPFC and hippocampus exhibited lower neural activity and the amygdala appeared to have higher neural activity when PTSD patients suffered from a trauma event [28]. However, these data were examined in the neuroimaging research but not in the other approaches. Therefore, the present study used the labeling approach of BDNF protein and BDNF mRNA to reexamine how the contribution of the neural connections among the mPFC, amygdala, and hippocampus regulated fear behavior of PTSD symptoms, especially for the situational reminder phase.

To target these emerged issues, this study concerned whether a footshock-induced severe traumatic memory event produced a fear response in the animal model of PTSD during the situational reminder phase. Moreover, the present work examined whether the mPFC (e.g., Cg1, PrL, and IL), hippocampus (e.g., CA1, CA2, CA3, and DG), amygdala, and piriform cortex (PC) exhibited higher BDNF protein and BDNF mRNA expression for PTSD-like rats, and it also tested the connections among the mPFC (i.e., Cg1, PrL, and IL), hippocampus (i.e., CA1, CA2, CA3, and DG), amygdala, and PC by analyzing the data of BDNF or BDNF mRNA in the third retrieval session of situational reminder.

2. Experimental Procedure

2.1. Animals. Forty-six male Wistar rats were purchased from BioLASCO Taiwan Co., Ltd. (Yilan County, Taiwan). At the beginning of the experiments, the weight of each rat was 250–350 g. All the rats were group-housed, two per plastic cage, with wooden bedding in the cage. The cages were kept in a colony room with a constant temperature (approximately $23 \pm 2^{\circ}$C) and light phase between 6:00 a.m. and 6:00 p.m. Food and water were provided *ad libitum*. The experiments were carried out in compliance with the American Psychological Association ethical standards for the treatment of animals. A description of the details of the treatment was submitted and received approval (ethical protocol # 1080008) from the Institutional Animal Care and Use Committee (IACUC) of Fo Guang University. Every effort was made to minimize the animals' suffering and the number of animals used.

2.2. Apparatus. The inescapable footshock apparatus is a box with a surrounding plastic shell measuring 60 cm × 60 cm × 72 cm high. The floor of the apparatus comprises metal grids (0.3 cm diameter at 0.7 cm grid intervals).

2.3. Behavioral Procedure. The experimental procedure is shown in Figure 1(a). Following the seven-day adaptation phase was the conditioning phase, where the rats were divided into nonfootshock (control group, $n = 12$) and footshock ($n = 12$) groups. During this phase, the rats in the footshock group received an inescapable footshock (3 mA, 10 seconds) and were then kept for two minutes in the footshock box. The rats in the control group were placed in the chamber for an equivalent period without receiving a footshock. Following this, rats were reexposed to the footshock box for two minutes to induce situational reminders once a day for three days. The experimental procedure of the PTSD animal model in situational reminder was referred from the previous studies [10, 14].

To examine BDNF proteins in the selected brain areas, immunohistochemical (IHC) staining was conducted on the nonfootshock ($n = 4$) and footshock ($n = 6$) groups

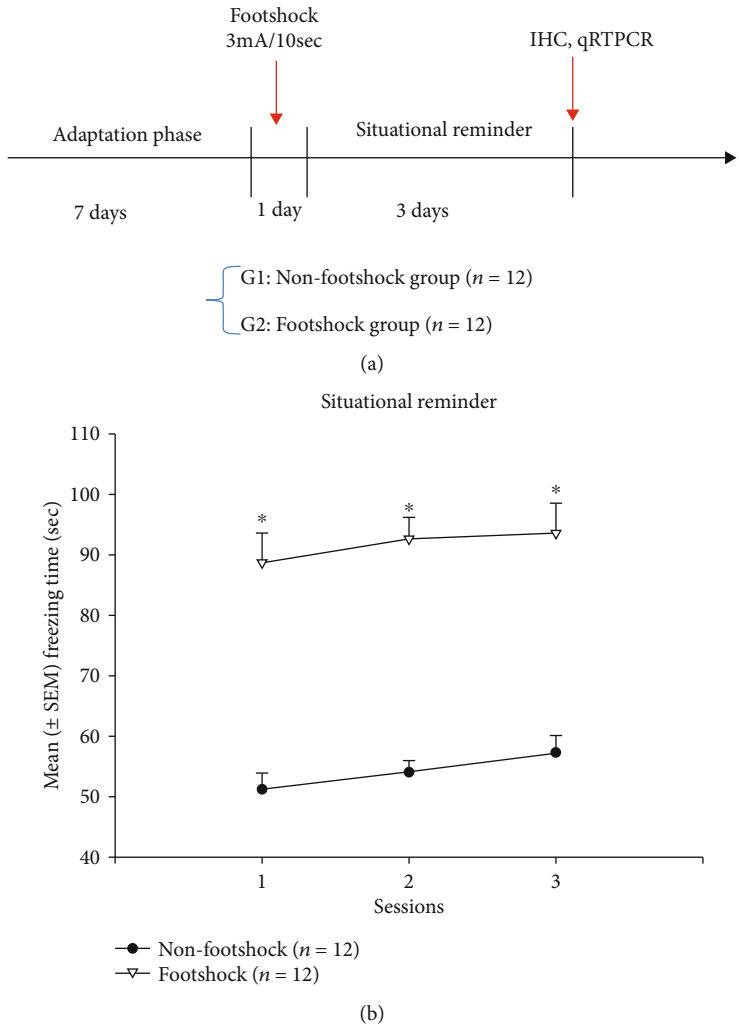

Figure 1: (a) Schematic representation of the experiment paradigm. After the seven-day adaptation phase, 3 mA footshock for 10 seconds was applied for fear conditioning, and freezing levels were measured for three sessions during situational reminder. Two hours after the third retrieval session of freezing behavior measurement, the rats were euthanized and their brain tissues were collected and further processed for immunohistochemical staining and qRT-PCR analysis. (b) Mean (±SEM) freezing time for three sessions during situational reminder. Conditioned freezing behavior was measured in the nonfootshock ($n = 12$) and footshock ($n = 12$) groups. $^*p < 0.05$ when comparing the nonfootshock and footshock groups.

following the third session of the situational reminder phase. The quantitative real-time polymerase chain reaction (qRT-PCR) method was performed on the nonfootshock ($n = 6$) and footshock ($n = 6$) groups to measure BDNF mRNA expression. Because fear behavior is a crucial PTSD symptom, the study addressed whether such behavior occurred in the third retrieval session. Thus, in the third retrieval session, qRT-PCR was performed to label BDNF proteins and BDNF mRNA levels.

The animals were euthanized, and their brain tissues were collected for further analysis of BDNF expression by IHC staining or BDNF mRNA levels. BDNF-positive nuclei were determined in conditioned fear-associated brain regions, including the Cg1, PrL, IL, hippocampus (CA1, CA2, CA3, and DG), amygdala, and PC. BDNF mRNA levels were labeled in the mPFC, hippocampus, amygdala, and PC.

2.4. Behavioral Testing. Situational reminders were conducted to reexperience the PTSD trauma event by measuring freezing behavior in rats, which was video recorded for two minutes in the previous environment which was associated with footshock. Freezing behavior comprises an index of fear responses, defined as the absence of all movements except respiration [29].

2.5. Immunohistochemical Staining of BDNF. Based on the previous findings related to the time course of BDNF protein expression [30], the immunohistochemical staining with BDNF was performed 60~90 minutes after the final session of freezing behavior measurement. The rats were euthanized with an overdose of sodium pentobarbital. Then, the rats were perfused with 0.9% sodium chloride followed by 4% paraformaldehyde in 0.1 M phosphate-buffered saline (PBS). After perfusion, the brain tissues were removed and

postfixed in 4% paraformaldehyde for three days. Following this, the brain tissues were stored in 30% sucrose until the brain sank. Later, a brain microdissection procedure was performed. The brain tissue was embedded by using frozen gel (Tissue-Tek O.C.T. compound) before sectioning. The frozen brain was placed in the platform of the microtome, and during the brain microdissection, coronal sections were cut 40 μm thick in a freezing microtome chamber. The temperature in the microtome chamber was maintained at -20°C. The coronal sections of the brain were collected in 0.1 M PBS. Anterior and posterior coordinates were by the brain map of rats [31].

Alternate sections were picked, and free-floating sections were washed once for 10 minutes in 0.1 M PBS and then immersed in 3% hydrogen peroxide (H_20_2) to block endogenous peroxidase and 1% Triton X-100 to enhance membrane permeability. After rinsing in 0.1 M PBS, the brain slices were submerged in normal goat serum with 0.1% Triton (NGST) for one hour and incubated overnight at 4°C with an anti-BDNF antibody (Millipore/AB1513, 1 : 500). The following day, the brain slices were rinsed for 10 minutes in 0.1 M PBS and incubated in a secondary biotinylated rabbit anti-sheep IgG antibody (1 : 500, BA-6000, Vector Laboratories, CA, USA) in 1% NGST at room temperature for one hour. The slices were then rinsed again in 0.1 M PBS for 10 minutes, and the bound secondary antibody was placed in an avidin-biotin solution in 0.1 M PBS (ABC kit, Vector Laboratories, CA, USA) for one hour. After this, the slices were rinsed once again in 0.1 M PBS for 10 minutes and then incubated with a chromogen reaction solution (PBS, pH 7.4, 3% H_2O_2, 25% nickel, and 0.03% 3,3′-diaminobenzidine) for 10 minutes. Finally, all sections were rinsed in a PBS solution and mounted onto gelatin-coated slides. For quantifying BDNF expression, nuclei with positive dark-point immunoreactivity were counted visually at 20x magnification. The counting software ImageJ was applied to count the c-Fos-positive neurons. The counts of the slices for each brain subarea were averaged for each group.

2.6. Real-Time Quantitative PCR of BDNF. Total RNA was extracted using the TRIzol reagent (Invitrogen, Carlsbad, CA, USA) according to the manufacturer's instructions. Total RNA was used for cDNA synthesis with random hexamers. The next step was the reverse transcription PCR amplification of BDNF. The amplification was initiated with a pair of BDNF primers (forward: 5′-AAAACCATAAGGAC GCGGACTT-3′; reverse: 5′-AAAGAGCAGAGGAGGC TCCAA-3′) in a total reaction volume of 20 μl, undergoing a denaturation stage at 95°C for 10 minutes, followed by 28 cycles of denaturation at 95°C for one minute, primer annealing at 55°C for 30 seconds, and extension at 72°C for 45 seconds. Once the cycling steps were complete, the final extension was at 72°C for five minutes. The reactions were repeated three times and were performed in an ABI PRISM 7500 Sequence Detection System (Applied Biosystems, Thermo Fisher Scientific, USA). The mean expression level of the housekeeping gene with a pair of beta-actin primers (forward: 5′CAACTTGATGTATGAAGGCTTTGGT-3′; reverse: 5′-ACTTTTATTGGTCTCAAGTCAGTGTACAG-3′) was used as the internal control to normalize the variability of BDNF expression levels. The relative changes in gene expression were analyzed using the $2^{-\Delta\Delta CT}$ method, as described in a previous study [32].

2.7. Statistical Analysis. A two-way mixed (group vs. session) analysis of variance (ANOVA) was performed for the freezing time. BDNF expression and normalized BDNF mRNA were analyzed using an independent t-test for a specific brain area of the nonfootshock and footshock groups. To examine the relationship between freezing response and the BNDF expressions or freezing response and BDNF mRNA, Pearson correlation tests were conducted. Values of $p < 0.05$ were considered to be statistically significant. The heat map of the neural networks in the determined brain areas was transformed from Pearson correlation coefficient values and illustrated by MATLAB free packages (The MathWorks, Inc., Natick, MA, USA). Note that the higher value of the Pearson correlation coefficient indicated a long-wave color. The lower value of the Pearson correlation coefficient showed a short-wave color. The values of power were analyzed following Pearson correlation tests.

3. Results

3.1. Freezing Behavior Tests during the Situational Reminder. In this study, a single severe footshock was paired with the context of the footshock box. Then, the animals encountered an experimental procedure of situational reminders in the footshock box. In this procedure, animals were given without any footshock once a day for three days to mimic patients with PTSD who have reexperienced a traumatic memory. By testing freezing behavior during situational reminder, a two-way mixed ANOVA (footshock vs. session) indicated that a significant difference occurred in the group ($F_{1,22} = 98.00$, $p < 0.05$; partial eta square = 0.82, power = 1.00). Nonsignificant differences occurred in session ($F_{2,44} = 1.62$, $p > 0.05$; partial eta square = 0.07, power = 0.32) and in the interaction of the group and session ($F_{2,44} = 0.07$, $p > 0.05$; partial eta square = 0.003, power = 0.06). The results highlight that footshock treatments significantly increased freezing time compared to the nonfootshock group for three sessions during situational reminder (Figure 1(b)).

3.2. BDNF Immunohistochemical Staining during Situational Reminder and Fear Behavior in PTSD-Associated Brain Areas. By investigating the involvement of brain areas in the BDNF expression of the nonfootshock and footshock groups, an independent t-test indicated that the footshock group experienced significant increases in BDNF expression in the Cg1 ($t(8) = -6.17$, $p < 0.05$; Figure 2(a)), PrL ($t(8) = -5.07$, $p < 0.05$; Figure 2(b)), and amygdala ($t(8) = -8.17$, $p < 0.05$; Figure 2(h)). In contrast, the BDNF expression of the footshock group in the IL ($t(8) = 3.86$, $p < 0.05$; Figure 2(c)), CA1 ($t(8) = 7.35$, $p < 0.05$; Figure 2(d)), CA2 ($t(8) = 6.14$, $p < 0.05$; Figure 2(e)), CA3 ($t(8) = 6.21$, $p < 0.05$; Figure 2(f)), and DG ($t(8) = 4.80$, $p < 0.05$; Figure 2(g)) showed a significant decrease

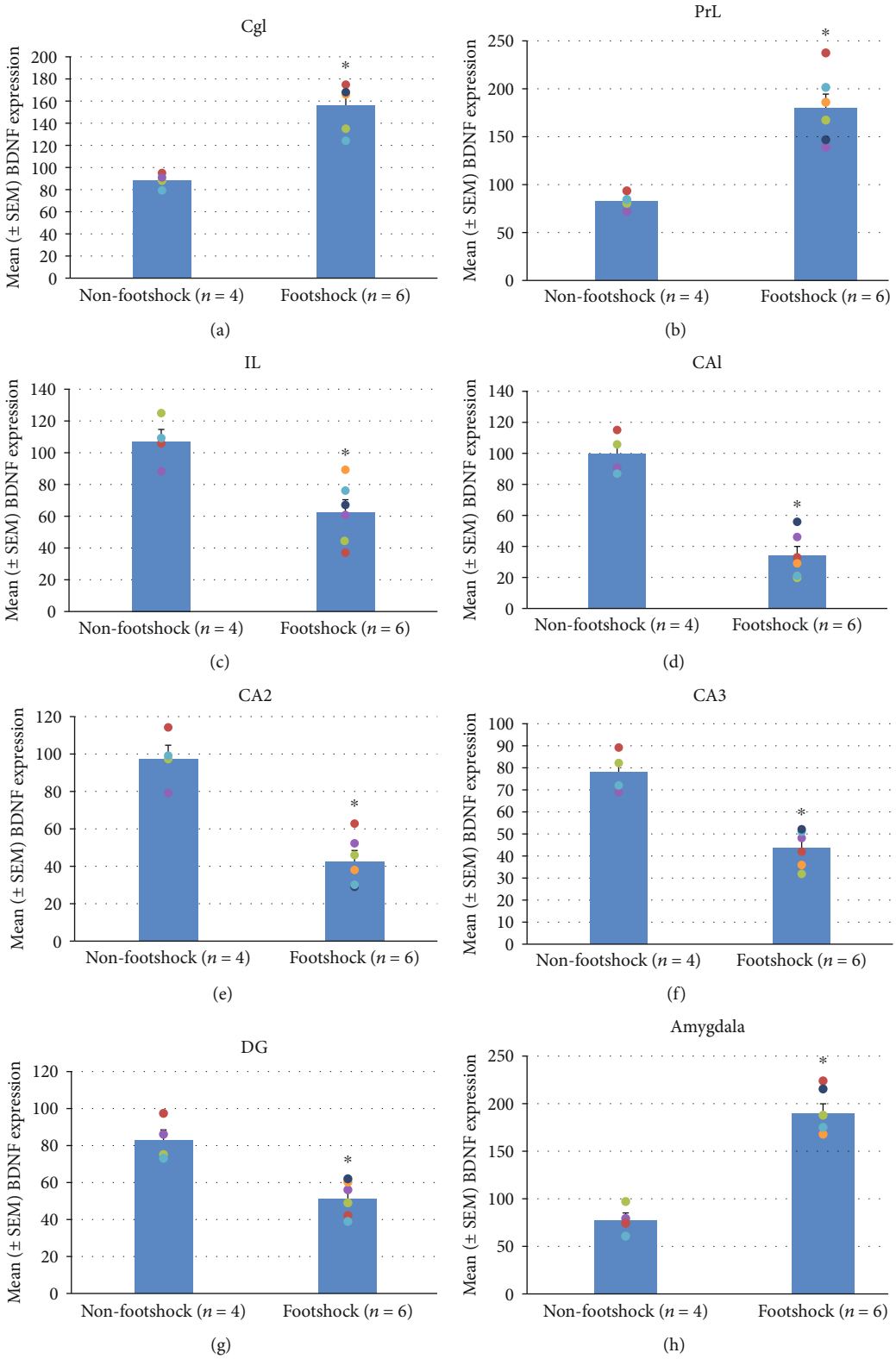

Figure 2: Continued.

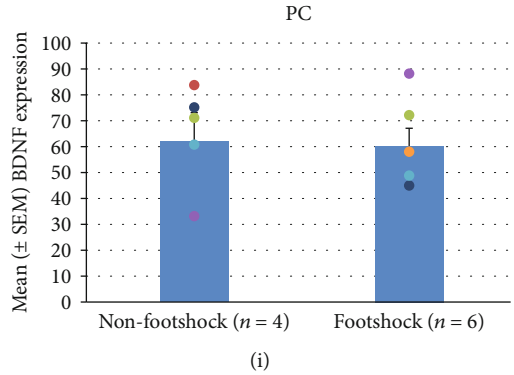

Figure 2: (a–i) Mean (±SEM) BDNF-positive cells per slice in footshock ($n = 4$) and nonfootshock ($n = 6$) groups. The number of BDNF-positive cells was counted in the PTSD-associated regions, including the Cg1; PrL; IL; hippocampal areas CA1, CA2, CA3, and DG; amygdala; and PC. $^{*}p < 0.05$ when comparing the nonfootshock and footshock groups.

compared to that of the nonfootshock group. The BDNF expression of the PC between the nonfootshock and footshock groups had no significant differences ($t(8) = 0.17$, $p > 0.05$; Figure 2(i)). To compare both of these groups, the BDNF expression of the determined brain areas is shown in Figures 3(a)–3(c). These results suggest that the Cg1, PrL, IL, CA1, CA2, CA3, DG, and amygdala were shown to have higher BDNF protein expression in the PTSD during situational reminder.

3.3. Quantification of BDNF mRNA Levels during Situational Reminder and Fear Behavior in PTSD-Associated Brain Areas. The BDNF mRNA levels were further determined by qRT-PCR. An independent t-test indicated that significantly higher BDNF mRNA levels occurred in the mPFC in the footshock group ($t(10) = -2.79$, $p < 0.05$; Figure 4(a)) and amygdala ($t(10) = -2.16$, $p = 0.05$; Figure 4(b)). The hippocampus showed significantly decreased BDNF mRNA levels in the footshock group ($t(10) = 2.54$, $p < 0.05$; Figure 4(c)). A nonsignificant difference occurred in the PC ($t(10) = 0.69$, $p > 0.05$; Figure 4(d)). The mPFC, amygdala, and hippocampus therefore mediate the BDNF mRNA levels.

3.4. Pearson Correlation Tests for Freezing Behavior and BDNF Protein Expressions in the Third Session of Situational Reminder. Rats induced freezing behavior following severe footshock treatment and were then placed in the same footshock box to induce fear behavior for three sessions during situational reminder. To examine the relationship between footshock-induced freezing behavior as a PTSD symptom and BDNF protein expressions in the brain, we assessed the relationship between freezing levels and BDNF protein expressions using Pearson correlation tests. The results indicated that freezing levels were positively associated with BDNF protein levels in the Cg1 ($r = 0.72$, $p < 0.05$), PrL ($r = 0.76$, $p < 0.05$), and amygdala ($r = 0.75$, $p < 0.05$). The associations in the subregions of the hippocampus were negatively correlated, including those in the CA1 ($r = -0.76$, $p < 0.05$), CA2 ($r = -0.75$, $p < 0.05$), and CA3 ($r = -0.83$, $p < 0.05$). However, freezing levels and BDNF protein expressions were not significantly correlated in the IL ($r = -0.61$, $p > 0.05$), DG ($r = -0.60$, $p > 0.05$), or PC ($r = -0.49$, $p > 0.05$; Table 1). Therefore, from the analysis of the relationship between freezing behavior and BDNF protein expressions, a positive correlation occurred in the Cg1, PrL, and amygdala; however, a negative correlation was found in the CA1, CA2, CA3, and amygdala.

3.5. Pearson Correlation Tests for Freezing Behavior and BDNF mRNA Levels in the Third Session of Situational Reminder. We also tested the relationship between freezing behavior and BDNF mRNA levels using Pearson correlation tests. It was found that a positively significant correlation occurred in the mPFC ($r = 0.80$, $p < 0.05$) and amygdala ($r = 0.84$, $p < 0.05$). A negative correlation was noted in the hippocampus ($r = -0.62$, $p < 0.05$). A nonsignificant correlation occurred in the PC ($r = -0.28$, $p > 0.05$; Table 2). Therefore, from the analysis of the relationship between freezing behavior and BDNF mRNA levels, positive correlations were observed in the mPFC and amygdala; however, a negative correlation occurred in the hippocampus.

3.6. Neural Connection Analysis of Regional BDNF Protein Expression. To test the neural connection of BDNF protein expression, we used a Pearson correlation analysis. For the nonfootshock and footshock groups, the values of Pearson correlation tests were shown to be 0.991~0.097 and -0.740~0.006, respectively. Moreover, the power values were 0.940~0.051 for the nonfootshock group and 0.436~0.050 for the footshock group. Thus, Pearson correlation coefficients were transferred to a heat map with colors to examine the relationship among the selected brain areas in BDNF expression. BDNF protein-level associations were analyzed in both nonfootshock (Figure 5(a)) and footshock (Figure 5(b)) groups. The heat map of the nonfootshock group exhibited many yellow and red colors, thus showing a higher correlation than any other comparison of brain areas (Figure 5(a)). However, after the footshock treatments, comparisons of all brain areas appeared to show more blue colors in the heat map, indicating that a footshock-induced traumatic event disrupted the relationship between all brain areas (Figure 5(b)). It was suggested that lower BDNF correlation levels were found in the brain following PTSD, thus representing a negatively regional connection in the third retrieval

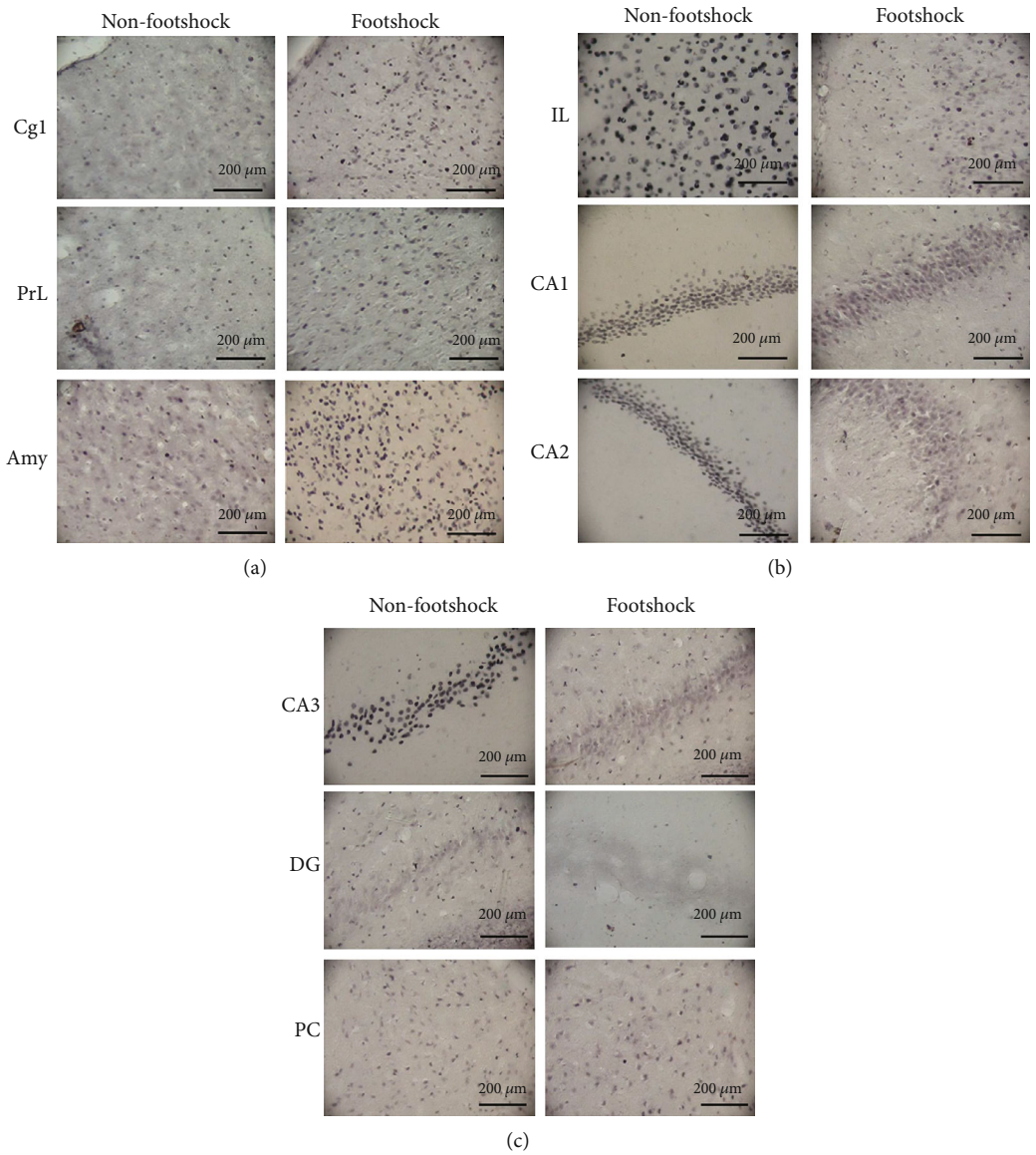

Figure 3: (a–c) Representative photomicrographs of BDNF-positive cells in the region of the Cg1; PrL; IL; hippocampal areas CA1, CA2, CA3, and DG; amygdala; and PC.

session of situational reminder. Furthermore, the neural connections during the third retrieval session of situational reminder for all neural substrates showed that a large amount of positive connectivity and a small amount of negative connectivity in nonfootshock (Figure 5(c)) become a lot of negative connectivity and less positive connectivity in BDNF expression in footshock (Figure 5(d)).

3.7. Neural Connection Analysis of Regional BDNF mRNA Levels. To test the neural connection of BDNF mRNA levels, we used a Pearson correlation analysis. For the nonfootshock and footshock groups, the values of Pearson correlation tests were shown to be 0.783~0.135 and -0.547~0.116, respectively. Moreover, the power values were 0.519~0.057 for the nonfootshock group and 0.203~0.055 for the footshock group. The value of the Pearson correlation coefficient was transferred into the heat map with color to examine the relationship among the mPFC, amygdala, hippocampus, and PC in BDNF mRNA levels for both nonfootshock and footshock groups (Figure 6). During the third retrieval session of situational reminder, the nonfootshock group revealed to have higher correlation values for the mPFC with the hippocampus and PC, the mPFC and hippocampus, and the mPFC and PC (Figure 6(a)); however, the Pearson correlation coefficients decreased for almost all comparisons for all determined brain areas in the footshock group (Figure 6(b)). Therefore, it appears that PTSD in situational reminders interferes with connections between the mPFC, amygdala, hippocampus, and PC in the brain, and it induces lower BDNF mRNA levels in footshock. It indicated that when compared with the nonfootshock and footshock groups, the connections of the neural network for all determined brain areas changed from having increased positive connectivity to decreased positive connectivity and enhanced negative

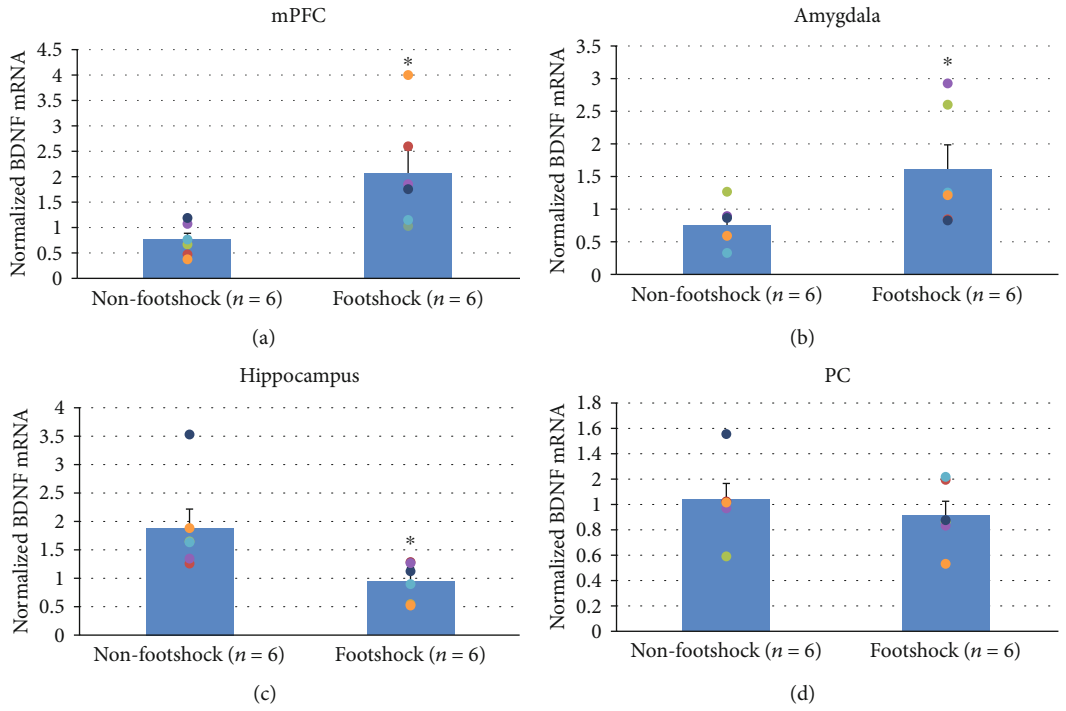

Figure 4: Normalized BDNF mRNA in the mPFC, amygdala, hippocampus, and PC in footshock ($n = 6$) and nonfootshock ($n = 6$) groups. $^*p < 0.05$ when comparing the nonfootshock and footshock groups.

Table 1: Pearson correlation tests conducted to analyze the relationship between freezing behavior and BDNF protein expression levels in selected brain areas ($n = 10$) during the final retrieval session of situational reminders.

	Cg1	PrL	IL	CA1	CA2	CA3	DG	Amygdala	PC
r	0.72	0.76	-0.61	-0.76	-0.75	-0.83	-0.60	0.75	-0.49
p	<0.05*	<0.05*	ns	<0.05*	<0.05*	<0.05*	ns	<0.05*	ns

Table 2: Pearson correlation tests conducted to analyze the relationship between freezing behavior and BDNF mRNA levels in selected brain areas ($n = 12$) during the final retrieval session of situational reminders.

	mPFC	Amygdala	Hippocampus	PC
r	0.80	0.84	-0.62	-0.28
p	<0.05*	<0.05*	<0.05*	ns

connectivity in BDNF mRNA levels, especially in the situational reminder phase (Figures 6(c) and 6(d)).

4. Discussion

The present study results showed that the footshock rats still induced a severe freezing behavior in the third retrieval session of situational reminder and the behavioral data were consistent with the previous evidence [10, 13, 14]. The mPFC (i.e., Cg1 and PrL) and the amygdala appeared to have higher BDNF protein expression. In contrast, part of the mPFC (i.e., IL) and the hippocampus (i.e., CA1, CA2, CA3, and DG) showed lower BDNF protein expression in the third retrieval session of situational reminder. In the BDNF mRNA levels, the results were very similar to those in BDNF protein expression. The levels of BDNF mRNA were higher in the mPFC and amygdala but lower in the hippocampus for the footshock group in the third retrieval session of situational reminder.

The neural connection analysis suggested that some connections between the mPFC, amygdala, and hippocampus changed the connection property from positive to negative. These connections included the PrL projections to the subareas of the mPFC (i.e., PrL-Cg1 and PrL-IL) and the subareas of the hippocampus (i.e., PrL-CA2, PrL-DG, and PrL-CA3), the amygdala projections (i.e., IL-amygdala, amygdala-CA2, and amygdala-PC), and the projections of the IL-PC, PC-CA3, and CA1-CA2. Therefore, the situational reminder of traumatic memory weakened the neural network of the mPFC, amygdala, and hippocampus that exhibited negative connections.

4.1. The mPFC and PTSD. A growing body of evidence has shown that the subregions of the mPFC (such as the PrL, IL, and Cg1) play separate roles in fear conditioning and PTSD symptoms [33]. Previous studies have reported some controversial evidence in this regard [20, 34–37]. For example, a study of fear conditioning discrimination showed that

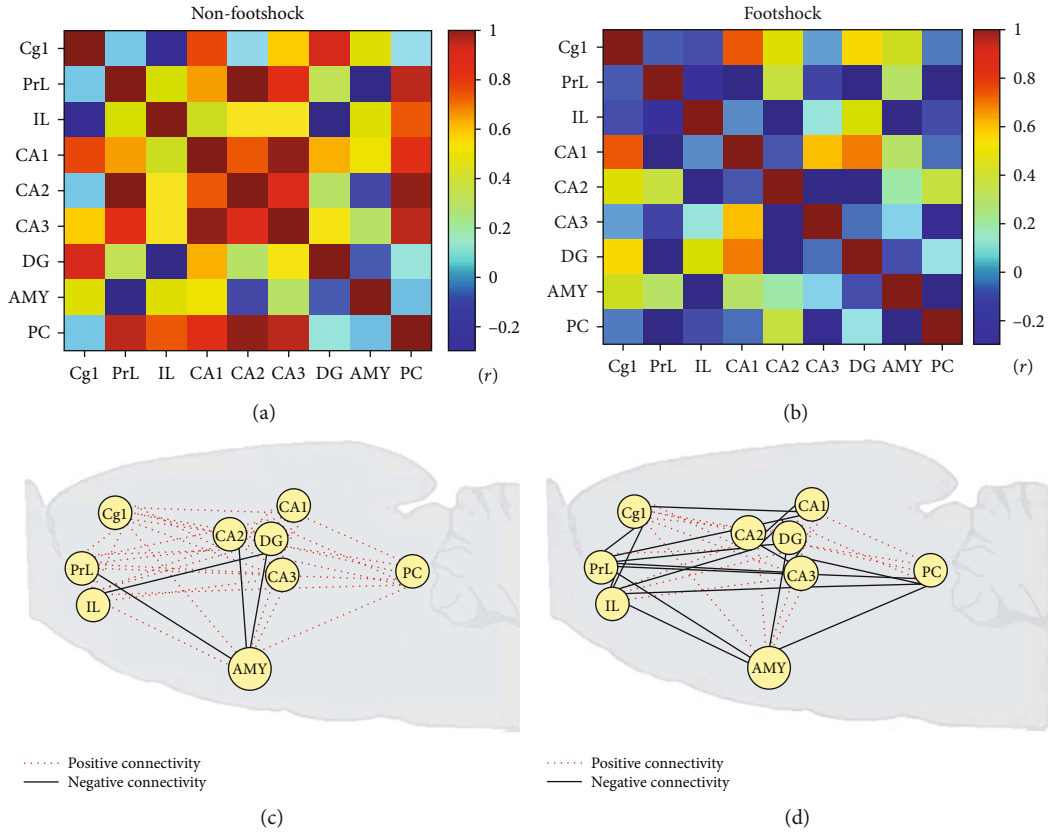

Figure 5: Pearson's correlation coefficient of BDNF protein expression in (a) nonfootshock ($n = 4$) and (b) footshock ($n = 6$) and the connectivity in (c) nonfootshock ($n = 4$) and (d) footshock ($n = 6$) between regions, including the Cg1; PrL; IL; hippocampal areas CA1, CA2, CA3, and DG; amygdala; and PC. Note that the red dotted line represents positive connectivity. The black line represents negative connectivity.

the subdivisions of the mPFC activated different responses to fear discrimination learning, and the PrL and IL seemingly contributed counterbalanced roles in fear discrimination learning [34]. A previous study has reported that animals with a single prolonged-stress PTSD procedure revealed to have significantly lower BDNF expression in the hippocampus and mPFC and decreased phosphorylated TrkB receptors in the ventral mPFC. However, microinfusions of BDNF in the IL (but not in the PrL or hippocampus) reduced the impairment of fear extinction but not extinction training. BDNF microinjections in the IL significantly activated TrkB phosphorylation in the IL, indicating that the signaling of BDNF to TrkB receptors in the IL (but not the PrL and hippocampus) regulates fear extinction memory [35]. Using the resting-state method of functional magnetic resonance imaging, a study examined brain mechanisms of PTSD and found that PTSD patients appeared to have a higher level of functional connectivity in the left posterior hippocampus and bilateral posterior cingulate cortex compared to the trauma-exposed control group, indicating that the cingulate cortex of the mPFC may be involved in PTSD fear behavior [36].

The present study focused on the situational reminder of traumatic memory, and the Cg1 and PrL of the mPFC showed higher BDNF expression; however, the IL exhibited lower BDNF expression. The results of BNDF labeling were seemingly consistent with the viewpoint of the PrL, IL, and Cg1's different levels of involvement in fear memory. During situational reminder, the Cg1 and PrL might enhance synaptic plasticity, but the IL reduces synaptic plasticity for regulating situational reminder. In other words, in the retrieval fear memory, the Cg1 and PrL neurons may be involved in the BDNF synaptic plasticity to ensure a connection with the relevant neural substrates. However, the BDNF synaptic plasticity of the IL neurons was likely weakened to connect with adjacent neurons.

4.2. The Amygdala and PTSD. Previous studies suggested that the amygdala regulated negative emotional responses and was involved in fear conditioning [38]. Moreover, the amygdala was shown to encode aversive and negative stimuli, and then, this negative information was associated with the contextual stimulus [39]. PTSD symptoms are present in fear and negative emotional responses, and the amygdala plays an essential role in PTSD [40]. For example, PTSD research on animals using the predator scent model showed that excitations of the BLA through high-frequency stimulations could interfere with predator scent-related anxiety and avoidance responses [41]. The inescapable footshock model of PTSD showed that animals with footshock treatments exhibited a higher expression of norepinephrine in the amygdala. In contrast, bilateral microinfusions of the beta-adrenergic receptor antagonist propranolol revealed a lower locomotive activity,

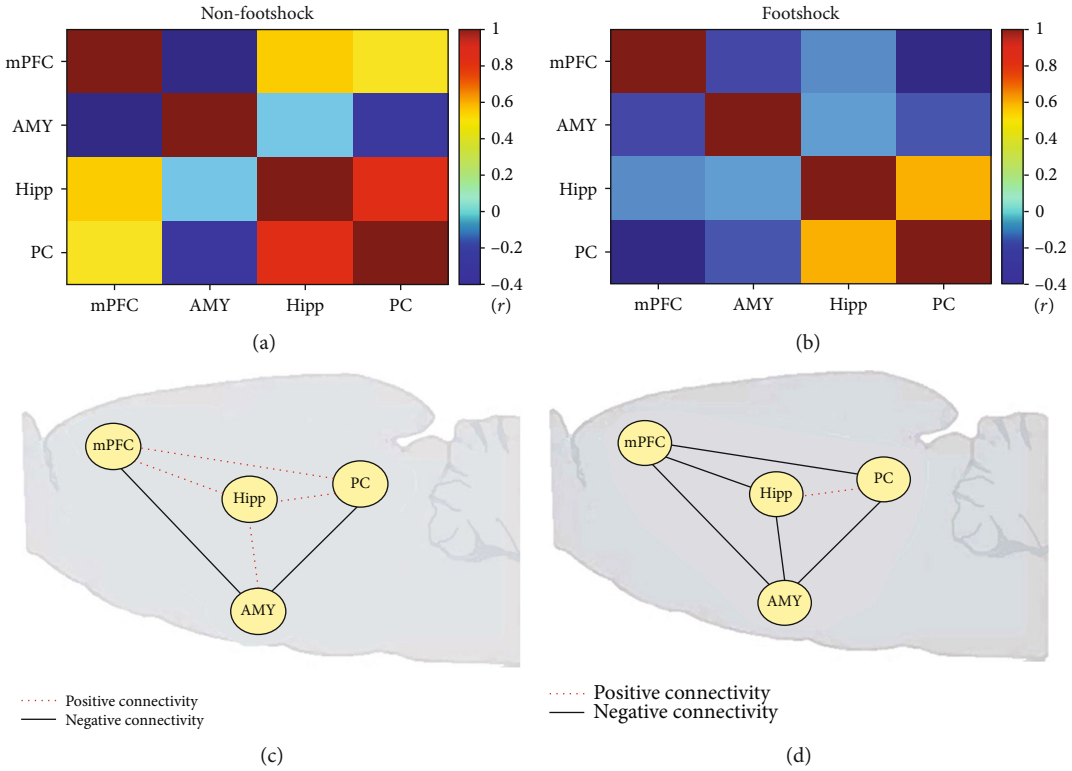

Figure 6: Pearson's correlation coefficient of BDNF mRNA levels in (a) nonfootshock ($n = 6$) and (b) footshock ($n = 6$) and the connectivity in (c) nonfootshock ($n = 6$) and (d) footshock ($n = 6$) between regions, including the Cg1; PrL; IL; hippocampal areas CA1, CA2, CA3, and DG; amygdala; and PC. Note that the red dotted line represents positive connectivity. The black line represents negative connectivity.

indicating that the activity of the amygdala's adrenergic neurons mediated PTSD symptoms [42]. A manganese-enhanced magnetic resonance imaging study indicated that PTSD animals induced higher signals in the BLA and striatum and lower activity in the IL in a single prolonged-stress PTSD model. This indicated that the prefrontal cortex inhibited the neuronal activity of the amygdala and striatum under the single prolonged-stress procedure [43]. Furthermore, a recent single prolonged-stress procedure in a PTSD animal model found that anxiety behavior and fear memory occurred one day after the procedure and were associated with decreased activated glutamate neurons and increased activated GABA neurons in the BLA. Ten days after the procedure, the animals exhibited enhanced anxiety and impaired fear memory associated with increased glutamate and GABA transmissions in the BLA, indicating that the different PTSD stages showed a distinct pattern of glutamate and GABA neuron activities in the amygdala [44].

The present result showed that BDNF protein expression was higher in the amygdala during situational reminders. This finding supports the view that the amygdala regulates fear-related PTSD symptoms; moreover, the BDNF involvement of the amygdala in the present result has extended the previous evidence in the studies of behavioral pharmacology and magnetic resonance imaging.

4.3. The Hippocampus and PTSD. Accumulated evidence has shown that the hippocampus governs context-related conditioned learning [45–47], in which the contextual environment (i.e., the CS) is conditioned by a physiological or survival stimulus (i.e., the US) [48]. Because the US is a fear-related aversive and negative effect, the contextual CS has the aversive fear effect, following the aversive conditioning of the CS and US; this is termed fear conditioning [39]. Accordingly, the hippocampus does not mediate the reward or aversive valence itself; instead, the hippocampus only regulates a single and whole ensemble of contextual components [39].

On the other hand, the subareas of the hippocampus (i.e., the CA1, CA2, CA3, and DG) may play different roles in fear conditioning and fear extinction memory [23, 26, 49]. For example, under a long-term stress treatment, the CA1 of the hippocampus exhibited decreased BDNF mRNA expression and increased *TrkB* mRNA expression in the predator scent-induced stress paradigm [26], indicating that the CA1 was involved in the stress event. BDNF protein expression of the DG was lower in cue fear conditioning, and the DG plays an inhibitory role in cue fear conditioning [23]. Another study used the contextual fear conditioning paradigm and showed that lesions of the CA3 enhanced fear behavior in the acquisition stage of fear conditioning. Moreover, lesions of the CA1 and DG impaired freezing behavior in the retrieval stage of fear memory, indicating that the CA3 mediated the acquisition of fear memory and the CA1 and DG regulated the retrieval of fear memory [49].

In the present PTSD study, the CA1, CA2, CA3, and DG of the hippocampus all exhibited significantly lower BDNF expression in the third retrieval session of situational

reminder. Therefore, our data are not consistent with this prior evidence. This discrepancy in evidence may be due to the different paradigms and stages of fear conditioning in PTSD. This issue should be investigated in further studies.

4.4. Neural Connections among the mPFC, Amygdala, and Hippocampus for PTSD during the Situational Reminder. Previous literature has reported that the mPFC, amygdala, and hippocampus were connected for playing different roles in PTSD [28, 50]. For example, a neuroimaging review suggested that during the sympathetic stage of PTSD, the mPFC and hippocampus both revealed hypoactivity associated with the hyperactivity of the amygdala [28]. This viewpoint was supported by another study, which indicated that exposing patients to severe stress produced deficits in the mPFC inhibition to suppress the hyperactivity of the amygdala [50]. For example, in severe stress, the mPFC loses its inhibitory function to the amygdala, and the deficit of the hippocampus disrupts the function of declarative memory but facilitates the nondeclarative memory of fear conditioning [50]. Another study found the mPFC and the hippocampus to be negatively connected to the amygdala, whereas the mPFC and hippocampus were positively connected [28]. In this neural relationship of the mPFC, hippocampus, and amygdala, the neural activity of the mPFC and hippocampus appeared lower, but a higher neural activity of the amygdala occurred when PTSD patients experienced a severe stress event, indicating the contribution of the neural connection in regulating PTSD symptoms [28]. However, the present data were not completely consistent with the previous viewpoint in neuroimaging research—namely, the fact that the neurons of the mPFC and hippocampus were shown to have a lower activity and the amygdala neurons exhibited a higher activity when patients experienced PTSD symptoms [28]. Our data showed that there was higher BDNF expression in the Cg1, PrL, and amygdala; however, the IL, CA1, CA2, CA3, and DG exhibited lower expression in BDNF protein tests. In our study, the PrL and IL played an opposite role in fear behavior during situational reminders, supporting the findings [33]. The data discrepancy between previous studies and ours may be due to inconsistent results from the different testing stages of PTSD and fear conditioning. In our study, we manipulated the retrieval of fear memory during situational reminder; however, the previous study conducted a fear conditioning and acquisition phase or fear extinction phase. These different testing phases may have led to the discrepancy in the results. Therefore, the acquisition, retrieval, and extinction of fear memory should be considered expressing the different patterns of neural network activity among the prefrontal cortex, amygdala, and hippocampus. Whether or not the different stages of PTSD appear in the varying neural connection patterns should be scrutinized in future studies.

4.5. Issue and Limitations. Some limitations should be a matter of concern. First, the issue of whether the immunohistochemical staining method was a suitable way to label BDNF proteins should be discussed. In the present study, it used immunohistochemical staining with the BDNF protein after behavioral testing. However, this method has a shortage such that the antibody of BDNF did not stain the right cellular and subcellular elements. The BDNF protein was located in the Trk receptor and surrounding postsynaptic neuronal membranes but not inside neuronal membranes [17]. BDNF is taken up by the presynaptic neurons via axonal retrograde transport into the cell body of this presynaptic neuron resulting in neuronal survival [51]. Therefore, the present data of BDNF protein expression with immunohistochemical staining have a limitation for BDNF labeling in a correct cellular element. In contrast, the western blot and ELISA approach with BDNF should be considered to prevent the deficits of the immunohistochemical staining method in further studies. Second, the small sample size for numerous Pearson correlation tests in BDNF protein and BDNF mRNA measurements should be a matter of concern because fewer data might lead to lower power values. In the neuroscience field, the small sample size ($n = 4$-6) is often used to compare the different effects between control and experimental groups with the t-test or F-test. However, the Pearson correlation test with the small sample size should be further considered for its effect size and power value.

To test BDNF protein and BDNF mRNA expression for comparing the nonfootshock and footshock groups, the PrL and IL, respectively, showed increases and decreases in the BDNF protein expression for the footshock group; however, the BDNF mRNA expression in the mPFC was lower in the footshock group. These results showed a conflict between the BDNF mRNA and BDNF protein expressions. This discrepancy in data might be due to the fact that the assessment of BDNF mRNA focused on the whole mPFC; however, the measurement of BDNF protein expression narrows down the subareas of the mPFC (i.e., PrL and IL). Thus, it shows the different functions between the PrL and IL. Furthermore, why did the PrL and IL appear to have an opposite expression in BDNF protein expression? A possible explanation is that the data of BDNF protein was consistent with the viewpoint that the PrL plays a role to enhance fear behavior, but the IL was involved in the reduction of fear behavior [52]. The present issue that whether the subareas of the mPFC contribute a different function to the fear conditioning and PTSD symptoms should be scrutinized in further studies.

4.6. Conclusion. In the retrieval of situational reminders, the subareas of the mPFC such as Cg1 and PrL and the amygdala showed a higher BDNF protein expression. However, the IL and the subareas of the hippocampus including CA1, CA2, CA3, and DG revealed a lower BDNF protein expression. The data of the BDNF mRNA levels were similar to those of BDNF protein expression: the levels of BDNF mRNA were higher in the mPFC and amygdala but lower in the hippocampus for the footshock group. In the neural connection analysis, we found that some connections between the mPFC, amygdala, and hippocampus changed the connection property from positive to negative. These connections included the PrL projections to the subareas of the mPFC (i.e., PrL-Cg1 and PrL–IL) and the subareas of the hippocampus (i.e., PrL-CA2, PrL-DG, and PrL-CA3), the amygdala projections (i.e., IL-amygdala, amygdala-CA2, and amygdala-PC), and

the projections of the IL-PC, PC-CA3, and CA1-CA2. The reexperience of PTSD traumatic memory is seemingly to weaken the neural network of the mPFC, amygdala, and hippocampus that exhibited negative connections.

Data Availability

The raw data can be accessed through the following link: https://www.dropbox.com/sh/ao9rnafpinp6qxb/AADqYPNwXL1rXWv5ehUKdfvha?dl=0.

Conflicts of Interest

The authors declare no conflict of interest.

Acknowledgments

This research was supported by funding from the Ministry of Science and Technology of the Republic of China (Taiwan) (MOST 107-2410-H-431-004 and MOST 108-2410-H-431-009 to Dr. A.C.W. Huang and MOST 106-2321-B-001-043 and MOST 108-2320-B-001-024 to Dr. B.C. Shyu). We also acknowledge the support from the Institute of Biomedical Sciences, Academia Sinica, Taiwan.

References

[1] N. J. Bush, "Post-traumatic stress disorder related to cancer: hope, healing, and recovery," *Oncology Nursing Forum*, vol. 37, no. 5, pp. E331–E343, 2010.

[2] M. Kangas, J. L. Henry, and R. A. Bryant, "Predictors of posttraumatic stress disorder following cancer," *Health Psychology*, vol. 24, no. 6, pp. 579–585, 2005.

[3] G. P. Owens, D. G. Baker, J. Kasckow, J. A. Ciesla, and S. Mohamed, "Review of assessment and treatment of PTSD among elderly American armed forces veterans," *International Journal of Geriatric Psychiatry*, vol. 20, no. 12, pp. 1118–1130, 2005.

[4] C. H. Wu, S. H. Chen, L. J. Weng, and Y. C. Wu, "Social relations and PTSD symptoms: a prospective study on earthquake-impacted adolescents in Taiwan," *Journal of Traumatic Stress*, vol. 22, no. 5, pp. 451–459, 2009.

[5] American Psychiatric Association, *Diagnostic and Statistical Manual of Mental Disorders: DSM-5*, American Psychiatric Association, Washington, DC, 5th edition, 2013.

[6] H. Glover, "The treatment of posttraumatic stress disorder (PTSD)," *Psychosomatic Medicine*, vol. 59, no. 1, pp. 70-71, 1997.

[7] R. Yehuda, A. C. McFarlane, and A. Y. Shalev, "Predicting the development of posttraumatic stress disorder from the acute response to a traumatic event," *Biological Psychiatry*, vol. 44, no. 12, pp. 1305–1313, 1998.

[8] A. L. Mahan and K. J. Ressler, "Fear conditioning, synaptic plasticity and the amygdala: implications for posttraumatic stress disorder," *Trends in Neurosciences*, vol. 35, no. 1, pp. 24–35, 2012.

[9] A. M. Rasmusson and D. S. Charney, "Animal models of relevance to PTSD," *Annals of the New York Academy of Sciences*, vol. 821, 1 Psychobiology, pp. 332–351, 1997.

[10] J. C. Kung, T. C. Chen, B. C. Shyu, S. Hsiao, and A. Huang, "Anxiety- and depressive-like responses and c-fos activity in preproenkephalin klockout mice: oversensitivity hypothesis of enkephalin deficit-induced posttraumatic stress disorder," *Journal of Biomedical Science*, vol. 17, no. 1, p. 29, 2010.

[11] R. S. Pynoos, R. F. Ritzmann, A. M. Steinberg, A. Goenjian, and I. Prisecaru, "A behavioral animal model of posttraumatic stress disorder featuring repeated exposure to situational reminders," *Biological Psychiatry*, vol. 39, no. 2, pp. 129–134, 1996.

[12] A. Segev, N. Korem, T. Mizrachi Zer-Aviv et al., "Role of endocannabinoids in the hippocampus and amygdala in emotional memory and plasticity," *Neuropsychopharmacology*, vol. 43, no. 10, pp. 2017–2027, 2018.

[13] M. Tanaka, H. Li, X. Zhang et al., "Region- and time-dependent gene regulation in the amygdala and anterior cingulate cortex of a PTSD-like mouse model," *Molecular Brain*, vol. 12, no. 1, p. 25, 2019.

[14] L. M. Zhang, W. W. Zhou, Y. J. Ji et al., "Anxiolytic effects of ketamine in animal models of posttraumatic stress disorder," *Psychopharmacology*, vol. 232, no. 4, pp. 663–672, 2015.

[15] S. C. Danzer, K. R. C. Crooks, D. C. Lo, and J. O. McNamara, "Increased expression of brain-derived neurotrophic factor induces formation of basal dendrites and axonal branching in dentate granule cells in hippocampal explant cultures," *The Journal of Neuroscience*, vol. 22, no. 22, pp. 9754–9763, 2002.

[16] A. E. Autry and L. M. Monteggia, "Brain-derived neurotrophic factor and neuropsychiatric disorders," *Pharmacological Reviews*, vol. 64, no. 2, pp. 238–258, 2012.

[17] M. M. Poo, "Neurotrophins as synaptic modulators," *Nature Reviews Neuroscience*, vol. 2, no. 1, pp. 24–32, 2001.

[18] K. Mogi, Y. Ishida, M. Nagasawa, and T. Kikusui, "Early weaning impairs fear extinction and decreases brain-derived neurotrophic factor expression in the prefrontal cortex of adult male C57BL/6 mice," *Developmental Psychobiology*, vol. 58, no. 8, pp. 1034–1042, 2016.

[19] L. Hou, Y. Qi, H. Sun et al., "Applying ketamine to alleviate the PTSD-like effects by regulating the HCN1-related BDNF," *Progress in Neuro-Psychopharmacology & Biological Psychiatry*, vol. 86, pp. 313–321, 2018.

[20] O. Soler-Cedeno, O. Torres-Rodriguez, F. Bernard, L. Maldonado, A. Hernandez, and J. T. Porter, "Plasticity of NMDA receptors at ventral hippocampal synapses in the infralimbic cortex regulates cued fear," *eNeuro.*, vol. 6, no. 2, pp. ENEURO.0354–ENEU18.2019, 2019.

[21] M. R. Bennett and J. Lagopoulos, "Stress and trauma: BDNF control of dendritic-spine formation and regression," *Progress in Neurobiology*, vol. 112, pp. 80–99, 2014.

[22] H. Cohen, E. Vainer, K. Zeev, J. Zohar, and A. A. Mathe, "Neuropeptide S in the basolateral amygdala mediates an adaptive behavioral stress response in a rat model of posttraumatic stress disorder by increasing the expression of BDNF and the neuropeptide YY1 receptor," *European Neuropsychopharmacology*, vol. 28, no. 1, pp. 159–170, 2018.

[23] A. M. Rasmusson, L. Shi, and R. Duman, "Downregulation of BDNF mRNA in the hippocampal dentate gyrus after re-exposure to cues previously associated with footshock," *Neuropsychopharmacology*, vol. 27, no. 2, pp. 133–142, 2002.

[24] L. Ni, Y. Xu, S. Dong et al., "The potential role of the HCN1 ion channel and BDNF-mTOR signaling pathways and synaptic transmission in the alleviation of PTSD," *Translational Psychiatry*, vol. 10, no. 1, p. 101, 2020.

[25] R. Sharma, P. Sahota, and M. M. Thakkar, "Short-term sleep deprivation immediately after contextual conditioning inhibits BDNF signaling and disrupts memory consolidation in predator odor trauma mice model of PTSD," *Brain Research*, vol. 1750, article 147155, 2021.

[26] N. Kozlovsky, M. A. Matar, Z. Kaplan, M. Kotler, J. Zohar, and H. Cohen, "Long-term down-regulation of BDNF mRNA in rat hippocampal CA1 subregion correlates with PTSD-like behavioural stress response," *The International Journal of Neuropsychopharmacology*, vol. 10, no. 6, pp. 741–758, 2007.

[27] L. Saur, L. T. Neves, S. Greggio et al., "Ketamine promotes increased freezing behavior in rats with experimental PTSD without changing brain glucose metabolism or BDNF," *Neuroscience Letters*, vol. 658, pp. 6–11, 2017.

[28] L. M. Shin, S. L. Rauch, and R. K. Pitman, "Amygdala, medial prefrontal cortex, and hippocampal function in PTSD," *Annals of the New York Academy of Sciences*, vol. 1071, no. 1, pp. 67–79, 2006.

[29] S. L. Young and M. S. Fanselow, "Associative regulation of Pavlovian fear conditioning: unconditional stimulus intensity, incentive shifts, and latent inhibition," *Journal of Experimental Psychology. Animal Behavior Processes*, vol. 18, no. 4, pp. 400–413, 1992.

[30] S. S. Shi, S. H. Shao, B. P. Yuan, F. Pan, and Z. L. Li, "Acute stress and chronic stress change brain-derived neurotrophic factor (BDNF) and tyrosine kinase-coupled receptor (TrkB) expression in both young and aged rat hippocampus," *Yonsei Medical Journal*, vol. 51, no. 5, pp. 661–671, 2010.

[31] G. Paxinos and C. Watson, *The Rat Brain in Stereotaxic Coordinates*, Academic Press, Burlington, MA, 6th edition, 2007.

[32] K. J. Livak and T. D. Schmittgen, "Analysis of relative gene expression data using real-time quantitative PCR and the $2^{-\Delta\Delta CT}$ method," *Methods*, vol. 25, no. 4, pp. 402–408, 2001.

[33] T. F. Giustino and S. Maren, "The role of the medial prefrontal cortex in the conditioning and extinction of fear," *Frontiers in Behavioral Neuroscience*, vol. 9, p. 298, 2015.

[34] A. Corches, A. Hiroto, T. W. Bailey et al., "Differential fear conditioning generates prefrontal neural ensembles of safety signals," *Behavioural Brain Research*, vol. 360, pp. 169–184, 2019.

[35] T. Kataoka, M. Fuchikami, S. Nojima et al., "Combined brain-derived neurotrophic factor with extinction training alleviate impaired fear extinction in an animal model of post-traumatic stress disorder," *Genes, Brain and Behavior*, vol. 18, no. 7, article e12520, 2019.

[36] B. L. Malivoire, T. A. Girard, R. Patel, and C. M. Monson, "Functional connectivity of hippocampal subregions in PTSD: relations with symptoms," *BMC Psychiatry*, vol. 18, no. 1, p. 129, 2018.

[37] R. Marek and P. Sah, "Neural circuits mediating fear learning and extinction," *Advances in Neurobiology*, vol. 21, pp. 35–48, 2018.

[38] J. E. LeDoux, "Emotional memory systems in the brain," *Behavioural Brain Research*, vol. 58, no. 1-2, pp. 69–79, 1993.

[39] N. Chaaya, A. R. Battle, and L. R. Johnson, "An update on contextual fear memory mechanisms: transition between amygdala and hippocampus," *Neuroscience and Biobehavioral Reviews*, vol. 92, pp. 43–54, 2018.

[40] I. Liberzon and C. S. Sripada, "The functional neuroanatomy of PTSD: a critical review," *Progress in Brain Research*, vol. 167, pp. 151–169, 2008.

[41] B. A. Dengler, S. A. Hawksworth, L. Berardo, I. McDougall, and A. M. Papanastassiou, "Bilateral amygdala stimulation reduces avoidance behavior in a predator scent posttraumatic stress disorder model," *Neurosurgical Focus*, vol. 45, no. 2, article E16, 2018.

[42] G. Ronzoni, A. del Arco, F. Mora, and G. Segovia, "Enhanced noradrenergic activity in the amygdala contributes to hyperarousal in an animal model of PTSD," *Psychoneuroendocrinology*, vol. 70, pp. 1–9, 2016.

[43] V. M. Piggott, K. E. Bosse, M. J. Lisieski et al., "Single-prolonged stress impairs prefrontal cortex control of amygdala and striatum in rats," *Frontiers in Behavioral Neuroscience*, vol. 13, p. 18, 2019.

[44] Q. Fang, Z. Li, G. D. Huang et al., "Traumatic stress produces distinct activations of GABAergic and glutamatergic neurons in amygdala," *Frontiers in Neuroscience*, vol. 12, p. 387, 2018.

[45] T. Bast, W. N. Zhang, and J. Feldon, "Dorsal hippocampus and classical fear conditioning to tone and context in rats: effects of local NMDA-receptor blockade and stimulation," *Hippocampus*, vol. 13, no. 6, pp. 657–675, 2003.

[46] R. J. McDonald and N. M. White, "A triple dissociation of memory systems: hippocampus, amygdala, and dorsal striatum," *Behavioral Neuroscience*, vol. 107, no. 1, pp. 3–22, 1993.

[47] M. A. Richmond, B. K. Yee, B. Pouzet et al., "Dissociating context and space within the hippocampus: effects of complete, dorsal, and ventral excitotoxic hippocampal lesions on conditioned freezing and spatial learning," *Behavioral Neuroscience*, vol. 113, no. 6, pp. 1189–1203, 1999.

[48] I. P. Pavlov, *Conditioned reflexes*, I. P. Pavlov, Ed., Oxford University Press, Oxford, UK, 1927.

[49] I. Lee and R. P. Kesner, "Differential contributions of dorsal hippocampal subregions to memory acquisition and retrieval in contextual fear-conditioning," *Hippocampus*, vol. 14, no. 3, pp. 301–310, 2004.

[50] B. M. Elzinga and J. D. Bremner, "Are the neural substrates of memory the final common pathway in posttraumatic stress disorder (PTSD)?," *Journal of Affective Disorders*, vol. 70, no. 1, pp. 1–17, 2002.

[51] P. S. DiStefano, B. Friedman, C. Radziejewski et al., "The neurotrophins BDNF, NT-3, and NGF display distinct patterns of retrograde axonal transport in peripheral and central neurons," *Neuron*, vol. 8, no. 5, pp. 983–993, 1992.

[52] J. Peters, P. W. Kalivas, and G. J. Quirk, "Extinction circuits for fear and addiction overlap in prefrontal cortex," *Learning & Memory*, vol. 16, no. 5, pp. 279–288, 2009.

Hindawi
Behavioural Neurology
Volume 2021, Article ID 6639255, 6 pages
https://doi.org/10.1155/2021/6639255

Research Article

Does the Personality of Patients with Parkinson's Disease Affect the Decision to Perform Deep Brain Stimulation Surgery? A Cross-Sectional Study in a Chinese Cohort

Wei Lin,[1] **Dan Wang**,[1] **Likun Yang**,[1] **Jie Zhu**,[1] **Jingjie Ge**,[2] **Chuantao Zuo**,[2] **and Yuhai Wang**[1]

[1]*Department of Neurosurgery, Joint Logistics Support Unit No. 904 Hospital, School of Medicine, Anhui Medical University, Wuxi, China*
[2]*PET Center, Huashan Hospital, Fudan University, Shanghai, China*

Correspondence should be addressed to Yuhai Wang; wangyuhai67@126.com

Received 11 November 2020; Revised 14 December 2020; Accepted 30 December 2020; Published 27 January 2021

Academic Editor: Muh-Shi Lin

We investigated whether the personality of patients with Parkinson's disease (PD) before subthalamic brain stimulation differed from patients receiving drug treatments and whether the personality of patients affected surgical decisions. We recruited 38 patients with advanced PD scheduled for deep brain stimulation (DBS), 40 patients with PD receiving the very best medical treatment, and 51 healthy control subjects. All participants were evaluated by the Minnesota multiphasic personality inventory-1 (MMPI-1). PD patients who were candidates for DBS did not exhibit any significant differences in personality when compared with PD patients who were treated with drugs. Compared with healthy controls, patients with PD had remarkably higher MMPI-1 scores for spiritual quality, neuroticism, and introversion, but significantly lower scores for socialization. In addition, patients with PD were more submissive, more dependent on others, and less active in social activities. Our data indicated that the main deciding factor relating to whether to undergo DBS was the disease itself and not the pathological personality. However, neurotic and psychotic symptoms accompanying PD may influence the effect of DBS. We found that greater benefit is obtained by surgical or medical interventions if abnormal neurotic characteristics are considered early in the course of PD.

1. Introduction

Parkinson's disease (PD) is the second most common degenerative disorder and is characterized by both motor and nonmotor symptoms. PD also has an extensive negative effect on the mental health of patients and presents with a wide range of psychiatric disorders involving depressive symptoms and general anxiety disorders. Rigidity, introversion, and cautiousness have all been proposed as typical personality characteristics of patients with PD [1].

Previous cross-sectional studies have compared the personalities of patients with PD to those of healthy subjects (HS) or patients with other neurological diseases such as Alzheimer's disease and suggested that PD patients are more introverted, apprehensive, tense, driven, and cautious. These data suggested the existence of "Parkinson's disease-specific personality" [2, 3]. Personality traits are known to affect perceptions of the overall impact of this disease on function, as well as general well-being (Lahey, 2009). Some studies of PD reported that there was no correlation that links personality traits to clinical features, such as disease duration and Hoehn and Yahr (H&Y) stage. However, other studies have presented contradictory findings [4–6].

Previous studies have suggested that certain personality qualities are typical of PD and may be linked to neurotransmitter alterations caused by disease progression or

treatments. It is speculated that these personality traits are early manifestations of neurochemical changes during PD [7, 8].

The Minnesota multiphasic personality inventory (MMPI) (Hathaway 1940) is the most widely studied personality test and is commonly used to examine personality traits, as well as psychopathology. However, only specially trained psychologists can administer this personality test. Some previous studies have used the MMPI-1 to investigate personality characteristics in PD patients [9].

Since its introduction in the early 1990s, deep brain stimulation (DBS) is widely regarded as the second milestone in the treatment of PD after dopamine replacement therapy. However, the postoperative effects of DBS are known to depend on a variety of different factors, including disease-specific pathopsychological symptoms [10, 11].

In this study, we investigated the personality of PD patients at our hospital prior to DBS surgery (PD-DBS) or the best form of medical treatment (PD-MED). This study sought to determine if there were personality differences between these two groups of PD patients and the personality characteristics of healthy subjects at our center.

2. Materials and Methods

2.1. Subjects. PD patients were recruited into the study a week before DSB surgery (PD-DBS; 38 patients) or treatment with drugs (PD-MED; 40 patients). Fifty-one healthy participants were also recruited as healthy controls (HC). We recorded a range of demographic data, including age, education level, gender, medical history, and levodopa and dopamine agonist usage. Further neuropsychological examinations were performed on every subject.

Patients were included if they had received a clinical diagnosis of idiopathic PD based on the British Parkinson's Disease Society Brain Bank Criteria for at least 5 years [12]. Patients were excluded if they had other known neurodegenerative and/or psychiatric disorders.

2.2. Personality Assessment. All PD subjects were asked to take anti-Parkinsonian medication prior to evaluation.

2.2.1. MMPI Assessment. Each patient was given a psychometric assessment using the Chinese version of the MMPI [13], which involves 566 statements that are answered as "true" or "false." The results were scored in a standard profile consisting of 3 "validity scales" and 10 "personality scales." The validity scales involved lie (L), fake (F), K correction, and defensive responses (K). Personality scales involved states of hypochondriasis (Hs), schizophrenia (Sc), depression (D), hysteria (Hy), masculinity-femininity (Mf), paranoia (Pa), psychasthenia (Pt), psychopathic deviate (Pd), mania (Ma), and social introversion (Si). Six clinical factors were also considered: P (including positive loads of F, PA, Pt, Ma, and SC and negative loads of L and K), N (including Hs, Hy, and D), I (including Pt, D, and Si), F (Pa), M (Mf), and A (including high negative loads of Pd and a medium negative load of Pa). This approach was used as described previously (James N. Butcher, 1976).

2.2.2. QUIP PD-Short Assessment. All subjects were tasked to complete a questionnaire relating to impulsive comprehensive disorders in Parkinson's disease (QUIP PD-short). This is a comprehensive screening test that evaluates a wide range of impulsive compulsive behaviors [14]. Scoring above a predetermined threshold indicates that the patient answered the test with bias, thus invalidating the personality scale results. The results of the MMPI test are presented as normalized t-scores. Scale scores indicate psychological dysfunction when the t-value was >60. Absolute scores are presented as means of the normalized t-scores.

2.3. Statistical Methods. All clinical parameters were indicated as the mean ± standard deviation (SD) or as percentages in the case of categorical variables. Dr. Zhang and his team considered 60 points as the demarcation point. Sensitivity, specificity, and interpreter reliability were calculated by comparing normal subjects versus those with mental disorders. Thus, the cutoff threshold was set at 60.

All patients, as well as healthy controls, were compared using one-way analysis of variance (ANOVA) for continuous parameters. Chi-squared tests were used to compare categorical parameters, and $p < 0.05$ was regarded as being statistically significant.

2.4. Ethical Considerations. This study was approved by the local ethics committee. All procedures adhered to the ethical guidelines of the responsible committee on human experimentation (institutional and national) and the Helsinki Declaration of 1975 (revised in 2000).

3. Results

In total, 129 subjects were recruited into the study: 51 in the healthy control group, 38 in the PD-DBS group, and 40 in the PD-MED group (Table 1). The basic characteristics of the 38 PD-DBS patients were as follows: mean age = 62.76 ± 9.31 years, mean H&Y score = 3.52 ± 0.80, mean disease duration = 11.53 ± 4.65, and mean Unified Parkinson's Disease Rating Scale (UPDRS) part III score = 45.63 ± 12.61. The basic characteristics of the 40 PD-MED were as follows: mean age = 67.43 ± 10.03 years, mean H&Y score = 2.60 ± 1.24, mean disease duration = 7.97 ± 6.36 years, and mean UPDRS score = 35.97 ± 18.04. The mean age of the 51 participants in the HS group was 57.49 ± 6.74 years. There were no statistically significant differences between the two groups with regard to age, gender, total levodopa equivalent dosage (total LEDD), or the use of levodopa and DA agonist LED ($p \geq 0.05$). Even more, no statistically significant differences were detected between the two groups with regard to H&Y stage, disease duration, and UPDRS III scores ($p \geq 0.05$), thus indicating that the condition of the patients in the PD-DBS group was similar to PD patients with the best medical treatment.

We found no significant differences between the two groups with regard to the QUIP PD-short neuropsychological evaluation ($p > 0.05$, Table 2). However, one-way ANOVA revealed significant differences in all 13 subscales

Table 1: Demographics and clinical feathers in all subjects.

	PD				
	PD-DBS (38)	PD-MED (40)	p value	HC (51)	p value
Age (years)	62.76 ± 9.31	67.43 ± 10.03	0.057	57.49 ± 6.74	0.067
Duration (years)	11.53 ± 4.65	7.97 ± 6.36	0.074	3.82 ± 3.71	—
H&Y stage	3.52 ± 0.80	2.60 ± 1.24	0.198	2.18 ± 1.33	—
Sex (F/M), no.	17 : 21	14 : 26	0.380	31 : 20	0.052
Total LEDD (mg)	795.0 ± 288.0	608.3 ± 150.6	0.199		
Levodopa (mg/d)	610.0 ± 176.1	454.2 ± 150.3	0.154	—	—
DA agonist LED (mg/d)	100.8 ± 83.7	125.0 ± 38.7	0.528		—
UPDRS III	45.63 ± 12.61	35.97 ± 18.04	0.0735		

Note: data are given as the mean ± standard deviation. UPDRS III: Unified Parkinson's Disease Rating Scale, part III. Note: DA agonist-LED (DA-LED, mg/d) = piribedil (mg/d) × 1 + pramipexole (mg/d) × 100. Total LED (TLED, mg/d) = regular levodopa dose (mg/d) × 1 + levodopa CR dose (mg/d) × 0.75 + DA-LED, and plus [regular levodopa dose (mg/d) + CR levodopa dose (mg/d) × 0.75] × 0.33 if taking COMT-I.

Table 2: Comparison between patients with and without ICD behaviors.

Variable	PD-DBS (38)	PD-MED (40)	p value
QUIP disorders			
Any 1 or more disorders	2	3	0.833
Gambling	1	1	1.0
Sex	0	1	—
Buying	1	1	1.0
Eating	0	0	—
Hobbyism	0	0	—
Punding	0	0	—

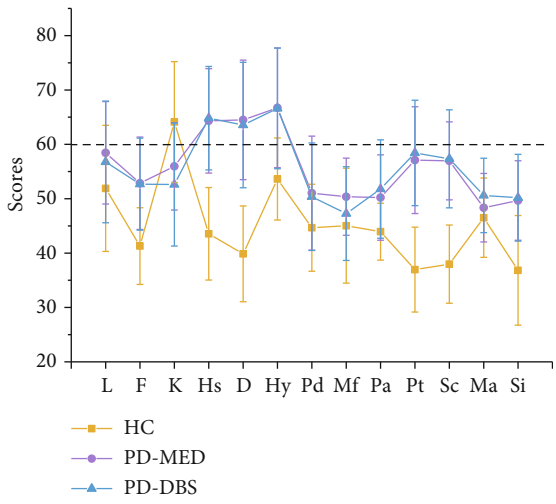

Figure 1: Scores of validity scales and personality scales in three groups of subjects. Note: HC: healthy control; PD-MED: drug-treated PD patients; PD-DBS: STN-DSB surgery; MMPI-1: Minnesota multiphasic personality inventory-1; L: lie; F: fake; K: K correction and defensive responses; Hs: hypochondriasis; D: depression; Hy: hysteria; Pd: psychopathic deviate; Mf: masculinity/femininity; Pa: paranoia; Pt: psychasthenia; Sc: schizophrenia; Ma: hypomania; Si: social introversion.

when compared between the three groups (PD-MED, PD-DBS, and HC) (Figures 1 and 2).

Significant differences were detected between the groups when considering the three corrected scales ($p \leq 0.01$). Analyses of 10 clinical scales revealed differences between the groups ($p \leq 0.01$) and significant differences in the Mf scale ($p \leq 0.01$) and Ma scale ($p = 0.09$). Moreover, the mean scores for the PD-DBS and PD-MED were >60 for Hy, D, and Hs. Using the N factor scale, the mean scores for the two PD groups were >65 and were both significantly higher than that of the HC group. However, post hoc analysis failed to identify any significant differences between the PD groups.

4. Discussion

To the best of our knowledge, this is the first study to investigate the personalities of PD patients prior to DBS or medical treatment. No significant differences were detected between the PD-DBS and PD-MED groups with regard to the dimensions of temperament, and the two groups exhibited similar psychotic characteristics. These data indicated that patients undergoing surgery do not have special personality traits; rather, they are part of the wider PD population.

Statistically significant differences were reported between the PD-DBS and PD-MED patients with regard to the H&Y stage, disease duration, and UPDRS III scores. These data indicated that PD was more severe in the PD-DBS group and that these patients required surgical intervention because medication was not sufficiently effective.

No significant differences were detected between the PD-DBS and PD-MED groups with regard to LEDD and DA drug usage, thus ruling out any influence that may have been created by these drugs. Analysis of QUIP scales further indicated that Compulsive Disorder (OCD) does not affect the decision to operate. After excluding impulsive factors, we investigated whether personality factors had an effect on surgical decisions within our patient population.

It has been reported that patients who develop PD often show a typical premorbid personality profile that is characterized by industriousness, inflexibility, cautiousness, and low impulsivity; these persist after the disease begins to affect

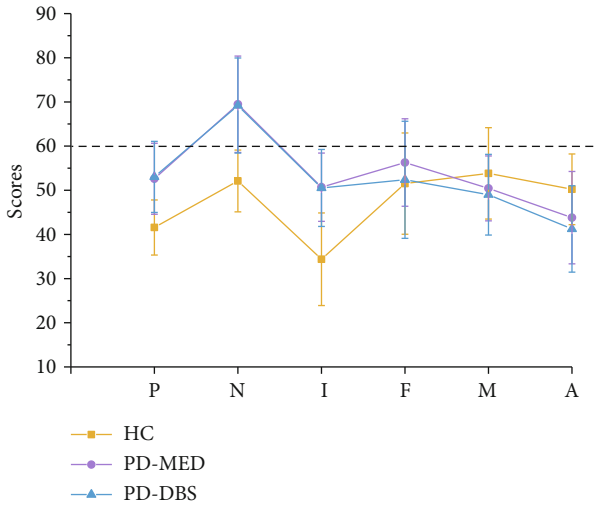

Figure 2: Scores of clinical factors in three groups of subjects. Note: P: including positive loads of F, PA, Pt, Ma, and SC and negative loads of L; N: including Hs, Hy, and D; I: including Pt, D, Si, F, Pa, M, and Mf; A: including high negative loads of Pd and medium negative load of Pa.

the motor system. However, other studies show that in addition to the innate factors that may affect personality, personality changes that develop with PD gradually become obsessive, dependent, affectively inconstant, passive, industrious, worried, and sick body perception, when compared with healthy controls [15, 16].

Although it is difficult to differentiate between premorbid personality features from those that develop after the appearance of the disease's typical manifestations, this should not prevent further attempts to reexamine the premorbid personality using newer hostility, as well as personality rating scales. A previous study investigated 6,822 participants over 40 years and used MMPI scales to monitor extraversion (sensation seeking, hypomania, and positive emotionality), introversion (social introversion and constraint), and neuroticism (psychasthenia, pessimistic personality, and depression) and found that only neuroticism was significantly correlated with the development of PD later in life [17]. Our results are consistent with these previous findings; the neuroticism score of our PD patients (>65) was significantly higher than that of the HC group, thus indicating a characteristic personality that is associated with PD.

Neuroticism derived from the Hs, D, and Hy scales showed considerable correlation with the subsequent development of PD. This relationship was primarily due to the anxious personality scale (psychasthenia). The correlation between the pessimistic personality trait and the absence of depression was poor. The neuroticism personality trait refers to negative emotions to threat, frustration, or loss and is typified by anxiety, moodiness, worry, envy, and holding grudges [18]. Neuroticism has been demonstrated to elevate the risk of depression in PD and can potentially aggravate the disease. Collectively, these observations imply that neuroticism is a hallmark personality of PD; this is consistent with our observations of PD-MED and PD-DBS patients. A mean neuroticism factor score that is higher than the HC group indicates emotional instability, disease progression, or poor disease control, thus suggesting that high levels of neuroticism may predispose patients to a reduced quality of life or poorer disease control [19]. Thus, we need to place greater emphasis on neuroticism, especially after DBS. A profound understanding of the role of neuroticism may help to improve the treatment of PD patients with high levels of neuroticism.

The D scale is related to psychopathic features and neurotic disorders. Depression is a clinical symptom of a variety of disorders, including bad moods, schizophrenia, bipolar depression, OCD, and anxiety disorder. Some studies have found that characteristic personalities, such as neuroticism, OCD, and anxiety disorder, are related to defects in the distribution of dopamine. However, other studies, involving neuroanatomical and functional studies, have indicated that it is not easy to conclude that dopamine distribution is the only cause [4, 20, 21]. Some studies suggest that DBS in PD results in personality changes, including an augmented impulsive profile, despite reduced levels of L-dopa and DA, thus supporting the idea of a primary behavioral effect caused by DBS [22, 23]. A recent study reported self-perceived personality changes in 6 out of 27 (22%) STN-DBS patients and identified that preoperative hypomania was the most remarkable predictor for personality change. Nevertheless, standard measurement scales did not sufficiently reflect personality or mood changes that were perceived subjectively by patients [24].

Chronic diseases can exert a notable long-term influence on personality, profoundly impacting the outcome of DBS. Relative to healthy controls, we found that our PD patients exhibited significant differences in three dimensions (spirit, neuroticism, and introversion), a significantly lower socialization dimension, greater levels of submissiveness, greater dependence on others, and less engagement in social activities. The MMPI characteristics of PD patients taking medications were consistent with those of PD patients prior to STN-DBS surgery. PD patients also exhibited some personality changes prior to surgery. Thus, it is very important to consider the mental state of PD patients prior to surgery.

Future research should be aimed at overcoming these limitations such as the number of the patients and longitudinal personality changes and thus validate the occurrence of changes in personality traits after DBS, to better determine whether specific personality traits can predict the progression of the disease or the effects of interventions such as DBS.

5. Conclusion

Chronic diseases can exert significant long-term influences on personality. These personality factors, particularly neuroticism, although are not factors in deciding whether to undergo operation, may have a significant effect on the postoperative effects of DBS.

Data Availability

All the clinical data used to support the findings of this study may be released upon application to the data access manager, who can be contacted at +8613812512187.

Ethical Approval

This study was conducted in accordance with the 2016/679 EU regulations. All of the subjects provided written informed consent in accordance with the Declaration of Helsinki. Ethical approval for this study was granted by the ethics committee of the IRCCS Istituto Auxologico Italiano.

Conflicts of Interest

None of the authors have any conflicts of interest to declare.

Authors' Contributions

Wei Lin was responsible for study design. Dan Wang and Shibai Sun were responsible for all patient assessments. Jie Zhu was responsible for patient neurological examinations. Jirong Dong and Likun Yang contributed to designing the study. Yuhai Wang critically revised the manuscript. All authors approved the final version of the manuscript. Wei Lin and Dan Wang contributed equally to this work. Yuhai Wang is the senior author.

Acknowledgments

We would particularly like to thank all patients and healthy individuals who participated in the study as well as medical staff and research assistants for their contributions to the study. This work was supported by the Wuxi health commission (CSZ0N1729).

References

[1] G. Santangelo, F. Piscopo, P. Barone, and C. Vitale, "Personality in Parkinson's disease: clinical, behavioural and cognitive correlates," *Journal of the Neurological Sciences*, vol. 374, pp. 17–25, 2017.

[2] J. H. Bower, B. R. Grossardt, D. M. Maraganore et al., "Anxious personality predicts an increased risk of Parkinson's disease," *Movement Disorders*, vol. 25, no. 13, pp. 2105–2113, 2010.

[3] M. F. Damholdt, M. B. Callesen, and A. Møller, "Personality characteristics of depressed and non-depressed patients with Parkinson's disease," *The Journal of Neuropsychiatry and Clinical Neurosciences*, vol. 26, no. 4, pp. 329–334, 2014.

[4] V. S. Kostić, D. Lečić, Z. Kovačević, S. Filipović, and N. Sternic, "The premorbid personality of patients with Parkinson's disease: evidence with the Tridimensional Personality Questionnaire," *European Journal of Neurology*, vol. 1, pp. 249–252, 1995.

[5] P. McNamara, R. Durso, and E. Harris, "Alterations of the sense of self and personality in Parkinson's disease," *International Journal of Geriatric Psychiatry*, vol. 23, no. 1, pp. 79–84, 2008.

[6] C. Volpato, M. Signorini, F. Meneghello, and C. Semenza, "Cognitive and personality features in Parkinson disease: 2 sides of the same coin?," *Cognitive and Behavioral Neurology*, vol. 22, no. 4, pp. 258–263, 2009.

[7] V. Kaasinen, E. Nurmi, J. Bergman et al., "Personality traits and brain dopaminergic function in Parkinson's disease," *Proceedings of the National Academy of Sciences of the United States of America*, vol. 98, no. 23, pp. 13272–13277, 2001.

[8] M. A. Menza, L. I. Golbe, R. A. Cody, and N. E. Forman, "Dopamine-related personality traits in Parkinson's disease," *Neurology*, vol. 43, 3, Part 1, pp. 505–508, 1993.

[9] L. Ishihara and C. Brayne, "What is the evidence for a premorbid parkinsonian personality: a systematic review," *Movement Disorders*, vol. 21, pp. 1066–1072, 2006.

[10] P. E. Mosley and R. Marsh, "The psychiatric and neuropsychiatric symptoms after subthalamic stimulation for Parkinson's disease," *The Journal of Neuropsychiatry and Clinical Neurosciences*, vol. 27, no. 1, pp. 19–26, 2015.

[11] V. Voon, C. Kubu, P. Krack, J. L. Houeto, and A. I. Tröster, "Deep brain stimulation: neuropsychological and neuropsychiatric issues," *Movement Disorders*, vol. 21, Supplement 14, pp. S305–S327, 2006.

[12] A. J. Hughes, S. E. Daniel, L. Kilford, and A. J. Lees, "Accuracy of clinical diagnosis of idiopathic Parkinson's disease: a clinico-pathological study of 100 cases," *Journal of Neurology, Neurosurgery, and Psychiatry*, vol. 55, no. 3, pp. 181–184, 1992.

[13] W. Z. Song, "Report of a trial of Minnesota Multiphasic Personality Inventory (MMPI) in some districts of our country (author's transl)," *Zhonghua Shen Jing Jing Shen Ke Za Zhi*, vol. 13, no. 3, pp. 157–160, 1980.

[14] D. Weintraub, E. Mamikonyan, K. Papay, J. A. Shea, S. X. Xie, and A. Siderowf, "Questionnaire for impulsive-compulsive disorders in Parkinson's Disease-Rating Scale," *Movement Disord.*, vol. 27, no. 2, pp. 242–247, 2012.

[15] J. S. PRICHARD, R. S. SCHWAB, and W. A. TILLMANN, "The effects of stress and the results of medication in different personalities with Parkinson's disease," *Psychosomatic Medicine*, vol. 13, no. 2, pp. 106–111, 1951.

[16] C. J. Todes and A. J. Lees, "The pre-morbid personality of patients with Parkinson's disease," *Journal of Neurology, Neurosurgery, and Psychiatry*, vol. 48, no. 2, pp. 97–100, 1985.

[17] M. Poletti and U. Bonuccelli, "Personality traits in patients with Parkinson's disease: assessment and clinical implications," *Journal of Neurology*, vol. 259, no. 6, pp. 1029–1038, 2012.

[18] B. B. Lahey, "Public health significance of neuroticism," *The American Psychologist*, vol. 64, no. 4, pp. 241–256, 2009.

[19] G. M. Pontone, Z. Mari, K. Perepezko, H. D. Weiss, and S. S. Bassett, "Personality and reported quality of life in Parkinson's disease," *International Journal of Geriatric Psychiatry*, vol. 32, no. 3, pp. 324–330, 2017.

[20] N. Bódi, S. Kéri, H. Nagy et al., "Reward-learning and the novelty-seeking personality: a between- and within-subjects study of the effects of dopamine agonists on young Parkinson's patients," *Brain*, vol. 132, pp. 2385–2395, 2009.

[21] T. Ishii, N. Sawamoto, H. Tabu et al., "Altered striatal circuits underlie characteristic personality traits in Parkinson's disease," *Journal of Neurology*, vol. 263, no. 9, pp. 1828–1839, 2016.

[22] M. Denheyer, Z. H. Kiss, and A. M. Haffenden, "Behavioral effects of subthalamic deep brain stimulation in Parkinson's disease," *Neuropsychologia*, vol. 47, no. 14, pp. 3203–3209, 2009.

[23] J. L. Houeto, V. Mesnage, L. Mallet et al., "Behavioural disorders, Parkinson's disease and subthalamic stimulation," *Journal of Neurology, Neurosurgery, and Psychiatry*, vol. 72, no. 6, pp. 701–707, 2002.

[24] L. Castelli, P. Perozzo, M. Caglio et al., "Does subthalamic stimulation induce personality modifications in Parkinson's disease? A Rorschach Test explorative study," *Acta Neurologica Belgica*, vol. 108, no. 1, pp. 5–8, 2008.

Hindawi
Behavioural Neurology
Volume 2021, Article ID 8886004, 8 pages
https://doi.org/10.1155/2021/8886004

Research Article

Ultrarapid Endoscopic-Aided Hematoma Evacuation in Patients with Thalamic Hemorrhage

Kuan-Yu Chen,[1] **Woon-Man Kung**,[2] **Lu-Ting Kuo**,[3] **and Abel Po-Hao Huang**[3]

[1]*School of Medicine, National Taiwan University, Taipei, Taiwan*
[2]*Department of Exercise and Health Promotion, College of Kinesiology and Health, Chinese Culture University, Taipei, Taiwan*
[3]*Division of Neurosurgery, Department of Surgery, National Taiwan University Hospital and National Taiwan University College of Medicine, Taipei, Taiwan*

Correspondence should be addressed to Abel Po-Hao Huang; how.how0622@gmail.com

Received 7 August 2020; Revised 4 September 2020; Accepted 12 January 2021; Published 21 January 2021

Academic Editor: Chung-Feng Kao

Thalamic hemorrhage bears the worst outcome among supratentorial intracerebral hemorrhage (ICH). Minimally invasive endoscopic-aided surgery (MIS) has been proved to be safe and effective in evacuating ICH. However, the ideal timing of MIS is still a controversy. In this study, we present our experience in the treatment of patients with thalamic hemorrhage by ultrarapid MIS evacuation. This retrospective analysis enrolled seven patients treated with ultrarapid MIS evacuation of thalamic hemorrhage. Seven patients treated with EVD with similar ICH score were included as match control. Primary endpoints included rebleeding, morbidity, and mortality. Hematoma evacuation rate was evaluated by comparing the pre- and postoperative computed tomography (CT) scans. Glasgow Outcome Scale Extended (GOSE) and modified Rankin Score (mRS) were noted at the 6-month and 1-year postoperative follow-up. Among the seven patients, six were accompanied with intraventricular hemorrhage. All patients received surgery within 6 hours after the onset of stroke. The mean hematoma volume was 35 mL, and the mean operative time was 116.4 minutes. The median hematoma evacuation rate was 74.9%. There was no rebleeding or death reported after the surgery. The median GOSE and mRS were 3 and 5, respectively, at 6 months postoperatively. Further, 1-year postoperative median GOSE and mRS were 3 and 5, respectively. The data suggest that the ultrarapid MIS technique is a safe and effective way in the management of selected cases with thalamic hemorrhage, with favorable long-term functional outcomes. However, a large, prospective, randomized-controlled trial is needed to confirm these findings.

1. Introduction

Spontaneous intracerebral hemorrhage (ICH) is a common neurosurgical emergency. The incidence of ICH is around 24 per 100,000 person-years in white people, 23 per 100,000 person-years in black people, and 52 per 100,000 person-years in Asian people [1]. Roughly 10 to 15% of ICH cases involve the thalamus. Thalamic hemorrhage bears the worst outcome among supratentorial ICH. Hematoma of the thalamus may expand and affect different proximal structures (e.g., the ventricle, globus pallidus, and internal capsule), leading to different extent of disability and mortality.

Due to its deeply seated anatomy, thalamic hemorrhage is hard to evacuate. Recently, minimally invasive endoscopic-aided surgery (MIS) for evacuating ICH has been considered as a safe and effective approach, showing with lower morbidity and mortality than the traditional craniotomy [2–4]. Many factors such as hematoma volume, intraventricular extension, and location of hematoma have been found to be associated with the prognosis of MIS [5]. However, the ideal timing to perform minimally invasive surgery (MIS) is still a controversy. It has been reported that early surgery performed within 6 to 24 hours ICH is ideal for MIS [6]; however, whether the ultrarapid MIS performed within 6 hours after ICH is favorable to patients is still under debate.

In this study, we focus on the surgical management of thalamic hemorrhage and present our experience in treating thalamic hemorrhage using ultrarapid MIS evacuation by

comparing the postoperative outcomes between patients receiving ultrarapid MIS evacuation and patients using extraventricular drainage (EVD) without thalamic hematoma evacuation.

2. Materials and Methods

2.1. Patient Selection. In this study, we included patients with ICH fulfilling the following criteria: (1) thalamic hemorrhage with >20 mL hematoma volume, accompanied with or without intraventricular hemorrhage (IVH) and acute hydrocephalus and (2) had undergone MIS within 24 hours after the onset of stroke. Moreover, we included another matched (control) group with thalamic hemorrhage fulfilling the following criteria: (1) ICH score ≥ 2, (2) had undergone unilateral or bilateral EVD without thalamic hematoma evacuation, and (3) had undergone EVD placement within 24 hours after the onset of stroke. Patients were excluded if they had met anyone of the following criteria: (1) ICH caused by the trauma, tumor, and coagulopathy (prothrombin time international normalized ratio (PT INR) > 1.3, partial thromboplastin time (PTT) > 35.5 seconds, and platelet count < 100, 000/mL); (2) with end-stage renal disease or Child-Pugh Class C cirrhosis; (3) taking antiplatelet or anticoagulation medications, (4) with preoperative Glasgow coma scale (GCS) score of <4 or >14; and (5) without the data on follow-up computed tomography (CT) result within 3 days or lost to follow-up at 6 months. Both MIS and EVD groups were managed by the same clinical surgical team at National Taiwan University Hospital.

The study was designed and conducted in accordance with the applicable local regulations and the ethical principles of the Declaration of Helsinki and was approved by Institutional Review Board (IRB) of National Taiwan University Hospital (IRB number: 201611058RINA). Written informed consent was waived as this is a retrospective research.

2.2. For the Removal of IVH. We used the ipsilateral Kocher point as the entry point for MIS and inserted external ventricular drain (EVD) through the operative tract for removing the IVH. A flexible endoscope with the free-hand technique was applied to evacuate massive hematoma in the third and fourth ventricles of patients with massive IVH. Also, bilateral EVD placement might be conducted.

Under general anesthesia, a 3.5 to 4.0 cm linear skin incision was made, followed by a burr hole (1.5-2.0 cm in diameter) drilling. Intraoperative sonography (ALOKA Prosound alpha 5 SV with UST-5268P-5 Multi-Frequency Phased Array Burr-hole Probe, 3.0-7.5 MHz, Tokyo, Japan) was applied to locate hematoma or ventricle before conducting cruciate durotomy and small corticotomy. A custom-made transparent plastic sheath (10 mm in outer diameter, with various lengths depending on surgeon's choice as well as the estimated length measured on preoperative CT scan) was inserted along the planned trajectory with the stylet. After removal of the stylet, the endoscope (4 mm, 0° rod-lens endoscope, and 18 cm in length; Karl Storz, Tuttlingen, Germany) was introduced into the transparent sheath to provide visualization when removing the hematoma.

Following our procedure of hematoma removal described in previous studies [4, 7], we entered the ventricle to evacuate IVH first. Next, we identified the rupture site of thalamic hemorrhage and evacuated the hematoma using the penetrating technique with an 8 Fr. angled suction in the working space of the sheath. A flexible endoscope (outer diameter: 2.5 mm; Karl Storz) could be introduced as an alternative to facilitate the removal of hematoma and to avoid excessive rotation or significant manipulation of the sheath enclosed in the brain parenchyma.

For most cases, ICH could be evacuated without active or pronounced bleeding during the operation. For patients with intraoperative bleeding, we applied the "wait-and-see saline irrigation" method to stop the bleeding when bleeding from a small artery or perforating vessel was found. For patients with intraoperative bleeding, we applied the "wait-and-see saline irrigation" method to stop the bleeding when bleeding from a small artery or perforating vessel was found. If the bleeding had not been stopped, the balanced irrigation-suction technique was then used to identify the bleeding site [8], where we injected FloSeal Hemostatic Matrix via a specialized 3 mm flexible catheter into the hematoma cavity to achieve hemostasis. Then, cotton was used for coverage, followed by normal saline to remove the residual FloSeal Hemostatic Matrix.

2.3. Clinical Follow-Up. All patients were followed up by brain CT within 3 days after the operation. The hematoma evacuation rate was calculated using the following formula: [(Preoperative hematoma volume − Postoperative hematoma volume)/preoperative hematoma volume] × 100%.

Primary endpoints included rebleeding, morbidity, and mortality after the surgery. The Glasgow Outcome Scale Extended (GOSE) score and the modified Rankin Score (mRS) were evaluated at 6-month and 1-year postoperative follow-up either at an outpatient department or by phone.

2.4. Statistical Analysis. Descriptive analysis and linear regression were conducted using SPSS (Statistical Package for the Social Sciences). Continuous variables were presented as mean, standard deviation (SD), median, and range, while the categorical variables were summarized as number and percentage. No imputation was applied for missing data.

3. Results

3.1. Baseline Characteristics. Table 1 summarizes patients' characteristics and surgical outcome. In the MIS group, seven patients receiving MIS within 24 hours of ictus were enrolled, including four men and three women at a mean age (mean ± SD) of 66.6 ± 10.5 years (range: 53-87 years); while in the EVD group, seven patients without hematoma evacuation were enrolled, including five men and two women at a mean age (mean ± SD) of 68.2 ± 12.4 years (range: 56-81 years). In the MIS group, six out of seven patients accompanied with IVH (three men and three women), while in the EVD group, all patients had IVH. Patients in the MIS group had higher preoperative hematoma volume and ICH score than those in the EVD group; however, the MIS group

Table 1: Demographics, clinical characteristics, and outcomes.

Parameters	MIS ($N = 7$)	EVD ($N = 7$)
Age (years), mean ± SD	66.6 ± 10.5	68.2 ± 12.4
Male, *n* (%)	4 (57.1)	2 (28.6)
ICH volume (mL), mean ± SD	35 ± 8.5	18.0 ± 8.5
ICH score, mean ± SD	3.0 ± 0.76	2.3 ± 0.5
Evacuation rate (%), median	74.9	—
Operation time (min), mean ± SD	116.4 ± 37.7	61.0 ± 18.1
Time to operation (hours)	3.1 ± 0.95	6.0 ± 4.5
Within 6 hr, *n* (%)	7 (100.0)	5 (71.4)
Within 6-24 hr, *n* (%)	0 (0.0)	2 (28.6)
ICU stay	20 ± 8.3	22 ± 7.8
Hospital stay	34.6 ± 13.5	48.7 ± 17.7
Initial GCS, median	8	8
1-month GCS, median	10	11
6-month GCS, median	10	12
1-year GCS, median	10	12
6-month GOSE, median	3	3
6-month mRS, median	5	5
1-year GOSE, median	3	3
1-year mRS, median	4	4
Rebleeding, *n* (%)	0 (0.0)	1 (14.3)
Morbidity, *n* (%)	1 (14.3)	4 (57.1)
VP shunt	1 (14.3)	4 (57.1)
Tracheostomy	0 (0.0)	4 (57.1)
Death, *n* (%)	0 (0.0)	0 (0.0)

Abbreviations: SD: standard deviation; ICH: intracerebral hemorrhage; GCS: Glasgow Coma Scale; GOSE: Glasgow Outcome Scale Extended; mRS: modified Rankin Score.

demonstrated shorter hospital stay and ICU stay than the EVD group.

3.2. Postoperative Outcomes. Postoperative outcomes in terms of rebleeding, morbidity, death, and functional outcomes are also summarized in Table 1. The incidences of postoperative rebleeding and morbidity were both higher in the EVD group than the MIN group. In the MIN group, there was neither rebleeding nor death reported after the surgery and only one patient received ventriculoperitoneal shunt (VP shunt) after the surgery. In the EVD group, one patient had rebleeding after the surgery and four patients experienced morbidity (received VP shunt and tracheostomy). No death was reported after the surgery in both groups.

For the consciousness evaluation, both groups showed improved GCS score from 8 preoperatively to 10 (MIS group) and 12 (EVD group) at 6 months postoperatively, which was sustained until 1 year. The distribution of functional outcome is presented in Figure 1, showing a sustained functional outcome in both groups after 6 months. In the MIS group, the median GOSE scores at 6 months and 1 year were both 3, with five patients graded as 3 or above. The median mRS at 1 year postoperatively was 4, with three patients showing good functional recovery (i.e., mRS ≤ 3). The EVD group demonstrated similar functional outcome as the MIS group, with a median GOSE score of 3 at both 6 months and 1 year, with six patients graded as 3 or above. The median mRS at 1 year postoperatively was 5, with one patient showing good functional recovery (i.e., mRS ≤ 3).

3.3. Correlation Analysis. The correlation analysis of 1-year mRS and preoperative hematoma volume revealed an *R*-squared of 0.1575 (Figure 2). The correlation analysis of 1-year mRS and initial GCS score showed an *R*-squared of 0.5181 (Figure 3).

3.4. Illustrative Case. A 71-year-old man was hospitalized due to sudden onset of left hemiparesis. He was brought to the emergency department within an hour. His consciousness level deteriorated soon from an initial GCS score of E3V5M6 to a score of E2V1M5, with preferential gaze to the right side. The CT scan revealed right thalamic hemorrhage with IVH and acute obstructive hydrocephalus. The volume of the hematoma was around 50 mL (Figure 4(a)). The patient was treated with MIS evacuation of ICH and IVH. The postoperative CT scan revealed minimal (around 5 mL) thalamic hematoma at the right side and residual hematoma at ventricles (Figure 4(b)). Bilateral EVDs were kept for three days after the operation, with no ventriculoperitoneal *shunt* implantation or intraventricular injection of anticoagulants. His GCS score was improved to E4V2M6 at one month after the surgery.

4. Discussion

According to the timing of surgery, surgeries can be classified into ultraearly (within 6 h after ICH), early (within 6–24 h after ICH), and delayed (4 days after ICH) surgeries [6, 9]. In this retrospective study of seven patients receiving ultrarapid MIS evacuation of thalamic hemorrhage, we observed a good surgical outcome, with no postoperative rebleeding or death noted. In addition, consciousness level and functional outcomes were improved after the surgery. Our data suggested that ultrarapid evacuation of thalamic hemorrhage via MIS may be an optimal surgical approach for selected patients with thalamic hemorrhage.

According to the American Heart Association/American Stroke Association guidelines for the management of spontaneous ICH [10], in patients with IVH and hydrocephalus, ventricular drainage is reasonable, especially for those with decreased level of consciousness. Whether or not removal of thalamic hematoma will improve outcome is still controversial. In recent years, we have performed aggressive evacuation of thalamic hematoma along with IVH removal in early thalamic ICH evacuation. Most of the surgeries were done within 6 hours after the onset of stroke. Since EVD is the most frequently used for thalamic hemorrhage with IVH, we took the EVD group as the matched control in this study, of which the ICH score is similar with the MIS group. Despite the patients receiving MIS evacuation bear higher volume of thalamic hemorrhage, the result showed that patients underwent early MIS evacuation had no rebleeding, lower shunt dependency, no tracheostomy rate, and shorter ICU stay as

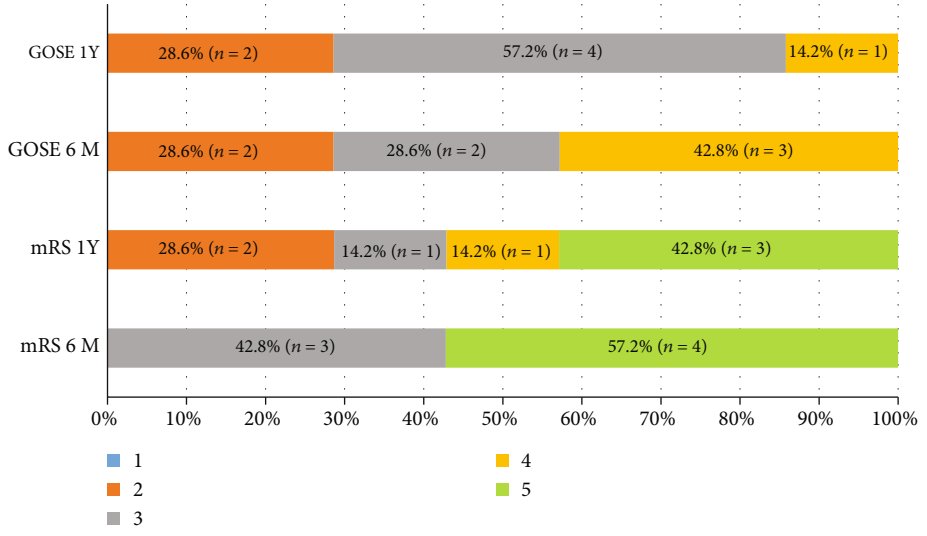

(a)

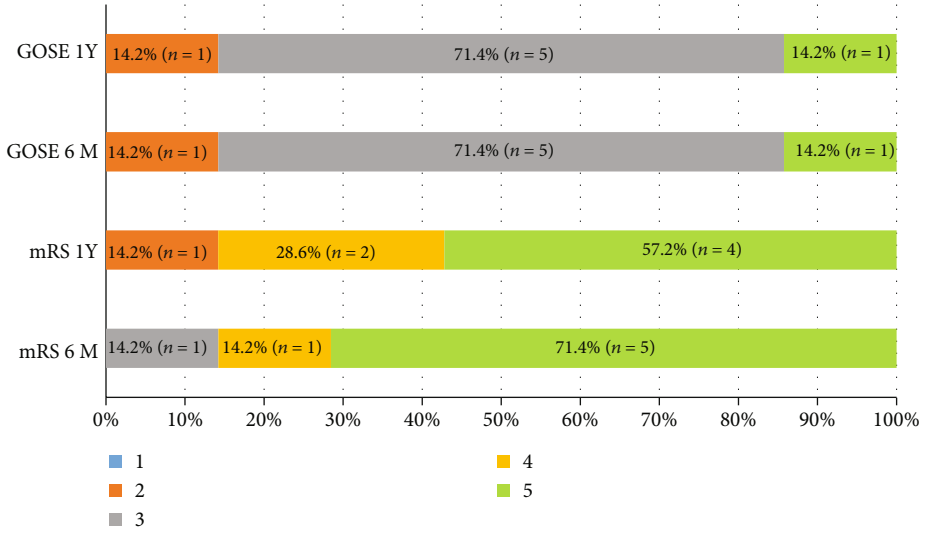

(b)

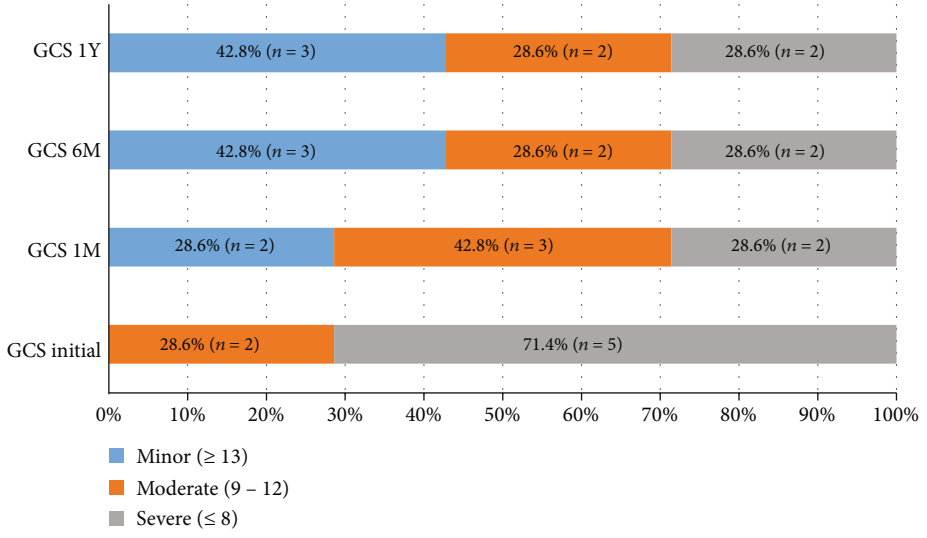

(c)

Figure 1: Continued.

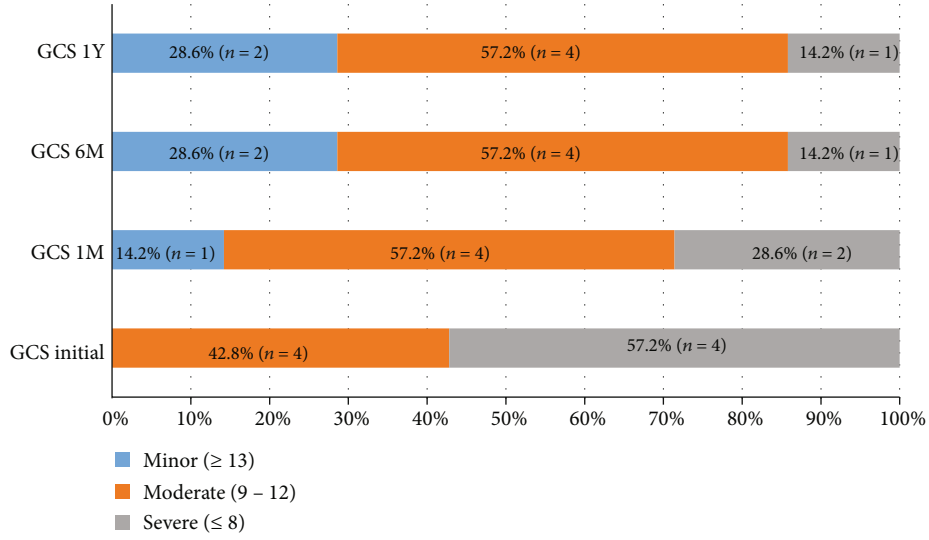

(d)

Figure 1: Distribution of functional outcomes. (a) Functional outcomes of the MIS group. (b) Functional outcomes of the EVD group. (c) Glasgow Coma Scale score of the MIS group. (d) Glasgow Coma Scale score of the EVD group.

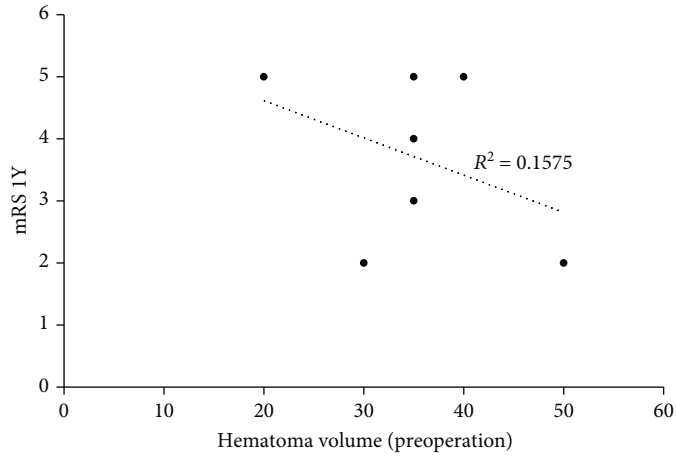

Figure 2: Correlation analysis of 1-year mRS and preoperative hematoma volume.

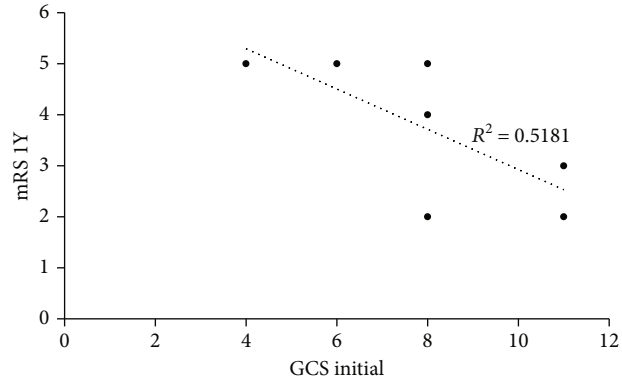

Figure 3: Correlation analysis of 1-year mRS and initial GCS score.

well as hospital stay. Moreover, better functional outcome was revealed in the MIS group. This result is compatible with the study conducted by Scaggiante et al. [11], which concluded that with a time to evacuation within 72 hours and 24hours, morbidity and mortality improved significantly in the MIS group over the other treatment group. Moreover, our study suggested that with a time to evacuation within 6 hours, MIS evacuation demonstrated efficacy over EVD placement.

It is well known that the local mass effect of hematoma can contribute to elevate intracranial pressure (ICP) and therefore elicit pathological cascades provoking biochemical toxicity. With the favorable outcome observed in this study, we suggested that the early evacuation of ICH can stop the expansion of initial hematoma and prevent associated pathological cascades. Similarly, a previous study has proved that decreasing the clot size to 15 mL or less may ameliorate the

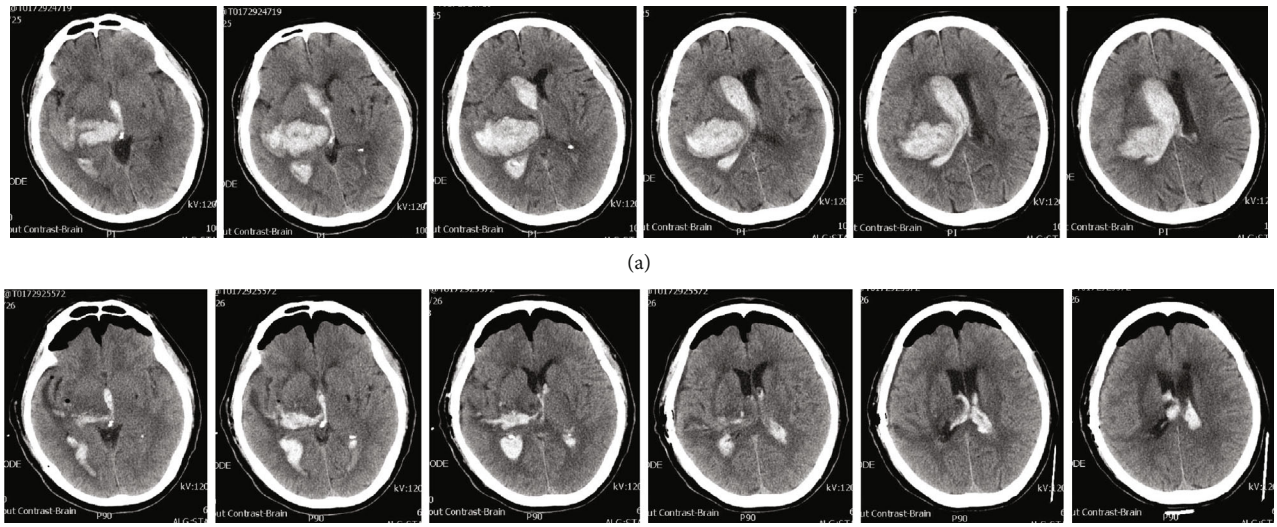

(a)

(b)

Figure 4: Axial CT scans. (a) Preoperative thalamic hematoma which ruptured into the ventricle. (b) Postoperative residual thalamic hematoma and intraventricular hematoma.

functional outcome [12]. Another study also demonstrated that early and minimally invasive gross-total removal of ICH can decrease the ICH-associated secondary injury [13].

However, according to the American Heart Association/American Stroke Association guidelines, timing to perform surgery for ICH remains controversial; furthermore, it was suggested that ultrarapid surgery may escalate the possibility of rebleeding. However, this statement was established on the limited evidence from one study comparing 11 patients undergoing traditional craniotomy within 4 hours of ICH onset with those undergoing traditional craniotomy within 12 hours. The rebleeding rate was 40% in the early surgery (within 4 hours) group, whereas the rebleeding rate was 12% in the late surgery (within 12 hours) group [14]. However, patients' characteristics, ICH severity, surgical method, timing of surgery, and surgeon's experience are all critical prognostic factors. It is inappropriate to conclude that an ultraearly surgery is detrimental to ICH patients. Moreover, unlike our study using the MIS, which has the advantage of minimizing the blood loss, the study applied the traditional craniotomy, which may incur more blood loss and increase the risk of rebleeding. For MIS, the rebleeding problem can be simply solved by applying local hemostatic matrix [7].

In addition to direct injury, ICH can cause secondary brain injury through late-phase inflammatory reactions. Previous studies have proved that degradation of hemin (the oxidized form of heme) can cause cell or brain tissue damage through direct cytotoxic effects [15].The key enzyme of heme catabolism is heme oxygenase-1 (OH-1), which is activated after the onset of ICH. OH-1 catalyzes heme and produces free iron, which is further oxidized into Fe^{3+} and contributes to oxidative stress, brain edema, neuronal death, and blood-brain barrier damage. Several animal studies have shown that OH-1 can be rapidly activated at 6 hours after ICH and reaches a peak at 3 to 7 days [16, 17]. In clinical studies, Liu et al. have discovered a significant increase of OH-1-positive cells, OH-1 protein expression level, and OH-1 RNA transcription level at 6 hours after the onset of ICH. In addition, inflammatory cytokines (e.g., TNF-α, IL-1, and IL-10) were also increased significantly at 6 hours after the onset of ICH, which led to the increase of cell apoptosis in brain tissues surrounding the hematoma [18]. These findings may indicate that hematoma evacuation within 6 hours after ICH has the potential to alleviate the cytotoxic cascade caused by heme degradation and further improve the surgical and functional outcomes.

Hematoma volume, initial GCS, and the presence of acute hydrocephalus are generally considered the prognostic factors of ICH evacuation. However, our preliminary result shows low correlation between hematoma volume and 1-year mRS and moderate correlation between initial GCS score and 1-year mRS. This contradicted to previous studies which proved that hematoma volume is the most powerful determinant of outcome [19]. One possible explanation for the differing results may have to do with the fact that we performed MIS instead of traditional craniotomy. Technically, it is difficult to remove the thalamic hemorrhage by traditional craniotomy as it may incur worse prognosis, especially for large hematoma [20, 21]. In contrast, MIS can be done quickly (within 1.5 hours) to prevent secondary injury and cause minimal damage to the brain tissue, which may benefit the functional outcomes.

Since the thalamus is anatomically proximal to the brainstem and ventricle, patients with thalamic hemorrhage have a higher chance of intraventricular extension (which leads to IVH and hydrocephalus) and midbrain compression or destruction, which may lead to the poor prognosis. Likewise, previous studies have reported that thalamic hemorrhage is inherited with poor outcome than other types of ICH [4, 7, 22]. To evacuate thalamic hemorrhage efficiently while preserving functions, our primary goal was to ease the acute hydrocephalus and elevated ICP. In this study, thalamic hemorrhage volume were >30 mL in most cases, which affected not only the thalamus but also proximal structures such as internal capsule, putamen, globus pallidus, and

ventricles. We entered the thalamus only after identifying the rupture site during surgery. Such concept of taking IVH evacuation as the priority has been proved to result in better clinical outcomes, including lower shunt-dependent rate, lower pneumonia rate, and higher GOSE score [23].

Theoretically, to remove IVH as the priority may lead to lower clearance rate of thalamic hematoma; however, some of our cases demonstrated a high clearance rate of up to 90% or above. Before the thalamic hematoma hardens, the hematoma would enter the ventricle through the rupture site, where we could use the suction to evacuate the hematoma. It is opposite to the common belief that delayed evacuation is technically simpler due to partial liquefaction of the hematoma. Our concept concurs with a study which suggests that operation should be conducted in an ultrarapid manner within 24 hours after the onset of ICH since ICH usually begins to harden about 24 hours after the onset [24].

In fact, thalamic hemorrhage in most patients of this study expended laterally to critical functional areas, such as internal capsule and lentiform nucleus. Some neuroanatomical structures, such as corticospinal tract that passes through posterior limb of internal capsule, were damaged due to the hemorrhage expansion. Although we performed ultraearly MIS after the onset of ICH, the damage in critical areas had already occurred, which may explain the poor functional outcomes (mRS > 3) observed in some patients. Such findings were also reported and discussed in some studies [25, 26].

This study has some limitations. First, the selection of patients may result in biases. This study excluded patients with poor prognosis, such as patients with a lower GCS score (≤3), with trauma, with coagulopathy, or receiving antiplatelets or anticoagulants, and there were no patients undergoing MIS at more than 6 hours after the onset. Second, this study had a small sample size of seven patients only. With these limitations, the study results should be interpreted with caution. Further large-scale investigation is essential to confirm the findings in our study.

5. Conclusions

The timing to perform MIS is an important factor for surgical and functional outcomes. Although the evacuation of thalamic ICH is difficult due to the location, the results in this research indicate that MIS evacuation of thalamic hemorrhage within 6 hours is safe and effective. Moreover, this study shows that it led to improved outcome in selected patients. To our knowledge, this is the first study to focus on the benefit of ultrarapid MIS evacuation for thalamic hemorrhage.

Data Availability

The data used to support the findings of this study are available via contacting the corresponding author.

Ethical Approval

The study was approved by the institutional review board (IRB) of National Taiwan University Hospital (IRB number: 201611058RINA).

Conflicts of Interest

The authors declare that there is no conflict of interest regarding the publication of this paper.

Authors' Contributions

Kuan-Yu Chen and Woon-Man Kung contributed equally to this work.

Acknowledgments

The authors acknowledge Ministry of Science and Technology and the assistance from Formosa Biomedical Technology Corp. CRO Division in the editorial support.

References

[1] A. CJJv, L. MJA, R. GJE, T. Ivd, A. Algra, and K. CJM, "Incidence, case fatality, and functional outcome of intracerebral haemorrhage over time, according to age, sex, and ethnic origin: a systematic review and meta-analysis," *Lancet Neurology*, vol. 9, no. 2, pp. 167–176, 2010.

[2] T. Nagasaka, M. Tsugeno, H. Ikeda, T. Okamoto, S. Inao, and T. Wakabayashi, "Early recovery and better evacuation rate in neuroendoscopic surgery for spontaneous intracerebral hemorrhage using a multifunctional cannula: preliminary study in comparison with craniotomy," *Journal of Stroke and Cerebrovascular Diseases*, vol. 20, no. 3, pp. 208–213, 2011.

[3] D. Y. Cho, C. C. Chen, C. S. Chang, W. Y. Lee, and M. Tso, "Endoscopic surgery for spontaneous basal ganglia hemorrhage: comparing endoscopic surgery, stereotactic aspiration, and craniotomy in noncomatose patients," *Surgical neurology*, vol. 65, no. 6, pp. 547–555, 2006.

[4] L. T. Kuo, C. M. Chen, C. H. Li et al., "Early endoscope-assisted hematoma evacuation in patients with supratentorial intracerebral hemorrhage: case selection, surgical technique, and long-term results," *Neurosurgical Focus*, vol. 30, no. 4, 2011.

[5] M. R. Gaab, "Intracerebral hemorrhage (ICH) and intraventricular hemorrhage (IVH): improvement of bad prognosis by minimally invasive neurosurgery," *World Neurosurgery*, vol. 75, no. 2, pp. 206–208, 2011.

[6] W. M. Wang, C. Jiang, and H. M. Bai, "New insights in minimally invasive surgery for intracerebral hemorrhage," *Frontiers of Neurology and Neuroscience*, vol. 37, pp. 155–165, 2016.

[7] H. T. Luh, A. P. Huang, S. H. Yang et al., "Local hemostatic matrix for endoscope-assisted removal of intracerebral hemorrhage is safe and effective," *Journal of the Formosan Medical Association*, vol. 117, no. 1, pp. 63–70, 2018.

[8] T. Nagasaka, S. Inao, H. Ikeda, M. Tsugeno, and T. Okamoto, "Inflation-deflation method for endoscopic evacuation of intracerebral haematoma," *Acta neurochirurgica*, vol. 150, no. 7, pp. 685–690, 2008.

[9] L. B. Morgenstern, R. F. Frankowski, P. Shedden, W. Pasteur, and J. C. Grotta, "Surgical treatment for intracerebral hemorrhage (STICH): a single-center, randomized clinical trial," *Neurology*, vol. 51, no. 5, pp. 1359–1363, 1998.

[10] Hemphill JC 3rd, S. M. Greenberg, C. S. Anderson et al., "Guidelines for the management of spontaneous intracerebral hemorrhage: a guideline for healthcare professionals from the

American Heart Association/American Stroke Association," *Stroke*, vol. 46, no. 7, pp. 2032–2060, 2015.

[11] J. Scaggiante, X. Zhang, J. Mocco, and C. P. Kellner, "Minimally invasive surgery for intracerebral hemorrhage," *Stroke*, vol. 49, no. 11, pp. 2612–2620, 2018.

[12] D. F. Hanley, R. E. Thompson, M. Rosenblum et al., "Efficacy and safety of minimally invasive surgery with thrombolysis in intracerebral haemorrhage evacuation (MISTIE III): a randomised, controlled, open-label, blinded endpoint phase 3 trial," *The Lancet*, vol. 393, no. 10175, pp. 1021–1032, 2019.

[13] Y. Zuo, G. Cheng, D. K. Gao et al., "Gross-total hematoma removal of hypertensive basal ganglia hemorrhages: a long-term follow-up," *Journal of the Neurological Sciences*, vol. 287, no. 1-2, pp. 100–104, 2009.

[14] L. B. Morgenstern, A. M. Demchuk, D. H. Kim, R. F. Frankowski, and J. C. Grotta, "Rebleeding leads to poor outcome in ultra-early craniotomy for intracerebral hemorrhage," *Neurology*, vol. 56, no. 10, pp. 1294–1299, 2001.

[15] S. R. Robinson, T. N. Dang, R. Dringen, and G. M. Bishop, "Hemin toxicity: a preventable source of brain damage following hemorrhagic stroke," *Redox Report*, vol. 14, no. 6, pp. 228–235, 2009.

[16] S. Okubo, G. Xi, R. F. Keep, K. M. Muraszko, and Y. Hua, "Cerebral hemorrhage, brain edema, and heme oxygenase-1 expression after experimental traumatic brain injury," in *Brain Edema XV*, pp. 83–87, Springer Vienna, Vienna, 2013.

[17] Y. Liu, Z. Zhang, B. Luo, H. J. Schluesener, and Z. Zhang, "Lesional accumulation of heme oxygenase-1+ microglia/macrophages in rat traumatic brain injury," *Neuroreport*, vol. 24, no. 6, pp. 281–286, 2013.

[18] B. Liu, B. Hu, S. Shao et al., "CD163/hemoglobin oxygenase-1 pathway regulates inflammation in hematoma surrounding tissues after intracerebral hemorrhage," *Journal of Stroke and Cerebrovascular Diseases*, vol. 24, no. 12, pp. 2800–2809, 2015.

[19] Y. Béjot, C. Aboa-Eboulé, M. Hervieu et al., "The deleterious effect of admission hyperglycemia on survival and functional outcome in patients with intracerebral hemorrhage," *Stroke*, vol. 43, no. 1, pp. 243–245, 2012.

[20] A. Mendelow, B. Gregson, H. Fernandes et al., "Early surgery versus initial conservative treatment in patients with spontaneous supratentorial intracerebral haematomas in the International Surgical Trial in Intracerebral Haemorrhage (STICH): a randomised trial," *Lancet*, vol. 365, no. 9457, pp. 387–397, 2005.

[21] A. D. Mendelow, B. A. Gregson, E. N. Rowan, G. D. Murray, A. Gholkar, and P. M. Mitchell, "Early surgery versus initial conservative treatment in patients with spontaneous supratentorial lobar intracerebral haematomas (STICH II): a randomised trial," *Lancet*, vol. 382, no. 9890, pp. 397–408, 2013.

[22] A. Tanaka, S. Yoshinaga, Y. Nakayama, M. Kimura, and M. Tomonaga, "Cerebral blood flow and clinical outcome in patients with thalamic hemorrhages: a comparison with putaminal hemorrhages," *Journal of the Neurological Sciences*, vol. 144, no. 1-2, pp. 191–197, 1996.

[23] Y. Shimizu, K. Tsuchiya, and H. Fujisawa, "Endoscopic surgery for thalamic hemorrhage with intraventricular hemorrhage: effects of combining evacuation of a thalamic hematoma to external ventricular drainage," *Asian Journal of Neurosurgery*, vol. 14, no. 4, pp. 1112–1115, 2019.

[24] T. Nishihara, K. Nagata, S. Tanaka et al., "Newly developed endoscopic instruments for the removal of intracerebral hematoma," *Neurocritical Care*, vol. 2, no. 1, pp. 67–74, 2005.

[25] B. L. Neisewander, K. Hu, Z. Tan et al., "Location of thalamic hemorrhage impacts prognosis," *World Neurosurgery*, vol. 116, pp. e525–e533, 2018.

[26] V. Eslami, P. Tahsili-Fahadan, L. Rivera-Lara et al., "Influence of intracerebral hemorrhage location on outcomes in patients with severe intraventricular hemorrhage," *Stroke*, vol. 50, no. 7, pp. 1688–1695, 2019.

Hindawi
Behavioural Neurology
Volume 2021, Article ID 8824011, 6 pages
https://doi.org/10.1155/2021/8824011

Research Article

Efficacy of a Smart Antisnore Pillow in Patients with Obstructive Sleep Apnea Syndrome

Tsung-Te Chung,[1,2] **Ming-Tsung Lee**,[3,4] **Ming-Chou Ku**,[5] **Kai-Chieh Yang**,[2] **and Cheng-Yu Wei**[6]

[1]*Department of Otolaryngology, Show Chwan Memorial Hospital, Changhua 500, Taiwan*
[2]*Sleep Center, Chang Bing Show Chwan Memorial Hospital, Changhua 505, Taiwan*
[3]*Research Assistant Center, Show Chwan Memorial Hospital, Changhua 500, Taiwan*
[4]*Department of Nursing, Hungkuang University, Taichung 433, Taiwan*
[5]*Department of Orthopedics, Show Chwan Memorial Hospital, Changhua 500, Taiwan*
[6]*Department of Exercise and Health Promotion, College of Kinesiology and Health, Chinese Culture University, Taipei 111, Taiwan*

Correspondence should be addressed to Cheng-Yu Wei; yuyu@seed.net.tw

Received 12 August 2020; Revised 8 December 2020; Accepted 2 January 2021; Published 15 January 2021

Academic Editor: Muh-Shi Lin

Objective. Untreated obstructive sleep apnea syndrome (OSAS) increases the risk of cardiovascular, dementia, and motor vehicle accident events. However, continuous positive airway pressure (CPAP) which is the gold standard treatment is not acceptable for many patients with OSAS. Development of devices for the patients of nonadherence to CPAP is necessary. *Materials and Methods*. We evaluated the effect of the smart antisnore pillow (SAP) in patients with OSAS in a prospective, noncontrolled, nonrandomized, pilot study. According to the apnea-hypopnea index (AHI), they were divided into two groups: mild-to-moderate OSAS group and severe OSAS group. Single-night polysomnography (PSG) with application of a SAP was performed. Thirty patients, 15 males and 15 females, 33–82 years old (mean age, 59.3 ± 12.9 years), completed the smart antisnore pillow therapy test. Among them, 23 patients had mild-to-moderate OSAS. *Results*. The SAP significantly improved the snore number ($p = 0.018$), snore index ($p = 0.013$), oxygen denaturation index ($p = 0.001$), total AHI ($p = 0.002$), and supine AHI ($p = 0.002$) in the mild-to-moderate OSAS group, but there was no significant improvement in the severe OSAS group. *Conclusions*. We concluded that the SAP is an effective positional therapy device for patients with OSAS of mild-to-moderate severity.

1. Introduction

Obstructive sleep apnea syndrome (OSAS) is characterized by snoring, sleep-related breathing pause, and daytime sleepiness [1] and is a result of a partial or complete collapse of the upper airways during sleep [2]. Patients with OSAS have an increased risk for hypertension, stroke, dementia, cardiac arrhythmias, and motor vehicle accidents [3].

The common treatment options for OSAS include continuous positive airway pressure (CPAP), upper airway surgery, and oral appliance use. Positional therapy (PT) can also be used, which includes methods for preventing patients with OSAS from sleeping in the worst sleeping position, usually the supine position. PT is regarded as an effective secondary therapy for OSAS in the American Academy of Sleep Medicine (AASM) practice guidelines [4]. It has been found to have a significant influence on snoring, OSAS severity, and apnea-hypopnea index (AHI). PT has a potential value in position-dependent snoring and OSAS treatment [5].

There are many devices used to prevent patients with OSAS from sleeping in the supine position by strapping an object, such as a ball or a vest, on their back [6–8]. However, these devices are redundant during sleep for most people and might cause discomfort, resulting in a poor long-term compliance [7, 9]. Pillows are habitual devices used during sleep to keep the head in a comfortable position. However, limited studies have been published on the effect of positional pillows for reducing the AHI and/or OSAS [10–12], and these

pillows were usually made with a special shape, enabling neck extension [10, 11] or maintaining a person's head in the lateral position [12, 13].

Smart antisnoring pillows (SAP) are innovative devices that have an ordinary pillow shape, enabling sleeping in a natural position. These devices contain a shift control assembly base and mobile foam. The SAP device can detect the sleeper's snore by its audio sensors which are situated in the SAP device's lateral portion. The mobile foam can shift horizontally back and forth automatically after detecting a person's snoring sound, thereby changing their head and/or neck position. The mobile foam movement will stop until the snoring is undetected. The aim of this study was to evaluate the efficacy of SAP devices in the treatment of patients with OSAS.

2. Methods

2.1. Protocol Design and Participants. This was a single-center, single-treatment, noncontrolled, nonrandomized study. The patients were recruited from the population of the Chang Bing Show Chwan Memorial Hospital Sleep Center. The inclusion criteria were as follows: (1) age > 18 years, (2) clinical history of OSAS (snoring or breathing pause at sleep, daytime sleepiness) over 6 months, and (3) overnight baseline polysomnography (PSG) confirming an AHI ≥ 5 events/hour. The exclusion criteria included (1) serious medical or psychiatric diseases, such as heart failure, stroke, or chronic respiratory disorders, and (2) neck or shoulder problems preventing sleeping in a lateral position or turning the head. The eligible patients underwent a second, experimental, overnight PSG with the SAP device within 2 months after the baseline PSG.

This study was approved by the Institutional Review Board of Show Chwan Memorial Hospital. Informed consent was obtained from all patients before enrolment in this study. This study was performed in compliance with the Declaration of Helsinki.

2.2. Measurement of Sleep Quality. Sleep quality in this study was measured using two sleep questionnaires: the Pittsburgh Sleep Quality Index (PSQI) and the Epworth Sleepiness Scale (ESS). Patients completed these questionnaires prior to the baseline PSG.

2.3. PSG. PSG recording was performed in the Chang Bing Show Chwan Memorial Hospital Sleep Center Laboratory, which was accredited by the Taiwan Society of Sleep Medicine, using a digital polygraph system (Embla N7000, Broomfield, CO, USA) while the patients were breathing room air. Snoring was recorded using a piezo snore sensor positioned at the neck, over the larynx. A body position sensor was attached on the patients' anterior chest to define the posture, which was defined as supine and nonsupine (including right side, left side, or prone). Synchronized digital video recordings were also obtained on all patients and reviewed during the scoring process to confirm the body position. The sleep stage and obstructive respiratory events were scored according to the 2007 AASM manual. Snoring events were confirmed after deleting the abnormal spike wave. The noise caused by the SAP motion and operating shift control assembly was small and would not cause PSG snoring sensor recording errors. Obstructive apnea was defined as a 90% reduction in oronasal airflow for at least 10 seconds with continued ribcage and/or abdominal excursions. Hypopnea was defined as a 30% reduction in the airflow for at least 10 seconds with >3% oxygen desaturation. AHI was defined as the mean number of obstructive apnea and hypopnea events per hour of sleep.

2.4. Description of the SAP Device. The SAP device (US Patent No. US7676870 B2) is 50 cm × 30 cm × 11.5 cm in size and shaped as a usual pillow. It is composed of a shift control assembly base and a mobile seat foam. Two audio sensors that detect a person's snoring sound are situated in the lateral portion of the pillow (Figure 1(a)). When a snoring sound is detected, the shift control assembly is automatically activated to induce movement in the mobile seat. The mobile foam shifts horizontally back and forth, thus achieving movement of the head and/or neck, until the snoring ceases or the snore volume is undetectable (Figure 1(b)). In the present study, the SAP was set to trigger motion after detecting four consecutive snoring sounds.

2.5. Statistical Analysis. Continuous data were expressed as mean ± standard deviation, and categorical data were expressed as numbers with percentages. Based on the baseline AHI, patients were divided into two groups: mild-to-moderate OSAS group ($5 \leq \text{AHI} \leq 30$) and severe OSAS group (AHI > 30). The paired t-test or Wilcoxon's signed-rank test was used to compare the differences in the snoring number, snoring index, and AHI between the baseline and SAP therapy PSG. A two-tailed p value < 0.05 was considered statistically significant. Data analysis was performed using the statistical package IBM SPSS Statistics for Windows, version 24.0 (IBM Corp., Armonk, NY, USA).

3. Results

3.1. Demographic and Clinical Characteristics. Thirty patients, 15 males and 15 females, completed baseline PSG and SAP therapy PSG. All patients tolerated the experimental SAP treatment well. The mean age was 59.3 ± 12.9 (range, 33–82) years, the mean body mass index (BMI) was 27.6 ± 3.6 (range, 21.5–38.9) kg/m^2, and the mean neck circumference was 37.03 ± 3.32 cm. The mean ESS and PSQI scores were 7.5 ± 3.5 and 9.10 ± 3.93, respectively. The patients' demographic characteristics are summarized in Table 1.

3.2. PSG. The baseline AHI for all patients was in the range from 5.2 to 75.1 events/hour. There were 23 patients with mild-to-moderate OSAS and seven with severe OSAS. The SAP therapy AHI was in the range from 0.7 to 82.2 events/hour. The total AHI decreased in 22 patients (73%) and increased in 8 patients (27%) with the SAP therapy. The individual baseline and SAP therapy AHIs are shown in Figure 2.

The characteristics of the baseline and SAP therapy PSG for all patients are shown in Table 2. The SAP significantly decreased the snore number and snore index from

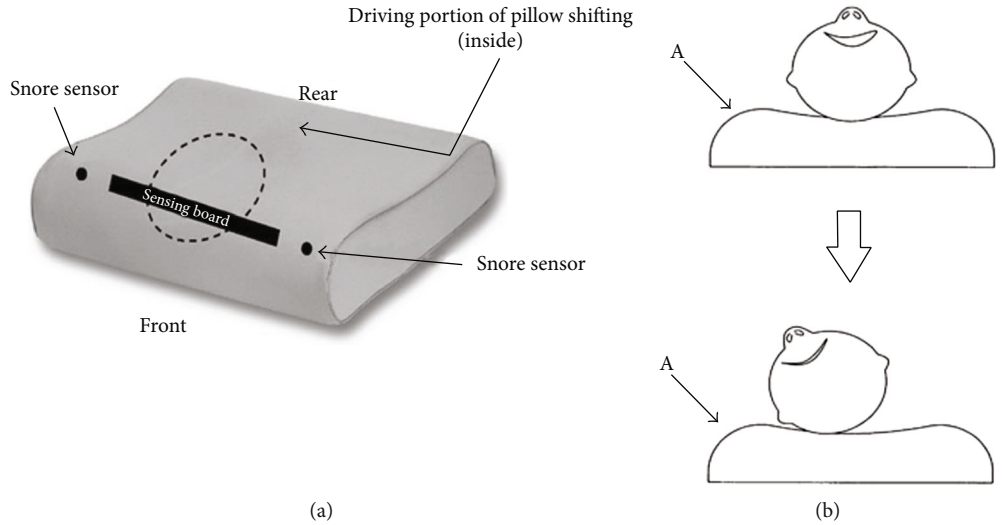

Figure 1: (a) Diagram of the smart antisnore pillow (SAP) device. (b) The working diagram of SAP: the head changes position when the snore sensors detect snoring and the SAP mobile foam shifts horizontally (A: snore sensor; ⟶: points out A's location).

Table 1: Demographic characteristics of 30 patients.

Variable	Numbers/mean ± SD
Female/male	15/15
Age (years)	59.30 ± 12.93
BMI (kg/m^2)	27.35 ± 3.62
ESS	7.53 ± 3.53
PSQI	9.10 ± 3.93
Neck circumference (cm)	37.03 ± 3.32

Data are given as numbers or mean ± SD. BMI: body mass index; ESS: Epworth Sleepiness Scale; PSQI: Pittsburgh Sleep Quality Index.

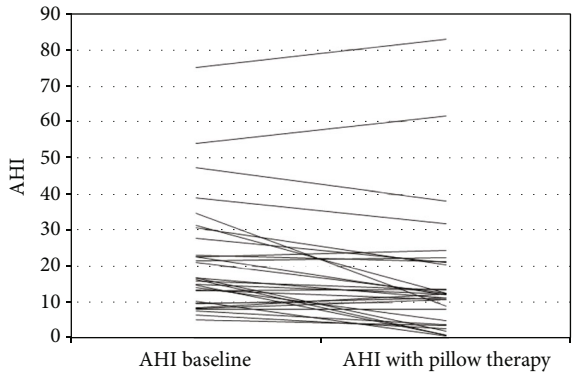

Figure 2: The individual effect of SAP therapy on the apnea-hypopnea index in 30 patients with obstructive sleep apnea.

2406.7 ± 1173.5 to 1693.8 ± 1071.4 events ($p = 0.004$) and from 501.5 ± 235.1 to 360.9 ± 218.1 events/hour ($p = 0.003$), respectively. The oxygen desaturation index (ODI) decreased from 15.8 ± 16.3 to 7.8 ± 2.5 ($p = 0.007$), but the average oxygen saturation did not show obvious change ($p = 0.322$). The mean AHI also significantly decreased from 21.8 ± 15.7 to 16.5 ± 17.8 events/hour ($p = 0.001$). In particular, the supine AHI was significantly decreased from 27.3 ± 17.5 to 20.4 ± 19.9 events/hour ($p = 0.005$), but the SAP has no significant effect on the nonsupine AHI ($p = 0.984$). Although stage N1 increased from 36.9 ± 20.1 to 45.9 ± 24.0 ($p = 0.037$) after SAP therapy, there was no obvious change in sleep efficiency, stages N2 and N3, and REM stage.

Comparison of the significant PSG variables, snoring number, snore index, and total and supine AHI between the baseline and SAP therapy PSG in the mild-to-moderate OSAS and severe OSAS groups is presented in Table 3. The SAP had a significant effect in decreasing the ODI, snoring number, snore index, and total and supine AHI in the mild-to-moderate OSAS group but had no significant effect in the severe OSAS group. Furthermore, the SAP had no significant effect on the average oxygen saturation and nonsupine AHI in both groups.

4. Discussion

CPAP is the gold standard treatment for OSAS [14]. Untreated OSAS increases the risk of fatal cardiovascular events [15]. In addition, those patients are also associated with significant psychosocial consequences, such as decreased quality of life, impaired cognitive function, and increased depressive symptoms [16]. Despite the known risks of untreated OSAS and documented benefits of CPAP, nonadherence to therapy is a major issue. The CPAP adherence rates are variable; in the Asian populations, the rates are 38–90% [17–24], whereas in the Western populations, there is a 37.3–87.5% adherence rate [25–30]. There are many factors affecting the CPAP adherence in patients with OSAS, including age, comorbidities, ESS score, AHI, treatment titration procedures, device factors (cost, inconvenience, and discomfort), and psychological and social factors [14, 19, 20, 24]. Thus, PT or alternative therapies are valuable for patients with OSAS with nonadherence to CPAP.

In this study, the SAP device could reduce the total and supine AHI, snore number, and snore index in patients with mild-to-moderate OSAS. To the best of our knowledge, SAP

Table 2: Polysomnographic variables of baseline and SAP therapy of 30 patients.

Variable	Baseline	SAP therapy	p value
Sleep efficiency (%)	77.8 ± 12.1	75.7 ± 13.8	0.473
Stage N1 (%)	36.9 ± 20.1	45.9 ± 24.0	0.037
Stage N2 (%)	49.0 ± 20.6	43.1 ± 22.1	0.157
Stage N3 (%)	1.1 ± 3.0	0.2 ± 0.4	0.132
REM (%)	13.0 ± 7.7	10.8 ± 5.3	0.086
Supine body position (%)	74.3 ± 23.7	73.1 ± 24.8	0.783
Nonsupine body position (%)	25.7 ± 23.7	26.9 ± 24.8	0.781
Arousal index (events/hour)	30.0 ± 19.7	32.91 ± 13.2	0.346
Average oxygen saturation (%)	91.0 ± 17.3	94.2 ± 2.3	0.322
ODI (events/hour)	15.8 ± 16.3	7.8 ± 2.5	0.007
Snore number	2406.7 ± 1173.5	1693.8 ± 1071.4	0.004
Snore index (events/hour)	501.5 ± 235.1	360.9 ± 218.1	0.003
AHI (events/hour)	21.8 ± 15.7	16.5 ± 17.8	0.001
Supine AHI (events/hour)	27.3 ± 17.5	20.4 ± 19.9	0.005
Nonsupine AHI (events/hour)	4.0 ± 6.3	4.1 ± 9.3	0.984

Data are given as mean ± SD. SAP: smart antisnore pillow; REM: rapid eye movement; ODI: oxygen denaturation index; AHI: apnea-hypopnea index.

Table 3: The effects of SAP in different baseline AHI severity categories.

Numbers	$5 \leq AHI \leq 30$			$AHI > 30$		
	23			7		
Variable	Baseline	SAP	p value	Baseline	SAP	p value
Average oxygen saturation (%)	94.5 ± 1.6	95.9 ± 1.3	0.072	92.5 ± 3.1	92.4 ± 3.4	0.958
ODI (events/hour)	10.3 ± 1.9	2.9 ± 2.6	0.001	28.5 ± 19.4	14.6 ± 8.7	0.244
Snore number	2528.0 ± 1231.3	1786.6 ± 1050.7	0.018	2007.9 ± 924.5	1388.7 ± 1165.5	0.063
Snore index (events/hour)	524.8 ± 247.9	377.0 ± 218.7	0.013	425.0 ± 181.2	307.9 ± 224.2	0.176
AHI (events/hour)	14.8 ± 6.2	10.3 ± 7.2	0.002	44.6 ± 15.9	36.6 ± 27.0	0.128
Supine AHI (events/hour)	21.4 ± 13.5	14.5 ± 12.2	0.002	46.9 ± 15.0	40.0 ± 28.1	0.398
Nonsupine AHI (events/hour)	14.7 ± 11.5	11.8 ± 15.0	0.401	24.3 ± 20.7	19.3 ± 12.7	0.655

Data are given as mean ± SD. SAP: smart antisnore pillow; ODI: oxygen denaturation index; AHI: apnea-hypopnea index.

is the first mobile positional therapy device to alter a person's head and/or neck position without changing the trunk position. At the same time, the arousal index did not increase during SAP therapy. The traditional PT included preventing patients with OSAS from sleeping in the supine position and keeping the trunk in a lateral position [31]. However, some studies showed that the head and/or neck position can affect the upper airway with the trunk in the supine position. Head posture had a marked effect on the collapsibility and site of collapse of the passive upper airway by anaesthesia [32]. The sniffing position with neck extension could increase the oropharyngeal airway size to maximum and decrease the closing pressures of the oropharynx and velopharynx in paralyzed patients with OSAS [33]. In a drug-induced sleep endoscopic observation, head rotation improved the upper airway collapse in supine-sleeping patients with OSAS [34]. van Kesteran and colleagues used two position sensors to detect the head and body position simultaneously during sleep. Their data showed that in 46.2% of the trunk supine position-dependent group, the head position considerably influenced the AHI (AHI was >5 higher when the head was also in a supine position compared to when the head was turned to the side). AHI might be alleviated through rotation of the head sideways while the trunk remains in a supine position [35]. In our study, the SAP device could reduce the supine AHI in patients with OSAS, indicating that the SAP-induced change in the head and neck position could open the collapsed upper airway even when the truck remained in a supine position. This result was similar to that of van Kesteran et al.'s investigation. The SAP had no significant improvement effect on the nonsupine AHI. These results implied that the SAP motion would not change the head and neck position significantly when a person's trunk is in a lateral and prone position.

The ODI is the average number of times per hour that oxygen saturation decreases per hour. It has a stronger

correlation and is a better predictor for AHI in patients with OSAS [36]. In our study, the SAP device also improved the parameter in patients with mild-to-moderate OSAS. The ODI was associated with hypertension [37]. Further studies should be designed for the long-term usage of the SAP device.

Our study has some limitations. First, we recognize the limited number of patients in this study. Second, the single-night baseline and SAP therapy PSG might have induced first-night effect bias. Third, we did not follow-up the AHI and adherence after long-term usage of SAP therapy.

5. Conclusions

In conclusion, the SAP is an effective positional therapy device that can improve the total and supine AHI, snore number, and snore index in patients with mild-to-moderate OSAS by shifting their head and neck position. However, this device had no significant effect in patients with severe OSAS. Future studies should be directed towards understanding the oropharyngeal anatomic change during SAP activity, its long-term effect, neck comfort, and patients' compliance.

Data Availability

Data measured or analysed during this study are available from the corresponding author on request.

Conflicts of Interest

The authors declare that there is no conflict of interest regarding the publication of this paper.

Acknowledgments

This study was supported by Hong Jian Technology Co., Ltd.

References

[1] K. P. Strohl and S. Redline, "Recognition of obstructive sleep apnea," *American Journal of Respiratory and Critical Care Medicine*, vol. 154, no. 2, pp. 279–289, 1996.

[2] M. S. Badr, "Pathophysiology of upper airway obstruction during sleep," *Clinics in Chest Medicine*, vol. 19, no. 1, pp. 21–32, 1998.

[3] T. Young, J. Skatrud, and P. E. Peppard, "Risk factors for obstructive sleep apnea in adults," *JAMA*, vol. 291, no. 16, pp. 2013–2016, 2004.

[4] Adult Obstructive Sleep Apnea Task Force of the American Academy of Sleep Medicine, "Clinical guideline for the evaluation, management and long-term care of obstructive sleep apnea in adults," *Journal of Clinical Sleep Medicine*, vol. 5, no. 3, pp. 263–276, 2009.

[5] M. J. Ravesloot, J. P. van Maanen, L. Dun, and N. de Vries, "The undervalued potential of positional therapy in position-dependent snoring and obstructive sleep apnea-a review of the literature," *Sleep and Breathing*, vol. 17, no. 1, pp. 39–49, 2013.

[6] J. T. Maurer, B. A. Stuck, G. Hein, T. Verse, and K. Hormann, "Schlafapnoetherapie mit einer neuartigen Rückenlage-Verhinderungs-Weste," *DMW - Deutsche Medizinische Wochenschrift*, vol. 128, no. 3, pp. 71–75, 2003.

[7] A. Oksenberg, D. Silverberg, D. Offenbach, and E. Arons, "Positional therapy for obstructive sleep apnea patients: a 6-month follow-up study," *The Laryngoscope*, vol. 116, no. 11, pp. 1995–2000, 2006.

[8] M. A. Skinner, R. N. Kingshott, S. Filsell, and D. R. Taylor, "Efficacy of the 'tennis ball technique' versus nCPAP in the management of position-dependent obstructive sleep apnoea syndrome," *Respirology*, vol. 13, no. 5, pp. 708–715, 2008.

[9] S. Wenzel, E. Smith, R. Leiacker, and Y. Fischer, "Efficacy and longterm compliance of the vest preventing the supine position in patients with obstructive sleep apnea," *The Laryngorhinootologie*, vol. 86, no. 8, pp. 579–583, 2007.

[10] C. A. Kushida, S. Rao, C. Guilleminault et al., "Cervical positional effects on snoring and apneas," *Sleep Research Online*, vol. 2, no. 1, pp. 7–10, 1999.

[11] C. A. Kushida, C. M. Sherrill, S. C. Hong, L. Palombini, P. Hyde, and W. C. Dement, "Cervical positioning for reduction of sleep-disordered breathing in mild-to-moderate OSAS," *Sleep And Breathing*, vol. 5, no. 2, pp. 71–78, 2001.

[12] N. A. Zuberi, K. Rekab, and H. V. Nguyen, "Sleep apnea avoidance pillow effects on obstructive sleep apnea syndrome and snoring," *Sleep And Breathing*, vol. 8, no. 4, pp. 201–207, 2004.

[13] J. Newell, O. Mairesse, and D. Neu, "Can positional therapy be simple, effective and well tolerated all together? A prospective study on treatment response and compliance in positional sleep apnea with a positioning pillow," *Sleep And Breathing*, vol. 22, no. 4, pp. 1143–1151, 2018.

[14] A. M. Sawyer, N. S. Gooneratne, C. L. Marcus, D. Ofer, K. C. Richards, and T. E. Weaver, "A systematic review of CPAP adherence across age groups: clinical and empiric insights for developing CPAP adherence interventions," *Sleep Medicine Reviews*, vol. 15, no. 6, pp. 343–356, 2011.

[15] T. Young, M. Palta, J. Dempsey, J. Skatrud, S. Weber, and S. Badr, "The occurrence of sleep-disordered breathing among middle-aged adults," *New England Journal of Medicine*, vol. 328, no. 17, pp. 1230–1235, 1993.

[16] T. Akashiba, S. Kawahara, T. Akahoshi et al., "Relationship between quality of life and mood or depression in patients with severe obstructive sleep apnea syndrome," *Chest*, vol. 122, no. 3, pp. 861–865, 2002.

[17] D. S. Hui, D. K. Choy, T. S. Li et al., "Determinants of continuous positive airway pressure compliance in a group of Chinese patients with obstructive sleep apnea," *Chest*, vol. 120, no. 1, pp. 170–176, 2001.

[18] S. F. Hussain, M. Irfan, Z. Waheed, N. Alam, S. Mansoor, and M. Islam, "Compliance with continuous positive airway pressure (CPAP) therapy for obstructive sleep apnea among privately paying patients- a cross sectional study," *BMC Pulmonary Medicine*, vol. 14, no. 1, p. 188, 2014.

[19] C. H. K. Lee, L. C. Leow, P. R. Song, H. Li, and T. H. Ong, "Acceptance and adherence to continuous positive airway pressure therapy in patients with obstructive sleep apnea (OSA) in a Southeast Asian privately funded healthcare system," *Sleep Science*, vol. 10, no. 2, pp. 57–63, 2017.

[20] B. Tan, A. Tan, Y. H. Chan, Y. Mok, H. S. Wong, and P. P. Hsu, "Adherence to continuous positive airway pressure therapy in Singaporean patients with obstructive sleep apnea," *American Journal of Otolaryngology*, vol. 39, no. 5, pp. 501–506, 2018.

[21] T. Tanahashi, J. Nagano, Y. Yamaguchi, C. Kubo, and N. Sudo, "Factors that predict adherence to continuous positive airway pressure treatment in obstructive sleep apnea patients: a

prospective study in Japan," *Sleep and Biological Rhythms*, vol. 10, no. 2, pp. 126–135, 2012.

[22] T. Tokunaga, T. Ninomiya, Y. Kato et al., "Long-term compliance with nasal continuous positive airway pressure therapy for sleep apnea syndrome in an otorhinolaryngological office," *European Archives of Oto-Rhino-Laryngology*, vol. 270, no. 8, pp. 2267–2273, 2013.

[23] Y. Wang, W. Gao, M. Sun, and B. Chen, "Adherence to CPAP in patients with obstructive sleep apnea in a Chinese population," *Respiratory Care*, vol. 57, no. 2, pp. 238–243, 2012.

[24] M.-C. Yang, C.-Y. Lin, C.-C. Lan et al., "Factors affecting CPAP acceptance in elderly patients with obstructive sleep apnea in Taiwan," *Respiratory Care*, vol. 58, no. 9, pp. 1504–1513, 2013.

[25] R. Budhiraja, C. A. Kushida, D. A. Nichols et al., "Predictors of sleepiness in obstructive sleep apnoea at baseline and after 6 months of continuous positive airway pressure therapy," *European Respiratory Journal*, vol. 50, no. 5, 2017.

[26] C. L. Chai-Coetzer, Y.-M. Luo, N. A. Antic et al., "Predictors of long-term adherence to continuous positive airway pressure therapy in patients with obstructive sleep apnea and cardiovascular disease in the SAVE study," *Sleep*, vol. 36, no. 12, pp. 1929–1937, 2013.

[27] A. R. Jacobsen, F. Eriksen, R. W. Hansen et al., "Determinants for adherence to continuous positive airway pressure therapy in obstructive sleep apnea," *PLoS One*, vol. 12, no. 12, article e0189614, 2017.

[28] A. Lanza, S. Mariani, M. Sommariva et al., "Continuous positive airway pressure treatment with nasal pillows in obstructive sleep apnea: long-term effectiveness and adherence," *Sleep Medicine*, vol. 41, pp. 94–99, 2018.

[29] A. McMillan, D. J. Bratton, R. Faria et al., "Continuous positive airway pressure in older people with obstructive sleep apnoea syndrome (PREDICT): a 12-month, multicentre, randomised trial," *The Lancet Respiratory Medicine*, vol. 2, no. 10, pp. 804–812, 2014.

[30] N. Nadal, J. de Batlle, F. Barbé et al., "Predictors of CPAP compliance in different clinical settings: primary care versus sleep unit," *Sleep and Breathing*, vol. 22, no. 1, pp. 157–163, 2018.

[31] R. D. Cartwright, "Effect of sleep position on sleep apnea severity," *Sleep*, vol. 7, no. 2, pp. 110–114, 1984.

[32] J. H. Walsh, K. J. Maddison, P. R. Platt, D. R. Hillman, and P. R. Eastwood, "Influence of head extension, flexion, and rotation on collapsibility of the passive upper airway," *Sleep*, vol. 31, no. 10, pp. 1440–1447, 2008.

[33] S. Isono, A. Tanaka, T. Ishikawa, Y. Tagaito, and T. Nishino, "Sniffing position improves pharyngeal airway patency in anesthetized patients with obstructive sleep apnea," *Anesthesiology*, vol. 103, no. 3, pp. 489–494, 2005.

[34] F. Safiruddin, I. Koutsourelakis, and N. de Vries, "Analysis of the influence of head rotation during drug-induced sleep endoscopy in obstructive sleep apnea," *The Laryngoscope*, vol. 124, no. 9, pp. 2195–2199, 2014.

[35] E. R. van Kesteren, J. P. van Maanen, A. A. Hilgevoord, D. M. Laman, and N. de Vries, "Quantitative effects of trunk and head position on the apnea hypopnea index in obstructive sleep apnea," *Sleep*, vol. 34, no. 8, pp. 1075–1081, 2011.

[36] F. Chung, P. Liao, H. Elsaid, S. Islam, C. M. Shapiro, and Y. Sun, "Oxygen desaturation index from nocturnal oximetry: a sensitive and specific tool to detect sleep-disordered breathing in surgical patients," *Anesthesia & Analgesia*, vol. 114, no. 5, pp. 993–1000, 2012.

[37] F. Frangopoulos, I. Nicolaou, S. Zannetos, N.-T. Economou, T. Adamide, and G. Trakada, "Association between respiratory sleep indices and cardiovascular disease in sleep apnea-a community-based study in Cyprus," *Journal of Clinical Medicine*, vol. 9, no. 8, p. 2475, 2020.

Hindawi
Behavioural Neurology
Volume 2021, Article ID 8866763, 7 pages
https://doi.org/10.1155/2021/8866763

Research Article

Prevalence and Associated Factors of Visual Hallucinations in Patients with Vascular Cognitive Impairment

Chih-Lin Chen,[1] Min-Hsien Hsu,[2] Chao-Hsien Hung,[1] Pai-Yi Chiu,[2,3] and Chung-Hsiang Liu[4]

[1]*Department of Neurology, Chang Bing Show Chwan Memorial Hospital, Changhua 505, Taiwan*
[2]*Department of Neurology, Show Chwan Memorial Hospital, Changhua 500, Taiwan*
[3]*Department of Nursing, College of Nursing and Health Sciences, Da-Yeh University, Dacun, Changhua 515, Taiwan*
[4]*Department of Neurology, China Medical University Hospital, Taichung 404, Taiwan*

Correspondence should be addressed to Pai-Yi Chiu; paiyibox@gmail.com and Chung-Hsiang Liu; greengen@gmail.com

Received 2 September 2020; Revised 16 December 2020; Accepted 30 December 2020; Published 11 January 2021

Academic Editor: Muh-Shi Lin

Visual hallucinations (VHs) are striking features for dementia, especially dementia with Lewy bodies (DLB). We aimed to study the frequency and associated factors of VH in vascular cognitive impairment (VCI) and investigate the feasibility of clinically diagnosing the mixed pathology of VCI with DLB. This is a multicentre registration study. A consecutive series of VCI patients with and without dementia were enrolled. Frequency of VH and associated factors, including age, gender, education, disease severity, DLB clinical features, vascular risk factors, cognitive function, and neuropsychiatric symptoms, were compared between VCI with VH (VH+) and without VH (VH−). Among the 1281 patients analysed, 155 (12.1%) had VH. The VH+ group was older ($t = 5.07$; $p < 0.001$), was more likely to be female ($\chi^2 = 13.46$; $p < 0.001$), and has a higher clinical dementia rating ($\chi^2 = 70.51$; $p < 0.001$). After adjusting for age, gender, and disease severity, the VH+ group had poorer cognition and more severe neuropsychiatric symptoms. The VH+ group was more associated with DLB features in fluctuating cognition (OR = 2.48; $p < 0.001$), parkinsonism (OR = 1.85; $p = 0.001$), rapid eye movement (REM) behavioral disorder (OR = 4.56; $p < 0.001$), and ≧2 DLB core features (OR = 26.01; $p < 0.001$). VCI patients with VH tend to have more severe dementia, neuropsychiatric symptoms, and poorer cognitive function. Additionally, highly associated with clinical DLB features in VCI with VH raised the possibility of mixed pathology with DLB in this group. More than two core features in VCI might help in diagnosing a mixed pathology with DLB.

1. Introduction

Vascular cognitive impairment (VCI) or vascular dementia (VaD) is the second most common form of dementia [1]. Visual hallucinations (VHs) occasionally occur in patients with VCI, having a great impact on both patients and their caregivers [2–4]. Robust evidence has shown that VH is more common in patients that have dementia with Lewy bodies (DLB) than in Alzheimer's disease (AD), VaD, or other forms of dementia [2, 5–7]. Therefore, VH, along with fluctuations in cognition, parkinsonism, and rapid eye movement (REM) sleep behavior disorder (RBD), is the core clinical feature for clinically diagnosing DLB. Previous studies have shown that prevalence of characteristic VH (complex, well-formed, and detailed VH) is much higher in DLB compared to other forms of dementia [5–8]. In our previous research article, we also provided evidence of VH in AD should also be considered the mixed pathologies with DLB [8]. However, few studies have addressed the prevalence and association factors of VH in patients with VCI or other non-DLB dementia [2].

The connection between the core clinical features for diagnosing DLB with Lewy body pathology is based mainly on the findings of clinical and pathological studies of DLB. These demonstrated relatively good specificity, accuracy, and variable sensitivity [9–11]. This is revised from the previous consensus criteria, which excluded DLB in subjects with CVD or other brain disorders [12, 13]. The newest consensus

criteria for DLB in 2017 stated that patients with DLB and comorbidities such as CVD or other brain disorders should not be excluded from potentially having DLB and that a mixed pathology should be considered [7]. Therefore, it is reasonable to propose in cases with VCI that if there is one typical core feature for diagnosing DLB, i.e., VH, mixed pathology with DLB should be investigated if at least one of the other core clinical DLB features or indicative biomarkers is present. According to the consensus criteria for DLB, two core features or one core feature plus one indicative biomarker is required for diagnosing probable DLB [7]. Furthermore, clinical-pathological studies on non-DLB dementia also provide evidence for mixed pathology of AD with DLB in cases where AD is comorbid with core DLB features [8, 14–16].

Diagnosing VH in dementia, especially in an amnesia-predominant disease like AD, is often confounded with a false memory of remote events due to impairment of source monitoring [17–19]. In that case, VH is usually less complex not persistent and is associated with delusions [20, 21]. This makes it difficult to differentiate with a remote memory of confabulations. However, complex, well-formed, and detailed VH, which is considered more characteristic for VH in DLB, should be more specific than actual VH. This type of impairment could be considered as a target feature for predicting mixed Lewy body dementia and other brain disorders.

To investigate the possible mixed Lewy body pathology in VCI with VH, in this study, only characteristic complex, well-formed, and detailed VHs were regarded as DLB type VH. These patients were allocated to the VH+ group. Due to the high specificity of clinically diagnosing DLB according to the consensus criteria, we proposed that by observing its association with other DLB clinical features, we can predict the possible mixed Lewy body pathology in VCI with VH. Besides, we also investigated the associated factors of VH in VCI including the demographical data, VCI subtypes, CVD subtypes, cognitive, neuropsychiatric, and vascular risk factors. Additionally, we investigated possible explanations of the associations.

2. Materials and Methods

2.1. Participants. This is a cross-sectional retrospective study. From October 2015 to July 2019, a consecutive series of participants from 3 regional hospitals in Taiwan were registered. A diagnosis of VCI was made according to the criteria for probable VaD, possible VaD, and vascular mild cognitive impairment (MCI) in the 2011 American Heart Association/American Stroke Association (AHA/ASA) criteria for VCI [22]. All patients had received at least a cerebral computed tomography (CT) or a cerebral magnetic resonance imaging (MRI) and a set of blood screening tests for ruling out other possibilities of cognitive decline. The following information was used in this study:

(1) Age, gender, education, disease duration, vascular risk factors (VRFs), and current medication

(2) Dementia severity using the Clinical Dementia Rating (CDR) scale and the sum of boxes of CDR (CDR-SB) [23]

(3) Clinical Lewy body dementia (LBD) features, including cognitive fluctuations, parkinsonism, RBD, auditory hallucinations (AHs), delusions, and depression [7]

(4) Cognitive performance on the Montreal Cognitive Assessment (MoCA) [24] and the Cognitive Abilities Screening Instrument, Chinese version (CASI C-2.0) [25]

(5) Activities of daily living assessment by Instrumental Activities of Daily Living (IADL) scale [26]

(6) Neuropsychiatric symptoms in the 12-item version of the Neuropsychiatric Inventory (NPI) based on observations within the past month [27]

2.2. Assessment of VH and Other DLB Core Clinical Features. Each patient and his or her primary caregiver were interviewed by a trained neuropsychologist for assessing VH and other core clinical features. VH was diagnosed when a clinical history of recurrent well-formed, complex, and detailed VH was present. The fluctuation of cognition was diagnosed when a Mayo Fluctuation Composite Score (MFCS) > 2 was present [28]. Parkinsonism was diagnosed when bradykinesia plus at least one of the following was present: resting tremor, rigidity, and instability. RBD was diagnosed according to the minimal criteria for clinically diagnosing RBD [29].

2.3. Data Analysis. For the statistical analyses, SPSS version 22.0 for Windows (IBM, SPSS Inc., Chicago) was used. Comparisons were made between the VH+ and VH- groups in terms of the demographic data, including CDR, clinical features, IADL, MoCA, CASI, and composite scores of the NPI. All data were analysed using an independent t-test, and the odds ratios (ORs) were adjusted for age, gender, and dementia severity. VCI subtypes (vascular MCI, probable VaD, and possible VaD) and CVD subtypes (multi-infarct, strategic infarct, subcortical lacunes, Binswanger disease, complex combination, hemorrhage, and others) were analysed using the chi-square test. DLB core clinical features (fluctuation, parkinsonism, and RBD), VRFs, and current medication were analysed using the chi-square test. All ORs were adjusted for age, gender, and dementia severity. To compare the associations between clinical symptoms/sign characteristic of DLB and neuroimaging variables between the VH+ and VH- groups, all ORs were adjusted for age, gender, and dementia severity.

2.4. Ethical Considerations. The participants were selected from a dementia database of Show Chwan Healthcare System. The study design was retrospective, and the data were analysed anonymously. The Committee for Medical Research Ethics of Show Chwan Memorial Hospital reviewed the project, and the Data Inspectorate approved the study.

Table 1: Demographic and background characteristics of VCI patients with or without visual hallucinations (VHs) adjusted for age, gender, and disease severity by CDR.

	Mean (SD, range)		Nonadjusted		Adjusted	
	VH+, mean (SD)	VH−, mean (SD)	t/χ^2	p	OR (95% CI)	p
N	155	1126				
Age, years	79.6 (8.9)	75.2 (10.3)	5.07	<0.001	NA	
CDR 0.5/1/2/3	12/40/54/49	407/311/256/152	70.51	<0.001	NA	
Gender, female (%)	98 (63.2)	535 (47.9%)	13.46	<0.001	NA	
Education, years	3.4 (3.9)	5.0 (4.5)	-4.41	<0.001	0.97 (0.93-1.02)	NS
Duration, years	3.9 (6.0)	3.1 (5.3)	1.82	NS	1.02 (0.99-1.05)	NS
Dementia, N (%)	152 (98.1)	939 (83.4)	23.22	<0.001	4.43 (1.35-14.53)	<0.001
CDR-SB	11.6 (4.8)	7.6 (5.5)	9.67	<0.001	1.16 (1.04-1.28)	0.007
IADL	1.0 (1.9)	2.9 (3.1)	-10.65	<0.001	0.85 (0.76-0.94)	0.002
MoCA	5.1 (5.5)	8.5 (7.3)	-6.86	<0.001	1.02 (0.97-1.06)	NS
CASI	31.8 (24.7)	44.7 (28.0)	-6.01	<0.001	1.02 (1.00-1.03)	0.012
NPI	17.4 (14.8)	8.0 (9.4)	7.66	<0.001	1.06 (1.04-1.07)	<0.001
VaMCI/PrVaD/PoVaD	3/88/64	187/561/378	23.43	<0.001	NA	
CVD subtypes	Mi 19/St 28/Sc 26/Bw 40/Cc 25/He 3/Ot 14	Mi 129/St 169/Sc 279/Bw 226/Cc 208/He 56/Ot 59	15.80	NS	NA	

VCI: vascular cognitive impairment; VH: visual hallucination; N: number of cases; NA: not applicable; NS: nonsignificance; OR: odds ratio. Adjusted ORs of variables were ORs adjusted for age and disease severity by Clinical Dementia Rating (CDR) scale; CDR-SB: sum of boxes of CDR; IADL: Instrumental Activities of Daily Living; MoCA: Montreal Cognitive Assessment; CASI: Cognitive Abilities Screening Instrument; NPI: total score of 12-domain Neuropsychiatric Inventory; VaMCI/PrVaD/PoVaD: vascular mild cognitive impairment/probable vascular dementia/possible vascular dementia; CVD: cerebrovascular disease; Mi: multi-infarct; St: strategic infarct; Sc: subcortical lacunes; Bw: Binswanger disease; Cc; complex combination; He: hemorrhage; Ot: others.

3. Results

Among the 1281 patients with VCI, 155 (12.1%) had VH and 1126 (87.9%) did not. Compared with the VH- group, the VH+ group was older (79.6 vs. 75.2; $t = 5.07$ and $p < 0.001$), more likely to be female (63.2% vs. 47.9%; $\chi^2 = 13.46$ and $p < 0.001$), and had a higher dementia severity according to the CDR ($\chi^2 = 70.51$ and $p < 0.001$). After adjusting for age, gender, and dementia severity by CDR, poorer IADL (OR = 0.85; $p = 0.002$), higher prevalence of dementia (OR = 4.43; $p < 0.001$), CDR-SB (OR = 9.67; $p < 0.001$), CASI (OR = 1.02; $p = 0.012$), and total score of NPI (OR = 1.06; $p < 0.001$) were found in the VH+ group compared to the VH- group. Disease duration, VCI subtypes, and CVD subtypes were not different between the VH+ and VH- groups. Comparisons between the demographic and background data are summarized in Table 1.

Table 2 showed the clinical manifestations of VCI patients with or without VH in terms of DLB features, current medications, and VRFs adjusted for age, gender, and disease severity by CDR. Compared with the VH- group, the VH+ group had a significantly higher prevalence of all LBD features including cognitive fluctuations (OR = 2.48; $p < 0.001$), parkinsonism (OR = 1.85; $p = 0.001$), RBD (OR = 4.56; $p < 0.001$), and ≧2 DLB core features (OR = 26.01; $p < 0.001$). Compared with the VH- group on current medication, the VH+ group was significantly more likely to be on anti-Parkinson's medication (OR = 2.35; $p = 0.010$). Compared with the VH- group on VRFs, the VH+ group was significantly more likely to have hypertension (OR = 1.47; $p = 0.032$), diabetes (OR = 1.86; $p = 0.001$), and heart disease (OR = 2.12; $p = 0.002$).

Table 3 demonstrates the relationship between the cerebral CT/MRI of the VH+ group and the VH- group. After adjusting for age, gender, and dementia severity by CDR, the VH+ group had a significantly higher MTA scale (OR = 1.27; $p = 0.010$). The Fazekas scale, global atrophy scale, cerebral microbleeds (cortical, subcortical, or total), and Evans' index were not different between the two groups.

Figure 1 demonstrates the percentage frequency of clinical symptom/signs that are characteristic of the DLB of VH+ compared to VH−. After having adjusted for age, gender, and disease severity, the VH+ group had a higher frequency in almost all the features including depression (OR = 1.90; $p < 0.01$), delusion (OR = 4.97; $p < 0.001$), auditory hallucinations (OR = 11.48; $p < 0.001$), sleep disruption (OR = 2.70; $p < 0.001$), acting out in dreams (OR = 4.44; $p < 0.01$), violent sleep (OR = 6.19; $p < 0.001$), postural instability (OR = 2.72; $p < 0.001$), rigidity (OR = 1.90; $p < 0.001$), bradykinesia (OR = 1.95; $p < 0.001$), action tremor (OR = 2.16; $p < 0.001$), resting tremor (OR = 1.84; $p < 0.01$), and disorganized speech (OR = 3.41; $p < 0.001$).

4. Discussion

Mixed degenerative pathologies, for example, Alzheimer's or Lewy body disease with cerebrovascular disease are highly prevalent according to pathological studies [30–33]. Some of these studies also revealed a high prevalence of cerebrovascular pathologies in the brain of patients with LBD [31–33].

Table 2: Clinical manifestation of VCI patients with or without visual hallucinations (VHs).

	N (%)		Nonadjusted		Adjusted	
	VH+ (*N* = 155)	VH− (*N* = 1126)	χ^2	*p*	OR (95% CI)	*p*
DLB core features						
Fluctuation	90 (58.1)	309 (27.4)	59.57	<0.001	2.48 (1.69-3.63)	<0.001
Parkinsonism	75 (48.4)	371 (33.0)	14.25	<0.001	1.85 (1.30-2.63)	0.001
RBD	38 (24.5)	73 (6.5)	55.98	<0.001	4.56 (2.86-7.26)	<0.001
≧2 core features*	129 (83.2)	166 (14.8)	360.11	<0.001	26.01 (16.23-41.67)	<0.001
Current medication						
Anti-Parkinson	14 (9.0)	45 (4.0)	7.86	0.005	2.35 (1.22-4.52)	0.010
Antipsychotics	9 (5.8)	41 (3.6)	1.70	NS	1.73 (0.80-3.75)	NS
Antidementia	14 (9.0)	69 (6.1)	1.90	NS	1.12 (0.60-2.29)	NS
Vascular risk factors						
Hypertension	83 (53.5)	548 (48.7)	1.30	NS	1.47 (1.03-2.09)	0.032
Diabetes	61 (39.4)	320 (28.4)	7.80	0.005	1.86 (1.29-2.69)	0.001
Hyperlipidemia	40 (25.8)	261 (23.2)	0.52	NS	1.38 (0.92-2.06)	NS
Heart disease	27 (17.4)	119 (10.6)	66.33	0.012	2.12 (1.32-3.43)	0.002

VCI: vascular cognitive impairment; VH: visual hallucination; *N*: number of cases; NA: not applicable; NS: nonsignificance; OR: odds ratio. Adjusted ORs of variables were ORs adjusted for age, gender, and disease severity by Clinical Dementia Rating (CDR) scale; CI: confidence interval; DLB: dementia with Lewy bodies; RBD: REM sleep behavior disorder; *core features including fluctuation, parkinsonism, RBD, and VH; heart disease including coronary artery disease, heart failure, arrhythmia, and valvular heart disease.

Table 3: Cerebral CT/MRI manifestation of VCI patients with or without visual hallucinations (VHs).

	Mean (SD)		Nonadjusted		Adjusted	
	VH+ (*N* = 155)	VH− (*N* = 1126)	t/χ^2	*p*	OR (95% CI)	*p*
Fazekas scale	2.2 (1.0)	1.9 (1.0)	2.91	0.004	1.07 (0.88-1.31)	NS
MTA scale	2.6 (1.1)	2.1 (1.2)	4.96	<0.001	1.27 (1.06-1.52)	0.010
Global atrophy scale	1.6 (0.8)	1.5 (0.7)	2.09	0.031	0.99 (0.75-1.30)	NS
Cerebral microbleeds*, *N* (%)	29 (30.3)	305 (40.1)	4.95	0.026	0.63 (0.39-1.02)	NS
Evans' index	0.29 (0.04)	0.28 (0.05)	1.69	0.091	0.07 (0.00-14.50)	NS

VCI: vascular cognitive impairment; VH: visual hallucination; *N*: number of cases; NA: not applicable; NS: nonsignificance; MTA: medial temporal lobe atrophy; OR: odds ratio. Adjusted ORs of variables were ORs adjusted for age, gender, and disease severity by Clinical Dementia Rating scale. *Cerebral microbleeds in MRI T2 gradient imaging among 94 VH+ and 760 VH−.

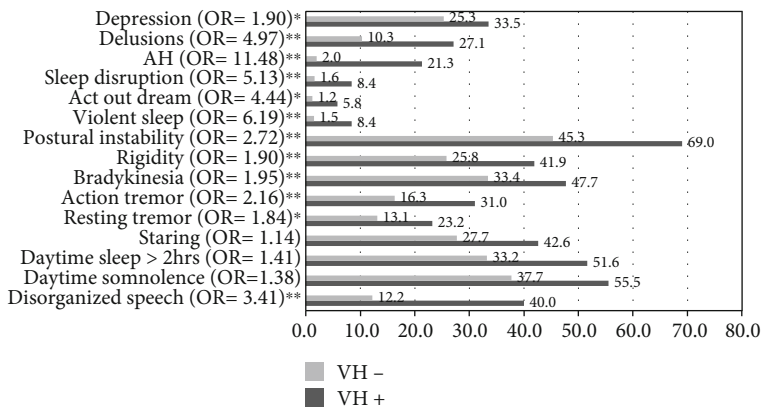

Figure 1: Percentage frequency of clinical feature characteristic of Lewy body dementia of VH+ compared to VH−. AH: auditory hallucination; ORs of variables were adjusted for age and disease severity as per the Clinical Dementia Rating scale. $^{*}p < 0.01$; $^{**}p < 0.001$.

Likewise, Lewy body pathology has been found in VaD autopsy cases [34]. However, most of the mixed pathological dementia cases were diagnosed postmortem. How to make a clinical diagnosis while alive is becoming an important issue. For studying nonmotor symptoms associated with vascular parkinsonism, Levin et al. proposed that nonmotor symptoms such as hallucinations may indicate another diagnosis or mixed pathology [35]. Our findings are consistent with

this. In this study, at least two core features for clinically diagnosing DLB were much higher in the VCI with the VH group compared to the non-VH group with an OR 26. All of the core features (fluctuations, RBD, and parkinsonism) were much higher in the VH group. Therefore, by highlighting the diagnostic differences between typical DLB type VHs (complex, well-formed, and detailed VH), we have provided a way for clinically diagnosing mixed DLB in other brain disorders such as VCI. We consider these findings as to the most important of the current study.

Besides this, our study focused on the associated factors of VH in VCI. We have had several other significant findings. Firstly, typical DLB type VH is not frequently observed in patients with VCI, with a prevalence of only 12.1%. VH in VCI was found to be more prevalent in those that are older, female, and have advanced dementia. These findings are consistent with our previous study that examined the gender differences of VH with DLB [36] as well as several other studies that focused on psychotic symptoms in vascular or degenerative dementia [4, 15, 37]. Even if these demographical factors have been adjusted for, the VH+ group still presented poorer cognitive function, ADL, and more severe neuropsychiatric symptoms. This may impact the quality of life of both patients and caregivers and also result in a greater caregiver burden [38, 39]. For the diagnosis of probable DLB, at least 2 core clinical features or one core clinical feature plus at least one indicative biomarker is necessary. Therefore, we analysed the symptoms of the associated core features (parkinsonism, fluctuation, and RBD) demonstrated on Figure 1 and found that symptoms of RBD have highest odds ratio (OR); however, the prevalence of RBD in VCI is relatively low (less than 5%) which might offset the diagnostic power of RBD in mixed DLB with VCI. On the contrary, although ORs for association of parkinsonism or fluctuation are both somewhat lower than RBD in VCI with VH, the prevalence of most of the symptoms of parkinsonism or fluctuation is higher than 50% which raised the power of the diagnosis of mixed pathologies of DLB in VCI with VH. Secondly, a significantly higher prevalence of VRFs, including hypertension, diabetes, and heart disease, was associated with the VH+ group in this study. However, hyperlipidemia was not. These results can be considered novel findings for VH in VCI. Similar studies on VRF association with neuropsychiatric symptoms in MCI or dementia have seldom been studied and remain controversial. Besides, none of them directly addressed to VH in VCI. A previous study concluded that VRFs were important modifiers of the risk of psychosis in AD [40]. Another study revealed that cholesterol is a significant factor for NPS occurring in AD [41]. A study from Cache County found that hypertension was associated with a higher risk of delusions, anxiety, and agitation/aggression, but not psychotic symptoms in AD. No significant associations were observed between neuropsychiatric symptoms and diabetes, hyperlipidemia, or heart disease [42]. Hypertension and previous CVD were the most prevalent risk factors for neuropsychiatric symptoms in VaD and mixed-type dementia [43]. Thirdly, it was revealed in this study that only medial temporal lobe atrophy had a modest association with VH in VCI. White matter lesions (WMLs) according to the Fazekas scale, global atrophy, cerebral microbleeds, and ventricle sizes were not associated. These findings were not consistent with previous studies regarding degenerative dementia that showed that WHLs are highly associated with neuropsychiatric symptoms in AD, DLB, or Parkinson disease with dementia (PDD) [44–46].

This study has several limitations. Firstly, this is a cross-sectional association study. Therefore, causal relationships to VH in VCI cannot be made. Secondly, dopamine transporter imaging, I123MIBG, or polysomnography, being indicative biomarkers for DLB, were not done in this study. The findings of the study were analysed purely according to the clinical manifestation plus brain structure imaging. Therefore, objective evidence of the mixed pathology with LBD was lacking. Thirdly, no pathological data was able to prove the diagnostic accuracy of clinical diagnosing mixed Lewy body pathology in VCI with VH.

5. Conclusions

In conclusion, VCI patients with VH tend to have more severe dementia, neuropsychiatric symptoms, and poorer cognitive function. Besides, there is a possibility of mixed pathology with DLB in this group due to the clinical DLB features in VCI with VH being associated. More than two core features in VCI might help for diagnosing mixed pathology with DLB. VH in VaD or VCI has not been widely studied in the literature. However, the underlying pathophysiology of VH, especially associated with typical DLB type VH (complex, well-formed, and detailed) in VCI, could be due to a mixed pathology with Lewy body disease such as DLB. Hence, we propose this novel concept along with a method for diagnosing mixed VCI with DLB. Further biomarker and pathological studies are warranted to prove its feasibility.

Data Availability

The data that support the findings of this study are available from the corresponding author upon reasonable request.

Conflicts of Interest

The authors declare that there is no conflict of interest regarding the publication of this article.

Acknowledgments

We would like to thank Dr. Ming-Tsung Lee at the Research Assistant Center of Show Chwan Memorial Hospital for his feedback and suggestions during the experimental design and statistical analysis stages.

References

[1] J. T. O'Brien, T. Erkinjuntti, B. Reisberg et al., "Vascular cognitive impairment," *Lancet Neurology*, vol. 2, no. 2, pp. 89–98, 2003.

[2] C. Ballard, D. Neill, J. O'Brien, I. G. McKeith, P. Ince, and R. Perry, "Anxiety, depression and psychosis in vascular

dementia: prevalence and associations," *Journal of Affective Disorders*, vol. 59, no. 2, pp. 97–106, 2000.

[3] D. R. Lee, I. McKeith, U. Mosimann, A. Ghosh-Nodyal, and A. J. Thomas, "Examining carer stress in dementia: the role of subtype diagnosis and neuropsychiatric symptoms," *International Journal of Geriatric Psychiatry*, vol. 28, no. 2, pp. 135–141, 2013.

[4] M. Caputo, R. Monastero, E. Mariani et al., "Neuropsychiatric symptoms in 921 elderly subjects with dementia: a comparison between vascular and neurodegenerative types," *Acta Psychiatrica Scandinavica*, vol. 117, no. 6, pp. 455–464, 2008.

[5] J. Bjoerke-Bertheussen, U. Ehrt, A. Rongve, C. Ballard, and D. Aarsland, "Neuropsychiatric symptoms in mild dementia with Lewy bodies and Alzheimer's disease," *Dementia and Geriatric Cognitive Disorders*, vol. 34, no. 1, pp. 1–6, 2012.

[6] C. Ballard, C. Holmes, I. McKeith et al., "Psychiatric morbidity in dementia with Lewy bodies: a prospective clinical and neuropathological comparative study with Alzheimer's disease," *The American Journal of Psychiatry*, vol. 156, no. 7, pp. 1039–1045, 1999.

[7] I. G. McKeith, B. F. Boeve, D. W. Dickson et al., "Diagnosis and management of dementia with Lewy bodies: fourth consensus report of the DLB Consortium," *Neurology*, vol. 89, no. 1, pp. 88–100, 2017.

[8] P. Y. Chiu, M. H. Hsu, C. W. Wang, C. T. Tsai, and M. C. Pai, "Visual hallucinations in Alzheimer's disease is significantly associated with clinical diagnostic features of dementia with Lewy bodies," *PLoS One*, vol. 12, no. 10, article e0186886, 2017.

[9] I. G. McKeith, C. G. Ballard, R. H. Perry et al., "Prospective validation of consensus criteria for the diagnosis of dementia with Lewy bodies," *Neurology*, vol. 54, no. 5, pp. 1050–1058, 2000.

[10] G. Rizzo, S. Arcuti, M. Copetti et al., "Accuracy of clinical diagnosis of dementia with Lewy bodies: a systematic review and meta-analysis," *Journal of Neurology, Neurosurgery, and Psychiatry*, vol. 89, no. 4, pp. 358–366, 2018.

[11] T. Nihashi, K. Ito, and T. Terasawa, "Diagnostic accuracy of DAT-SPECT and MIBG scintigraphy for dementia with Lewy bodies: an updated systematic review and Bayesian latent class model meta-analysis," *European Journal of Nuclear Medicine and Molecular Imaging*, vol. 47, no. 8, pp. 1984–1997, 2020.

[12] I. G. McKeith, D. Galasko, K. Kosaka et al., "Consensus guidelines for the clinical and pathologic diagnosis of dementia with Lewy bodies (DLB): report of the consortium on DLB international workshop," *Neurology*, vol. 47, no. 5, pp. 1113–1124, 1996.

[13] I. G. McKeith, D. W. Dickson, J. Lowe et al., "Diagnosis and management of dementia with Lewy bodies: third report of the DLB Consortium," *Neurology*, vol. 65, no. 12, pp. 1863–1872, 2005.

[14] J. A. Schneider, Z. Arvanitakis, L. Yu, P. A. Boyle, S. E. Leurgans, and D. A. Bennett, "Cognitive impairment, decline and fluctuations in older community-dwelling subjects with Lewy bodies," *Brain*, vol. 135, no. 10, pp. 3005–3014, 2012.

[15] E. Sinforiani, M. Terzaghi, C. Pasotti, C. Zucchella, E. Zambrelli, and R. Manni, "Hallucinations and sleep-wake cycle in Alzheimer's disease: a questionnaire-based study in 218 patients," *Neurological Sciences*, vol. 28, no. 2, pp. 96–99, 2007.

[16] D. Tsuang, E. B. Larson, E. Bolen et al., "Visual hallucinations in dementia: a prospective community-based study with autopsy," *The American Journal of Geriatric Psychiatry*, vol. 17, no. 4, pp. 317–323, 2009.

[17] E. Attali, F. De Anna, B. Dubois, and G. D. Barba, "Confabulation in Alzheimer's disease: poor encoding and retrieval of over-learned information," *Brain*, vol. 132, no. 1, pp. 204–212, 2008.

[18] G. D. Barba, Z. Nedjam, and B. Dubois, "Confabulation, executive functions, and source memory in Alzheimer's disease," *Cognitive Neuropsychology*, vol. 16, no. 3-5, pp. 385–398, 1999.

[19] A. P. Weiss and S. Heckers, "Neuroimaging of hallucinations: a review of the literature," *Psychiatry Research: Neuroimaging*, vol. 92, no. 2-3, pp. 61–74, 1999.

[20] C. Ballard, I. McKeith, R. Harrison et al., "A detailed phenomenological comparison of complex visual hallucinations in dementia with Lewy bodies and Alzheimer's disease," *International Psychogeriatrics*, vol. 9, no. 4, pp. 381–388, 1997.

[21] L. Van Assche, E. Van Aubel, L. Van de Ven, F. Bouckaert, P. Luyten, and M. Vandenbulcke, "The neuropsychological profile and phenomenology of late onset psychosis: a cross-sectional study on the differential diagnosis of very-late-onset schizophrenia-like psychosis, dementia with Lewy bodies and Alzheimer's type dementia with psychosis," *Archives of Clinical Neuropsychology*, vol. 34, no. 2, pp. 183–199, 2019.

[22] P. B. Gorelick, A. Scuteri, S. E. Black et al., "Vascular contributions to cognitive impairment and dementia: a statement for healthcare professionals from the American Heart Association/American Stroke Association," *Stroke*, vol. 42, no. 9, pp. 2672–2713, 2011.

[23] J. C. Morris, "The Clinical Dementia Rating (CDR): current version and scoring rules," *Neurology*, vol. 43, no. 11, pp. 2412–2414, 1993.

[24] K. L. Chen, Y. Xu, A. Q. Chu et al., "Validation of the Chinese version of Montreal cognitive assessment basic for screening mild cognitive impairment," *Journal of the American Geriatrics Society*, vol. 64, no. 12, pp. e285–e290, 2016.

[25] E. L. Teng, K. Hasegawa, A. Homma et al., "The Cognitive Abilities Screening Instrument (CASI): a practical test for cross-cultural epidemiological studies of dementia," *International Psychogeriatrics*, vol. 6, no. 1, pp. 45–58, 1994.

[26] M. P. Lawton and E. M. Brody, "Assessment of older people: self-maintaining and instrumental activities of daily living," *Gerontologist*, vol. 9, 3 Part 1, pp. 179–186, 1969.

[27] J. L. Cummings, M. Mega, K. Gray, S. Rosenberg-Thompson, D. A. Carusi, and J. Gornbein, "The Neuropsychiatric Inventory: comprehensive assessment of psychopathology in dementia," *Neurology*, vol. 44, no. 12, pp. 2308–2314, 1994.

[28] T. J. Ferman, G. E. Smith, B. F. Boeve et al., "DLB fluctuations: specific features that reliably differentiate DLB from AD and normal aging," *Neurology*, vol. 62, no. 2, pp. 181–187, 2004.

[29] L. Vignatelli, F. Bisulli, A. Zaniboni et al., "Interobserver reliability of ICSD–R minimal diagnostic criteria for the parasomnias," *Journal of Neurology*, vol. 252, no. 6, pp. 712–717, 2005.

[30] K. A. Jellinger, "Prevalence and impact of cerebrovascular lesions in Alzheimer and Lewy body diseases," *Neurodegenerative Diseases*, vol. 7, no. 1-3, pp. 112–115, 2010.

[31] L. White, "Brain lesions at autopsy in older Japanese-American men as related to cognitive impairment and dementia in the final years of life: a summary report from the Honolulu-Asia Aging Study," *Journal of Alzheimer's Disease*, vol. 18, no. 3, pp. 713–725, 2009.

[32] J. De Reuck, V. Deramecourt, F. Auger et al., "Cerebrovascular lesions in mixed neurodegenerative dementia: a

neuropathological and magnetic resonance study," *European Neurology*, vol. 78, no. 1-2, pp. 1–5, 2017.

[33] J. De Reuck, C. A. Maurage, V. Deramecourt et al., "Aging and cerebrovascular lesions in pure and in mixed neurodegenerative and vascular dementia brains: a neuropathological study," *Folia Neuropathologica*, vol. 56, no. 2, pp. 81–87, 2018.

[34] A. D. Korczyn, "The complex nosological concept of vascular dementia," *Journal of the Neurological Sciences*, vol. 203-204, pp. 3–6, 2002.

[35] O. S. Levin, A. S. Chimagomedova, N. A. Skripkina, E. A. Lyashenko, and O. V. Babkina, "Nonmotor symptoms in vascular and other secondary parkinsonism," *International Review of Neurobiology*, vol. 134, pp. 1303–1334, 2017.

[36] P. Y. Chiu, P. R. Teng, C. Y. Wei, C. W. Wang, and C. T. Tsai, "Gender difference in the association and presentation of visual hallucinations in dementia with Lewy bodies: a cross-sectional study," *International Journal of Geriatric Psychiatry*, vol. 33, no. 1, pp. 193–199, 2018.

[37] A. Cagnin, F. Gnoato, N. Jelcic et al., "Clinical and cognitive correlates of visual hallucinations in dementia with Lewy bodies," *Journal of Neurology, Neurosurgery, and Psychiatry*, vol. 84, no. 5, pp. 505–510, 2013.

[38] Y. R. Zweig and J. E. Galvin, "Lewy body dementia: the impact on patients and caregivers," *Alzheimer's Research & Therapy*, vol. 6, no. 2, p. 21, 2014.

[39] E. Svendsboe, T. Terum, I. Testad et al., "Caregiver burden in family carers of people with dementia with Lewy bodies and Alzheimer's disease," *International Journal of Geriatric Psychiatry*, vol. 31, no. 9, pp. 1075–1083, 2016.

[40] C. E. Fischer, W. Qian, T. A. Schweizer et al., "Lewy bodies, vascular risk factors, and subcortical arteriosclerotic leukoencephalopathy, but not Alzheimer pathology, are associated with development of psychosis in Alzheimer's disease," *Journal of Alzheimer's Disease*, vol. 50, no. 1, pp. 283–295, 2016.

[41] J. R. Hall, A. R. Wiechmann, L. A. Johnson et al., "The impact of APOE status on relationship of biomarkers of vascular risk and systemic inflammation to neuropsychiatric symptoms in Alzheimer's disease," *Journal of Alzheimer's Disease*, vol. 40, no. 4, pp. 887–896, 2014.

[42] K. A. Treiber, C. G. Lyketsos, C. Corcoran et al., "Vascular factors and risk for neuropsychiatric symptoms in Alzheimer's disease: the Cache County Study," *International Psychogeriatrics*, vol. 20, no. 3, pp. 538–553, 2008.

[43] J. I. Siqueira-Neto, O. M. Pontes-Neto, F. de Assis Carvalho do Vale et al., "Neuropsychiatric symptoms (NPS) in patients with pure vascular dementia (VaD) and mixed dementia (MD) from a memory outpatient clinic in Southeast Brazil," *Dementia & Neuropsychologia*, vol. 7, no. 3, pp. 263–268, 2013.

[44] N. D. Prins and P. Scheltens, "White matter hyperintensities, cognitive impairment and dementia: an update," *Nature Reviews Neurology*, vol. 11, no. 3, pp. 157–165, 2015.

[45] H. Joki, Y. Higashiyama, Y. Nakae et al., "White matter hyperintensities on MRI in dementia with Lewy bodies, Parkinson's disease with dementia, and Alzheimer's disease," *Journal of the Neurological Sciences*, vol. 385, pp. 99–104, 2018.

[46] R. González-Redondo, J. Toledo, P. Clavero et al., "The impact of silent vascular brain burden in cognitive impairment in Parkinson's disease," *European Journal of Neurology*, vol. 19, no. 8, pp. 1100–1107, 2012.

Hindawi
Behavioural Neurology
Volume 2020, Article ID 8875087, 8 pages
https://doi.org/10.1155/2020/8875087

Research Article

Basolateral Amygdala but Not Medial Prefrontal Cortex Contributes to Chronic Fluoxetine Treatments for PTSD Symptoms in Mice

Ying Hao Yu,[1,2] Chen Yin Ou,[1] Bai Chuang Shyu,[3] and Andrew Chih Wei Huang[1]

[1]*Department of Psychology, Fo Guang University, Yilan County 26247, Taiwan*
[2]*Department of Biotechnology and Animal Science, National Ilan University, Yilan County 26247, Taiwan*
[3]*Institute of Biomedical Sciences, Academia Sinica, Taipei, Taiwan*

Correspondence should be addressed to Bai Chuang Shyu; bmbai@gate.sinica.edu.tw
and Andrew Chih Wei Huang; acwhuang@gmail.com

Received 13 August 2020; Revised 16 October 2020; Accepted 2 November 2020; Published 25 November 2020

Academic Editor: Muh-Shi Lin

Do chronic fluoxetine treatments reduced footshock-induced posttraumatic stress disorder (PTSD) symptoms, including fear and comorbid depression, in the situational reminder phase? Moreover, are the subareas of the medial prefrontal cortex (mPFC), including the cingulate cortex 1 (Cg1), prelimbic cortex (PrL), infralimbic cortex (IL), and basolateral amygdala (BLA), involved in the fluoxetine amelioration of PTSD symptoms? These two crucial issues were addressed in the present study. All mice were injected with chronic fluoxetine or normal saline treatments for the adaptation (14 days), footshock fear conditioning (1 day), and situational reminder (3 days) phases. After adaptation, the mice were subjected to footshock (2 mA, 10 seconds) or nonfootshock and stayed 2 min in a footshock box for 2 min for fear conditioning. Later, they were placed in the footshock box for 2 min in the situational reminder phase. In the final session of the situational reminder phase, a forced swimming test (FST) and immunohistochemical staining were conducted. The results indicated that footshock induced fear and comorbid depression. Meanwhile, chronic fluoxetine treatments reduced fear and depression behaviors. The Cg1, PrL, IL, and BLA were seemingly to increase c-Fos expression after footshock-induced PTSD symptoms in the situational reminder phase. The fluoxetine treatments reduced only the BLA's c-Fos expression. The findings suggest that BLA contributes to the fluoxetine amelioration of PTSD symptoms; however, the mPFC, including the Cg1, PrL, and IL, did not mediate PTSD symptoms' amelioration stemming from fluoxetine. The present data might help us to further understand the neural mechanism of fluoxetine treatments in PTSD symptoms.

1. Introduction

Posttraumatic stress disorder (PTSD) is associated with reexperiencing a traumatic memory, emotional numbering, hyperarousal, the avoidance of cue-associated trauma, and fear and horror [1]. Moreover, PTSD patients suffer from comorbid depression and anxiety symptoms [2, 3]. Previous studies of PTSD involving animal models often examined fear conditioning or fear extinction [4]; however, the present study used the situational reminder procedure with the traumatic memory associated with the context. This kind of study was aimed at mimicking the reexperiencing of a traumatic memory of PTSD symptoms in humans [5, 6].

Fluoxetine is a category of specific serotonin reuptake inhibitor (SSRI) drugs and can effectively ameliorate depressive behavior for patients with major depression disorder [7]. Recently, some studies have shown that fluoxetine might be an effective drug for reducing PTSD's symptoms and for changing its pathological response in the brain [8–11]. For example, PTSD patients who had suffered traumatic events early in life were each given 20-80 mg/day for a continuous period of 8 to 32 weeks, and it decreased the severity of their

PTSD symptoms [8]. Microinjections of fluoxetine into the amygdala or hippocampus were found to reduce neurometabolic abnormalities in the amygdala or hippocampus in a single-prolonged, stress-induced PTSD animal model [9]; moreover, another study demonstrated that chronic treatments of fluoxetine could prevent inflammatory gene expression in the anterior cingulate cortex and decrease PTSD symptoms [11]. Fluoxetine administrations in PTSD patients were also shown to recover PTSD-induced synaptic protein loss and dysfunction behaviors [10]. Therefore, SSRI drug fluoxetine is a crucial treatment for PTSD symptoms. This current study examined whether PTSD's fear and comorbid depression behaviors were decreased by fluoxetine treatments, especially in the situational reminder phase of a traumatic memory.

A growing body of evidence has shown that the medial prefrontal cortex (mPFC)-amygdala pathway plays an essential role in regulating PTSD symptoms [12–14]. For example, some recent evidence has suggested that mPFC has an emotional downregulation function to inhibit the negative emotions of the amygdala, whereas the amygdala transfers its property and valence of emotions to the mPFC for the interpretation of emotions [15]. Therefore, the information in mPFC-amygdala connectivity is reciprocal between these two areas [16]. Some studies have demonstrated that the mPFC normally inhibits the activity of the amygdala, resulting in the extinction of fear conditioning [17, 18]. Moreover, the mPFC-amygdala circuitry can be altered by fear-conditioned learning and is involved in the extinction and reinstatement of fear [19]. A neuroimaging study showed that the mPFC-amygdala pathway may govern stress and anxiety disorders [20]. Furthermore, there is an inhibition deficit from the mPFC to the amygdala due to the PTSD symptoms. Moreover, PTSD patients showed hypoactivity of the mPFC and hyperactivity of the amygdala [13].

Recently, many studies have narrowed down the subarea of the mPFC and amygdala, and this line of studies showed that the subareas of the mPFC and amygdala contributed to different functions in the fear conditioning and fear extinction of the PTSD symptoms [4, 21–23]. For example, a review paper reported that the prelimbic cortex (PrL) of mPFC regulates fear expression; meanwhile, the infralimbic cortex (IL) of mPFC controls fear suppression [4]. Moreover, another study demonstrated that the activity of the PrL neurons promotes the extinction of fear conditioning; however, the neuronal activity of the IL inhibits fear behavior after extinction [22]. In addition, BLA, a portion of the amygdala in the basolateral parts, was involved in PTSD symptoms [21, 23]. For example, the high-frequency stimulation of the bilateral BLA was shown to reduce the avoidance behavior in the predator scent-induced PTSD animal model [21]. Furthermore, the transcription factor NF-κB inhibitions of BLA interfered with the amygdala-dependent auditory fear conditioning in the memory retention phase of PTSD [23]. However, no research has systematically examined whether Cg1, PrL, IL, and BLA are involved in fluoxetine treatments for PTSD symptoms. Therefore, this issue was addressed in the present study.

Altogether, the present study addressed the following issues: (a) Do fluoxetine treatments reduce footshock-induced freezing behavior in the situational reminder phase, and do they also ameliorate PTSD's comorbid depression behavior? (b) Are the subareas of the mPFC, including the Cg1, PrL, and IL, and the BLA, involved in PTSD's fear and comorbid depressive behaviors following situational reminders? (c) Do the Cg1, PrL, IL, and BLA contribute to fluoxetine treatments in PTSD's fear and depression symptoms?

2. Material and Methods

2.1. Animals. Thirty-nine C57BL/6J male mice were bought from the National Laboratory for Animal Breeding and Research Center, Taipei, Taiwan. At the beginning of the experiment, all mice weighed 25-35 grams. The mice were group-housed with another three mice in the plastic cages with wooden bedding. The cage was placed in a colony room with a constant temperature (approximately $23 \pm 2^{\circ}$C) and a light phase between 6:00 a.m. and 6:00 p.m. Food and water were provided *ad libitum*. The experiments were performed in compliance with the American Psychological Association ethical standards for the treatment of animals. A description of the details of the treatment was submitted and received approval from a local ethics committee. Every effort was made to minimize the animals' suffering and the number of animals used.

2.2. Apparatus. The inescapable footshock apparatus is a box with a surrounding plastic shell measuring 60 cm × 60 cm × 72 cm high. The floor of the apparatus is made of metal grids (0.3 cm diameter at 0.7 cm grid intervals).

2.3. Behavioral Procedure. The procedure of the experiment is shown in Figure 1. After the 14-day adaptation phase, all mice underwent the footshock phase for one day. In this period of time, all mice were intraperitoneally injected normal saline or fluoxetine, placed 2 min in the footshock box, and placed into the nonfootshock/saline, footshock/saline, and footshock/fluoxetine groups ($n = 8$ per group; footshock amount was 2 mA, 10 s). Later, the situational reminder was conducted once a day for three days. All mice were placed 2 min in the same footshock box for situational reminders to reexperience traumatic memories once a day for three days. On the last day of the situational reminders, all mice were also tested using the FST for 5 min. After 120 min of FST testing, all mice were sacrificed, and the brains were removed to label immunohistochemical staining with the c-Fos protein for the specific brain areas. The saline or fluoxetine was continuously administered for the adaptation (14 days), footshock (one day), and situational reminder (three days) phases among the nonfootshock/saline, footshock/saline, and footshock/fluoxetine groups.

2.4. Immunohistochemical Staining: c-Fos. Following the last day of the situational reminder test, and 120 min later, all rats were sacrificed via sodium pentobarbital overdose. All mice were perfused with a 0.1-M sodium phosphate-buffered saline buffer (PBS; 100 ml) followed by 4% paraformaldehyde (400 ml) in a 0.1-M PBS buffer. The brain was dissected and postfixed for one day. The tissues of the brain

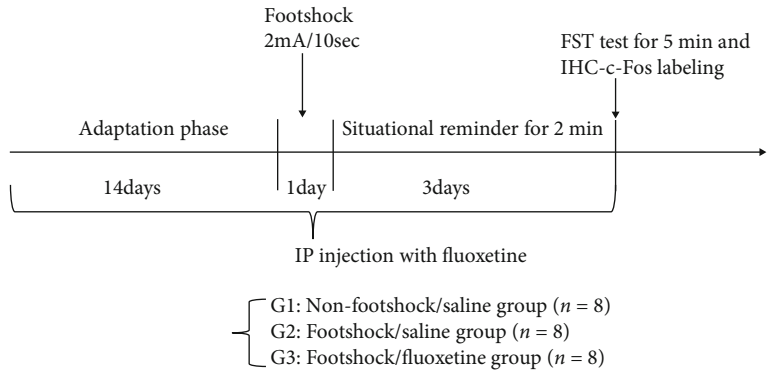

Figure 1: The experimental procedure. After the 14-day adaptation phase, a 2-mA footshock for 10 seconds was applied for fear conditioning, and the freezing time was measured for 2 min during one session a day in the situational reminder sessions. Later, the mice's floating behavior was measured for 5 min in the FST. Following the final session of freezing and floating behavior measurements, 120 mice were sacrificed, and their brain tissues were labeled using immunohistochemical staining with c-Fos proteins.

were transferred to 30% sucrose for cryoprotection until the brain tissues sunk to the bottom of the solution. Each whole brain was cut into 40-micrometer coronal sections on a freezing and sliding microtome. All sections of the brain area were then labeled with c-Fos proteins.

For labeling the c-Fos protein, the brain sections were washed once for 15 min in 0.1-M PBS, permeabilized in 3% H_2O_2 for 1 h, washed three times in 2% phosphate-buffered saline with Tween 20 (PBST) buffer for 20 min, and soaked in 3% normal goat serum and 1% bovine serum albumin for 1 h. Later, the brain sections were washed twice for 15 min with PBST. Then, the sections were incubated at 4°C overnight with rabbit anti-Fos antibody (Abcam Biotechnology Inc., AB190289, 1 : 1000) for labeling c-Fos. The sections were washed with PBST twice for 15 min and incubated with a biotinylated goat antirabbit secondary antibody (Vector Lab BA-1000, 1 : 500) for 1 h. Later, the sections were washed for 10 min with PBS. The secondary antibody was amplified using the ABC kit (Vector Lab ABC Kit, PK-6100). The positive expression of the brain nucleus was measured via quantification for the selected brain areas. In general, every third section of each brain slice was determined for counting. The c-Fos-positive neurons for each brain session were counted using the software ImageJ. Each group was to be averaged to count the expressions of the c-Fos protein for each brain subarea.

2.5. Drugs. Fluoxetine and sodium chloride were purchased from Sigma-Aldrich Company (St. Louis, MO, USA). Sodium chloride was dissolved in distilled water and prepared in 0.9% normal saline. Fluoxetine was dissolved in 0.9% normal saline. Fluoxetine and sodium chloride were administered intraperitoneally. The injection volume of fluoxetine and sodium chloride was 1 ml/kg. The dose of 2.5 mg/kg fluoxetine was used in the behavioral test. The dose of fluoxetine and the continuous fluoxetine injections for 14 days came from the previous study [24].

2.6. Statistical Analysis. A 3×3 two-way mixed (group vs. session) analysis of variance (ANOVA) was performed for the freezing time among the nonfootshock/saline, footshock/saline, and footshock/fluoxetine groups ($n = 8$ per group). When appropriate, Tukey's honest significant difference post hoc test was conducted. (a) indicated that $p < 0.05$ was considered to be statistically significant between the nonfootshock/saline and footshock/saline groups. (b) indicated that $p < 0.05$ was considered to be statistically significant between the footshock/saline and footshock/fluoxetine groups. One-way ANOVA was conducted to analyze the floating time among the nonfootshock/saline, footshock/saline, and footshock/fluoxetine groups ($n = 8$ per group). When appropriate, Fisher's least significant difference (LSD) post hoc test was conducted. (∗) and (#) indicated that $p < 0.05$ was considered to be statistically significant compared with the nonfootshock/saline and footshock/saline groups, respectively. c-Fos expression numbers were analyzed by one-way ANOVA for the specific brain areas, including Cg1, PrL, IL, BLA, and PC, among the nonfootshock/saline, footshock/saline, and footshock/fluoxetine groups ($n = 5$ per group). When appropriate, Tukey's honest significant difference post hoc test was conducted. (∗) and (#) indicated that $p < 0.05$ was considered to be statistically significant compared with the nonfootshock/saline and footshock/saline groups, respectively.

3. Results

3.1. Fluoxetine and Freezing Behavior Tests during Situational Reminders. After encountering severe footshock treatment, mice were placed in the same footshock box, and the freezing time was measured once a day for three days. This was referred to as the situational reminders of traumatic memory. A 3×3 mixed two-way ANOVA analysis revealed significant differences in the factors of group ($F(2, 21) = 73.69$, $p < 0.05$), session ($F(2, 42) = 16.17$, $p < 0.05$), and group × session ($F(4, 42) = 9.39$, $p < 0.05$). The post hoc with Tukey test showed that the freezing time of the footshock/saline group was significantly increased compared with the nonfootshock/saline group, indicating that the footshock treatment induced a strong freezing behavior over sessions 1-3 ($p < 0.05$). Moreover, the freezing time of the footshock/fluoxetine group was significantly decreased when

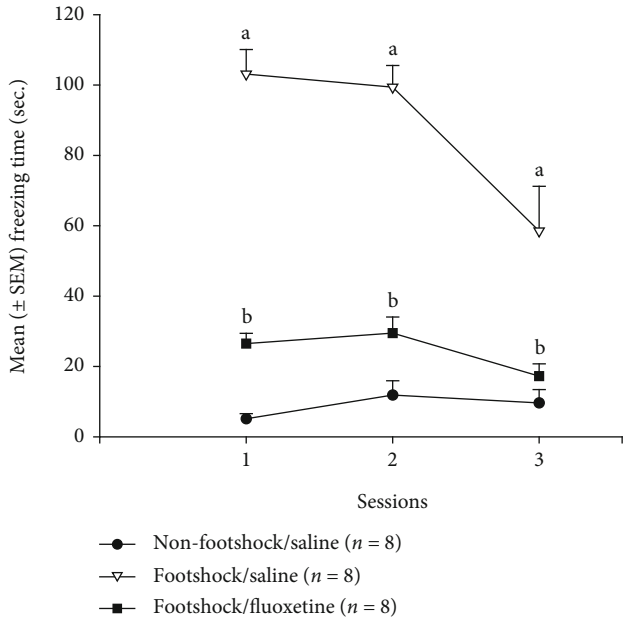

Figure 2: The mean (± SEM) freezing time (sec.) over three sessions of the situational reminder phase for the nonfootshock/saline, footshock/saline, and footshock/fluoxetine groups ($n = 8$, per group).

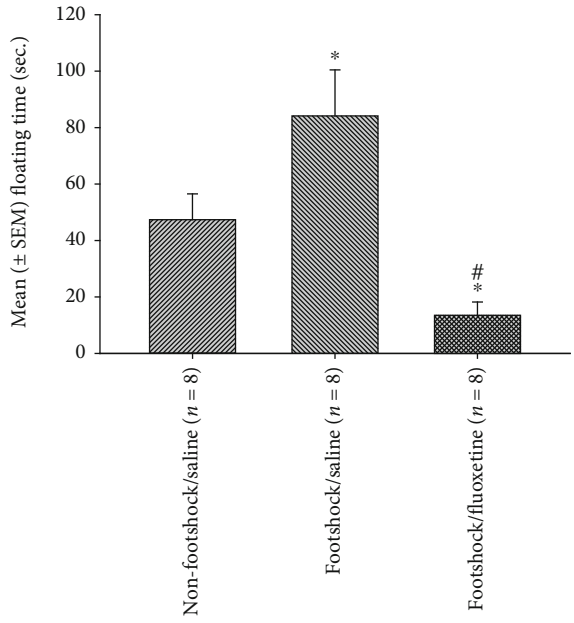

Figure 3: The mean (± SEM) floating time (sec.) in the forced swimming test for the nonfootshock/saline, footshock/saline, and footshock/fluoxetine groups ($n = 8$, per group).

compared with the footshock/saline group over sessions 1-3 ($p < 0.05$), indicating the antidepression drug, fluoxetine, and injections could reduce freezing behavior induced by the footshock treatment (Figure 2).

3.2. Fluoxetine and PTSD's Comorbid Depression. To test the PTSD's comorbid depression symptom of fluoxetine, one-way ANOVA was conducted. The results of the floating time in the FST test showed a significant difference in the factor of group ($F(2, 21) = 9.86$, $p < 0.05$). Furthermore, the post hoc with LSD indicated that the floating time of the footshock/saline group was significantly increased compared with the nonfootshock group ($p < 0.05$). The floating time of the footshock/fluoxetine group was significantly decreased compared with the nonfootshock/saline group ($p < 0.05$). Importantly, the floating time of the footshock/fluoxetine group was significantly decreased compared with the footshock/saline group ($p < 0.05$). In summary, the footshock treatment induced severe depression behavior in the FST test, and the treatment of fluoxetine could reduce the floating behavior. The results mean that injections of antidepression drug fluoxetine reduced PTSD's comorbid depression symptoms (Figure 3).

3.3. c-Fos Immunohistochemical Staining and the Amelioration of Fluoxetine in PTSD-Associated Brain Areas. For investigating the involvement of brain areas in the amelioration of fluoxetine treatments in PTSD symptoms, a one-way ANOVA analysis was conducted for c-Fos expressions among the nonfootshock/saline group, footshock/saline group, and footshock/fluoxetine group. The results showed that significant differences in the c-Fos expression occurred in the Cg1 ($F(2, 12) = 12.94$, $p < 0.05$), PrL ($F(2, 12) = 5.18$, $p < 0.05$), and BLA ($F(2, 12) = 10.34$, $p < 0.05$). However, there were no significant differences for the c-Fos expression in the IL ($F(2, 12) = 1.92$, $p > 0.05$) and PC ($F(2, 12) = 0.04$, $p > 0.05$). Furthermore, the c-Fos expression of the footshock/saline group was significantly increased compared with the nonfootshock/saline group in the Cg1, PrL, and BLA ($p < 0.05$), indicating that the footshock treatment induced c-Fos expression in the Cg1, PrL, and BLA. The footshock/fluoextine group showed a higher c-Fos expression compared with the nonfootshock/saline group ($p < 0.05$). Importantly, the c-Fos expression of the footshock/fluoxetine group was decreased more than that of the footshock/saline group only in the BLA ($p < 0.05$) but not in the other brain areas. The result of the BLA revealed that the antidepression drug fluoxetine reduced the c-Fos expression induced by footshock (Figures 4 and 5). In conclusion, the results mean that the Cg1, PrL, and BLA were involved in the footshock-induced PTSD symptoms. However, fluoxetine treatments could ameliorate footshock-induced c-Fos expression in the BLA.

4. Discussion

In the behavioral tests, footshock treatments induced a long-lasting freezing behavior over three sessions, as mice stayed in the same footshock box and encountered the situational reminders of the traumatic memories. Moreover, the PTSD mice with footshock produced comorbid depression behavior in floating in the FST task. Fluoxetine injections reduced freezing behavior in the situational reminder phase and comorbid depression behavior.

The data of the immunohistochemical staining with c-Fos showed that the subareas of the mPFC, including the Cg1 and PrL but not the IL, were involved in footshock-

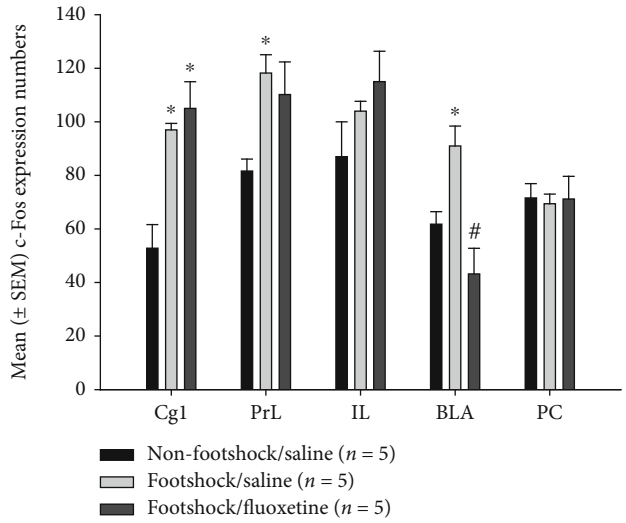

Figure 4: The mean (± SEM) c-Fos-positive neurons per slice in nonfootshock/saline, footshock/saline, and footshock/fluoxetine groups ($n = 5$, per group). The number of c-Fos-positive neurons was counted in the amelioration of fluoxetine for PTSD-associated regions, including the Cg1, PrL, IL, BLA, and PC.

induced PTSD symptoms, such as freezing and depression behaviors. Only the BLA was shown to be associated with a lower level of c-Fos expression in the footshock/fluoxetine group when compared with the footshock/saline group. The results of the BLA suggest that the fluoxetine treatments ameliorated the negative emotional response.

4.1. Comparing the Present Data and the Viewpoint of mPFC-Amygdala Dysfunction in PTSD. How the mPFC-amygdala neural pathway controls PTSD symptoms is an important issue. Based on the hypothesis regarding the mPFC-amygdala dysfunction in PTSD, the medial prefrontal cortex (mPFC) and the amygdala pathway interact with each other to govern emotional processing [25]. The mPFC projects to the amygdala and inhibits the neural activity of the amygdala; thus, the negative emotional effect of the amygdala is distinguished, and healthy people can control their emotional responses [17, 26]. In contrast, the amygdala also projects to the mPFC; thus, the negative emotional information of the amygdala transfers to the mPFC, and the mPFC plays a role in interpreting the valence of emotion from the amygdala for healthy people [17]. In PTSD patients, the neural activity of the amygdala was revealed to be hyperactive when one is reexperiencing a traumatic memory. Meanwhile, the mPFC was shown to be hypoactive; thus, the mPFC cannot inhibit the hyperactivity of the amygdala [27]. Patients with PTSD suffered from negative emotions continuously, and the mPFC-amygdala neural circuit revealed dysfunction [13, 27]. However, the present data were not consistent with this viewpoint regarding the mPFC-amygdala pathway—that the mPFC revealed hypoactivity and the BLA revealed hyperactivity. Instead, the present results showed that the subareas of the mPFC (such as the Cg1, PrL, and IL) and the BLA were associated with hyperactive c-Fos expression, indicating that the mPFC and amygdala exhibited hyperactivity after situational reminders of traumatic memories. This discrepancy in the data might stem from the several reasons outlined below. First, differences in the fear conditioning phase might have resulted in differences in the evidence. The previous studies often tested fear conditioning or fear extinction in the animal model of PTSD; however, the current study manipulated the situational reminder procedure of a traumatic memory. The manipulation of different phases of PTSD may have caused the inconsistent data between the previous studies and our study. Second, the discrepancy data for the previous studies and ours may be due to the differently determined locations of the mPFC and amygdala. The present study determined the location of the Cg1, PrL, and IL for counting the c-Fos expression based on the mouse brain in the seterotaxic coordinates of Paxinos and Franklin [28]. In our study, the range of the Cg1 was AP: +1.77~1.53 mm; ML: +0~0.7 mm; DV: -1~-2 mm. The range of the PrL was AP: +1.77~1.53 mm; ML: +0~0.7 mm; and DV: -1.5~-2.5 mm. The range of the IL was AP: +1.77~1.53 mm; ML: +0~0.7 mm; and DV: -2.5~-3.2 mm [28]. The chosen placements of the brain areas are a bit in the upper part of the brain. Whether the chosen location of the mPFC was due to the discrepancy should be addressed.

In conclusion, the present data on immunohistochemical staining with c-Fos proteins in the mPFC-amygdala neural circuit did not support the hypothesis of hypoactivity in the subareas of the mPFC (i.e., Cg1, PrL, and IL) and hyperactivity in the amygdala. Why this is should be scrutinized in further studies.

4.2. Fluoxetine Treatments for PTSD Symptoms. Although the SSRI drug fluoxetine is the first-line medication for treating PTSD symptoms, the effective rate of amelioration in PTSD symptoms is rarely higher than 60%, and less than 20~30% of PTSD patients can obtain full remissions following fluoxetine treatments [29, 30]. Therefore, the therapeutic effect of fluoxetine for PTSD symptoms has some limitations. The animal study showed that following juvenile stress, PTSD animals with chronic fluoxetine treatments at a juvenile age could reduce their PTSD anxiety behavior; however, chronic fluoxetine treatments in adult PTSD animals did not affect PTSD-induced anxiety behaviors. This indicates that the childhood period of time is critical for experiencing a therapeutic effect of fluoxetine for PTSD [31]. Nevertheless, many animal studies on PTSD have demonstrated that fluoxetine treatments can effectively reduce fear-related conditioning and PTSD symptoms. For example, a study on contextual fear conditioning showed that chronic fluoxetine treatments could prevent fear generalization, increase fear extinction, and avoid the occurrence of spontaneous fear recovery [32]. Moreover, previous PTSD animal studies related to the therapeutic effect of fluoxetine found that chronic treatments could decrease sensitized fear behavior [33], reduced hippocampus synaptic proteins [10], and prevented inflammatory responses [11]. Furthermore, the combined treatments of fluoxetine and treadmill exercises have been shown to alleviate PTSD animals' anxiety responses, inhibit the hypothalamus-pituitary-adrenal gland stress system, increase hippocampal brain-derived neurotrophic factor

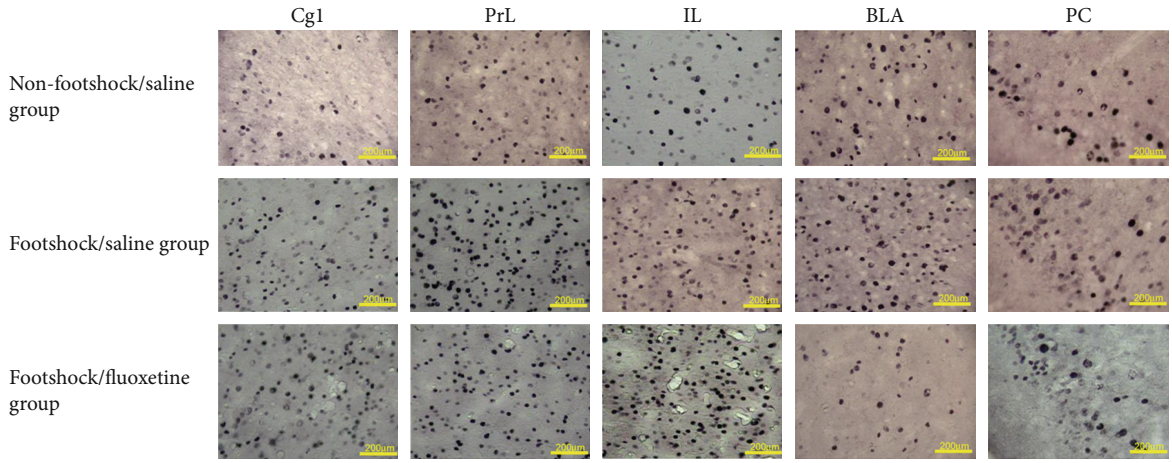

Figure 5: Representative photomicrographs of c-Fos immunoreactivity in the cingulated cortex area 1 (Cg1), prelimbic cortex (PrL), infralimbic cortex (IL), basolateral amygdala (BLA), and piriform cortex (PC) for the nonfootshock/saline, footshock/saline, and footshock/fluoxetine groups ($n = 5$, per group).

levels, and decrease apoptosis biomarkers. This means that fluoxetine had a therapeutic effect on ameliorating PTSD symptoms and neural and pathology responses [34]. Therefore, despite the fact that some research has suggested that fluoxetine treatments might not be fully effective for curing PTSD symptoms in the clinical setting, fluoxetine is seemingly able to ameliorate fear conditioning and PTSD symptoms in an animal model. Whether fluoxetine treatments can effectively reduce PTSD symptoms should be examined in further studies.

4.3. The Involvements of the Neural Substrates in Fluoxetine Treatments for PTSD Symptoms

4.3.1. The mPFC: the Cg1, PrL, and IL in Fluoxetine Amelioration to PTSD. The mPFC has been shown to play different functions, such as emotional regulation, hypothalamic–pituitary–adrenal stress system regulation, working memory, and cognitive execution. Moreover, after repeated stress-related experiences, the dysfunctions of the mPFC [35] and dopamine dysregulation within the mPFC [36] implicated a variety of psychopathologies, such as PTSD, revealing the mPFC's changes in a dendritic spine's density and morphology [35]. Recently, some studies have reported that the subareas of the mPFC-PrL and IL through different neural circuits connected to the subregions of the amygdala control fear expression and fear suppression, respectively [4, 37]. The stress-resilient and susceptible PTSD mice were found to show separated morphological changes in the mPFC; moreover, the stress-resilient mice decreased dendritic numbers in the PrL but increased dendritic numbers in the IL. However, the stress-susceptible mice appeared to only decrease in their dendritic numbers in the IL [38]. However, a little bit of research examined whether the mPFC regulated the fluoxetine amelioration of PTSD [39]. For example, a previous study showed that fluoxetine treatments decreased the freezing behavior and changed the PFC miRNA 1971 expression levels in the animal model of PTSD [39]. The present data showed that although the Cg1 and PrL contributed to the PTSD symptoms, including fear and depression, the Cg1, PrL, and IL were not involved in the PTSD amelioration after chronic fluoxetine treatments. This study might be the first to examine whether the subareas of the mPFC, such as the PrL, IL, and Cg1, contribute to fluoxetine treatments for PTSD using immunohistochemical staining. This issue of the involvement of the mPFC in the fluoxetine amelioration of PTSD symptoms should be scrutinized in further studies.

4.3.2. The Role of BLA in Fluoxetine Treatments of PTSD. Previously, most studies elucidated how BLA contributes to PTSD symptoms. For example, the bilateral stimulation of the amygdala decreased avoidance behavior in predator scent-induced PTSD [21]. Bilateral intra-BLA (but not central amygdala) infusions with sulfasalazine activated the inhibition of NF-κB and disrupted the retention of fear memory in auditory-induced fear conditioning [23]. With deep brain stimulation in the prefrontal cortex, fear and anxiety behaviors were facilitated; however, it decreased the activity of the BLA in the PTSD animal model [40]. Therefore, the BLA might govern fear and anxiety in the PTSD animal model.

On the other hand, fewer studies have examined whether the BLA is involved in fluoxetine treatments for PTSD [9, 11]. Fluoxetine treatments reduced neurometabolites, such as the *N*-acetylaspartate (NAA)/creatine (Cr) and choline moieties (Cho)/Cr ratios, in the amygdala in a single-prolonged stress animal model [9]. Repeated fluoxetine treatments were shown to avoid inflammatory gene expression in the anterior cingulate cortex but not in the BLA [11]. The present data showed that following the experience of footshock, chronic fluoxetine treatments reduced the c-Fos expression in the BLA compared with the group for footshock with saline injections. The findings were not fully consistent with the previous evidence. Whether the BLA was involved in the fluoxetine amelioration of PTSD should be further investigated.

4.4. Limitations. Some limitations should be concerned. First, the present study used the typical SSRI antidepressant drugs fluoxetine to ameliorate PTSD symptoms, including freezing and floating behaviors. However, this study did not comprehensively test the other SSRI drugs such as paroxetine or sertraline or the serotonin and norepinephrine reuptake inhibitors (SNRI) such as venlafaxine or duloxetine for the amelioration of PTSD symptoms. It is questioned that SSRIs or SNRIs reduce major depression symptoms; meanwhile, do the other SSRI or SNRI drugs also ameliorate PTSD symptoms, including freezing or floating behaviors? Obviously, this issue should be investigated in further studies. Second, are there any differences of c-Fos expression between the left and right BLA for the amelioration of PTSD symptoms with chronic fluoxetine treatments? In the present study, the left or right parts of the BLA were randomly chosen to count the numbers of c-Fos expression for each brain slice. This study did not, respectively, measure c-Fos expression in the left or right BLA. Thus, the present data of the c-Fos expression in the BLA cannot find a significant difference between the left and right parts of the BLA. This is the second limitation of the present study. This issue has emerged that whether a significant difference for the c-Fos expression occurred in the left and right BLA should be examined further.

4.5. Conclusion. Footshock induced fear behavior and comorbid depression in the situational reminder phase of a traumatic memory. However, the fear and comorbid depression were reduced by the chronic treatment of fluoxetine. In immunohistochemical staining data, the Cg1 and PrL (but not IL) of the mPFC, as well as the BLA, contribute to PTSD symptoms in fear and depression behaviors. Importantly, the BLA was involved in the amelioration of fluoxetine treatments in PTSD symptoms, including fear and depression. However, the other brain areas of the mPFC (such as the Cg1, PrL, and IL) did not regulate fluoxetine treatments in the reduction of the PTSD symptoms. This study is the first one that systematically examines the issue of whether the subareas of the mPFC (e.g., Cg1, PrL, and IL) and BLA are involved in fluoxetine treatments for PTSD symptoms. The present data might help us to further understand the neural mechanism of fluoxetine treatments in PTSD symptoms. Furthermore, the present findings should be considered for developing further pharmacological treatments, as these data can offer some clinical implications.

Data Availability

Data are available from the corresponding author upon reasonable request.

Conflicts of Interest

The authors declare no conflict of interest.

Acknowledgments

This research received support from the Ministry of Science and Technology of the Republic of China (Taiwan) (MOST 108-2410-H-431-009 to Dr. A.C.W. Huang and MOST 108-2320-B-001-024 to Dr. B.C. Shyu). This research received funding from the Ministry of Science and Technology of Taiwan (MOST 108-2410-H-431-009 to Dr. A.C.W. Huang and MOST 108-2320-B-001-024 to Dr. B.C. Shyu). We also thank the support from the Institute of Biomedical Sciences of Academia Sinica in Taiwan.

References

[1] D. J. Nutt and A. L. Malizia, "Structural and functional brain changes in posttraumatic stress disorder," *The Journal of Clinical Psychiatry*, vol. 65, Supplement 1, pp. 11–17, 2004.

[2] B. L. Green, J. L. Krupnick, J. Chung et al., "Impact of PTSD comorbidity on one-year outcomes in a depression trial," *Journal of Clinical Psychology*, vol. 62, no. 7, pp. 815–835, 2006.

[3] C. Zayfert, C. B. Becker, D. L. Unger, and D. K. Shearer, "Comorbid anxiety disorders in civilians seeking treatment for posttraumatic stress disorder," *Journal of Traumatic Stress*, vol. 15, no. 1, pp. 31–38, 2002.

[4] T. F. Giustino and S. Maren, "The role of the medial prefrontal cortex in the conditioning and extinction of fear," *Frontiers in Behavioral Neuroscience*, vol. 9, p. 298, 2015.

[5] R. S. Pynoos, R. F. Ritzmann, A. M. Steinberg, A. Goenjian, and I. Prisecaru, "A behavioral animal model of posttraumatic stress disorder featuring repeated exposure to situational reminders," *Biological Psychiatry*, vol. 39, no. 2, pp. 129–134, 1996.

[6] M. Tanaka, H. Li, X. Zhang et al., "Region- and time-dependent gene regulation in the amygdala and anterior cingulate cortex of a PTSD-like mouse model," *Molecular Brain*, vol. 12, no. 1, p. 25, 2019.

[7] G. Hancu, M. Carcu-Dobrin, M. Budau, and A. Rusu, "Analytical methodologies for the stereoselective determination of fluoxetine: an overview," *Biomedical Chromatography*, vol. 32, no. 1, 2018.

[8] J. Davidson, S. Roth, and E. Newman, "Fluoxetine in posttraumatic stress disorder," *Journal of Traumatic Stress*, vol. 4, pp. 419–423, 1991.

[9] F. Han, B. Xiao, L. Wen, and Y. Shi, "Effects of fluoxetine on the amygdala and the hippocampus after administration of a single prolonged stress to male Wistar rates: in vivo proton magnetic resonance spectroscopy findings," *Psychiatry Research*, vol. 232, no. 2, pp. 154–161, 2015.

[10] L. Herrmann, I. A. Ionescu, K. Henes et al., "Long-lasting hippocampal synaptic protein loss in a mouse model of posttraumatic stress disorder," *PLoS One*, vol. 7, no. 8, article e42603, 2012.

[11] C. Y. Kao, Z. He, A. S. Zannas et al., "Fluoxetine treatment prevents the inflammatory response in a mouse model of posttraumatic stress disorder," *Journal of Psychiatric Research*, vol. 76, pp. 74–83, 2016.

[12] L. M. Shin, S. L. Rauch, and R. K. Pitman, "Amygdala, medial prefrontal cortex, and hippocampal function in PTSD," *Annals of the New York Academy of Sciences*, vol. 1071, no. 1, pp. 67–79, 2006.

[13] M. Koenigs and J. Grafman, "Posttraumatic stress disorder: the role of medial prefrontal cortex and amygdala," *The Neuroscientist*, vol. 15, no. 5, pp. 540–548, 2009.

[14] R. C. Wolf and R. J. Herringa, "Prefrontal-amygdala dysregulation to threat in pediatric posttraumatic stress disorder," *Neuropsychopharmacology*, vol. 41, no. 3, pp. 822–831, 2016.

[15] M. J. Kim, R. A. Loucks, A. L. Palmer et al., "The structural and functional connectivity of the amygdala: from normal emotion to pathological anxiety," *Behavioural Brain Research*, vol. 223, no. 2, pp. 403–410, 2011.

[16] J. D. Townsend, S. J. Torrisi, M. D. Lieberman, C. A. Sugar, S. Y. Bookheimer, and L. L. Altshuler, "Frontal-amygdala connectivity alterations during emotion downregulation in bipolar I disorder," *Biological Psychiatry*, vol. 73, pp. 127–135, 2012.

[17] R. Marek, C. Strobel, T. W. Bredy, and P. Sah, "The amygdala and medial prefrontal cortex: partners in the fear circuit," *The Journal of Physiology*, vol. 591, no. 10, pp. 2381–2391, 2013.

[18] F. Sotres-Bayon, C. K. Cain, and J. E. LeDoux, "Brain mechanisms of fear extinction: historical perspectives on the contribution of prefrontal cortex," *Biological Psychiatry*, vol. 60, no. 4, pp. 329–336, 2006.

[19] R. M. Vouimba and M. Maroun, "Learning-induced changes in mPFC-BLA connections after fear conditioning, extinction, and reinstatement of fear," *Neuropsychopharmacology*, vol. 36, no. 11, pp. 2276–2285, 2011.

[20] L. M. Shin and I. Liberzon, "The neurocircuitry of fear, stress, and anxiety disorders," *Neuropsychopharmacology*, vol. 35, no. 1, pp. 169–191, 2010.

[21] B. A. Dengler, S. A. Hawksworth, L. Berardo, I. McDougall, and A. M. Papanastassiou, "Bilateral amygdala stimulation reduces avoidance behavior in a predator scent posttraumatic stress disorder model," *Neurosurgical Focus*, vol. 45, no. 2, article E16, 2018.

[22] J. Peters, P. W. Kalivas, and G. J. Quirk, "Extinction circuits for fear and addiction overlap in prefrontal cortex," *Learning & Memory*, vol. 16, no. 5, pp. 279–288, 2009.

[23] J. Si, J. Yang, L. Xue et al., "Activation of NF-κB in basolateral amygdala is required for memory reconsolidation in auditory fear conditioning," *PLoS One*, vol. 7, no. 9, article e43973, 2012.

[24] T. J. Mezadri, G. M. Batista, A. C. Portes, J. Marino-Neto, and C. Lino-de-Oliveira, "Repeated rat-forced swim test: reducing the number of animals to evaluate gradual effects of antidepressants," *Journal of Neuroscience Methods*, vol. 195, no. 2, pp. 200–205, 2011.

[25] E. A. Phelps, M. R. Delgado, K. I. Nearing, and J. E. LeDoux, "Extinction learning in humans: role of the amygdala and vmPFC," *Neuron*, vol. 43, no. 6, pp. 897–905, 2004.

[26] W. B. Hoover and R. P. Vertes, "Anatomical analysis of afferent projections to the medial prefrontal cortex in the rat," *Brain Structure & Function*, vol. 212, no. 2, pp. 149–179, 2007.

[27] M. Wicking, F. Steiger, F. Nees et al., "Deficient fear extinction memory in posttraumatic stress disorder," *Neurobiology of Learning and Memory*, vol. 136, pp. 116–126, 2016.

[28] G. Paxinos and K. B. J. Franklin, *The Mouse Brain in Stereotaxic Coordinates*, Academic Press, San Diego, 2001.

[29] J. Zohar, D. Amital, C. Miodownik et al., "Double-blind placebo-controlled pilot study of sertraline in military veterans with posttraumatic stress disorder," *Journal of Clinical Psychopharmacology*, vol. 22, no. 2, pp. 190–195, 2002.

[30] M. B. Stein, N. A. Kline, and J. L. Matloff, "Adjunctive olanzapine for SSRI-resistant combat-related PTSD: a double-blind, placebo-controlled study," *The American Journal of Psychiatry*, vol. 159, no. 10, pp. 1777–1779, 2002.

[31] L. Ariel, S. Inbar, S. Edut, and G. Richter-Levin, "Fluoxetine treatment is effective in a rat model of childhood-induced post-traumatic stress disorder," *Translational Psychiatry*, vol. 7, no. 11, p. 1260, 2017.

[32] L. K. Pedraza, R. O. Sierra, M. Giachero, W. Nunes-Souza, F. N. Lotz, and L. de Oliveira Alvares, "Chronic fluoxetine prevents fear memory generalization and enhances subsequent extinction by remodeling hippocampal dendritic spines and slowing down systems consolidation," *Translational Psychiatry*, vol. 9, no. 1, p. 53, 2019.

[33] A. Siegmund and C. T. Wotjak, "A mouse model of posttraumatic stress disorder that distinguishes between conditioned and sensitised fear," *Journal of Psychiatric Research*, vol. 41, no. 10, pp. 848–860, 2007.

[34] S. Shafia, A. A. Vafaei, S. A. Samaei et al., "Effects of moderate treadmill exercise and fluoxetine on behavioural and cognitive deficits, hypothalamic-pituitary-adrenal axis dysfunction and alternations in hippocampal BDNF and mRNA expression of apoptosis - related proteins in a rat model of post-traumatic stress disorder," *Neurobiology of Learning and Memory*, vol. 139, pp. 165–178, 2017.

[35] K. M. Moench and C. L. Wellman, "Stress-induced alterations in prefrontal dendritic spines: implications for post-traumatic stress disorder," *Neuroscience Letters*, vol. 601, pp. 41–45, 2015.

[36] C. M. V. Weele, C. A. Siciliano, and K. M. Tye, "Dopamine tunes prefrontal outputs to orchestrate aversive processing," *Brain Research*, vol. 1713, pp. 16–31, 2019.

[37] M. Arruda-Carvalho and R. L. Clem, "Prefrontal-amygdala fear networks come into focus," *Frontiers in Systems Neuroscience*, vol. 9, p. 145, 2015.

[38] A. Lguensat, Y. Bentefour, M. Bennis, S. Ba-M'hamed, and R. Garcia, "Susceptibility and resilience to PTSD-like symptoms in mice are associated with opposite dendritic changes in the prelimbic and infralimbic cortices following trauma," *Neuroscience*, vol. 418, pp. 166–176, 2019.

[39] U. Schmidt, L. Herrmann, K. Hagl et al., "Therapeutic action of fluoxetine is associated with a reduction in prefrontal cortical miR-1971 expression levels in a mouse model of posttraumatic stress disorder," *Frontiers in Psychiatry*, vol. 4, p. 66, 2013.

[40] R. Reznikov, F. R. Bambico, M. Diwan et al., "Prefrontal cortex deep brain stimulation improves fear and anxiety-like behavior and reduces basolateral amygdala activity in a preclinical model of posttraumatic stress disorder," *Neuropsychopharmacology*, vol. 43, no. 5, pp. 1099–1106, 2018.

Hindawi
Behavioural Neurology
Volume 2020, Article ID 1712604, 12 pages
https://doi.org/10.1155/2020/1712604

Research Article

Machine Learning Based on a Multiparametric and Multiregional Radiomics Signature Predicts Radiotherapeutic Response in Patients with Glioblastoma

Zi-Qi Pan, Shu-Jun Zhang, Xiang-Lian Wang, Yu-Xin Jiao, and Jian-Jian Qiu

Department of Radiation Oncology, Shanghai Huadong Hospital, Fudan University, Shanghai 200040, China

Correspondence should be addressed to Jian-Jian Qiu; qiujianjian@fudan.edu.cn

Received 13 July 2020; Revised 15 September 2020; Accepted 23 September 2020; Published 24 October 2020

Academic Editor: Muh-Shi Lin

Background and Objective. Although radiotherapy has become one of the main treatment methods for cancer, there is no noninvasive method to predict the radiotherapeutic response of individual glioblastoma (GBM) patients before surgery. The purpose of this study is to develop and validate a machine learning-based radiomics signature to predict the radiotherapeutic response of GBM patients. *Methods*. The MRI images, genetic data, and clinical data of 152 patients with GBM were analyzed. 122 patients from the TCIA dataset (training set: $n = 82$; validation set: $n = 40$) and 30 patients from local hospitals were used as an independent test dataset. Radiomics features were extracted from multiple regions of multiparameter MRI. Kaplan-Meier survival analysis was used to verify the ability of the imaging signature to predict the response of GBM patients to radiotherapy before an operation. Multivariate Cox regression including radiomics signature and preoperative clinical risk factors was used to further improve the ability to predict the overall survival (OS) of individual GBM patients, which was presented in the form of a nomogram. *Results*. The radiomics signature was built by eight selected features. The *C*-index of the radiomics signature in the TCIA and independent test cohorts was 0.703 ($P < 0.001$) and 0.757 ($P = 0.001$), respectively. Multivariate Cox regression analysis confirmed that the radiomics signature (HR: 0.290, $P < 0.001$), age (HR: 1.023, $P = 0.01$), and KPS (HR: 0.968, $P < 0.001$) were independent risk factors for OS in GBM patients before surgery. When the radiomics signature and preoperative clinical risk factors were combined, the radiomics nomogram further improved the performance of OS prediction in individual patients (*C*-index = 0.764 and 0.758 in the TCIA and test cohorts, respectively). *Conclusion*. This study developed a radiomics signature that can predict the response of individual GBM patients to radiotherapy and may be a new supplement for precise GBM radiotherapy.

1. Introduction

Glioblastoma is the most common malignant tumour of the central nervous system in adults. At present, the standard therapy for glioblastoma patients is surgery and radiotherapy and adjuvant or concurrent chemotherapy [1]. The median survival time of glioblastoma is 14-15 months [2]. However, in the actual clinical practice, the difference in OS of individual GBM patients is very significant [3–5]. As one of the main methods of cancer treatment, radiotherapy plays an important role in the comprehensive multimodal treatment of GBM. In the era of personalized medicine, the core principle of precision medicine is that cancer treatment should be adjusted according to the biological heterogeneity of individual patients. However, the current radiotherapy plan still assumes that each patient benefits from the same dose plan [6], ignoring the heterogeneity of individual tumour patients. It means that clinical practice needs a marker that can predict the response of radiotherapy to lead to more personalized clinical decision making or dose adjustments for patients.

Recent studies have developed and validated some genetic markers for predicting radiotherapeutic response in individual cancer patients. By clustering four different microarray experiments, Kim et al. built a radiotherapeutic response prediction signature [7] containing 31 genes. The 31-gene signature has been validated in independent clinical

datasets of different cancer types, including glioblastoma [8], low-grade gliomas [9], head and neck tumours [10], and oesophageal cancer [11]. Eschrich et al. constructed the tumour radiosensitivity index (RSI) [12], which has also been verified in a number of different types of tumour datasets [13].

However, the main drawback of these signatures for predicting response to radiotherapy is that tumour samples must be sequenced, which can only be performed after surgery or biopsy. At the same time, a GBM tissue biopsy is associated with a risk of neurological impairment, and the small samples obtained cannot reflect the overall heterogeneity of the whole tumour.

Therefore, in order to overcome these limitations, it is necessary to develop a noninvasive technology to identify the tumour response to radiotherapy. Radiomics has the advantages of being highly specific and noninvasive. It can mine high-throughput quantitative features from traditional medical images and apply them to clinical decision-making or improve the accuracy of diagnosis and prognosis [14, 15]. Compared with traditional methods, radiomics has two unique advantages. First, radiomics allows semiautomatic or automatic extraction of features and provides more quantitative data than qualitative analysis. Second, by extracting the features of different subregions, the tumour phenotype can be described in depth, which not only reflects the macroscopic characteristics of the tumour tissue but also reflects the molecular characteristics of tumour and the responsiveness to treatment [16–18]. The study by Grossmann et al. showed that extracting the image features of GBM from multiple sequences and multiple subregions can provide a variety of tumour biological information, including information about the cell cycle, inflammation, and immune response, which affects the prognosis of patients [19]. Beig et al. successfully constructed a radiomics scoring model to evaluate hypoxia in GBM patients by using the expression profiles of 21 genes related to the hypoxia pathway of GBM [20]. All of these indicate that radiomics is an extremely promising method to assist in the development of individualized treatment strategies for GBM [21].

This study hypothesized that the radiotherapeutic response of GBM patients may be related to the high-dimensional information in different subregions of MR images and developed a radiomics signature based on a machine learning algorithm to predict the radiotherapeutic response of GBM patients. The performance for predicting the OS of individual GBM patients was further improved by constructing a nomogram combining the imaging markers and clinical factors.

2. Methods and Materials

2.1. Patients. In this retrospective study, a total of 152 pathologically confirmed GBM patients were included: 122 from the TCGA-GBM [22] dataset in the cancer imaging database (TCIA) [23] and 30 from a local hospital dataset (January 2013 to February 2019). To evaluate the prognostic value of radiomics signature, OS was calculated as the time from the initial diagnosis to death or censure point (June 15, 2020) if patients were still alive. At the median 14.7-month follow-up, 11 (36.67%) patients from the local hospital were alive.

TCIA (http://www.cancerimagingarchive.net) is a publicly available database, and the medical images of patients are deidentified; therefore, it does not need the approval of the institutional review committee. The data from the local hospital were approved by the ethics committee of the hospital, and informed consent of the patients was waived. All images were obtained at the time of the initial diagnosis.

The inclusion criteria for the TCIA dataset used to build the radiomics signature were as follows: (1) newly diagnosed histologically confirmed GBM (WHO classification IV); (2) preoperative MRI images with a complete sequence, including T1-weighted, postcontrast T1-weighted, T2-weighted, and T2 flair (T1W, T1c, T2W, and T2FLAIR, respectively) images; (3) original dataset with corresponding gene expression values (HU-133A); and (4) satisfactory image quality.

Using patients from a local hospital ($n = 30$) and the TCIA dataset receiving radiotherapy ($n = 102$), the ability of the radiomics signature to predict individual GBM patients' radiotherapeutic responses was verified. The inclusion criteria for these data were as follows: (1) GBM (WHO classification IV) with newly diagnosed histology; (2) postoperative radiotherapy; (3) preoperative MRI images with complete sequences, including T1-weighted, postcontrast T1-weighted, T2-weighted, and T2 flair (T1W, T1c, T2W, and T2FLAIR, respectively); (4) satisfactory image quality; and (5) OS that could be achieved through follow-up. The flowchart of this study is shown in Figure 1. The detailed data exclusion process in TCIA is described in Supplement S1 and Figure S1, and the local dataset is described in Supplement S2 and Figure S2.

2.2. MRI Data Acquisition

2.2.1. MR Image Acquisition of TCIA Cohort. MRI was performed with a 1.5 or 3.0 T scanner before operation. In TCIA images, the T1 sequence parameters were as follows: TR/TE, 352-3379 msec/2.75-19 msec; and slice thickness, 1-5 mm. The parameters of the T1 enhancement sequence were as follows: repeat time (TR)/echo time (TE), 4.9–3285 msec/2.1–20 msec and slice thickness, 1–5 mm. The parameters of the T2 sequence were as follows: TR/TE, 700-6370 msec/15-120 msec and slice thickness, 1.5-5 mm. The parameters of the T2FLAIR sequence were as follows: TR/TE, 6000–11000 msec/34.6–155 msec and slice thickness, 2.5–5 mm.

2.2.2. Local Cohort MR Image Acquisition. Preoperative MRI was performed with a 3.0 T scanner (GE Signa HD xt) and 8-channel array coil. In the images from the local hospital, the parameters of the T1 sequence were as follows: TR/TE, 139-409 msec/2.46-2.48 msec and slice thickness, 5 mm. The parameters of the T1 enhancement sequence were as follows: TR/TE, 220–2300 msec/2.34–2.5 msec and slice thickness, 1-5 mm. The parameters of the T2 sequence were as follows: TR/TE, 4000-6000 msec/92-125 msec and slice thickness, 5 mm. The parameters of the T2FLAIR sequence were as follows: TR/TE, 7000–9000 msec/81–85 msec and slice thickness, 5 mm.

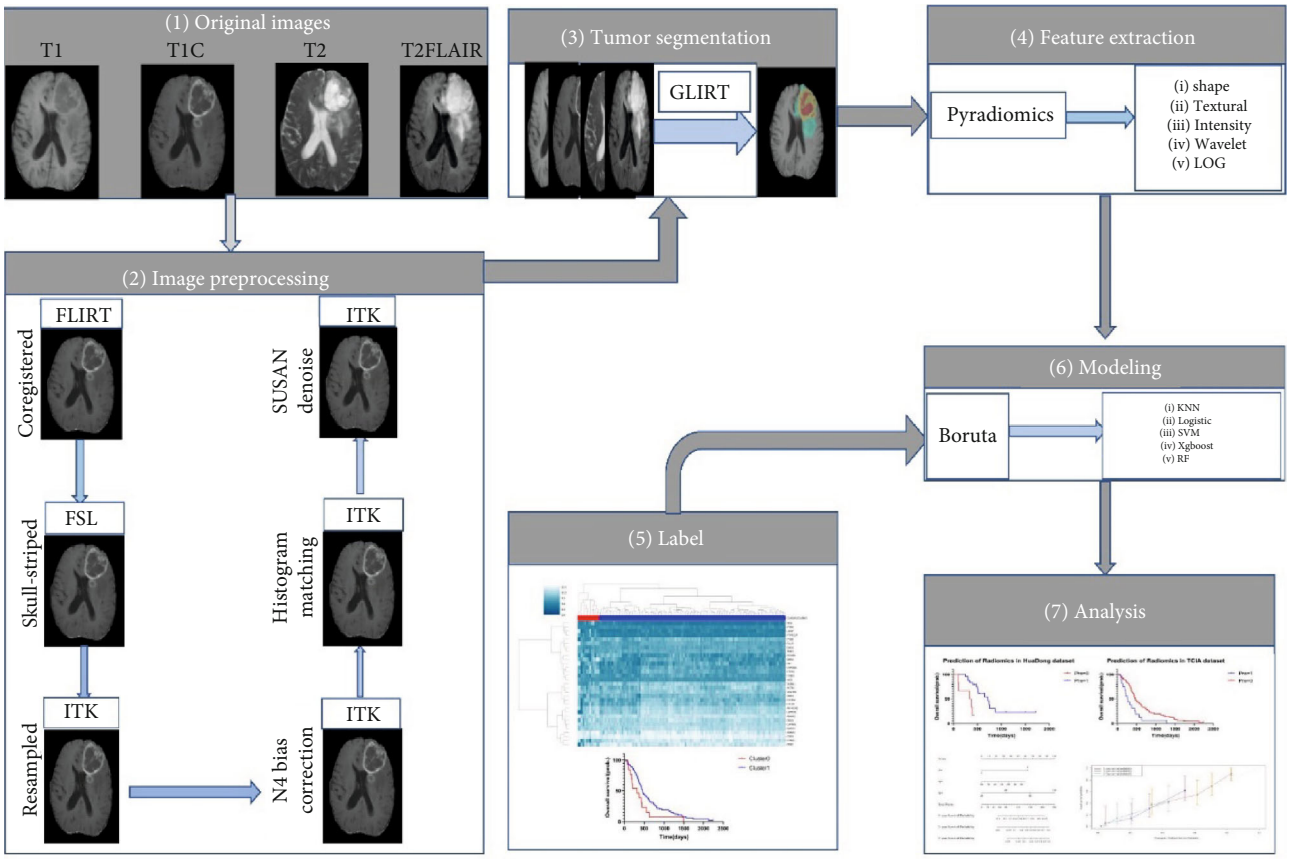

Figure 1: A flowchart describing the radiomics method for prediction of radiotherapy response. (1) Preprocess the original image; (2) delineate the subregion ROI by GLISTR; (3) feature extraction using pyradiomics; (4) 31-gene signature were used to predict the result of the corresponding data, and a label was generated. (5) Feature selection by the Boruta algorithm; (6) modeling by a variety of machine learning methods, ROC curve, and AUC evaluation model; (7) building a prediction model by combining radiomics signature features and clinical features, finally displaying the OS prediction results by nomogram.

2.3. Radiotherapeutic Response. The TCGA-GBM dataset in the TCGA (The Cancer Genome Atlas) database was used to evaluate the radiotherapeutic response of individual GBM patients. Gene expression data (HU-133A microarray) corresponding to the TCIA image data were obtained from the UCSC Xena browser (https://xenabrowser.net). According to the previous study [7] of Kim et al., a 31-gene model was used to evaluate the radiotherapeutic response, which is a model to calculate the SF2 (2 Gy survival fraction, which represented radiosensitivity) value distribution of individual patients through gene expression.

Based on the expression of the specific 31 genes in the TCGA dataset, the patients were divided into two groups by a hierarchical clustering method ($k = 2$): radiotherapy effective group (RE) and radiotherapy resistance group (RR). Kaplan-Meier survival analysis was performed to verify the prediction results of the 31-gene model.

2.4. Image Preprocessing and Tumour Segmentation. Image preprocessing was mainly performed through the FMRIB software library (http://fsl.fmrib.ox.ac.uk/fsl/fslwiki/FSL) and with Python's SimpleITK package. To increase the robustness of features as much as possible through preprocessing [24], the following steps were adopted in this study: use of FLIRT in FMRIB to coregister the same T1WI image [25] as the template. After skull stripping, the isotropic voxel was resampled [26] to $1 \times 1 \times 1\,\text{mm}^3$. N4ITK [27] was used to correct the bias field of each image sequence to eliminate the influence of pixel extremum in the image as much as possible. Since the image data were collected by different centres, a landmark-based method [28] was used to standardize the intensity. Then, the SUSAN method [29] (Smallest Univalue Segment Assimilating Nucleus) was used to smooth the image to reduce the interference of high-frequency intensity changes in different images. The image preprocessing process is shown in Figure 1.

GLISTR (glioma image segmentation and registration) software [30] was used to segment the image automatically. After preprocessing, the image was automatically divided into four segmentation subregions, i.e., the tumour enhancement area, tumour nonenhancement area, peritumoural edema area, and whole tumour. After that, two different radiotherapy doctors reviewed and revised the segmentation results together. Figure 2 shows an example of the segmentation results.

2.5. Radiomics Feature Extraction. Based on the above four subregions, five groups of features were extracted by

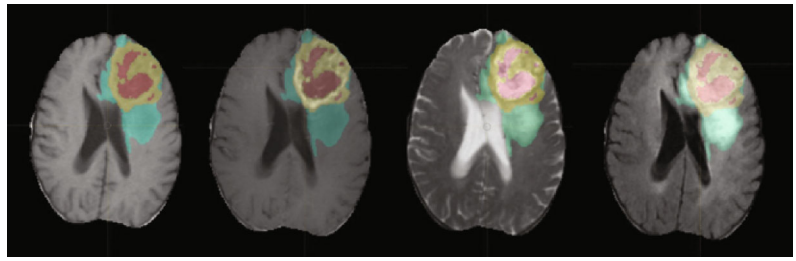

Figure 2: The segmentation result of tumour subregions overlapped on T1WI, CE-T1WI, T2WI, and FLAIR images.

pyradiomics including the following: (I) shape features, (II) intensity features, (III) texture features, (IV) intensity and texture features under wavelet transformation, and (V) intensity and texture features under Gaussian Laplace transformation. Shape features describe the shape and volume of the tumour. Intensity features refer to the first-order statistics of all voxel intensity values in the region of interest (ROI). Texture features use the Gray Level Cooccurrence Matrix (GLCM), Gray Level Dependence Matrix (GLDM), Gray Level Run-Length Matrix (GLRLM), Gray Level Size-Zone Matrix (GLSZM), and Neighbouring Gray Tone Difference Matrix (NGTDM) to quantify sharp changes in the gray spectrum. Wavelet and Gaussian Laplacian features are obtained by extracting voxel features and texture features, respectively, after applying wavelet or Gaussian Laplace transformation to the image. These two processes can obviously show the features of the image edge. Finally, for each image, 28496 features were extracted from four segmentation regions of four sequences. For the detailed definition of features, please refer to Supplement S3.

2.6. Radiomics Feature Selection. The Boruta algorithm [31] was used for feature selection. Boruta is a packing algorithm for selecting all relevant features. After comparing the importance of original features and random features for modeling, the important features were arranged from top to bottom, and the P values were corrected by the Benjamin Hochberg method to ensure their reliability. To ensure the robustness and replicability of features, 20 cases were randomly selected from all datasets. A region of interest (ROI) was generated after GLISTR automatic segmentation. The generated ROI was modified by different doctors to generate two independent groups of new ROIs.

The two new groups of new ROIs including four subregions were used to extract the corresponding radiomics features from four sequences of MRI images in 20 cases, and the intraclass correlation coefficient (ICC) of each feature was calculated [32]. Among them, the features with an ICC of 0.9 were considered to be robust [33] and were included in the study.

2.7. Radiomics Signature and Nomogram Construction. To develop the radiomics signature, all cases from the TCIA database were stratified and sampled by a computer-generated random number according to the ratio of 2 : 1 and were divided into a training set ($n = 82$) and a validation set ($n = 40$). Because the data from the RE and RR groups were unbalanced, the training set was first balanced by using the synthetic minority oversampling technique (SMOTE) algorithm [34]. The SMOTE algorithm is a kind of oversampling algorithm for fewer classes. It is generally considered that it can effectively balance imbalanced samples. Several machine learning algorithms, such as logistic regression (logistic), random forest (RF), support vector machine (SVM), k-nearest neighbour (KNN), and Xgboost (Xgboost, extreme gradient boosting), were used to model. The input of the model was the selected features, and the output was the results of the 31-gene model prediction.

The purpose of using these machine learning methods was to build a model to predict the radiotherapeutic response of GBM patients by inputting quantitative image features before surgery. Through 10-fold cross-validation, a grid search was carried out on the training set to determine the optimal tuning parameters of each machine learning algorithm. The AUC and ROC curve were used to evaluate the model in the training set and validation set, respectively, and the most suitable model was selected.

Due to the lack of gene expression data in local hospitals, we used an indirect method to verify the model independently. We hypothesized that among the 30 local GBM patients with basically the same treatment, the OS of the cluster with strong response to radiotherapy should be longer than that of the patients with radiotherapy resistance and was verified by Kaplan survival analysis. In order to further construct the OS prediction model for individual GBM patients, univariate and multivariate Cox regression models were used to evaluate the effects of the radiomics signature and clinical factors (such as KPS, age, gender, and tumour location) on OS. Multivariate Cox regression was performed for independent risk factors and presented in the form of a nomogram. The calibration curve was used to evaluate the consistency between the nomogram and the observed values, and the Harrell consistency index (C-index) was used to quantify the discrimination performance.

2.8. Statistical Analysis. All data were analyzed by SPSS (version 19.0), R software (3.4), and Python (3.7). Pearson's chi-squared test or Student's t-test (as appropriate) were performed with SPSS to evaluate the differences between the TCIA and local hospital datasets in terms of age, gender, KPS, survival status, OS, etc. The statistical significance levels were all two-sided, with the statistical significance level set at 0.05. The C-index was calculated with the "hmisc" software package. ROC curves were drawn using the "pROC" package. Feature selection used the R package which is "Boruta," and classifier building was mainly performed using the following

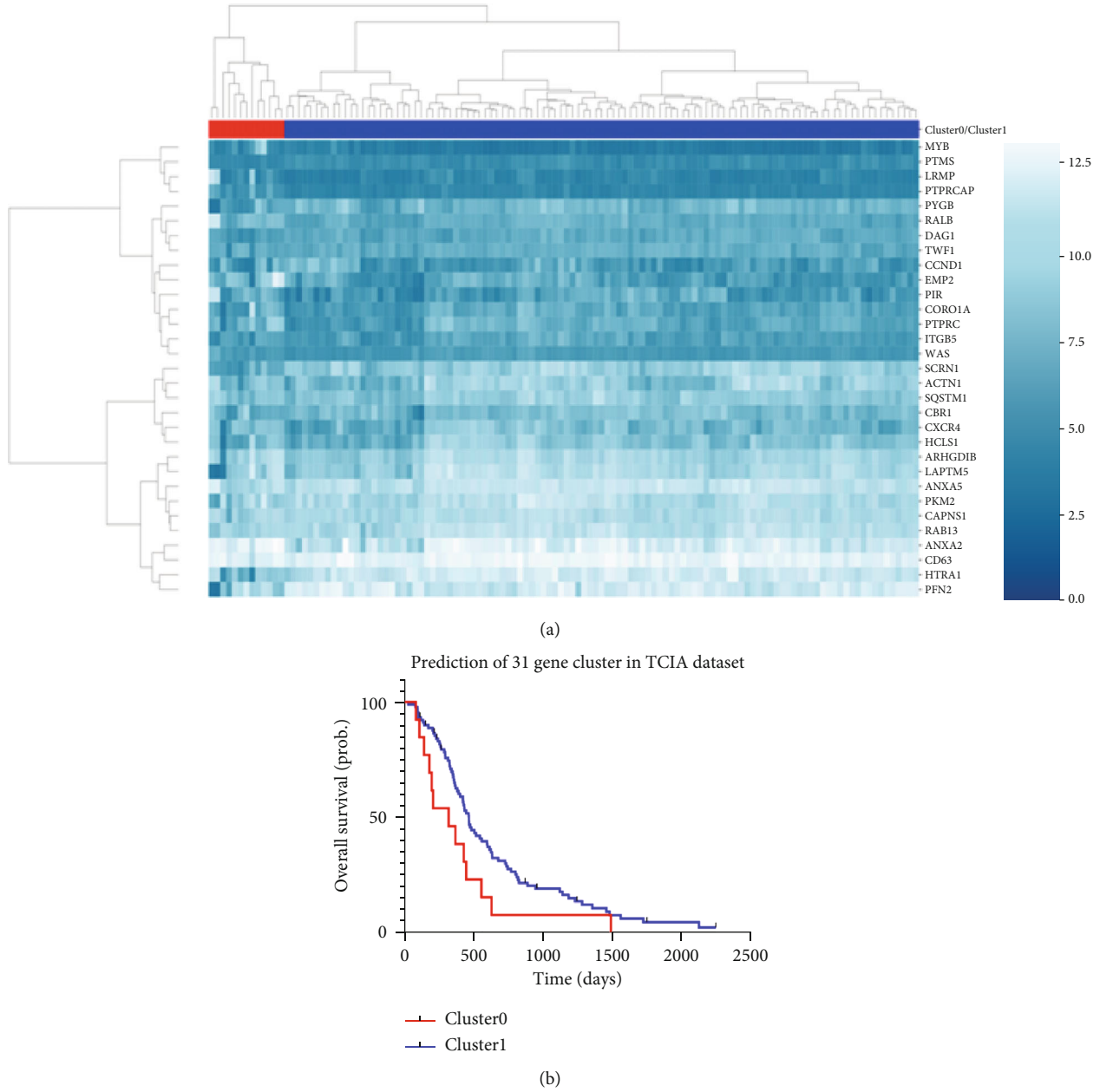

FIGURE 3: Hierarchical clustering was used to determine the expression pattern of the 31-gene signature on the samples from TCGA (Figure 3(a)). The samples in the red branch on the left side of the dendrogram are classified as Cluster0, while the samples in the blue branch on the right side are classified as Cluster1. After using Kaplan-Meier survival analysis, the prognosis of Cluster0 is different from that of Cluster1, so according to Kim et al.'s report, Cluster0 was subclassified as the radiotherapy resistance group (RR), whereas Cluster1 was a radiotherapy effective group (RE) (Figure 3(b)).

Python packages: "Gridsearchcv," "Sklearn," "SMOTE," and "Xgboost."

3. Results

3.1. Patient Characteristics. First, gene expression data of 122 patients were included in the 31-gene model to calculate the distribution of the SF2 value. In order to test the accuracy of this distribution, Kaplan survival analysis was performed in 102 patients who received radiotherapy. It can be seen that Cluster0 in the red part on the left side is the RR group, and Cluster1 in the blue part is the RE group ($P < 0.05$), as shown in Figure 3.

The clinical data and results of the model are summarized in Table 1. There was no significant difference in age, gender, KPS, and OS between the TCIA dataset and independent test group ($P > 0.05$). In this study, 122 cases from the TCIA dataset were divided into the RR group (13 cases) and the RE group (109 cases). The reason for this result is that the 31-gene model is a marker to distinguish the responsiveness

Table 1: Characteristics of patients in the TCIA and independent test datasets.

Characteristic	TCIA ($N = 102$)	Huadong ($N = 30$)	P
Ages (years)			0.856
Range	17-80	18-73	
Median	57.5	54	
Mean ± SD	56.10 ± 14.35	52 ± 13.68	
Gender, No. (%)			0.847
Female	40 (39.22%)	13 (43.33%)	
Male	62 (60.78%)	17 (56.67%)	
Status, No. (%)			0.0011
Alive	10 (9.8%)	11 (36.67%)	
Dead	92 (90.2%)	19 (63.33%)	
KPS			0.2795
KPS > 60	75	21	
KPS ≤ 60	17	9	
Not reported	10	0	
Tumour location			0.377
Frontal lobe	24	12	
Temporal lobe	43	11	
Parietal lobe	19	4	
Occipital lobe	8	3	
Insular lobe	6	0	
Callosum lobe	2	0	
OS (months)			0.6516
Range	1-74.87	3.3-52.43	
Median	14.30	14.77	
Mean ± SD	18.90 ± 15.23	17.53 ± 10.70	
31-gene prediction result			
RH	89	—	
RR	13	—	
Radiomics prediction result			0.8813
RH	85	24	
RR	17	6	

to radiotherapy in the sample, and the results of the cluster analysis depend on the sample size and median value.

3.2. Feature Selection. After using the Boruta algorithm for feature selection and applying the Benjamin Hochberg method to correct the P value, 8 features were retained, as shown in Table 2.

All features selected by the Boruta algorithm were qualified (the ICC value was higher than 0.9). A summary of the ICC results for the features can be found in Supplement S4 and Figure S3.

3.3. Radiomics Signature Construction. The AUCs of RF, SVM, KNN, logistic, and Xgboost were 0.980, 0.965, 0.969, 0.974, and 0.962, respectively, and 0.937, 0.874, 0.874, 0.931, and 0.880, respectively. The ROC curves of the five machine learning methods are shown in Figure 4, and the accuracy, sensitivity, and specificity of the model are summarized in Tables 3 and 4. Because of the best performance, the RF model was chosen as the final radiomics signature model.

3.4. Survival Analysis. Individual GBM patients' radiotherapeutic responses to radiotherapy in the TCIA ($n = 102$) and test ($n = 30$) datasets were predicted using radiomics signature.

After Kaplan-Meier analysis, as shown in Figure 5, the C-index of the radiomics signature in the TCIA and test datasets was 0.703 (95% CI: 0.642-0.764, $P < 0.001$) and 0.757 (95% CI: 0.663-0.851, $P = 0.001$), respectively.

3.5. Construction and Evaluation of Nomogram. Univariate and multivariate Cox regression analyses using the radiomics signature, age, and KPS as independent risk factors were performed (radiomics signature: HR: 0.290, 95% CI: 0.160-0.526, $P < 0.001$; age: HR: 1.023, 95% CI: 1.005-1.040, $P = 0.01$; and KPS: HR:0.968, 95% CI: 0.950-0.987, $P < 0.001$).

According to the relevant factors of the multivariate Cox regression analysis, the nomogram was constructed (Figure 5). The C-index of the nomogram in the TCIA dataset was 0.764 (95% CI: 0.723-0.806, $P < 0.001$), and that of the test dataset was 0.758 (95% CI: 0.667-0.838, $P < 0.001$), indicating that the prediction performance was improved. The calibration curves of 1-, 2-, or 3-year OS probability after radiotherapy are shown in Figure 6. The calibration curve of the nomogram shows that there is satisfactory consistency between the prediction and observation possibility of OS in 1, 2, and 3 years in the TCIA and independent test datasets.

4. Discussion

This study built a radiomics signature based on three texture, one shape, and four intensity features and verified that it can predict the response of individual patients to radiotherapy on an independent test dataset.

Since the model constructed in this study only predicted the results of a 31-gene model through preoperative images, it was not necessary to consider whether the patient had received radiotherapy in the modeling stage of this study. In the validation stage of this model, because the 31-gene model is only a model with predictive effect in patients who have received radiotherapy, only 102 of 122 patients who have received radiotherapy are included in the validation phase.

Different from other studies using radiomics to predict the response to radiotherapy [35], this study used a 31-gene signature. This is because there are many confounding factors in reflecting the response ability of patients to radiotherapy with clinical results. However, the 31-gene clustering model based on the SF2 value can only predict the individual's response ability after radiotherapy [7] and has been verified [8]. Therefore, the radiomics signature constructed in this study can be verified by a Kaplan-Meier survival curve; that is, the OS of the sensitive cluster is longer than that of the resistant cluster.

Since the model constructed in this study only predicted the results calculated by a 31-gene model through

Table 2: A summary of the high-throughput radiomics features extracted.

MRI sequences	Region	Group	Feature name	Type
T1WI	Whole tumour	Shape	MinorAxisLength	Origin
CE-T1WI	Edema	Texture	MeanAbsoluteDeviation	Wavelet-HHL
CE-T1WI	Enhancement	Texture	GLCM_JointEnergy	Wavelet-LLH
CE-T1WI	Enhancement	Texture	GLDM_DependenceNonUniformityNormalized	Wavelet-LLH
CE-T1WI	Enhancement	Intensity	90Percentile	Wavelet-LHH
CE-T1WI	Enhancement	Intensity	90Percentile	Wavelet-HLH
T2WI	Whole tumour	Intensity	90Percentile	Log-sigma-1-mm
T2WI	Nonenhancement	Texture	GLSZM-SizeZoneNonUniformity	Wavelet-LHH

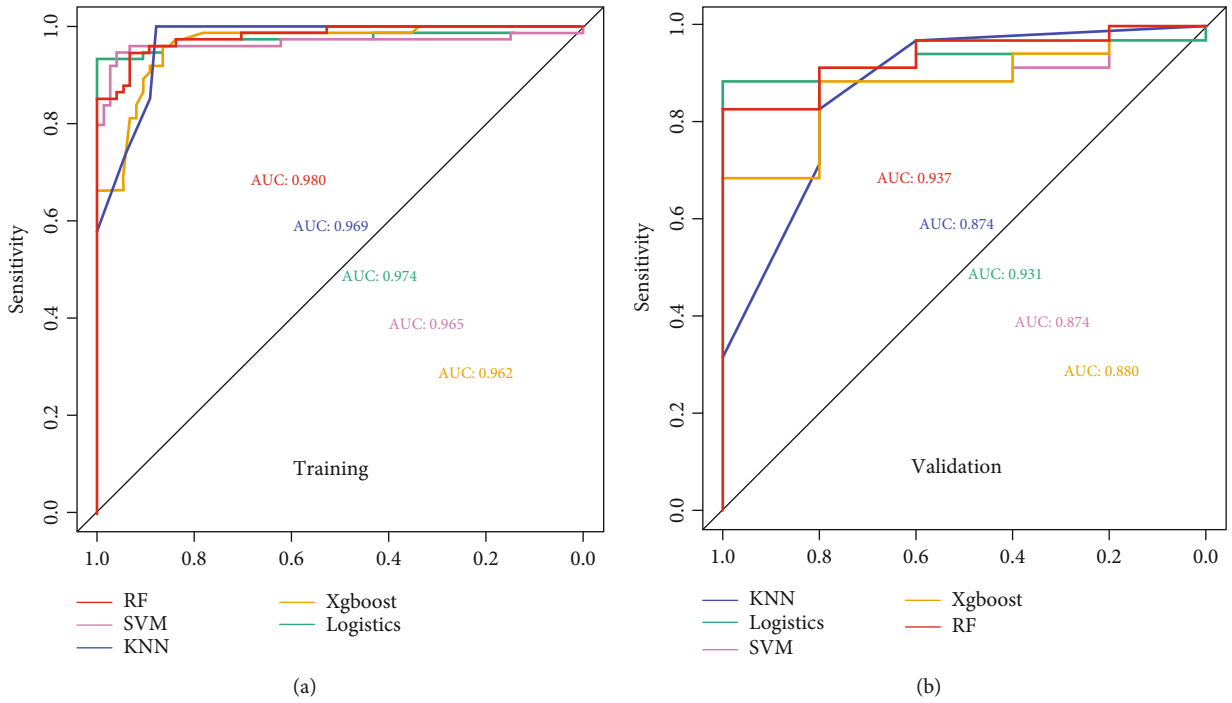

Figure 4: Receiver operating characteristic (ROC) curves of training (a) and validation (b) sets under different machine learning algorithms. It can be seen from the figure that the random forest algorithm performs best. KNN: *k*-nearest neighbour; logistics: logistic regression; SVM: support vector machine; Xgboost: extreme gradient boosting; RF: random forest.

Table 3: A summary of the AUC with different machine learning methods on the TCIA dataset.

Algorithm	AUC	95% CI	SENS	SPEC	ACC	*P*
RF	0.980	0.942-0.996	0.946	0.932	0.939	<2.2*e*-16
SVM	0.965	0.921-0.988	0.905	0.972	0.939	<2.2*e*-16
KNN	0.969	0.926-0.990	0.757	0.932	0.844	<2.2*e*-16
Logistic	0.974	0.933-0.993	0.932	1	0.966	<2.2*e*-16
Xgboost	0.962	0.917-0.987	0.865	0.905	0.885	<2.2*e*-16

SENS: sensitivity; SPEC: specificity; ACC: accuracy.

preoperative images, it was not necessary to consider whether the patient had received radiotherapy in the modeling stage of this study. In the validation stage of this model, because the 31-gene model is only a model with predictive effect in patients who have received radiotherapy, only 102 of 122 patients who have received radiotherapy are included in the validation phase.

In order to further improve the ability to predict the OS of individual patients, this study constructed a nomogram including the radiomics signature and preoperative clinical

Table 4: A summary of the AUC with different machine learning methods on the independent test dataset.

Algorithm	AUC	95% CI	SENS	SPEC	ACC	*P* value
RF	0.937	0.813-0.989	0.829	1	0.9	<2.2*e*-16
SVM	0.874	0.732-0.957	0.771	0.800	0.775	1.375*e*-08
KNN	0.874	0.731-0.958	0.714	0.800	0.725	7.63*e*-05
Logistic	0.931	0.805-0.987	0.886	1	0.900	<2.2*e*-16
Xgboost	0.880	0.738-0.961	0.886	0.800	0.875	6.851*e*-09

SENS: sensitivity; SPEC: specificity; ACC: accuracy.

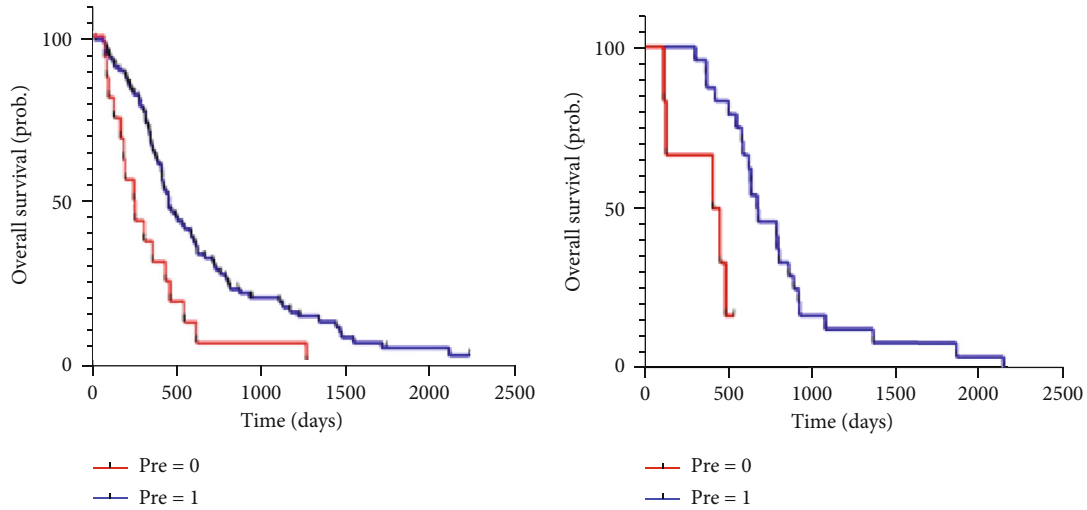

(a) Prediction of radiomics signature in TCIA dataset

(b) Prediction of radiomics signature in test dataset

Figure 5: Using Kaplan-Meier analysis to verify the performance of radiomics signature. The response ability of GBM patients to radiotherapy was successfully divided into the high-risk group (radiotherapy resistance group, pre = 0) and low-risk group (radiotherapy effective group, pre = 1) according to the prediction results of radiomics signature. There were significant differences in TCIA (a) and test (b) datasets between the high-risk group and the low-risk group.

factors. The *C*-index of the nomogram was 0.764 (95% CI: 0.723-0.806, $P < 0.001$) and 0.758 (95% CI: 0.667-0.838, $P < 0.001$) in the TCIA dataset and independent test dataset, which was higher than that with the single application of the radiomics signature (the *C*-index of the TCIA dataset was 0.703, 95% CI: 0.642-0.764, $P < 0.001$; and the *C*-index of the independent test dataset was 0.757, 95% CI: 0.663-0.851, $P = 0.001$), indicating that the combination of multiple risk factors can improve the ability to predict the OS of individual GBM patients. MGMT methylation or IDH mutation status was not included in this study because the purpose of this study was to build a radiomics signature to predict the response of individual GBM patients to radiotherapy by extracting preoperative imaging features. MGMT methylation and IDH mutation status need to be obtained after operation or biopsy, which undoubtedly limits the application of the nomogram in patients who cannot be operated.

Multiparameter imaging sequences contain the comprehensive information of the tumour; for instance, T1WI images reflect the anatomical information of the tumour, and CE-T1WI images include information regarding tumour local angiogenesis and blood-brain barrier damage. Previous studies have shown that multisequence imaging features can be used to predict the heterogeneity and gene expression of individual tumours. The radiomics signature included 1 edema subregion, 4 tumour enhancement subregions, 1 tumour nonenhancement subregion, and 2 overall tumour features. This may be because the nonenhancement subregion is related to the process of apoptosis. The features of the enhancement subregion are related to the process of signal transduction and protein folding, and the edema subregion mainly reflects the process of the cell cycle [19]. These tumour biological pathways are related to the function of the genes in the 31-gene signature and have been proven to be related to the response ability of cells to radiation [7].

The core of precision medicine is to make clinical decisions according to individual heterogeneity. For GBM, radiotherapy has become an important part of standard therapy. How to choose the most appropriate treatment strategy or adjust the radiotherapy dose parameters to better match the biological phenotypes of individual patients has become a problem.

In a recent study [36], the authors combined gene expression values with traditional LQ models to build a dose-response model for individual patients. According to the model, patients can be divided into several clusters, and the

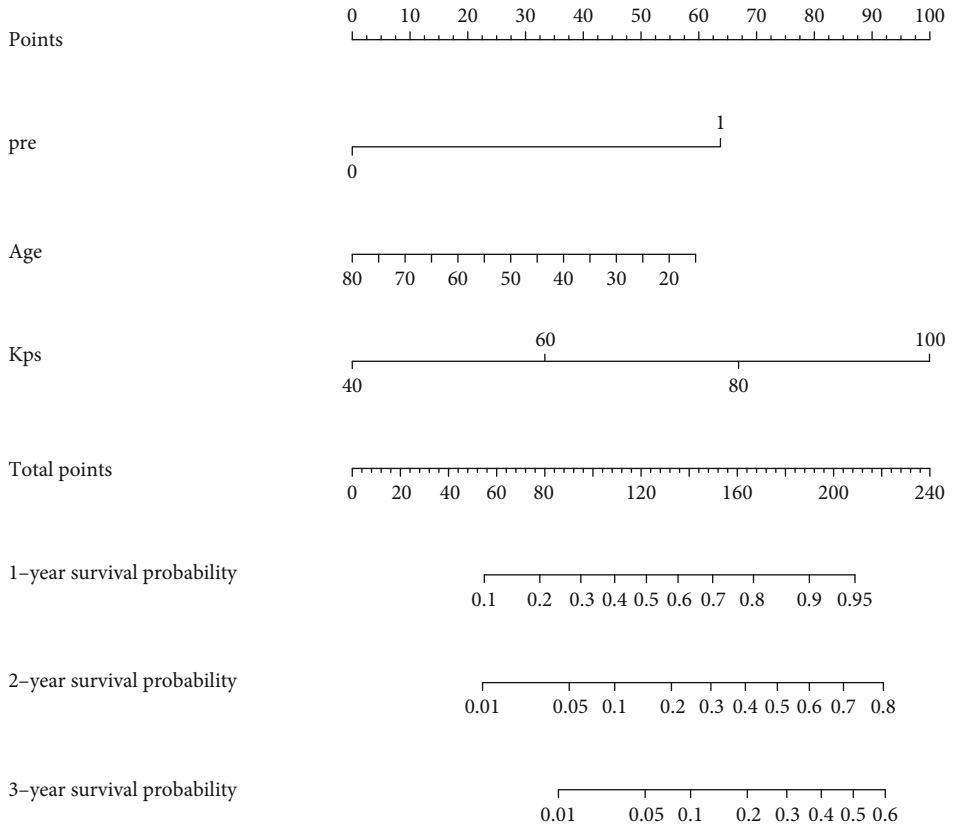

(a)

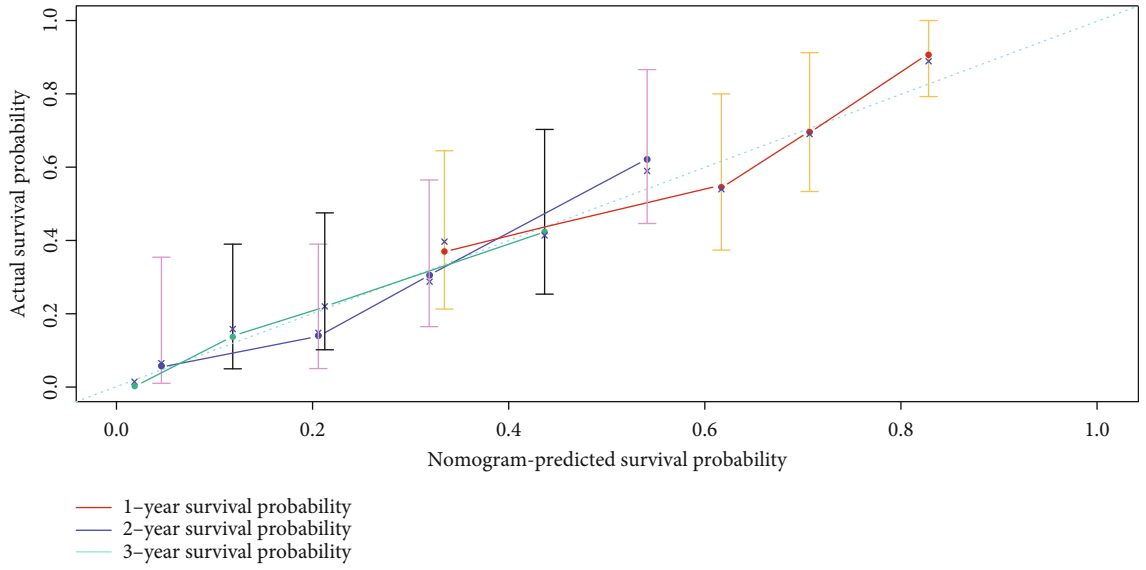

(b)

Figure 6: Continued.

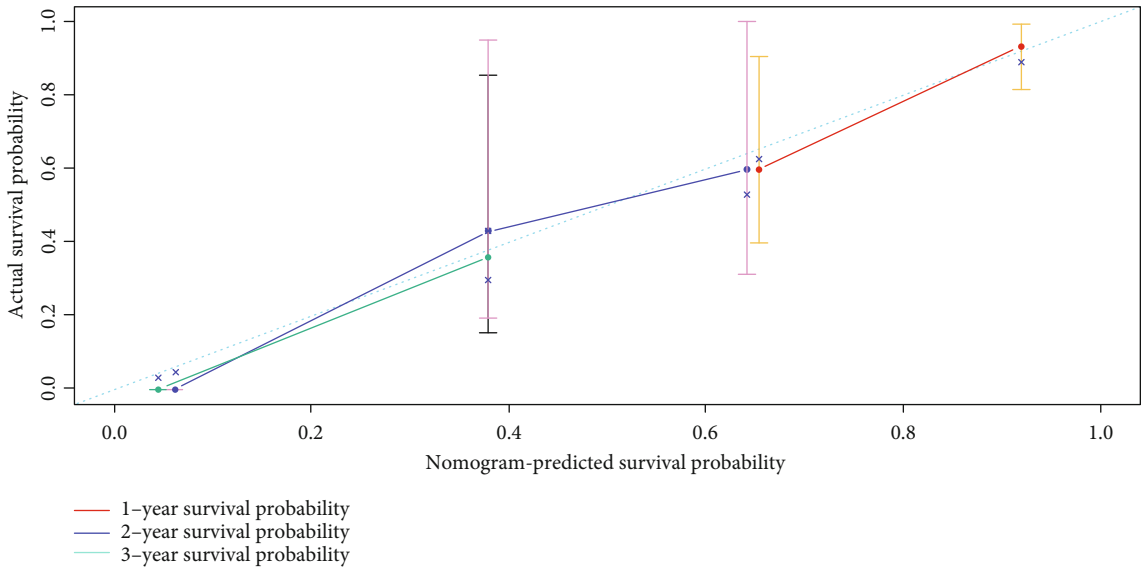

(c)

Figure 6: The nomogram constructed by radiomics signature, KPS, and age (a). The calibration curve of the nomogram shows that the prediction and observation possibilities of TCIA (b) and test (c) datasets are satisfactory.

response degree of each cluster to the same dose is very different. This shows that it is necessary to adjust the dose of radiotherapy for individual patients. At present, the recommended standard procedure postoperative treatment is the combination of conventional fractionated radiotherapy (RT) and temozolomide (TMZ), followed by adjuvant TMZ [37]. Neoadjuvant TMZ can improve the sensitivity of patients to radiotherapy [37], and a phase II clinical trial has confirmed that the use of neoadjuvant TMZ before radiotherapy can increase the OS of GBM patients [38]. Tumour-treating fields (TTFs) is the latest GBM recommended therapy in the NCCN (National Comprehensive Cancer Network) guidelines, and a previous clinical study found that in addition to its antimitotic effect, this technique can also specifically delay DNA repair and increase DNA-induced damage, thus increasing the radiosensitivity of tumour cells [39–40]. Therefore, it is very important to predict the response of GBM patients to radiotherapy. For those clusters with radiotherapy resistance, the individual clinical decision of using TTF or neoadjuvant TMZ before radiotherapy may prolong the OS of individual patients.

There are some limitations to this study. First, although the study included an independent test dataset, it had a relatively small sample size with retrospective data. Increasing the sample size to improve the robustness of the model is the main work in the next stage. To ensure the robustness and repeatability of the research, multicentre data should be collected. Second, limited by the TCIA database, only four kinds of conventional MRI sequences (T1WI, CE-T1WI, T2WI, and T2FLAIR) were used in the dataset in this study, but no other sequences (such as DCE or DTI) were included. Third, a more accurate OS should be from the time of radiotherapy to death or censure point. Although postoperative radiotherapy has been the standard treatment for GBM, due to the limitations of the TCIA dataset, detailed treatment information (such as the use and type of chemotherapy drugs, the dose of radiotherapy, or the start time of radiotherapy) cannot be obtained. Therefore, this study used the time from diagnosis to censure point as OS to roughly evaluate the impact of radiotherapy on survival. This rough evaluation has a certain impact on the accuracy of this study. Finally, although a variety of image preprocessing methods are used in this study, different imaging parameters and protocols still affect its radiologic characteristics to a certain extent. Moreover, most of the image parameters are removed from TCIA image data, so the normalization method cannot be used further. This is the main reason why the application of radiomics is currently limited.

5. Conclusion

In this study, a noninvasive radiomics signature was built by combining the previous 31-gene signature with radiomics, which was proven to predict the response of GBM patients to radiotherapy on independent test datasets. Compared with the 31-gene model prediction after surgery, the radiomics signature constructed by the machine learning algorithm can predict the response ability of radiotherapy before operation. The performance of predicting individual patients' OS can be further improved by using the constructed nomogram with the radiomics signature, age, and KPS, and this technique may be a new attempt for providing precise GBM radiotherapy.

Data Availability

The data from TCIA and UCSC can be downloaded from http://www.cancerimagingarchive.net and https://xenabrowser.net. The data from the local hospital can be obtained from the corresponding author as reasonably required.

Conflicts of Interest

The authors declare that they have no conflicts of interest.

Acknowledgments

This work was supported by the Shanghai Commission of Science and Technology (Grant No. 17411963600).

Supplementary Materials

Supplements S1 and S2 provide a text description of the screening criteria for samples from TCIA and local datasets and are accompanied by two flowcharts, Figures S1 and S2. These two parts are mentioned in Section 2.1 of the paper. Supplement S3 describes the definition and details of five groups of radiomics features, which are mentioned in Section 2.5 of the paper. Supplement 4 describes the robustness test by calculating the ICC values of the radiomics features and presenting the results in the form of graphs (Figure S3). This part is mentioned in Section 3.2 of the original text. *(Supplementary Materials)*

References

[1] Q. T. Ostrom, H. Gittleman, J. Xu et al., "CBTRUS statistical report: primary brain and other central nervous system tumors diagnosed in the United States in 2009-2013," *Neuro-Oncology*, vol. 18, Supplement 5, pp. v1–v75, 2016.

[2] R. Stupp, M. E. Hegi, W. P. Mason et al., "Effects of radiotherapy with concomitant and adjuvant temozolomide versus radiotherapy alone on survival in glioblastoma in a randomised phase III study: 5-year analysis of the EORTC-NCIC trial," *The Lancet Oncology*, vol. 10, no. 5, pp. 459–466, 2009.

[3] J. N. Scott, N. B. Rewcastle, P. M. A. Brasher et al., "Which glioblastoma multiforme patient will become a long-term survivor? A population-based study," *Annals of Neurology*, vol. 46, no. 2, pp. 183–188, 1999.

[4] D. Krex, B. Klink, C. Hartmann et al., "Long-term survival with glioblastoma multiforme," *Brain*, vol. 130, no. 10, Part 10, pp. 2596–2606, 2007.

[5] D. Armocida, A. Pesce, F. Di Giammarco, A. Frati, A. Santoro, and M. Salvati, "Long term survival in patients suffering from glio-blastoma multiforme: a single-center observational cohort study," *Diagnostics*, vol. 9, no. 4, p. 209, 2019.

[6] J. F. Torres-Roca, "A molecular assay of tumor radiosensitivity: a roadmap towards biology-based personalized radiation therapy," *Personalized Medicine*, vol. 9, no. 5, pp. 547–557, 2012.

[7] H. S. Kim, S. C. Kim, S. J. Kim et al., "Identification of a radiosensitivity signature using integrative metaanalysis of published microarray data for NCI-60 cancer cells," *BMC Genomics*, vol. 13, no. 1, p. 348, 2012.

[8] J. Meng, P. Li, Q. Zhang, Z. Yang, and S. Fu, "A radiosensitivity gene signature in predicting glioma prognostic via EMT pathway," *Oncotarget*, vol. 5, no. 13, pp. 4683–4693, 2014.

[9] G. Li, Y. Jiang, X. Lyu et al., "Gene signatures based on therapy responsiveness provide guidance for combined radiotherapy and chemotherapy for lower grade glioma," *Journal of Cellular and Molecular Medicine*, vol. 24, no. 8, pp. 4726–4735, 2020.

[10] X. Lyu, M. Zhang, G. Li, Y. Jiang, and Q. Qiao, "PD-1 and PD-L1 expression predicts radiosensitivity and clinical outcomes in head and neck cancer and is associated with HPV infection," *Journal of Cancer*, vol. 10, no. 4, pp. 937–948, 2019.

[11] Q. Zhang, Z. Bing, J. Tian et al., "Integrating radiosensitive genes improves prediction of radiosensitivity or radioresistance in patients with oesophageal cancer," *Oncology Letters*, vol. 17, no. 6, pp. 5377–5388, 2019.

[12] S. Eschrich, H. Zhang, H. Zhao et al., "Systems biology modeling of the radiation sensitivity network: a biomarker discovery platform," *International Journal of Radiation Oncology • Biology • Physics*, vol. 75, no. 2, pp. 497–505, 2009.

[13] S. A. Eschrich, W. J. Fulp, Y. Pawitan et al., "Validation of a radiosensitivity molecular signature in breast cancer," *Clinical Cancer Research*, vol. 18, no. 18, pp. 5134–5143, 2012.

[14] R. J. Gillies, P. E. Kinahan, and H. Hricak, "Radiomics: images are more than pictures, they are data," *Radiology*, vol. 278, no. 2, pp. 563–577, 2016.

[15] P. Lambin, R. T. H. Leijenaar, T. M. Deist et al., "Radiomics: the bridge between medical imaging and personalized medicine," *Nature Reviews Clinical Oncology*, vol. 14, no. 12, pp. 749–762, 2017.

[16] X. Jin, X. Zheng, D. Chen et al., "Prediction of response after chemoradiation for esophageal cancer using a combination of dosimetry and CT radiomics," *European Radiology*, vol. 29, no. 11, pp. 6080–6088, 2019.

[17] R. Sun, E. J. Limkin, M. Vakalopoulou et al., "A radiomics approach to assess tumour-infiltrating CD8 cells and response to anti-PD-1 or anti-PD-L1 immunotherapy: an imaging biomarker, retrospective multicohort study," *The Lancet Oncology*, vol. 19, no. 9, pp. 1180–1191, 2018.

[18] K. Nie, L. Shi, Q. Chen et al., "Rectal cancer: assessment of neoadjuvant chemoradiation outcome based on radiomics of multiparametric MRI," *Clinical Cancer Research*, vol. 22, no. 21, pp. 5256–5264, 2016.

[19] P. Grossmann, D. A. Gutman, W. D. Dunn Jr., C. A. Holder, and H. J. W. L. Aerts, "Imaging-genomics reveals driving pathways of MRI derived volumetric tumor phenotype features in glioblastoma," *BMC Cancer*, vol. 16, no. 1, p. 611, 2016.

[20] N. Beig, J. Patel, P. Prasanna et al., "Radiogenomic analysis of hypoxia pathway is predictive of overall survival in glioblastoma," *Scientific Reports*, vol. 8, no. 1, p. 7, 2018.

[21] J. E. Park and H. S. Kim, "Radiomics as a quantitative imaging biomarker: practical considerations and the current standpoint in neuro-oncologic studies," *Nuclear Medicine and Molecular Imaging*, vol. 52, no. 2, pp. 99–108, 2018.

[22] L. Scarpace, L. Mikkelsen, T. Cha et al., "Radiology Data from the Cancer Genome Atlas Glioblastoma Multiforme [TCGA-GBM] Collection," *The Cancer Imaging Archive*, vol. 11, no. 4, p. 1, 2016.

[23] F. W. Prior, K. Clark, P. Commean et al., "TCIA: an information resource to enable open science," in *2013 35th Annual International Conference of the IEEE Engineering in Medicine and Biology Society (EMBC)*, pp. 1282–1285, Osaka, Japan, 2013.

[24] H. Moradmand, S. M. R. Aghamiri, and R. Ghaderi, "Impact of image preprocessing methods on reproducibility of radiomic features in multimodal magnetic resonance imaging in glioblastoma," *Journal of Applied Clinical Medical Physics*, vol. 21, no. 1, Article ID 31880401, pp. 179–190, 2020.

[25] T. Rohlfing, N. M. Zahr, E. V. Sullivan, and A. Pfefferbaum, "The SRI24 multichannel atlas of normal adult human brain

structure," *Human Brain Mapping*, vol. 31, no. 5, pp. 798–819, 2010.

[26] I. Aganj, B. T. T. Yeo, M. R. Sabuncu, and B. Fischl, "On removing interpolation and resampling artifacts in rigid image registration," *IEEE Transactions on Image Processing*, vol. 22, no. 2, pp. 816–827, 2013.

[27] N. J. Tustison, B. B. Avants, P. A. Cook et al., "N4ITK: improved N3 bias correction," *IEEE Transactions on Medical Imaging*, vol. 29, no. 6, pp. 1310–1320, 2010.

[28] L. G. Nyúl, J. K. Udupa, and X. Zhang, "New variants of a method of MRI scale standardization," *IEEE Transactions on Medical Imaging*, vol. 19, no. 2, pp. 143–150, 2000.

[29] S. M. Smith and J. M. Brady, "SUSAN—a new approach to low level image processing," *International Journal of Computer Vision*, vol. 23, no. 1, pp. 45–78, 1997.

[30] A. Gooya, K. M. Pohl, M. Bilello et al., "GLISTR: glioma image segmentation and registration," *IEEE Transactions on Medical Imaging*, vol. 31, no. 10, pp. 1941–1954, 2012.

[31] M. B. Kursa and W. R. Rudnicki, "Feature selection with the Boruta package," *Journal of Statistical Software*, vol. 36, no. 11, pp. 1–3, 2010.

[32] J. P. Weir, "Quantifying test-retest reliability using the intraclass correlation coefficient and the SEM," *The Journal of Strength and Conditioning Research*, vol. 19, no. 1, pp. 231–240, 2005.

[33] T. K. Koo and M. Y. Li, "A guideline of selecting and reporting intraclass correlation coefficients for reliability research," *Journal of Chiropractic Medicine*, vol. 15, no. 2, pp. 155–163, 2016.

[34] T. Maciejewski and J. Stefanowski, "Local neighbourhood extension of SMOTE for mining imbalanced data," in *2011 IEEE Symposium on Computational Intelligence and Data Mining (CIDM)*, pp. 104–111, Paris, France, 2011.

[35] A. Mouraviev, J. Detsky, A. Sahgal et al., "Use of radiomics for the prediction of local control of brain metastases after stereotactic radiosurgery," *Neuro-Oncology*, vol. 22, no. 6, pp. 797–805, 2020.

[36] J. G. Scott, A. Berglund, M. J. Schell et al., "A genome-based model for adjusting radiotherapy dose (GARD): a retrospective, cohort-based study," *The Lancet Oncology*, vol. 18, no. 2, pp. 202–211, 2017.

[37] W. J. Kil, D. Cerna, W. E. Burgan et al., "In vitro and in vivo radiosensitization induced by the DNA methylating agent temozolomide," *Clinical Cancer Research*, vol. 14, no. 3, pp. 931–938, 2008.

[38] G. Shenouda, L. Souhami, K. Petrecca et al., "A phase 2 trial of neoadjuvant temozolomide followed by hypofractionated accelerated radiation therapy with concurrent and adjuvant temozolomide for patients with glioblastoma," *International Journal of Radiation Oncology • Biology • Physics*, vol. 97, no. 3, pp. 487–494, 2017.

[39] M. Giladi, A. Tichon, R. S. Schneiderman et al., "Alternating electric fields (TTFields) inhibit DNA damage repair response in cancer cell lines," *Neuro-Oncology*, vol. 15, pp. iii98–iii135, 2013.

[40] M. Giladi, M. Munster, R. S. Schneiderman et al., "Tumor treating fields (TTFields) sensitize glioma tumor cells to radiation therapy by delaying DNA damage repair through homologous recombination," *International Journal of Radiation Oncology • Biology • Physics*, vol. 93, no. 3, pp. E524–E525, 2015.

Hindawi
Behavioural Neurology
Volume 2020, Article ID 1080521, 12 pages
https://doi.org/10.1155/2020/1080521

Research Article

Wild Bitter Melon Exerts Anti-Inflammatory Effects by Upregulating Injury-Attenuated CISD2 Expression following Spinal Cord Injury

Woon-Man Kung,[1] **Chai-Ching Lin**,[2] **Chan-Yen Kuo**,[3] **Yu-Ching Juin**,[2] **Po-Ching Wu**,[4] **and Muh-Shi Lin**[2,5,6,7]

[1]*Department of Exercise and Health Promotion, College of Kinesiology and Health, Chinese Culture University, Taipei 11114, Taiwan*
[2]*Department of Biotechnology and Animal Science, College of Bioresources, National Ilan University, Yilan 26047, Taiwan*
[3]*Graduate Institute of Systems Biology and Bioinformatics, National Central University, Chungli 32001, Taiwan*
[4]*Department of Biomechatronic Engineering, College of Bioresources, National Ilan University, Yilan 26047, Taiwan*
[5]*Division of Neurosurgery, Department of Surgery, Kuang Tien General Hospital, Taichung 43303, Taiwan*
[6]*Department of Biotechnology, College of Medical and Health Care, Hung Kuang University, Taichung 43302, Taiwan*
[7]*Department of Health Business Administration, College of Medical and Health Care, Hung Kuang University, Taichung 43302, Taiwan*

Correspondence should be addressed to Muh-Shi Lin; neurosurgery2005@yahoo.com.tw

Received 4 May 2020; Revised 19 July 2020; Accepted 12 September 2020; Published 30 September 2020

Academic Editor: Péter Klivényi

Background. Spinal cord injuries (SCIs) induce secondary neuroinflammation through astrocyte reactivation, which adversely affects neuronal survival and eventually causes long-term disability. CDGSH iron sulfur domain 2 (CISD2), which has been reported to be involved in mediating the anti-inflammatory responses, can serve as a target in SCI therapy. Wild bitter melon (WBM; *Momordica charantia* Linn. var. abbreviata Ser.) contains an anti-inflammatory agent called alpha-eleostearic acid (α-ESA), a peroxisome proliferator-activated receptor-β (PPAR-β) ligand. Activated PPAR-β inhibits the nuclear factor κB (NF-κB) signaling pathway via the inhibition of IκB (inhibitor of NF-κB) degradation. The role of astrocyte deactivation and CISD2 in anti-inflammatory mechanisms of WBM in acute SCIs is unknown. *Materials and Methods*. A mouse model of SCI was generated via spinal cord hemisection. The SCI mice were administered WBM intraperitoneally (500 mg/kg bodyweight). Lipopolysaccharide- (LPS-) stimulated ALT cells (astrocytes) were used as an *in vitro* model for studying astrocyte-mediated inflammation post-SCI. The roles of CISD2 and PPAR-β in inflammatory signaling were examined using LPS-stimulated SH-SY5Y cells transfected with si-CISD2 or scramble RNA. *Results*. WBM mitigated the SCI-induced downregulation of CISD2, PPAR-β, and IκB and upregulation of glial fibrillary acidic protein (GFAP; marker of astrocyte reactivation) in the spinal cord of SCI mice. Additionally, WBM (1 μg/mL) mitigated LPS-induced CISD2 downregulation. Furthermore, SH-SY5Y neural cells with CISD2 knockdown exhibited decreased PPAR-β expression and augmented NF-κB signaling. *Conclusion*. To the best of our knowledge, this is the first study to report that CISD2 is an upstream modulator of the PPAR-β/NF-κB proinflammatory signaling pathway in neural cells, and that WBM can mitigate the injury-induced downregulation of CISD2 in SCI mice and LPS-stimulated ALT astrocytes.

1. Introduction

Most patients with acute spinal cord injuries (SCIs) exhibit disability. SCIs are associated with expensive and long-term healthcare. The pathophysiology of acute SCIs involves primary and secondary injuries. Primary injury to the spinal cord results in structural damage, disruption of cell membranes and vessels, and degeneration of myelin and axons,

which may lead to secondary injury [1]. In SCIs, the pathological mechanisms underlying secondary injuries involve inflammation, free radical production, hyperoxidation, and mitochondrial dysfunction [2, 3]. Extensive injuries to the central nervous system (CNS) may activate the astrocytes, which are the resident immune cells [4, 5]. In response to SCI, astrocytes secrete proinflammatory cytokines and chemokines, thereby inducing a shift in microglial polarization from the beneficial M2 phenotype toward the detrimental M1 phenotype [6–8]. The SCI-induced M1 microglial phenotype is associated with the attenuation of IL-4 expression [9, 10]. The aberrantly activated glial cells (astrocytes and microglia) produce nitric oxide and reactive oxygen species (ROS), which exacerbate the inflammatory response [11]. The activation of inflammatory cascades may be cytotoxic to some neurons and glial cells, which may result in irreversible neurological deficits [12, 13].

Wild bitter melon (WBM) (*Momordica charantia* Linn. var. abbreviata Ser.) belongs to the family Cucurbitaceae. In Asia and Europe, WBM is used as a medicinal herb to treat various pathological conditions, such as inflammation, hyperglycemia, bacterial infection, and oxidative stress [14]. Mice orally administered WBM exhibit upregulated expression of peroxisome proliferator-activated receptor-α (PPAR-α) and PPAR-γ mRNA, which are involved in hypolipidemic and insulin-sensitizing activities [14]. Additionally, WBM inhibits lipopolysaccharide- (LPS-) induced inflammatory responses in macrophages through the regulation of NF-κB activation [15]. Furthermore, WBM extracts have been demonstrated to scavenge free radicals [16], such as 2,2-diphenyl-1-picrylhydrazyl (DPPH) and hydroxyl radicals [17].

The triglycerides in the seed oils of the family Cucurbitaceae comprise conjugated linolenic acid. Alpha-eleostearic acid (α-ESA, 18 : 3, $\Delta^{9cis,11trans,13trans}$, 9*cis*, 11*trans*, 13*trans*-conjugated linolenic acid) is a linolenic acid, which is widely distributed among the members of the family Cucurbitaceae, including WBM and *Momordica charantia* (bitter gourd). α-ESA accounts for more than 60% of the total fatty acid composition in bitter gourd seed oil [18]. High-performance liquid chromatography revealed that α-ESA accounts for approximately 19% of the total fatty acid composition of the ethyl acetate extracts. The content of α-ESA in dried and fresh WBM is 7.1 g/kg and 0.42 g/kg, respectively. In WBM seed oil, α-ESA accounts for more than 30% of the total fatty acid content [19].

The ligands of PPAR-β (synonyms: PPAR-δ) include polyunsaturated fatty acids, such as conjugated linoleic acid [20]. α-ESA can be metabolized into conjugated linoleic acid in mice [21] and rats [22]. Therefore, α-ESA can be used as a natural ligand for PPAR-β. Moreover, PPAR-β has been reported to attenuate the production of transforming necrosis factor-α (TNF-α) in cardiomyocyte culture through the inhibition of the NF-κB (nuclear factor κB) signaling pathway [23]. In a mouse model of bleomycin-induced lung injury, the PPAR-β agonist GW0742 inhibited IκB (inhibitor of NF-κB) degradation, thereby consequently deactivating NF-κB [24]. WBM attenuated the generation of inflammatory responses in LPS-stimulated RAW 264.7 macrophages through the inhibition of NF-κB activation [15]. Thus, the interaction between α-ESA and PPAR-β may inhibit IκB degradation and subsequently attenuate NF-κB activation. The pathological mechanisms underlying traumatic SCIs involve mitochondrial oxidative stress and inflammation. Thus, WBM, which exhibits antioxidant and anti-inflammatory activities, may aid the management of acute SCIs.

CDGSH iron sulfur domain 2 (CISD2), known to be associated with aging, has been reported to be involved in conferring protection against mitochondrial dysfunction-induced inflammatory responses and apoptosis. Previously, we had demonstrated that CISD2 was significantly downregulated under conditions of CNS injury and disease, such as aging mouse brain [25] and hemisection injury to the spinal cord in rats [26]. Injury-induced CISD2 downregulation leads to neuroinflammation and mitochondrial dysfunction. Thus, CISD2 can serve as a potential therapeutic target for SCI. This study is aimed at evaluating the role of CISD2 in mediating the anti-inflammatory effects of WBM and the regulatory effects of CISD2 on the PPAR-β/NF-κB signaling pathway using the SCI mouse and *in vitro* cellular injury models.

2. Materials and Methods

2.1. Extract Preparation and Reagents. WBM dried at low temperature was used to prepare the extract. The WBM samples were ground into a powder and stored at -20°C. WBM powder was incubated with water at room temperature for 24 h with shaking. The suspension was centrifuged at 13,000 g and 4°C for 10 min to remove any residues. The supernatant was freeze-dried, and the lyophilized powder was incubated with ethanol at room temperature for 24 h with shaking. The samples were centrifuged at 13,000 g and 4°C for 10 min, and the supernatant was concentrated under vacuum and stored at -20°C. The concentrated extract was dissolved in absolute alcohol (≧99.8%) before analysis. Absolute alcohol was purchased from Sigma-Aldrich (St. Louis, MO, USA). α-ESA purchased from Cayman Chemical (Ann Arbor, MI, USA) was dissolved in absolute alcohol. LPS (obtained from *Escherichia coli* serotype 055:B5) was purchased from Sigma-Aldrich (St. Louis, MO, USA; L-2880).

2.2. Animals. Wild-type C57BL/6JNarl mice with an average weight of 22–28 g were obtained from the National Laboratory Animal Center (Taipei, Taiwan). The animals were maintained in a cage for at least 5 days (5 mice per cage) before arrival to our laboratory. The animals had *ad libitum* access to food and water and were maintained under a 12 h dark/light cycle. The experiments were performed according to the guidelines of the Experimental Animal Laboratory. The animal experiments were approved by the Animal Care and Use Committee at National Ilan University, Yilan, Taiwan (ethical approval code: 105-20).

2.3. Hemisection SCI in Mice. The animal model of acute SCI was generated as described in our previous study [27]. Briefly, the animals were divided into the following three groups: sham control, SCI, and WBM ($n = 6$/group). The mice were anesthetized using isoflurane and placed in a stereotactic apparatus (David Kopf Instruments, Tujunga, CA)

to secure the spinal cord. Posterior spinal decompression was performed under a dissecting microscope by performing laminectomy of the ninth to tenth thoracic vertebra without duraplasty. For hemisection of the spinal cord, the guide of the wire knife was positioned along the vertical plane close to the lateral surface in the lower thoracic vertebra of the spinal cord. The knife was turned medially and then extended 1.5 mm. The guide was lifted 4.0 mm to hemitransect the spinal cord. The sham control group underwent surgery, but hemisection of the spinal cord was not performed. The wound was closed in layers using sutures, and recovery was promoted using a heating pad (36.5°C). The animals were starved for 3 h after surgery. Postoperative care included rehydration using subcutaneous saline injection. The mice were returned to their preoperative housing conditions after surgery. A 5 mm section of the spinal cord with the lesion or a similar area in the sham control group was obtained for mRNA extraction and lysate preparation at 8 or 24 h posthemisection (each time point $n = 3$, total $n = 6$ for each experimental condition).

2.4. Treating SCI Mice with WBM. The mice in the WBM group were administered WBM intraperitoneally (500 mg/kg body weight; single dose) immediately after SCI. This dosage has been reported to protect mice against inflammation, oxidative stress [28], and hyperglycemia [29]. The mice in the SCI group were administered normal saline intraperitoneally (500 mg/kg body weight) immediately after SCI. The sham operation group was not administered either saline or WBM.

2.5. Neural Cell Lines. The astrocyte cell line (ALT, BCRC 60581) was purchased from the Bioresource Collection and Research Center (BCRC, Hsinchu, Taiwan). ALT cells were cultured in 90% Dulbecco's modified Eagle's medium (DMEM) supplemented with 1.5 g/L sodium bicarbonate and 10% fetal bovine serum (FBS). The SH-SY5Y cell line (ATCC, Manassas, VA, USA), derived from human neuroblastoma cells was cultured in DMEM/F-12 supplemented with 10% FBS in an incubator with an atmosphere of 5% CO_2 at 37°C.

2.6. Treatment of LPS-Stimulated ALT Cells with WBM. ALT cells (1×10^6) cultured in a 35 mm dish were stimulated using 20 μg/mL LPS. Next, the cells were treated with 1 μg/mL WBM or 0.28 μg/mL α-ESA for 24 h. Each experiment was performed at least two times with at least three different astrocyte cultures.

2.7. Quantitative Real-Time Polymerase Chain Reaction (qRT-PCR). Total RNA was extracted from the cultured cells using an extraction buffer (TRIzol/phenol/chloroform). The extracted RNA was reverse transcribed into cDNA using oligo-dT and SuperScript II Reverse Transcriptase (Invitrogen, Carlsbad, CA). The cDNAs were subjected to qRT-PCR to quantify the expression of the target genes. The housekeeping gene cyclophilin was used as an internal control. The PCR conditions were as follows: 25 cycles of 94°C for 1 min (denaturation), 55–60°C for 1 min (annealing), and 72°C for 1 min (extension). The primers used for qRT-PCR are shown in Table 1. The qRT-PCR was performed using SYBR Green on an ABI PRISM 7300 HT Real-Time PCR system (Applied Biosystems, Foster City, CA). The minor groove-binding probes and primers for the detection of target genes and cyclophilin were designed by ABI. The threshold cycle (C_t) (the cycle number at which the amount of the amplified target reached a fixed threshold) was determined. The C_t value of the target genes was normalized to that of cyclophilin. Three independent experiments were performed.

2.8. RNA Interference. CISD2 was knocked down in SH-SY5Y cells using small interfering RNA (siRNA). The cells were transfected with CISD2-specific siRNA (si-CISD2) or scrambled siRNA (Silencer® Predesigned siRNA; Ambion, Austin, TX) using Lipofectamine™ 2000 reagent (Invitrogen, Carlsbad, CA). The sequences of si-CISD2 were as follows: 5′-GUCCUCUCAUCCUGAAGAATT-3′ and 5′-UUCUUC AGGAUGAGAGGACTT-3′. At 5 h posttransfection, the Lipofectamine 2000-containing medium was replaced with culture medium to allow the cells to recover for 67 h. CISD2 knockdown efficiency was examined using qRT-PCR.

2.9. Immunoblotting. Total protein was extracted from the ALT astrocytes and spinal cord tissues using a lysis buffer (20 mM Tris-HCl, 0.1% sodium dodecyl sulfate (SDS), 0.8% NaCl, and 1% Triton X-100). The protein was subjected to gradient electrophoresis on a 12% gel. The resolved proteins were electroblotted onto a nitrocellulose membrane. The membrane was incubated with a blocking reagent. Next, the membrane was incubated with the following primary antibodies at 4°C for 12 h: anti-IκB alpha (E130) (1 : 2000; ab32518; Abcam, Cambridge, MA, USA), anti-PPAR-β (1 : 2000; ab23673; Abcam), anti-GFAP (1 : 2000; ab7260; Abcam), anti-β-actin (1 : 4000; ab8227; Abcam), and anti-CISD2 (1 : 500; PA5-34545; Thermo Fisher Scientific). The membrane was washed and incubated with goat anti-rabbit IgG (horseradish peroxidase- (HRP-) conjugated secondary antibody) (1 : 5000; 12-348; Merck Millipore) for 1 h. Protein bands were developed using the Immobilon™ Western Chemiluminescent HRP Substrate (WBKLS0500; Merck Millipore). Densitometric analysis of the protein bands was performed using ImageQuant™ LAS 4000 (GE Healthcare Life Sciences).

2.10. Cell Viability. The viability of ALT astrocytes was examined using the 3-(4,5-dimethylthiazol-2-yl)-2,5-diphenyltetrazolium bromide (MTT) assay. The cells were seeded in a 96-well microplate for 24 h before use. The WBM- or α-ESA-treated ALT cells were incubated with MTT for 4 h. Next, 0.4 N HCl (0.3 mL) in isopropanol was incubated with the mixture overnight to dissolve the formazan crystals. The absorbance of the mixture was measured at 600 nm using an enzyme-linked immunosorbent assay plate reader.

2.11. Statistical Analysis. The variables were subjected to the normality test. Variables exhibiting normal distribution were analyzed using the parametric tests, whereas those exhibiting nonnormal distribution were analyzed using the nonparametric tests. The P values in the normality test were >0.05.

Table 1: Primers.

Gene	Orientation	Sequence
IL-1β	Forward	5′-AGGCTCCGAGATGAACAA-3′
	Reverse	5′-AAGGCATTAGAAACAGTCC-3′
IL-4	Forward	5′-TCGGCATTTTGAACGAGGTC-3′
	Reverse	5′-GAAAAGCCCGAAAGAGTCTC-3′
IL-6	Forward	5′-CCACCAAGAACGATAGTCAA-3′
	Reverse	5′-TTTCCACGATTTCCCAGA-3′
GFAP	Forward	5′-CCAACCCGTTCCTCCATA-3′
	Reverse	5′-TCCGCCTGGTAGACATCA-3′
CISD2	Forward	5′-CTTGGAGACTGCTGGGTG-3′
	Reverse	5′-CTTTGCTAAGTCCTCGTC-3′
PPAR-β	Forward	5′-GCCGCCCTACAACGAGATCA-3′
	Reverse	5′-CCACCAGCAGTCCGTCTTTGT-3′
NF-κB p105 subunits	Forward	5′-CCAGGGTATGGCTACTCGAACT-3′
	Reverse	5′-GTGACCCCTGCGTTGGATT-3′
COX-2	Forward	5′-ACAAGCACAATAGACGCACAAGA-3′
	Reverse	5′-GGGAGGGCAATTATGATAAGGAT-3′
RANTES	Forward	5′-TGCCCACGTCAAGGAGTATTT-3′
	Reverse	5′-GGCGGTTCCTTCGAGTGA-3′
β-Actin	Forward	5′-CTGTCCCTGTATGCCTCTG-3′
	Reverse	5′-ATGTCACGCACGATTTCC-3′
GAPDH	Forward	5′-GGCAAATTCAACGGCACAGT-3′
	Reverse	5′-CGCTCCTGGAAGATGGTGAT-3′

Therefore, parametric tests were used for comparison of means among the experimental groups.

Independent two-sample t -tests were used to compare the means of the two groups. One-way analysis of variance was used to analyze the means of more than two groups.

3. Results

3.1. Effect of WBM and α-ESA on the Viability of ALT Cells. The effects of various concentrations of WBM (0.25–500 μg/mL) and α-ESA (0.07–11.1 μg/mL) on the viability of ALT cells were analyzed using the MTT assay. Compared with the untreated cells, the WBM- (6.25 μg/mL, Figure 1(a)) or α-ESA-treated cells (0.7 μg/mL, Figure 1(c)) exhibited significantly decreased viability. At concentrations of 0.25–6 μg/mL WBM (Figure 1(b)) or 0.07–0.56 μg/mL α-ESA (Figure 1(d)), the viability of ALT cells was greater than 80%. Subsequent *in vitro* experiments were performed using 1 μg/mL WBM and 0.28 μg/mL α-ESA as at these concentrations, the test agents did not exhibit any cytotoxic effects.

3.2. Effect of LPS on the Expression of Proteins Associated with Astrocyte Reactivation and Inflammation. LPS-stimulated ALT cells were used as an *in vitro* model of cellular injuries. This model recapitulates SCI-associated aberrant astrocyte activation and inflammation [25, 26, 30]. The cells were treated with 20 μg/mL LPS for 24 h and subjected to qRT-PCR and western blotting. The expression of GFAP ($P < 0.01$, Figure 2(a)), IL-1β ($P < 0.001$, Figure 2(c)), and IL-6 mRNA ($P < 0.001$, Figure 2(d)) was significantly upregulated in LPS-stimulated cells compared with that in the control cells. In contrast, the expression of IL-4 ($P < 0.001$, Figure 2(e)) and CISD2 mRNA ($P < 0.05$, Figure 2(f)) was significantly downregulated in LPS-stimulated cells when compared with that in the control cells. The expression of GFAP in ALT cells was quantified by western blotting. Compared with that in control cells, the expression of GFAP was significantly upregulated in LPS-stimulated ALT cells ($P < 0.001$, Figure 2(b)). These findings indicated that the mechanisms underlying injury-induced secondary damage involve aberrant activation of astrocytes, enhanced inflammatory response, and attenuated expression of IL-4 (potentially resulting in impaired polarization of anti-inflammatory M2 microglia) and CISD2.

3.3. WBM and α-ESA Attenuated LPS-Induced Changes in ALT Astrocytes. Next, the effects of WBM and α-ESA on the expression of IL-4 and CISD2 in LPS-stimulated ALT

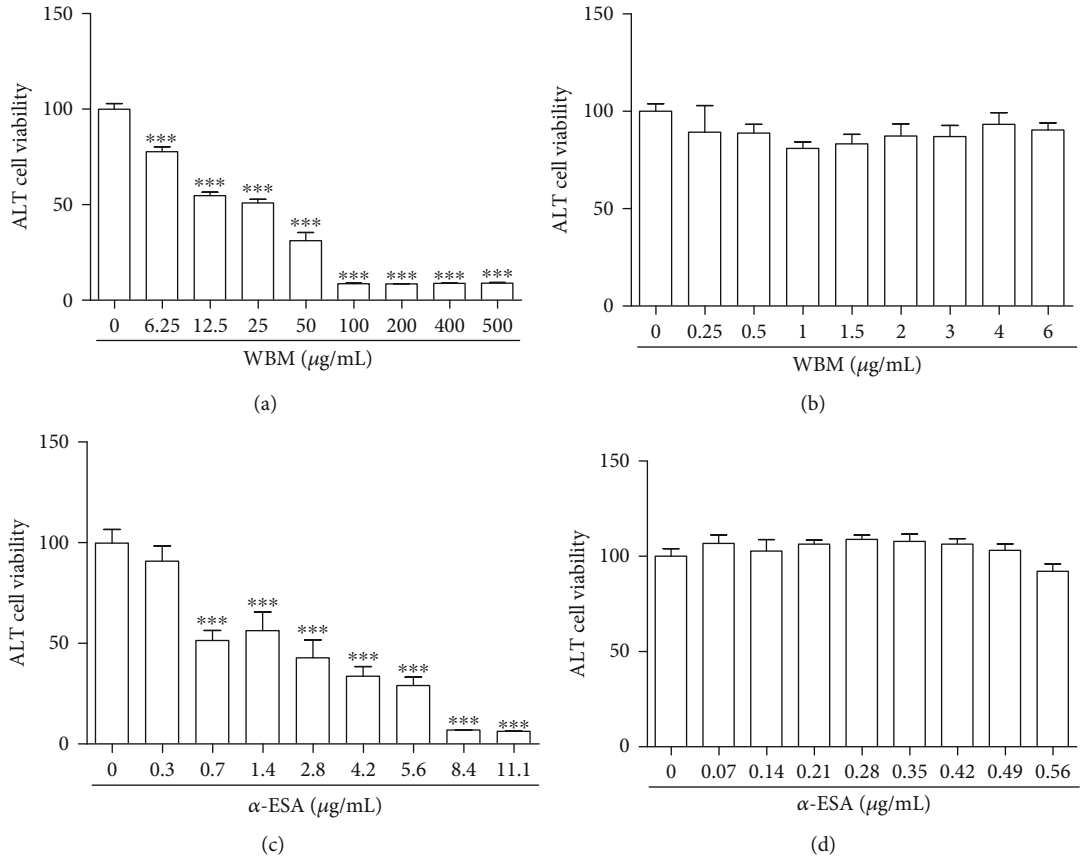

Figure 1: Cell survival, as measured by MTT assay, of ALT astrocytes following treatment with varying doses of WBM (0.25-500 μg/mL) (a) and α-ESA (0.07-11.1 μg/mL) (c). Concentrations with less cytotoxic effects were determined (>80% of cell viability) at 0.25-6 μg/mL in WBM (b) and 0.07-0.56 μg/mL in α-ESA (d). For *in vitro* experiments, 1 μg/mL WBM and 0.28 μg/mL α-ESA were selected. Vertical bars indicate the mean ± standard error of the mean (SEM) ($n = 3$). $^{***}P < 0.001$ vs. control. Pair-wise multiple comparisons between groups were determined using the Newman-Keuls method.

cells were evaluated. ALT cells were treated with 20 μg/mL LPS, 20 μg/mL LPS, and 1 μg/mL WBM, or 20 μg/mL LPS and 0.28 μg/mL α-ESA for 24 h, and subjected to qRT-PCR and western blotting.

Compared with LPS-stimulated ALT cells, ALT cells treated with WBM or α-ESA in the background of LPS stimulation exhibited significant downregulation of GFAP mRNA (both $P < 0.01$, Figure 2(a)) as well as protein levels (both $P < 0.01$, Figure 2(b)). Additionally, the expression of IL-1β ($P < 0.01$ or $P < 0.05$, respectively, Figure 2(c)) and IL-6 mRNA ($P < 0.001$ or $P < 0.001$, respectively, Figure 2(d)) in ALT cells treated with WBM or α-ESA in the background of LPS stimulation was lower than that in LPS-stimulated ALT cells. Moreover, the expression of IL-4 (both $P < 0.05$, Figure 2(e)) and CISD2 mRNA (both $P < 0.05$, Figure 2(f)) in ALT cells treated with WBM or α-ESA in the background of LPS stimulation was lower than that in LPS-stimulated ALT cells. These findings indicated that α-ESA is the bioactive component, and it is responsible for the anti-inflammatory effect of WBM. We hypothesized that the mechanism underlying the anti-inflammatory activity of WBM in LPS-stimulated ALT cells involves astrocyte deactivation, proinflammatory cytokine attenuation, and enhanced IL-4 and CISD2 expression.

3.4. Effect of CISD2 Knockdown on PPAR-β Expression and Inflammatory Response in the SH-SY5Y Cells. CISD2 has been reported to inhibit inflammation through the regulation of upstream components of the NF-κB signaling pathway [39]. Attenuation of CISD2 promotes inflammation in various CNS-associated conditions, such as aging [20], injuries, and degeneration [19]. α-ESA, a bioactive anti-inflammatory compound in WBM, serves as a PPAR-β ligand. Thus, α-ESA suppresses NF-κB signaling and downstream cytokine production by inhibiting IκB degradation. Next, the effects of WBM and α-ESA on the expression of CISD2 and PPAR-β, which are the upstream effectors of the NF-κB signaling pathway, were examined. SH-SY5Y cells are recognized as a well-established *in vitro* model to evaluate neural function. In this study, SH-SY5Y cells were transfected with si-CISD2 to knockdown CISD2. Previous studies have reported that si-CISD2 achieved approximately 60% knockdown efficiency in SH-SY5Y cells [26].

The results of qRT-PCR are shown in Figure 3(a). The band intensities reproducibly confirmed the anti-inflammatory effect of CISD2. Compared with the scramble siRNA-transfected cells, si-CISD2-transfected cells exhibited significant upregulation of NF-κB p105 ($P < 0.01$, Figure 3(b)), COX-2 ($P < 0.001$, Figure 3(c)), and RANTES

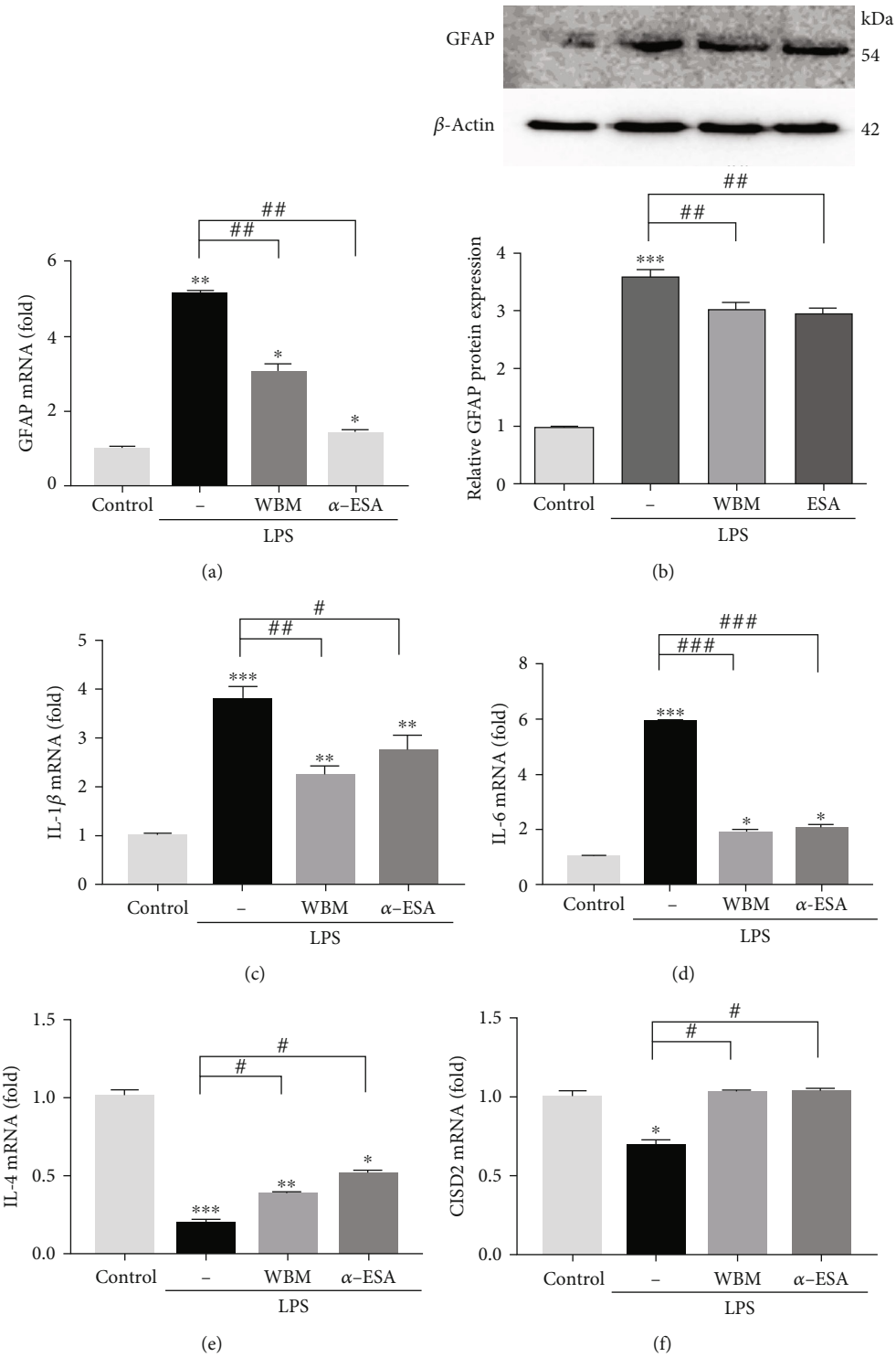

Figure 2: Injury-induced CISD2 downregulation, enhanced GFAP mRNA and protein expression, and proinflammation in LPS-challenged ALT astrocytes. WBM can prevent the abovementioned detrimental effects. Results of mRNA expression of GFAP (a), GFAP protein (b), mRNA expression of IL-1β (c), IL-6 (d), IL-4 (e), and CISD2 (f) in ALT cells with or without administration of WBM and α-ESA. Vertical bars indicate the mean ± standard error of the mean (SEM) of mRNA expression ($n = 3$). $^{*}P < 0.05$vs. control,$^{**}P < 0.01$vs. control,$^{***}P < 0.001$vs. control, $^{\#}P < 0.05$, $^{\#\#}P < 0.01$, and $^{\#\#\#}P < 0.001$indicate a significant difference. Pair-wise multiple comparisons between groups were performed using the Newman-Keuls method.

mRNA ($P < 0.01$, Figure 3(d)). Furthermore, the expression of PPAR-β mRNA in si-CISD2-transfected cells was significantly lower than that in the control cells (untreated with si-CISD2) ($P < 0.01$, Figure 3(e)). These findings indicated that CISD2 acts on the upstream components of the PPAR-β/NF-κB signaling pathway, and that it is involved in NF-

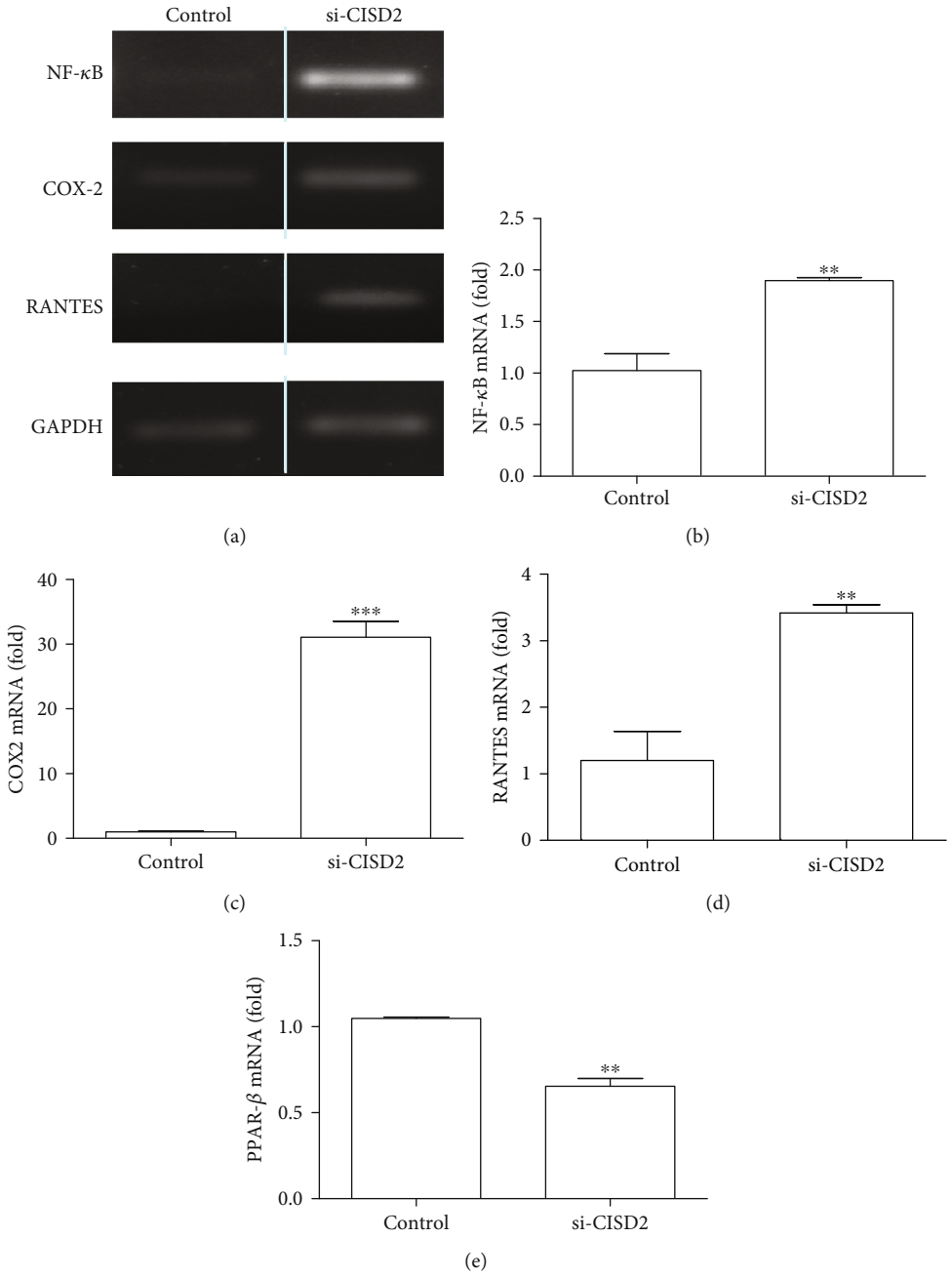

Figure 3: Knockdown of CISD2 expression in neural cells significantly influenced mRNA expression levels in PPAR-β, indicating upstream regulation of CISD2 on PPAR-β (a). mRNA levels of NF-κB, COX-2, and RANTES were determined by semiquantitative RT-PCR in neural cells with or without si-CISD2 transfection. The results shown are from one of the experiments that were repeated for at least 3 times. Quantification of relative band intensity of semiquantitative RT-PCR showed that CISD2 knockdown in neural cells led to enhanced mRNA expression levels in NF-κB (b) and downstream proinflammatory mediators including COX-2 (c) and RANTES (d). (e) Results of real-time qRT-PCR for mRNA levels of PPAR-β in neural cells with or without si-CISD2 transfection. Vertical bars indicate the mean ± standard error of the mean (SEM) of mRNA expression ($n = 3$). $^{**}P < 0.01$ and $^{***}P < 0.001$ indicate a statistically significant difference between the control and si-CISD2 groups using independent two-sample t-tests.

κB-mediated aberrant activation of astrocytes and proinflammatory cascades.

3.5. Effects of WBM on SCI Mice. Next, the effect of WBM on the expression of CISD2 in mice with hemisection SCI was evaluated. The SCI mice were intraperitoneally administered WBM (500 mg/kg body weight) or normal saline. At 24 h post-SCI, qRT-PCR was performed to analyze the expression of genes involved in astrocyte-mediated inflammation, such as GFAP, IL-4, and CISD2, in the damaged spinal cord. Compared with the sham control group, the SCI group exhibited upregulation of GFAP ($P < 0.001$, Figure 4(a)), IL-1β ($P < 0.001$, Figure 4(b)), and IL-6 mRNA ($P < 0.001$, Figure 4(c)) and downregulation of IL-4 ($P < 0.05$,

Figure 4(d)) and CISD2 mRNA ($P < 0.01$, Figure 4(e)). These findings suggested that SCIs result in inhibited IL-4 and CISD2 expression, aberrant astrocyte activation, and enhanced inflammation [26].

Compared with the SCI group, the WBM group exhibited downregulation of GFAP ($P < 0.01$, Figure 4(a)), IL-1β ($P < 0.001$, Figure 4(b)), and IL-6 mRNA ($P < 0.001$, Figure 4(c)) and upregulation of IL-4 ($P < 0.05$, Figure 4 (d)) and CISD2 mRNA ($P < 0.05$, Figure 4(e)). Thus, the anti-inflammatory effects of WBM in SCI mice may involve inhibition of astroglial activity, attenuation of glia-mediated inflammatory responses, and enhanced production of IL-4 (which potentially enhances the M2 microglial population) and CISD2.

3.6. Anti-Inflammatory Mechanisms of WBM in SCI Mice. Finally, we demonstrated that the CISD2/PPAR-β/NF-κB signaling pathway is involved in mediating the anti-inflammatory effect of WBM in mice with hemisection SCI. Western blotting was performed to evaluate the therapeutic effects of WBM with respect to the mouse spinal cord with or without SCI.

No detrimental effects were observed at 8 h post-SCI (Figures 5(a), 5(c), and 5(d)). Moreover, the expression of PPAR-β ($P < 0.05$, Figure 5(b)) and IκB proteins ($P < 0.001$, Figure 5(c)) in the injured spinal cord of the WBM group was upregulated compared to that in the injured spinal cord of the SCI group. However, WBM-mediated downregulation of GFAP and upregulation of CISD2 in mice with SCI were nonsignificant (Figures 5(a) and 5(d), respectively). The effects of WBM on the expression of GFAP and CISD2 were significant at 24 h post-SCI.

At 24 h post-SCI, compared with the sham group, the SCI group exhibited significant upregulation of GFAP ($P < 0.01$, Figure 5(h)) and significant downregulation of PPAR-β ($P < 0.01$, Figure 5(f)), IκB ($P < 0.001$, Figure 5(g)), and CISD2 proteins ($P < 0.01$, Figure 5(e)) in the injured spinal cord. Furthermore, compared with the SCI group, the WBM group exhibited significant downregulation of GFAP ($P < 0.01$, Figure 5(h)) and significant upregulation of PPAR-β ($P < 0.001$, Figure 5(f)), IκB ($P < 0.01$, Figure 5 (g)), and CISD2 proteins ($P < 0.01$, Figure 5(e)) in the injured spinal cord. These *in vivo* findings suggested that WBM mitigated the SCI-induced downregulation of CISD2 at mRNA and protein levels, and inhibited the PPAR-β/IκB/NF-κB signaling pathway, which was in agreement with the *in vitro* results.

4. Discussion

Various CNS-associated conditions, such as aging, neurodegeneration, and traumatic brain injury or SCIs are associated with inflammation [31–33] and mitochondrial dysfunction [34, 35]. Activated glial cell-mediated inflammation can contribute to mitochondrial dysfunction, which impairs mitochondrial dynamics and membrane permeabilization and promotes ROS production [36, 37]. Mitochondrial dysfunction can exacerbate the inflammatory response [38]. Prolonged inflammation and mitochondrial dysfunction may lead to irreversible neuronal deficits.

CISD2, an outer mitochondrial membrane protein, is reported to be involved in the maintenance of mitochondrial integrity and calcium metabolism, as well as in the inhibition of apoptosis. It is involved in maintaining the calcium pool in the endoplasmic reticulum (ER), so as to prevent Ca^{2+} surge [39]. Compared with the wild-type mice, the CISD2 knockout mice exhibit increased Ca^{2+} levels in the ER and cytoplasm [40], mitochondrial dysfunction, and enhanced cell death [41]. CISD2 can bind BCL2 and promote the formation of the BCL2-BECN1 complex, which inhibits Beclin 1, a promoter of apoptosis [42].

In addition to mitochondrial dysfunction, CISD2 mitigates CNS injury-induced inflammatory response. Aging, neurodegeneration, and trauma are associated with downregulated CISD2 expression, which enhances the inflammatory response and exacerbates mitochondrial dysfunction [25, 26]. Therefore, therapeutic targeting of CISD2 can aid in preventing the exacerbation of inflammation and mitochondrial dysfunction.

NF-κB signaling is active in the cytoplasm and mitochondrial intermembranous space. The NF-κB signaling pathway is involved in mediating phenomenon, such as mitochondrial dynamics and respiratory electron transport chain. Aberrant activation of NF-κB promotes mitochondrial dysfunction and apoptosis [43]. Additionally, the mechanisms underlying inflammation and mitochondrial dysfunction associated with aging, neurodegenerative disease, and head trauma or acute SCIs may involve aberrant NF-κB activation. Further studies are needed to elucidate the role of CISD2 in regulating the NF-κB signaling pathway.

BCL2 and NF-κB are the upstream targets of CISD2 [44]. In this study, we demonstrated that CISD2 regulates the upstream effectors (PPAR-β) of the PPAR-β/IκB/NF-κB signaling pathway. Additionally, the findings of this study indicated that the anti-inflammatory mechanism of CISD2 involves inhibition of NF-κB activity. Furthermore, CISD2 is an outer mitochondrial membrane structural protein that may be degraded during the pathological process of primary injury (in acute trauma) or secondary injury (in chronic inflammation) associated with CNS injury or disease. CISD2 is downregulated under nonstressed and injured conditions [25]. Insult-induced CISD2 downregulation results in the inhibition of NF-κB activity in the cytoplasm and mitochondria. This explains the wide range of harmful effects, including enhanced inflammation and mitochondrial dysfunction, associated with injury-induced CISD2 downregulation.

Previously, we had demonstrated that curcumin mitigated injury-induced CISD2 downregulation, suggesting that curcumin exerts a protective effect against inflammation and mitochondrial dysfunction in mice with hemisection SCI [26] and aged mice (104 weeks) [25]. CISD2 deficiency enhances the expression of iNOS and RANTES, which contributes to mitochondrial dysfunctions, such as low DeltaPsi(m) levels, high ROS levels, and augmented apoptosis, which are mitigated upon curcumin treatment [25]. In this study, WBM mitigated the injury-induced downregulation of CISD2, which inhibited the aberrant activation of glia

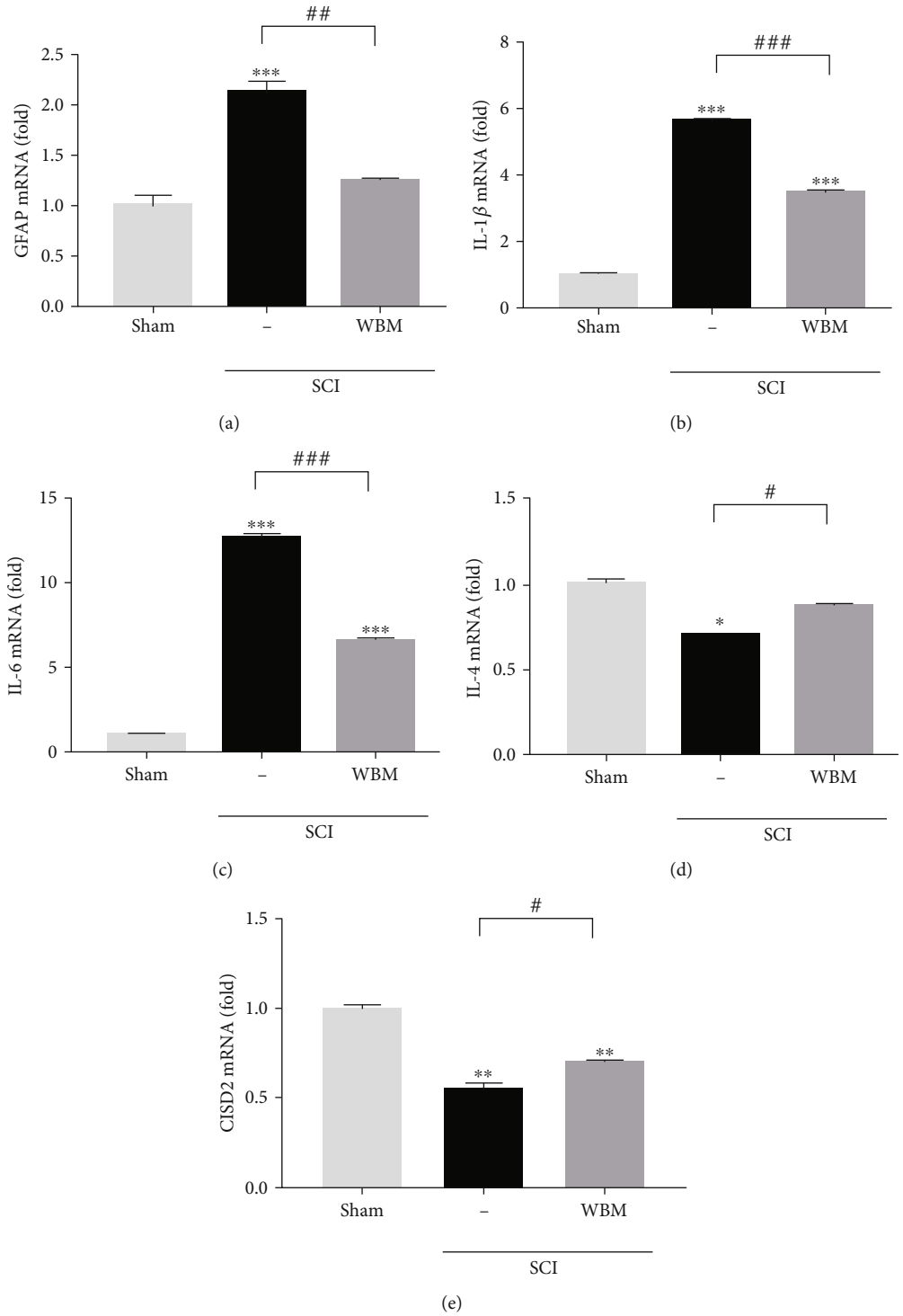

Figure 4: Traumatic insults upregulated GFAP and neuroinflammatory mediators and downregulated CISD2 mRNA expression *in vivo* 24 h after spinal cord hemisection in mice. WBM can *in vivo* rescue the abovementioned detrimental effects. Results of mRNA expression of GFAP (a), IL-1β (b), IL-6 (c), IL-4 (d), and CISD2 (e) for 3 conditions. Vertical bars indicate the mean ± standard error of the mean (SEM) of mRNA expression ($n = 3$). $^{**}P < 0.01$ vs. control, $^{***}P < 0.001$ vs. control, $^{\#\#}P < 0.01$, and $^{\#\#\#}P < 0.001$ indicate a significant difference. Pair-wise multiple comparisons between groups were performed using the Newman-Keuls method.

and proinflammatory cascades in SCI-hemisected mice and LPS-stimulated ALT cells. WBM enhanced the expression of CISD2, PPAR-β, and IκB proteins in the spinal cord of SCI mice. Hence, we hypothesized that WBM upregulates CISD2, which negatively regulates the PPAR-β/IκB/NF-κB signaling pathway and alleviates inflammation and mitochondrial dysfunction through NF-κB. Pharmacological agents that target CISD2 can be considered for treating

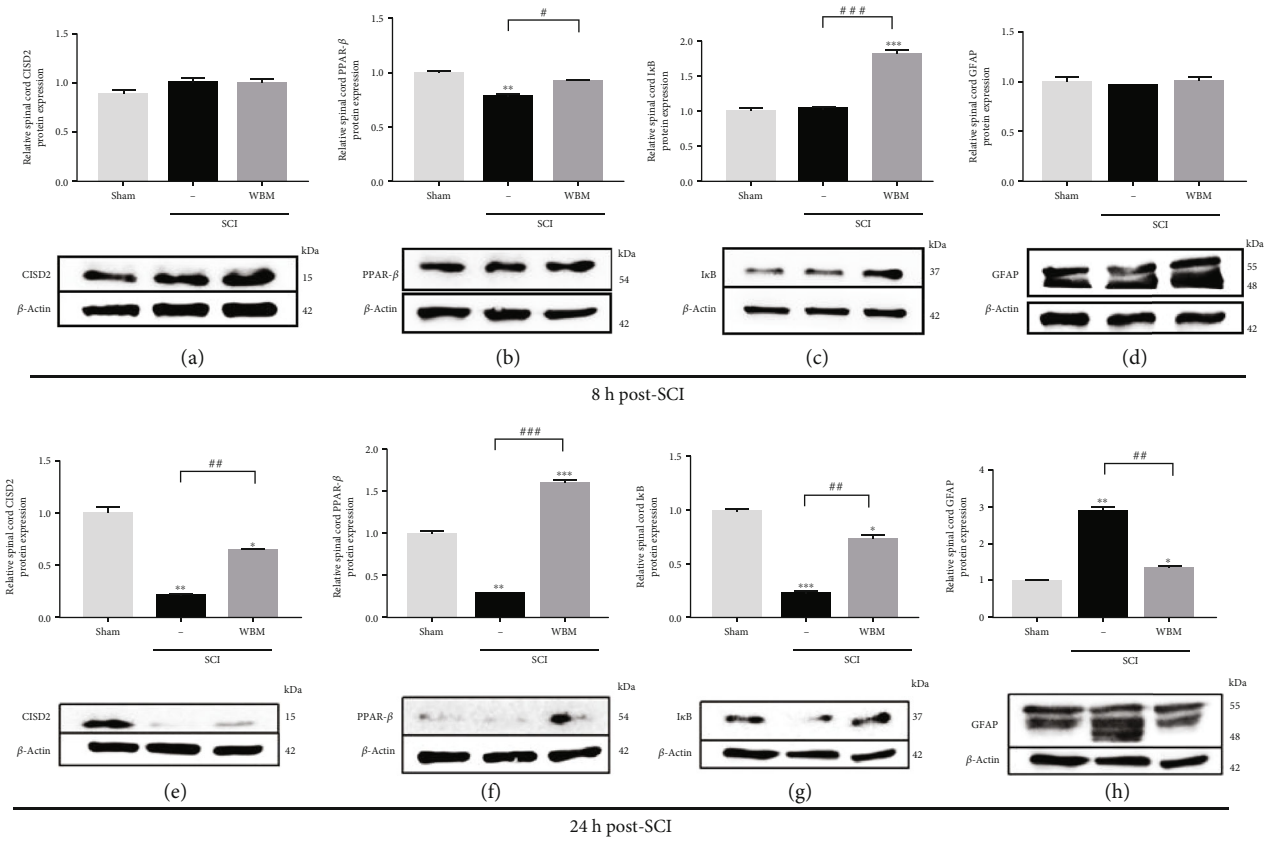

Figure 5: WBM abolished injury-triggered GFAP and attenuated injury-downregulated CISD2, PPAR-β, and IκB protein expression in mice 24 h following spinal cord hemisection *in vivo*. (a–d) *In vivo* mouse model of SCI. Results of protein expression of CISD2 (a), PPAR-β (b), IκB (c), and GFAP (d) for 3 conditions 8 h after SCI. (e–h) Results of protein expression of CISD2 (e), PPAR-β (f), IκB (g), and GFAP (h) for 3 conditions 24 h after SCI. The lower panel indicates representative immunoblot of the proposed protein expression, and β-actin (42 kDa) serves as an internal control. The results shown were from one of the experiments that were repeated for at least 3 times. The upper panel indicates the mean ± SEM of the proposed protein/β-actin band intensity in ratio to the control group. Anti-inflammatory effects of WBM on SCI can be postulated as CISD2 preservation, and the potential upstream regulation of CISD2 on PPAR-β, subsequent IκB stabilization, and therefore, NF-κB inhibition. Vertical bars indicate the mean ± standard error of the mean (SEM) of protein expression ($n = 3$). $^{*}P < 0.05$ vs. control, $^{**}P < 0.01$ vs. control, $^{***}P < 0.001$ vs. control, $^{\#}P < 0.05$, $^{\#\#}P < 0.01$, and $^{\#\#\#}P < 0.001$ indicate a significant difference. Pair-wise multiple comparisons between groups were performed using the Newman-Keuls method.

CNS injury or disease. Further studies are needed to elucidate the role of NF-κB activation in CISD2-mediated alleviation of inflammation and mitochondrial dysfunction.

This study has several limitations. The anti-inflammatory effects of WBM were evaluated based on the expression of CISD2 and attenuation of aberrant glial activation in SCI mice. However, the mechanism underlying injury-induced aberrant glial activation involves astrocyte-microglia interaction. In this study, WBM mitigated the injury-induced upregulation of GFAP in SCI mice and LPS-stimulated ALT cells. This indicated that WBM deactivated the astrocytes. WBM mitigated SCI-induced downregulation of IL-4 in mice with SCI. The loss of IL-4 promotes microglial polarization from M2 to M1 phenotype in IL-4 knockout mice [10]. Thus, WBM can potentially enhance the levels of anti-inflammatory M2 microglia in SCI mice. Further *in vivo* studies are needed to examine the mechanism underlying WBM-mediated microglial polarization in SCIs. Furthermore, si-CISD2 transfection revealed that the anti-inflammatory effects of CISD2 were associated with the regulation of PPAR-β, which positively regulates IκB, an inhibitor of NF-κB. Hence, we hypothesized that the injury-induced downregulation of CISD2 inhibited NF-κB activity in the cytoplasm and mitochondria, which resulted in enhanced inflammation and mitochondrial dysfunction. Future studies must elucidate the detailed mechanism underlying CISD2-mediated regulation of NF-κB and glial activation. However, the findings of this study indicated that CISD2 regulates inflammation and mitochondrial dysfunction via the inhibition of NF-κB.

In conclusion, WBM exerted its anti-inflammatory effects through the upregulation of CISD2 in SCI mice and LPS-stimulated ALT cells. CISD2 exhibits protective activity in SCI mice via NF-κB downregulation and astrocyte deactivation.

Data Availability

Answer: yes. Comment: the data used to support the findings of this study are included within the article.

Conflicts of Interest

No competing financial interests exist.

Authors' Contributions

Woon-Man Kung contributed in writing the original draft of the manuscript as well as in formal analysis. Chai-Ching Lin contributed in supervision, investigation, and formal analysis. Chan-Yen Kuo contributed in project administration and validation. Yu-Ching Juin contributed in project administration and methodology. Po-Ching Wu contributed resources as well as in supervision and investigation. Muh-Shi Lin contributed in funding acquisition; writing the original draft of the manuscript; writing, reviewing, and editing the final version of the manuscript; and in conceptualization.

Acknowledgments

Part of the information reported in Results was referenced from the master thesis of Yu-Ching Juin at the National Ilan University, Yilan, Taiwan. This work was supported by grants from the Kuang Tien General Hospital, Taiwan (Kuang Tien 105-07 and 106-12).

References

[1] B. K. Kwon, W. Tetzlaff, J. N. Grauer, J. Beiner, and A. R. Vaccaro, "Pathophysiology and pharmacologic treatment of acute spinal cord injury," *The Spine Journal*, vol. 4, no. 4, pp. 451–464, 2004.

[2] J. R. Bethea and W. D. Dietrich, "Targeting the host inflammatory response in traumatic spinal cord injury," *Current Opinion in Neurology*, vol. 15, no. 3, pp. 355–360, 2002.

[3] J. D. Houle and A. Tessler, "Repair of chronic spinal cord injury," *Experimental Neurology*, vol. 182, no. 2, pp. 247–260, 2003.

[4] S. J. Davies, P. M. Field, and G. Raisman, "Regeneration of cut adult axons fails even in the presence of continuous aligned glial pathways," *Experimental Neurology*, vol. 142, no. 2, pp. 203–216, 1996.

[5] K. S. Hung, S. L. Hwang, C. L. Ling et al., "Calpain inhibitor inhibits p35-p25-Cdk5 activation, decreases tau hyperphosphorylation, and improves neurological function after spinal cord hemisection in rats," *Journal of Neuropathology and Experimental Neurology*, vol. 64, no. 1, pp. 15–26, 2005.

[6] Y. Luo, M. A. Berman, Q. Zhai et al., "RANTES stimulates inflammatory cascades and receptor modulation in murine astrocytes," *Glia*, vol. 39, no. 1, pp. 19–30, 2002.

[7] C. H. Tator and M. G. Fehlings, "Review of the secondary injury theory of acute spinal cord trauma with emphasis on vascular mechanisms," *Journal of Neurosurgery*, vol. 75, no. 1, pp. 15–26, 1991.

[8] W. Liu, Y. Tang, and J. Feng, "Cross talk between activation of microglia and astrocytes in pathological conditions in the central nervous system," *Life Sciences*, vol. 89, no. 5-6, pp. 141–146, 2011.

[9] G. Volpin, M. Cohen, M. Assaf, T. Meir, R. Katz, and S. Pollack, "Cytokine levels (IL-4, IL-6, IL-8 and TGFβ) as potential biomarkers of systemic inflammatory response in trauma patients," *International Orthopaedics*, vol. 38, no. 6, pp. 1303–1309, 2014.

[10] X. Liu, J. Liu, S. Zhao et al., "Interleukin-4 is essential for microglia/macrophage M2 polarization and long-term recovery after cerebral ischemia," *Stroke*, vol. 47, no. 2, pp. 498–504, 2016.

[11] S. Li, L. Wang, M. A. Berman, Y. Zhang, and M. E. Dorf, "RNAi screen in mouse astrocytes identifies phosphatases that regulate NF-κB signaling," *Molecular Cell*, vol. 24, no. 4, pp. 497–509, 2006.

[12] K. S. Hung, S. H. Tsai, T. C. Lee, J. W. Lin, C. K. Chang, and W. T. Chiu, "Gene transfer of insulin-like growth factor-I providing neuroprotection after spinal cord injury in rats," *Journal of Neurosurgery. Spine*, vol. 6, no. 1, pp. 35–46, 2007.

[13] R. J. Hurlbert, "Strategies of medical intervention in the management of acute spinal cord injury," *Spine*, vol. 31, Supplement, pp. S16–S21, 2006.

[14] C. Y. Chao, M. C. Yin, and C. J. Huang, "Wild bitter gourd extract up-regulates mRNA expression of PPARα, PPARγ and their target genes in C57BL/6J mice," *Journal of Ethnopharmacology*, vol. 135, no. 1, pp. 156–161, 2011.

[15] C. K. Lii, H. W. Chen, W. T. Yun, and K. L. Liu, "Suppressive effects of wild bitter gourd (Momordica charantia Linn. var. abbreviata ser.) fruit extracts on inflammatory responses in RAW264.7 macrophages," *Journal of Ethnopharmacology*, vol. 122, no. 2, pp. 227–233, 2009.

[16] Y. L. Lu, Y. H. Liu, J. H. Chyuan, K. T. Cheng, and W. L. Liang, "Antioxidant activities of different wild bitter gourd (Momordica charantia L. var. abbreviata Seringe) cultivars," *Botanical Studies*, vol. 53, pp. 207–214, 2012.

[17] S. J. Wu and L. T. Ng, "Antioxidant and free radical scavenging activities of wild bitter melon (Momordica charantia Linn. var. abbreviata Ser.) in Taiwan," *LWT-Food Science and Technology*, vol. 41, no. 2, pp. 323–330, 2008.

[18] R. Rawat, X. H. Yu, M. Sweet, and J. Shanklin, "Conjugated fatty acid synthesis: residues 111 and 115 influence product partitioning of Momordica charantia conjugase," *The Journal of Biological Chemistry*, vol. 287, no. 20, pp. 16230–16237, 2012.

[19] C. Y. Chuang, C. Hsu, C. Y. Chao, Y. S. Wein, Y. H. Kuo, and C. J. Huang, "Fractionation and identification of 9c, 11t, 13t-conjugated linolenic acid as an activator of PPARα in bitter gourd (Momordica charantia L.)," *Journal of Biomedical Science*, vol. 13, no. 6, pp. 763–772, 2006.

[20] Y. Liu, J. K. Colby, X. Zuo, J. Jaoude, D. Wei, and I. Shureiqi, "The role of PPAR-δ in metabolism, inflammation, and cancer: many characters of a critical transcription factor," *International Journal of Molecular Sciences*, vol. 19, no. 11, p. 3339, 2018.

[21] G. F. Yuan, A. J. Sinclair, C. Q. Zhou, and D. Li, "α-Eleostearic acid is more effectively metabolized into conjugated linoleic acid than punicic acid in mice," *Journal of the Science of Food and Agriculture*, vol. 89, no. 6, pp. 1006–1011, 2009.

[22] T. Tsuzuki, Y. Tokuyama, M. Igarashi et al., "α-Eleostearic acid (9Z11E13E-18:3) is quickly converted to conjugated linoleic acid (9Z11E-18:2) in rats," *The Journal of Nutrition*, vol. 134, no. 10, pp. 2634–2639, 2004.

[23] G. Ding, L. Cheng, Q. Qin, S. Frontin, and Q. Yang, "PPARδ modulates lipopolysaccharide-induced TNFα inflammation signaling in cultured cardiomyocytes," *Journal of Molecular and Cellular Cardiology*, vol. 40, no. 6, pp. 821–828, 2006.

[24] M. Galuppo, R. di Paola, E. Mazzon et al., "GW0742, a high affinity PPAR-β/δ agonist reduces lung inflammation induced by bleomycin instillation in mice," *International Journal of Immunopathology and Pharmacology*, vol. 23, no. 4, pp. 1033–1046, 2010.

[25] C. C. Lin, T. H. Chiang, Y. Y. Sun, and M. S. Lin, "Protective effects of CISD2 and influence of curcumin on CISD2 expression in aged animals and inflammatory cell model," *Nutrients*, vol. 11, no. 3, p. 700, 2019.

[26] C. C. Lin, T. H. Chiang, W. J. Chen, Y. Y. Sun, Y. H. Lee, and M. S. Lin, "CISD2 serves a novel role as a suppressor of nitric oxide signalling and curcumin increases CISD2 expression in spinal cord injuries," *Injury*, vol. 46, no. 12, pp. 2341–2350, 2015.

[27] M. S. Lin, Y. H. Lee, W. T. Chiu, and K. S. Hung, "Curcumin provides neuroprotection after spinal cord injury," *The Journal of Surgical Research*, vol. 166, no. 2, pp. 280–289, 2011.

[28] K. H. Lu, H. C. Tseng, C. T. Liu, C. J. Huang, J. H. Chyuan, and L. Y. Sheen, "Wild bitter gourd protects against alcoholic fatty liver in mice by attenuating oxidative stress and inflammatory responses," *Food & Function*, vol. 5, no. 5, pp. 1027–1037, 2014.

[29] X.-Q. Yuan, X. Gu, J. Tang, and J. Wasswa, "Hypoglycemic effect of semipurified peptides from Momordica charantia L. var. Abbreviata Ser. in alloxan-induced diabetic mice," *Journal of Food Biochemistry*, vol. 32, no. 1, pp. 107–121, 2008.

[30] M. S. Lin, Y. Y. Sun, W. T. Chiu et al., "Curcumin attenuates the expression and secretion of RANTES after spinal cord injury in vivo and lipopolysaccharide-induced astrocyte reactivation in vitro," *Journal of Neurotrauma*, vol. 28, no. 7, pp. 1259–1269, 2011.

[31] N. J. Maragakis and J. D. Rothstein, "Mechanisms of disease: astrocytes in neurodegenerative disease," *Nature Clinical Practice. Neurology*, vol. 2, no. 12, pp. 679–689, 2006.

[32] S. Hickman, S. Izzy, P. Sen, L. Morsett, and J. el Khoury, "Microglia in neurodegeneration," *Nature Neuroscience*, vol. 21, no. 10, pp. 1359–1369, 2018.

[33] A. Ravari, T. Mirzaei, D. Kennedy, and M. Kazemi Arababadi, "Chronoinflammaging in Alzheimer: a systematic review on the roles of toll like receptor 2," *Life Sciences*, vol. 171, pp. 16–20, 2017.

[34] A. Navarro and A. Boveris, "Brain mitochondrial dysfunction in aging, neurodegeneration, and Parkinson's disease," *Frontiers in Aging Neuroscience*, vol. 2, p. 34, 2010.

[35] N. Sun, R. J. Youle, and T. Finkel, "The mitochondrial basis of aging," *Molecular Cell*, vol. 61, no. 5, pp. 654–666, 2016.

[36] J. van Horssen, P. van Schaik, and M. Witte, "Inflammation and mitochondrial dysfunction: A vicious circle in neurodegenerative disorders?," *Neuroscience letters*, vol. 710, article 132931, 2019.

[37] R. L. Hunter, N. Dragicevic, K. Seifert et al., "Inflammation induces mitochondrial dysfunction and dopaminergic neurodegeneration in the nigrostriatal system," *Journal of Neurochemistry*, vol. 100, no. 5, pp. 1375–1386, 2007.

[38] M. N. Valcárcel-Ares, R. R. Riveiro-Naveira, C. Vaamonde-García et al., "Mitochondrial dysfunction promotes and aggravates the inflammatory response in normal human synoviocytes," *Rheumatology (Oxford)*, vol. 53, no. 7, pp. 1332–1343, 2014.

[39] N. C. Chang, M. Nguyen, J. Bourdon et al., "Bcl-2-associated autophagy regulator Naf-1 required for maintenance of skeletal muscle," *Human Molecular Genetics*, vol. 21, no. 10, pp. 2277–2287, 2012.

[40] N. C. Chang, M. Nguyen, and G. C. Shore, "BCL2-CISD2: An ER complex at the nexus of autophagy and calcium homeostasis?," *Autophagy*, vol. 8, no. 5, pp. 856-857, 2014.

[41] Y. F. Chen, C. H. Kao, Y. T. Chen et al., "Cisd2 deficiency drives premature aging and causes mitochondria-mediated defects in mice," *Genes & Development*, vol. 23, no. 10, pp. 1183–1194, 2009.

[42] R. Kang, H. J. Zeh, M. T. Lotze, and D. Tang, "The Beclin 1 network regulates autophagy and apoptosis," *Cell Death and Differentiation*, vol. 18, no. 4, pp. 571–580, 2011.

[43] B. C. Albensi, "What is nuclear factor kappa B (NF-κB) doing in and to the mitochondrion?," *Frontiers in Cell and Development Biology*, vol. 7, p. 154, 2019.

[44] B. Chen, S. Shen, J. Wu et al., "CISD2 associated with proliferation indicates negative prognosis in patients with hepatocellular carcinoma," *International Journal of Clinical and Experimental Pathology*, vol. 8, no. 10, pp. 13725–13738, 2015.

Hindawi
Behavioural Neurology
Volume 2020, Article ID 1574816, 8 pages
https://doi.org/10.1155/2020/1574816

Research Article

Retinal Levels of Amyloid Beta Correlate with Cerebral Levels of Amyloid Beta in Young APPswe/PS1dE9 Transgenic Mice before Onset of Alzheimer's Disease

Xi Mei,[1] **Mengxiang Yang**,[2] **Lina Zhu**,[3] **Qi Zhou**,[1] **Xingxing Li**,[1] **Zhongming Chen**,[1] **and Chenjun Zou**[1]

[1]*Kangning Hospital of Ningbo, Ningbo City, Zhejiang Province, China*
[2]*Ningbo University, Ningbo City, Zhejiang Province, China*
[3]*Weifang Medical University, Weifang City, Shandong Province, China*

Correspondence should be addressed to Xi Mei; meixi18401856@163.com and Chenjun Zou; zouchenjunkn@163.com

Received 11 June 2020; Revised 15 September 2020; Accepted 16 September 2020; Published 24 September 2020

Academic Editor: Yu Yo Sun

Objectives. Retina abnormalities are related to cognitive disorders in patients with Alzheimer's disease (AD). Retinal amyloid beta (Aβ) can be labeled by curcumin. We measured Aβ content in the cerebrum and retina of APPswe/PS1dE9 (APP) transgenic mice with early age to investigate the correlation between cerebrum and retina. *Methods*. APP mice and age-matched wild-type mice were investigated every month from age 2 months to 6 months to assess changes in Aβ content in the retina and cerebrum. At the beginning of each month, mice were fed a curcumin diet (50 mg/kg/day) for 7 consecutive days. The Aβ levels in the retina and cerebrum were measured by ELISAs. Correlations were identified between retinal and cerebral Aβ contents using Pearson's correlation. *Results*. In the absence of curcumin, there was a significant correlation between Aβ contents in the retina and cerebrum of APP mice ($r = 0.7291$, $P = 0.0014$). With increasing age, Aβ-mediated degenerative change in the cerebrum ($P < 0.001$ in 5 months) and retina ($P < 0.01$ in 5 months) increased significantly. The inhibitory effect of curcumin on the Aβ level was significant in the cerebrum ($P < 0.001$) and retina ($P < 0.01$) of older APP mice in the early stage of life. *Conclusion*. We observed a significant correlation between the Aβ content in the retina and Aβ content in the cerebrum of APP mice. Our data suggest an appropriate time to measure retinal Aβ. Although curcumin can label Aβ in the retina, it also suppresses Aβ levels and weakens the degree of correlation between Aβ in cerebrum and retina tissues.

1. Introduction

Early diagnosis of Alzheimer's disease (AD) is essential for treatment [1]. Most diagnostic methods for AD are based on clinical symptoms [2]. Commonly, people in the presymptomatic stage of AD have no clinical symptoms (including impairment in episodic memory).

"Amyloid beta" (Aβ), which denotes peptides of 36-43 amino acids, is a major pathologic hallmark in the central nervous system (CNS) of patients with AD [3, 4]. Amyloidal precursor protein (APP) is first cleaved by the enzymes β-secretase and γ-secretase and then released into the space between cells [5]. Due to the different cleavage sites of γ-secretase, Aβ lengths are different. Soluble Aβ oligomers are more toxic than deposited plaques [6]. Although Aβ plaques are found in the brains of many elderly people without AD, they might be denoting a presymptomatic stage of AD.

Auxiliary diagnoses involve the examination of cerebrospinal fluid and positron emission tomography (PET) of Aβ plaques [7, 8]. The examination of cerebrospinal fluid Aβ is an invasive method. High cost of Aβ-PET limits its use in early diagnosis. Recent studies demonstrate the ability to detect CNS Aβ deposition via the use of plasma assessment of Aβ species [9, 10]. Due to the blood-brain barrier, plasma amyloid beta levels cannot reflect the real condition in the brain. Plasma concentrations of Aβ40 and Aβ42 have been shown to increase with age and in early AD but may decrease with advancing AD. However, no significant

differences in plasma Aβ concentrations have been reported between individuals with and without AD [11].

However, AD is a disease of the CNS, and Aβ may distribute in all parts of nervous tissue, including the cerebrum and retina [12]. Ocular amyloidal imaging has been used to diagnose AD and monitor, noninvasively, AD progression [13].

Although the identifiable difference in the retinal structure between AD patients and healthy people is not straightforward, and misdiagnoses can occur [14, 15], retinal Aβ plaques which can be labeled with curcumin may improve diagnostic accuracy [16, 17]. This method merits further study and development into a new diagnostic measurement. Moreover, curcumin is a safe, nontoxic lipophilic agent with antioxidant and anti-inflammatory properties [4]. Apart from being a valuable labeling agent, curcumin may also play an important part in the AD treatment without eliciting side effects [18, 19].

The biological basis of curcumin-labeled examination of the retina is good coherence between the cerebrum and retina. Retinal Aβ plaques can reflect Aβ plaques in the cerebrum. When is the best time to early detect Aβ and diagnose AD through the retina? What is the consistency between the cerebral Aβ and the retinal Aβ? In this brief research report, we elucidated Aβ content and its coherence in the cerebrum and retina of mice with early-age before the onset of AD.

2. Materials and Methods

2.1. Ethical Approval of the Study Protocol. The study protocol was approved by the Animal Care and Use Committee of the Medical School of Ningbo University (Ningbo, China). Animal experiments were undertaken according to the *Guide for the Care and Use of Laboratory Animals* (National Institutes of Health (Bethesda, MD, USA) publication number 80-23, revised 1996).

2.2. Animals. APPswe/PS1dE9 transgenic mice (APP) and age-matched wild type (WT) mice were provided by the Model Animal Research Center of Nanjing University (Nanjing, China). To exclude the effect of sex on results, only male mice were used. Animals were housed in cages in a room maintained at 22 ± 2°C and 60 ± 5% relative humidity under a 12 h light–dark cycle (lights on at 6 : 00 am). Water and food were freely available in their cages. Animal experiments were conducted outside of their housing area in a separate room.

2.3. Experimental Procedures. According to previous studies, amyloid-beta plaques in CNS of AD mice are markedly formed at 6 months of age [20]. Curcumin was administered to 2-, 3-, 4-, 5-, and 6-month old APP and WT mice for 7 consecutive days using the intragastric (i.g.) administration route.

Mice at the age of each month were divided into 4 experimental groups ($n \geq 3$ mice/group): (1) APP mice treated with curcumin (50 mg/kg/day) dissolved in phosphate-buffered saline (PBS, 0.1 mg/g), $n = 19$; (2) APP mice treated with the same volume of only PBS, $n = 17$; (3) WT mice treated with curcumin (50 mg/kg/day) dissolved in phosphate-buffered saline (PBS, 0.1 mg/g), $n = 18$; and (4) WT mice treated with the same volume of only PBS, $n = 17$.

The dose of curcumin used in this study was chosen according to previous animal studies and clinical trials [16, 21, 22]. According to previous studies, at high dosages, curcumin might prevent short-term recognition but not spatial memory. No signs of neurogenesis were evident, but reduced neuroinflammation was observed. The dose of the intragastric (i.g.) administration route has been shown to reduce the risk of vascular inflammation in the brain of AD subjects [19, 23].

Mice were sacrificed by neck amputation after the final administration. Then, the retina and cerebrums were isolated. Tissue samples were homogenized in RIPA Buffer (Beijing Solarbio Science & Technology, Beijing, China) at 1 : 10 (g/v) with 1% phenylmethylsulfonyl fluoride (Beijing Solarbio Science & Technology). Supernatant proteins were extracted after centrifugation (13,000 rpm or 20 min at 4°C). For each sample, 150 μL of extracted protein was used for detection. The Aβ concentration was quantified using a mouse total Aβ ELISA kit (Shanghai Yuanye BioTechnology, Shanghai, China) according to manufacturer protocols.

2.4. Materials. Curcumin (pure curcumin ≥ 80%, Hushi, Shanghai, China) was dissolved by phosphate-buffered saline (0.1 M Na_2HPO_4, 0.1 M KH_2PO_4, 0.1 M KCl, and 0.1 M NaCl, pH 7.4).

2.5. Enzyme-Linked Immune Sorbent Assay (ELISA). The Aβ level in the brain and retina was measured by ELISAs. Absorbance at 450 nm (at a reference wavelength of 690 nm) was measured by an absorbance reader (Sunrise™; Tecan, Geneva, Switzerland). The absorbance value was transformed into a concentration value by reading the absorbance of pure samples on a standard curve.

2.6. Aβ Immunohistochemistry. Briefly, after anesthetized, mice were perfused with saline until the limbs and the liver turn white, and then perfused with 4% paraformaldehyde until the tail became stiff. The brain tissue was dissected and incubated with 4% paraformaldehyde for 1 day. After being washed with PBS, the tissue was put in a centrifuge tube containing 30% sucrose solution until the brain tissue sunk to the bottom. A cryostat was used to cut the brain tissue into 25 μm thick brains. The sections were incubated in 1% BSA for 1 h and then incubated with β-amyloid antibody (1 : 500, Cell Signaling Technology) at 4°C overnight. The sections were washed 3 times with PBS, rinsed, and incubated with the secondary antibody at 37°C for 1 h. After staining with 4′,6-diamidino-2-phenylindole (DAPI) for 1 min, the sections were washed 3 times with PBS and imaged using a confocal fluorescence microscope.

2.7. Statistical Analyses. Data are the mean ± standard error (SE). Prism v7.0 (GraphPad, San Diego, CA, USA) was employed for statistical analyses. Differences among multiple mean ± SE values were assessed by one-way and two-way ANOVA, followed by Bonferroni's *post hoc* test. Differences

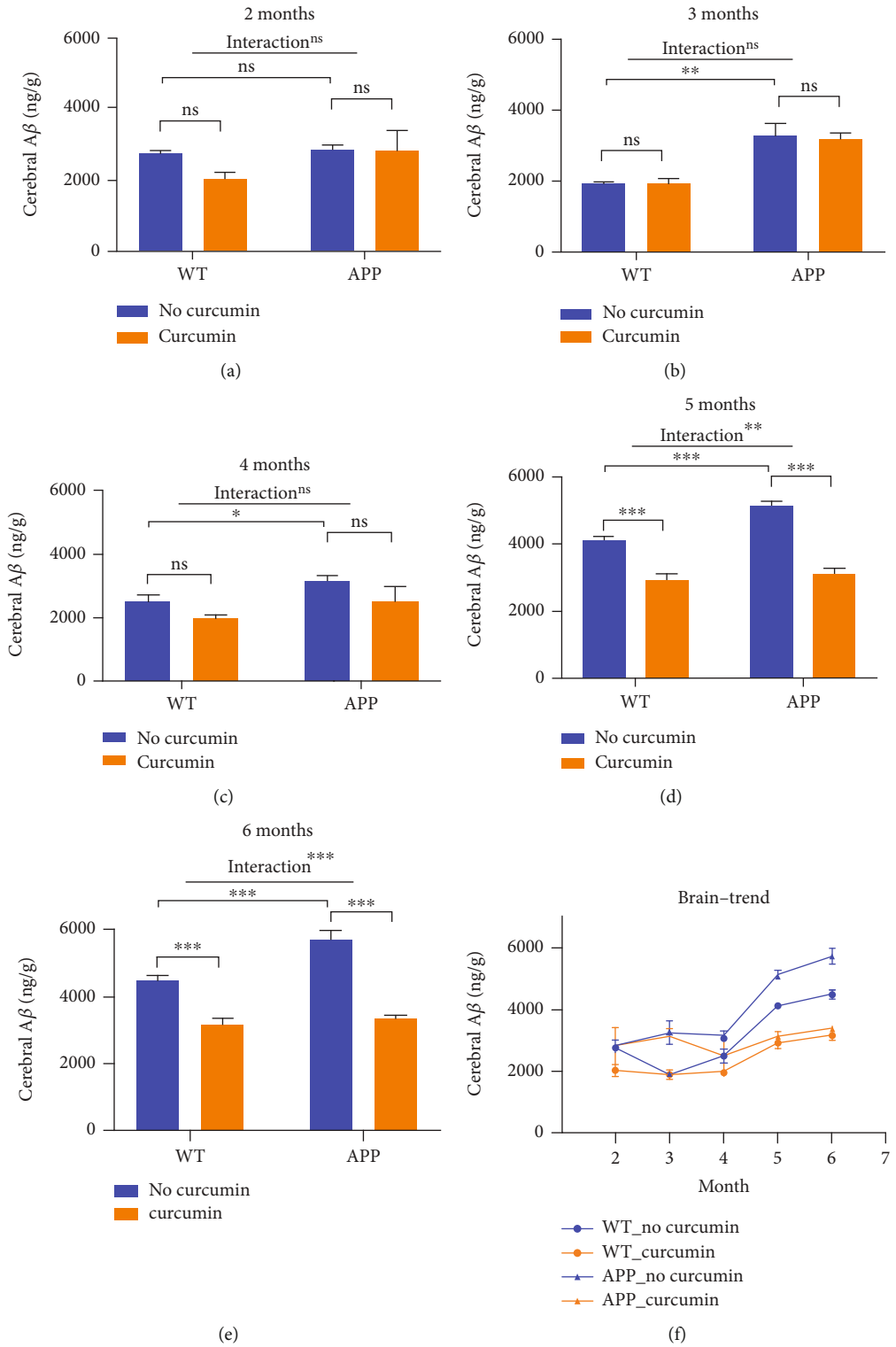

Figure 1: Effects of curcumin on the Aβ level in the cerebrum. Abbreviations: APP: APPswe/PS1dE9; WT: wild type; APP_C: APP mice given curcumin ($n = 19$); APP_N: APP mice not given curcumin ($n = 17$); WT_C: WT mice given curcumin ($n = 18$); WT_N: WT mice not given curcumin ($n = 17$); $^*P < 0.05$; $^{**}P < 0.01$; $^{***}P < 0.001$.

between two mean ± SE values were assessed by the unpaired t-test. The correlation between Aβ content in the retina and cerebrum in each group was tested using Pearson's correlation. $P < 0.05$ was considered significant.

3. Results

3.1. Aβ Accumulation with Increasing Age in the Cerebrum of Mice. Several works have shown abundant Aβ plaques in the

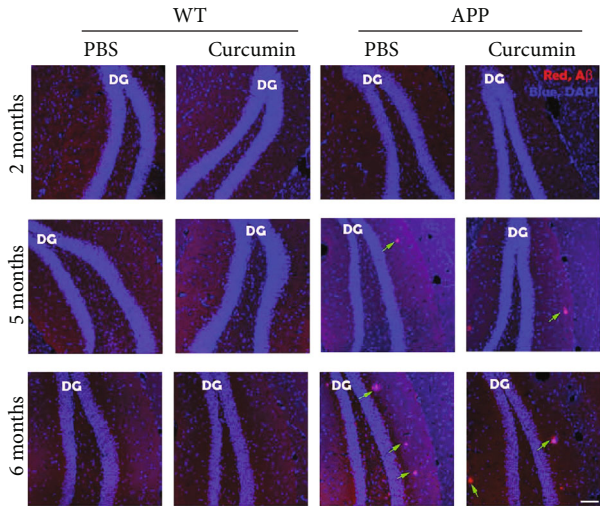

Figure 2: Aβ immunohistochemistry of hippocampus (red, Aβ; blue, DAPI). WT control brain exhibited no plaques in each group of age, while plaques of APP mice aged 5 and 6 months began to accumulate (green arrows). Abbreviations: APP: APPswe/PS1dE9; WT: wild type. Scale bar = 100 μm.

brain of APP transgenic mice older than 6 months [20]. Mice in the present study were aged 2-6 months, so Aβ plaques have not yet formed in the brain. Hence, we measured the Aβ concentration in the brain of each mouse using ELISAs. WT mice given or not given curcumin are represented as WT_C and WT_N, respectively. APP mice given or not given curcumin are represented as APP_C and APP_N, respectively.

Results revealed that Aβ was present in all four groups (WT_C, WT_N, APP_C, APP_N). Figure 1 shows the change in the Aβ level in the four groups with increasing age, as well as the effects of curcumin on the Aβ level in mouse brains. Aβ content was significantly higher in the APP_N group compared with that in the WT_N group ($P < 0.05$ from 3 month to 6 month). A two-way ANOVA (genotype × treatment) revealed a significant effect of genotype ($F(1, 8) = 100.5$, $P < 0.001$) from 3 months to 6 months.

From 5 months of age, the difference in the Aβ level between the curcumin administration group and no curcumin administration increased. The inhibitory effect of curcumin on the Aβ level was significant in the brain in 5 months, with 38.82% suppression by curcumin (APP_C *vs.* APP_N, $P < 0.001$). Images of Figure 2 show a progressive increase in plaque load of APP mice. The Aβ plaques began to accumulate from 5 months of age in tissue level.

3.2. Retinal Content of Aβ in Mice Aged 2-6 Months. Different from the cerebrum, there was no significant difference in the Aβ level in the retinas between the APP_N group and the WT_N group until 5 months in Figure 3. At 5 months of age, the difference between APP_C and APP_N was significant, with 15.96% inhibition by curcumin being recorded ($P < 0.01$).

3.3. Deposition Trend of Aβ in the Cerebrum and Retina. There was an age-related increase in the Aβ content, as shown in Figures 1(f) and 2(f). Aβ accumulation in the brain was different from 2 months to 6 months of age. At 5 months of age, curcumin had a significant effect on the Aβ content. The retinal content of Aβ in mice aged 2-4 months was not sensitive to the effects of curcumin.

Correlation analyses between the Aβ level in the retina and that in the cerebrum are shown in Figure 4. Using combined data from APP mice of all ages, the Aβ level in the retina was correlated positively with the Aβ level in the cerebrum. Without curcumin administration, the Aβ level in the retina was correlated significantly with the Aβ level in the cerebrum ($r = 0.7291$, $P < 0.01$). Coherence between the brain and retina was established gradually with increasing age.

4. Discussion

In 2009, Perez and coworkers suggested that Aβ deposition within the retina can contribute to retinal dysfunction [24]. Many studies have focused on finding the best time to detect Aβ deposition in the eye because it could aid the early diagnosis of AD in humans [25, 26]. Aside from Aβ deposition, studies have focused on retinal function (e.g., light reflection) in young mice with AD [12]. However, Aβ-mediated degenerative change in the cerebrum and retina before the onset of AD has not been studied.

APPswe/PS1dE9 transgenic mice display early onset of Aβ deposition in the CNS [27, 28]. Hence, APPswe/PS1dE9 transgenic mice could be an ideal model to study the Aβ-related pathogenic effects on the nervous system in early-stage AD and even stage before the onset of AD.

Using APPswe/PS1dE9 transgenic mice, our study reported that in early age just before AD onset, there was a correlation between amyloid-beta levels of cerebrum and retina. Researchers have found Aβ plaques on the retina with the aid of the fluorescence effect of curcumin [17]. We also investigated the effect of curcumin on Aβ levels in CNS. Oral administration of curcumin can not only label the amyloid-beta plaques in the retina which may be a window of AD noninvasive diagnosis as Koronyo et al.'s study but also suppress the amyloid-beta level and its correlation of cerebrum and retina.

Time is an important factor in AD pathology. Notably, the accumulation of amyloid-beta increased over time. At 5 months old, the Aβ content became significantly different between mice of APP and WT genotype. The difference between Aβ levels of curcumin and no curcumin groups was higher from 5 months to 6 months. Before 4 months, cerebral levels of amyloid-beta were more affected by genotype than curcumin.

In the cerebrum of young mice, the difference in the Aβ level between APP and WT came earlier than that in the retina. This finding may be because Aβ accumulates in the hippocampal region at the beginning of life and then diffuses to frontal and temporal cortices and other parts of the CNS [1]. With increasing age, the Aβ level in the retina of APPswe/PS1dE9 transgenic mice increased. This appears to resemble a process of age-related decrease in the number of synapses in retinal layers as a result of Aβ accumulation [29]. Aβ accumulation is the upstream event and can be

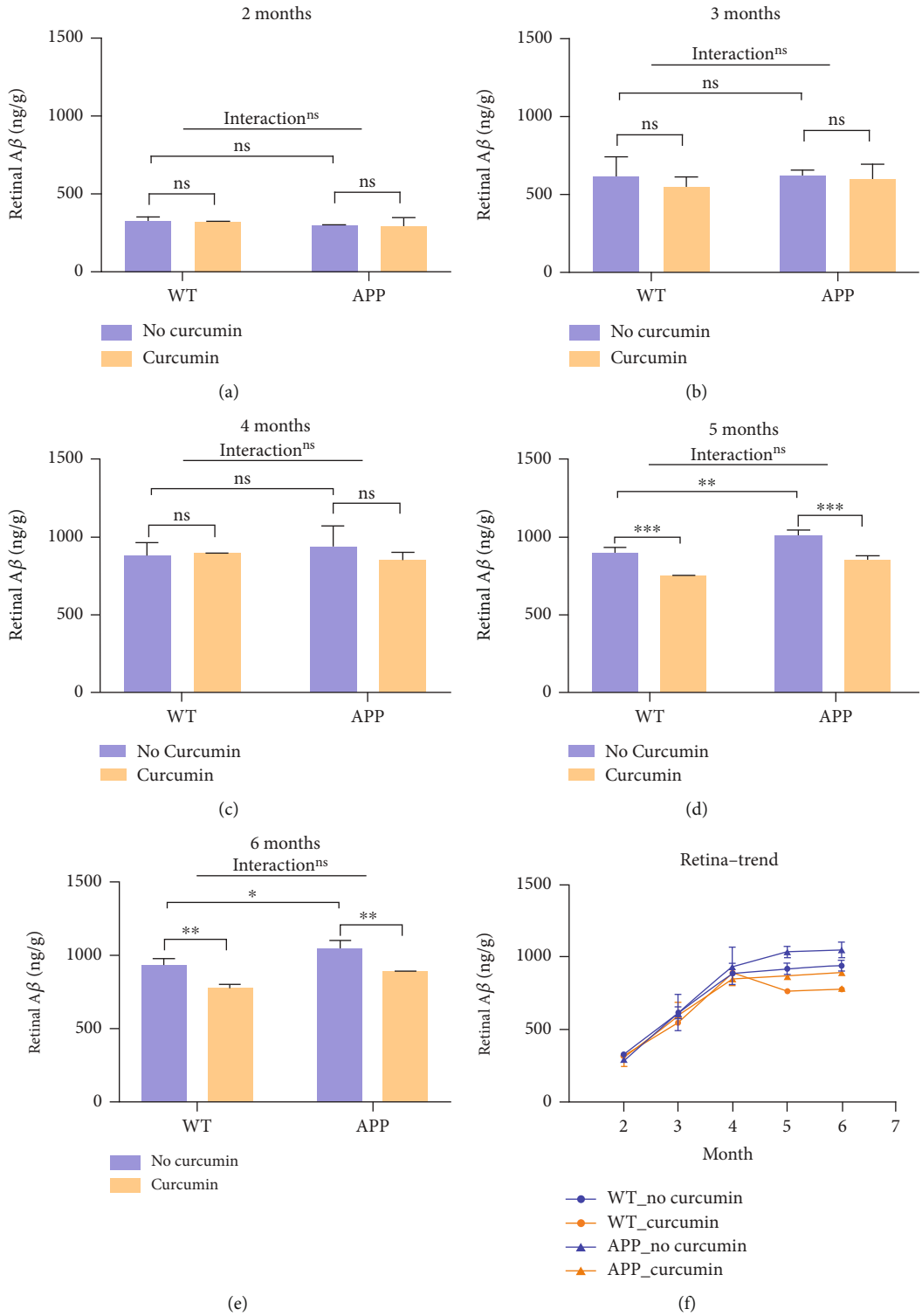

FIGURE 3: Effects of curcumin on the Aβ level in the retina. Abbreviations: APP: APPswe/PS1dE9; WT: wild type; APP_C: APP mice given curcumin ($n = 19$); APP_N: APP mice not given curcumin ($n = 17$); WT_C: WT mice given curcumin ($n = 18$); WT_N: WT mice not given curcumin ($n = 17$); $^*P < 0.05$; $^{**}P < 0.01$.

indirectly reflected by age-related increase in presynaptic and a decrease in postsynaptic retinal proteins in retinal plexiform layers [3, 29]. These phenotypes were similar to the brain. At this time (especially in 5-month-old mice), the amyloidal pathogenesis of AD compared with that in the normal retina could be distinguished. This may be the best time to detect amyloidal pathogenesis from retina for early diagnosis of AD.

Several research teams have used curcumin to label Aβ in the retina and brain [30]. Curcumin can also suppress Aβ

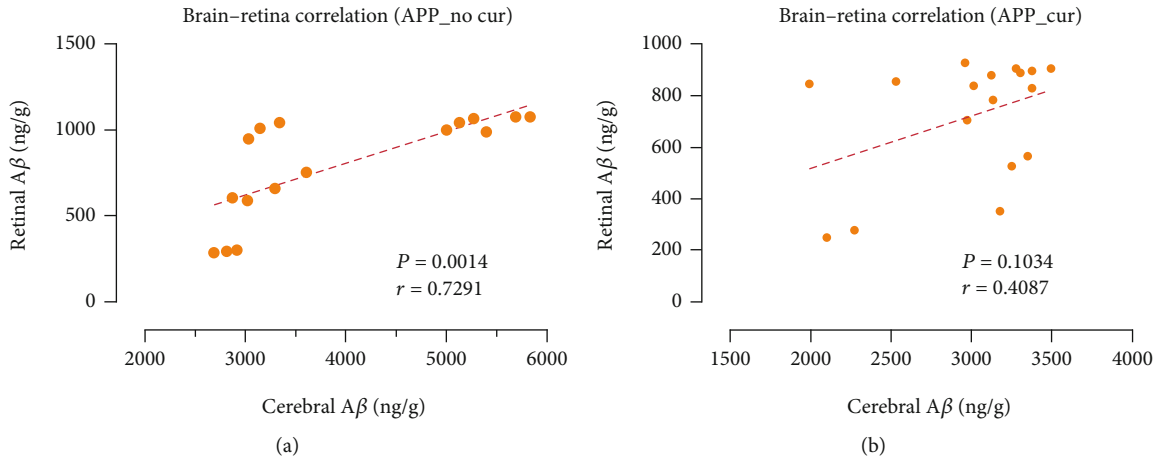

Figure 4: Correlations of the Aβ level in the cerebrum and retina of APP transgenic mice with (b) and without (a) administration of curcumin. Abbreviations: APP: APPswe/PS1dE9.

Table 1: RNFL thickness inpatients of different ages with neurodegenerative disease.

Age (years)	N	Female : male	Subjects	Cognitive evaluation	RNFL thickness	Reference
35.80 ± 9.48	49	26 : 23	Down syndrome	Temporal cortex MRI and PET	$r = 0.592^{*}$	[37]
43.4 ± 12.0	66	48 : 18	Multiple sclerosis	MRI	$B = 1.26^{**}$	[38]
56.0 (55.9 to 56.1)	32038	17172 : 14866	Cognitive decline	Cognitive function tests	$OR = 2.08^{***}$	[39]
65.36 ± 5.55	56	35 : 21	Preclinical AD	PET	-0.228^{*}	[41]
73.5 ± 6.0	63	32 : 31	AD	PET/CT	$AUC = 0.652^{*}$	[42]

$^{*}P < 0.05$; $^{**}P < 0.01$; $^{***}P < 0.001$; AD: Alzheimer's disease; MRI: magnetic resonance imaging; PET: positron emission tomography; CT: computed tomography; OR: odds ratio; AUC: area under the receiver operating characteristic curves (to assess the ability of RNFL thicknesses to discriminate AD cases from healthy people).

accumulation. In our study, curcumin decreased the Aβ level in the brain and retina of APPswe/PS1dE9 transgenic mice in the early stage of life, but it had a more potent inhibitory effect in older mice. Feeding demethylcurcumin or bisdemethylcurcumin to APPswe/PS1dE9 double-transgenic mice can upregulate the NEP expression in the brain and reduce Aβ accumulation in the hippocampus and cortices of mice at 4.5-5.5 months of age [31].

In the absence of curcumin, the trends of Aβ accumulation in APPswe/PS1dE9 transgenic mice and WT mice were inconsistent and continued to increase with increasing age. However, in APPswe/PS1dE9 transgenic mice, there was a significant correlation between the Aβ content in the retina and brain. In addition to Aβ, hyperphosphorylation of tau proteins disrupts the retinal structure and may contribute to visual deficits seen in APPswe/PS1dE9 transgenic mice [24, 32].

Besides the retina, other ocular changes occur in AD patients and animals: altered pupil flash response, Aβ aggregation in the lens, and abnormal pattern electroretinograms [33–36]. Hence, even though most AD-related disease occurs in the brain, AD can also affect the eye. The retina shares many features with the brain (embryological origin, anatomic (e.g., microvascular bed) and physiologic (e.g., blood-tissue barrier) characteristics) [14], so the relationship between the brain and retina merits further study.

Ocular imaging of Aβ in AD patients could facilitate noninvasive monitoring [13]. In humans, ophthalmic imaging methods are used to assess neurodegenerative disorders, such as AD and Parkinson's disease [15]. Presently and in the future, the relationship between the degree of cognitive impairment and retinal abnormality merits further the study (Table 1).

Aβ is also observed in virtually all people with Down syndrome aged > 40 years and leads to a clinical diagnosis of dementia [37]. Increased retinal nerve fiber layer (RNFL) thinning in adults with Down syndrome may represent early AD-related changes. Studies in other neurodegenerative diseases, such as multiple sclerosis and cognitive decline, have also suggested that a thinner RNFL may be a preclinical observation of dementia [38, 39].

As a potential contrast agent of AD retinal diagnosis, pharmacokinetics of curcumin in wild type and APP mice should be further explored. A previous study investigated a magnetic resonance imaging contrast agent [40]. They reported that no significant differences were observed in the plasma or brain kinetics of wild type and APP mice. Similar to curcumin, this contrast agent was previously shown to cross the blood-brain barrier and bind to amyloid plaques in the brain of AD transgenic mouse.

With the advent of advanced imaging technologies and Aβ biomarkers for clinical use, it is now possible to identify the effects of Aβ accumulation through noninvasive imaging of ocular structures in live patients. Optical coherence tomography angiography (OCTA) was used in clinical trials

of AD detection, but only revealed the structure of biological tissues, such as RNFL thickness and vessel density [39]. Therefore, a detection method based on pathological biomarkers is urgently needed. In the future, AD progression could be quantified by measurement of the retinal Aβ level. One limitation of the proposed method is that although curcumin can label Aβ in the retina, it also suppresses Aβ levels and weakens the degree of correlation between Aβ in cerebrum and retina tissues.

5. Conclusions

We observed a significant correlation between the Aβ content in the retina and Aβ content in the brain of young APP mice before the onset of AD. Our data provide a biological basis for supporting noninvasive detection of AD in the eye and also suggest a time to detect retinal Aβ. Although curcumin can label the Aβ, it can also suppress the Aβ level and weaken the degree of correlation.

Data Availability

All data are included in the manuscript. However, the raw data used and/or analyzed in the present study are available from the corresponding author on reasonable request.

Ethical Approval

The study protocol was approved by the Animal Care and Use Committee of the Medical School of Ningbo University (Ningbo, China). Animal experiments were undertaken according to the *Guide for the Care and Use of Laboratory Animals* (National Institutes of Health (Bethesda, MD, USA) publication number 80-23, revised 1996).

Conflicts of Interest

The authors declare that there is no conflict of interest.

Authors' Contributions

XM, MY, and LZ performed in vitro and in vivo experiments, contributed to data analysis, and writing of the manuscript. LZ, QZ, and XL contributed to animal experiments and data collection. ZC and CZ proofread the manuscript. All authors read and approved the final manuscript.

Acknowledgments

We thank Prof. Wei Cui of Ningbo University for providing the useful discussion. This study was supported by the Zhejiang Provincial Natural and Science Fund (LQ19F010003) and Natural Science Foundation of Ningbo (2019A610355).

References

[1] J. M. Long and D. M. Holtzman, "Alzheimer disease: an update on pathobiology and treatment strategies," *Cell*, vol. 179, no. 2, pp. 312–339, 2019.

[2] F. Jessen and L. Frolich, "ICD-11: neurocognitive disorders," *Fortschritte der Neurologie-Psychiatrie*, vol. 86, no. 3, pp. 172–177, 2018.

[3] J. Hardy and D. J. Selkoe, "The amyloid hypothesis of Alzheimer's disease: progress and problems on the road to therapeutics," *Science*, vol. 297, no. 5580, pp. 353–356, 2002.

[4] A. Shehzad, G. Rehman, and Y. S. Lee, "Curcumin in inflammatory diseases," *BioFactors*, vol. 39, no. 1, pp. 69–77, 2013.

[5] S. Makin, "The amyloid hypothesis on trial," *Nature*, vol. 559, no. 7715, pp. S4–s7, 2018.

[6] C. Haass and D. J. Selkoe, "Soluble protein oligomers in neurodegeneration: lessons from the Alzheimer's amyloid beta-peptide," *Nature Reviews. Molecular Cell Biology*, vol. 8, no. 2, pp. 101–112, 2007.

[7] E. Niemantsverdriet, J. Ottoy, C. Somers et al., "The cerebrospinal fluid Aβ1–42/Aβ1–40 ratio improves concordance with amyloid-PET for diagnosing Alzheimer's disease in a clinical setting," *Journal of Alzheimer's Disease*, vol. 60, no. 2, pp. 561–576, 2017.

[8] D. Tautvydaite, J. P. Antonietti, H. Henry, A. von Gunten, and J. Popp, "Relations between personality changes and cerebrospinal fluid biomarkers of Alzheimer's disease pathology," *Journal of Psychiatric Research*, vol. 90, pp. 12–20, 2017.

[9] V. Ovod, K. N. Ramsey, K. G. Mawuenyega et al., "Amyloid β concentrations and stable isotope labeling kinetics of human plasma specific to central nervous system amyloidosis," *Alzheimer's & Dementia : The Journal of the Alzheimer's Association*, vol. 13, no. 8, pp. 841–849, 2017.

[10] S. Palmqvist, S. Janelidze, E. Stomrud et al., "Performance of fully automated plasma assays as screening tests for Alzheimer disease-related β-Amyloid status," *JAMA neurology*, vol. 76, no. 9, p. 1060, 2019.

[11] K. Yaffe, A. Weston, N. R. Graff-Radford et al., "Association of plasma beta-amyloid level and cognitive reserve with subsequent cognitive decline," *JAMA*, vol. 305, no. 3, pp. 261–266, 2011.

[12] S. S. More, J. M. Beach, and R. Vince, "Early detection of amyloidopathy in Alzheimer's mice by hyperspectral endoscopy," *Investigative Ophthalmology & Visual Science*, vol. 57, no. 7, pp. 3231–3238, 2016.

[13] S. S. Ong, A. D. Proia, H. E. Whitson, S. Farsiu, P. M. Doraiswamy, and E. M. Lad, "Ocular amyloid imaging at the crossroad of Alzheimer's disease and age-related macular degeneration: implications for diagnosis and therapy," *Journal of Neurology*, vol. 266, no. 7, pp. 1566–1577, 2019.

[14] M. K. Ikram, C. Y. Cheung, T. Y. Wong, and C. P. L. H. Chen, "Retinal pathology as biomarker for cognitive impairment and Alzheimer's disease," *Journal of Neurology, Neurosurgery, and Psychiatry*, vol. 83, no. 9, pp. 917–922, 2012.

[15] A. Uchida, J. A. Pillai, R. Bermel et al., "Outer retinal assessment using spectral-domain optical coherence tomography in patients with Alzheimer's and Parkinson's disease," *Investigative Ophthalmology & Visual Science*, vol. 59, no. 7, pp. 2768–2777, 2018.

[16] M. Garcia-Alloza, L. A. Borrelli, A. Rozkalne, B. T. Hyman, and B. J. Bacskai, "Curcumin labels amyloid pathology in vivo, disrupts existing plaques, and partially restores distorted neurites in an Alzheimer mouse model," *Journal of Neurochemistry*, vol. 102, no. 4, pp. 1095–1104, 2007.

[17] Y. Koronyo, D. Biggs, E. Barron et al., "Retinal amyloid pathology and proof-of-concept imaging trial in Alzheimer's disease," *JCI Insight*, vol. 2, no. 16, 2017.

[18] J.-. X. Song, S. Malampati, Y. Zeng et al., "A small molecule transcription factor EB activator ameliorates beta-amyloid precursor protein and Tau pathology in Alzheimer's disease models," *Aging Cell*, vol. 19, no. 2, p. e13069, 2020.

[19] S. D. Voulgaropoulou, T. A. M. J. van Amelsvoort, J. Prickaerts, and C. Vingerhoets, "The effect of curcumin on cognition in Alzheimer's disease and healthy aging: a systematic review of pre-clinical and clinical studies," *Brain Research*, vol. 1725, p. 146476, 2019.

[20] M. Garcia-Alloza, E. M. Robbins, S. X. Zhang-Nunes et al., "Characterization of amyloid deposition in the APPswe/PS1dE9 mouse model of Alzheimer disease," *Neurobiology of Disease*, vol. 24, no. 3, pp. 516–524, 2006.

[21] J. B. Hoppe, K. Coradini, R. L. Frozza et al., "Free and nanoencapsulated curcumin suppress β-amyloid-induced cognitive impairments in rats: involvement of BDNF and Akt/GSK-3β signaling pathway," *Neurobiology of Learning and Memory*, vol. 106, pp. 134–144, 2013.

[22] S. K. Jain, J. Rains, J. Croad, B. Larson, and K. Jones, "Curcumin supplementation lowers TNF-alpha, IL-6, IL-8, and MCP-1 secretion in high glucose-treated cultured monocytes and blood levels of TNF-alpha, IL-6, MCP-1, glucose, and glycosylated hemoglobin in diabetic rats," *Antioxidants & Redox Signaling*, vol. 11, no. 2, pp. 241–249, 2009.

[23] F. Ullah, A. Liang, A. Rangel, E. Gyengesi, G. Niedermayer, and G. Munch, "High bioavailability curcumin: an anti-inflammatory and neurosupportive bioactive nutrient for neurodegenerative diseases characterized by chronic neuroinflammation," *Archives of Toxicology*, vol. 91, no. 4, pp. 1623–1634, 2017.

[24] S. E. Perez, S. Lumayag, B. Kovacs, E. J. Mufson, and S. Xu, "Beta-amyloid deposition and functional impairment in the retina of the APPswe/PS1DeltaE9 transgenic mouse model of Alzheimer's disease," *Investigative Ophthalmology & Visual Science*, vol. 50, no. 2, pp. 793–800, 2009.

[25] M. Koronyo-Hamaoui, Y. Koronyo, A. V. Ljubimov et al., "Identification of amyloid plaques in retinas from Alzheimer's patients and noninvasive in vivo optical imaging of retinal plaques in a mouse model," *NeuroImage*, vol. 54, Suppl 1, pp. S204–S217, 2011.

[26] Y. Koronyo, B. C. Salumbides, K. L. Black, and M. Koronyo-Hamaoui, "Alzheimer's disease in the retina: imaging retinal Aß plaques for early diagnosis and therapy assessment," *Neuro-Degenerative Diseases*, vol. 10, no. 1-4, pp. 285–293, 2012.

[27] S. E. Perez, S. Dar, M. D. Ikonomovic, S. T. DeKosky, and E. J. Mufson, "Cholinergic forebrain degeneration in the APPswe/PS1DeltaE9 transgenic mouse," *Neurobiology of Disease*, vol. 28, no. 1, pp. 3–15, 2007.

[28] S. E. Perez, O. Lazarov, J. B. Koprich et al., "Nigrostriatal dysfunction in familial Alzheimer's disease-linked APPswe/PS1 E9 transgenic mice," *The Journal of neuroscience : the official journal of the Society for Neuroscience*, vol. 25, no. 44, pp. 10220–10229, 2005.

[29] L. Y.-L. Chang, A. O. Ardiles, C. Tapia-Rojas et al., "Evidence of synaptic and neurochemical remodeling in the retina of aging degus," *Frontiers in Neuroscience*, vol. 14, p. 161, 2020.

[30] A. N. Lazar, S. Mourtas, I. Youssef et al., "Curcumin-conjugated nanoliposomes with high affinity for Aβ deposits: possible applications to Alzheimer disease," *Nanomedicine: Nanotechnology, Biology and Medicine*, vol. 9, no. 5, pp. 712–721, 2013.

[31] P.-T. Chen, Z.-t. Chen, W.-C. Hou, L.-C. Yu, and R. P.-Y. Chen, "Polyhydroxycurcuminoids but not curcumin upregulate neprilysin and can be applied to the prevention of Alzheimer's disease," *Scientific Reports*, vol. 6, no. 1, p. 29760, 2016.

[32] H. Zhao, R. Chang, H. Che et al., "Hyperphosphorylation of tau protein by calpain regulation in retina of Alzheimer's disease transgenic mouse," *Neuroscience Letters*, vol. 551, pp. 12–16, 2013.

[33] S. Frost, R. N. Martins, and Y. Kanagasingam, "Ocular biomarkers for early detection of Alzheimer's disease," *Journal of Alzheimer's Disease*, vol. 22, no. 1, pp. 1–16, 2010.

[34] A. Grimaldi, C. Brighi, G. Peruzzi et al., "Inflammation, neurodegeneration and protein aggregation in the retina as ocular biomarkers for Alzheimer's disease in the 3xTg-AD mouse model," *Cell Death & Disease*, vol. 9, no. 6, p. 685, 2018.

[35] C. Kerbage, C. H. Sadowsky, D. Jennings, G. D. Cagle, and P. D. Hartung, "Alzheimer's disease diagnosis by detecting exogenous fluorescent signal of ligand bound to beta amyloid in the lens of human eye: an exploratory study," *Frontiers in Neurology*, vol. 4, p. 62, 2013.

[36] R. Parthasarathy, K. M. Chow, Z. Derafshi et al., "Reduction of amyloid-beta levels in mouse eye tissues by intra-vitreally delivered neprilysin," *Experimental Eye Research*, vol. 138, pp. 134–144, 2015.

[37] M. J. Walpert, E. M. Normando, T. Annus et al., "Age-related retinal thickness in Down's syndrome: a high-risk population for dementia," *Alzheimer's & Dementia: Diagnosis, Assessment & Disease Monitoring*, vol. 11, no. 1, pp. 744–751, 2019.

[38] J. Frau, G. Fenu, A. Signori et al., "A cross-sectional and longitudinal study evaluating brain volumes, RNFL, and cognitive functions in MS patients and healthy controls," *BMC Neurology*, vol. 18, no. 1, p. 67, 2018.

[39] F. Ko, Z. A. Muthy, J. Gallacher et al., "Association of retinal nerve fiber layer thinning with current and future cognitive decline: a study using optical coherence tomography," *JAMA Neurology*, vol. 75, no. 10, pp. 1198–1205, 2018.

[40] K. K. Kandimalla, T. M. Wengenack, G. L. Curran, E. J. Gilles, and J. F. Poduslo, "Pharmacokinetics and amyloid plaque targeting ability of a novel peptide-based magnetic resonance contrast agent in wild-type and Alzheimer's disease transgenic mice," *The Journal of Pharmacology and Experimental Therapeutics*, vol. 322, no. 2, pp. 541–549, 2007.

[41] C. Y. Santos, L. N. Johnson, S. E. Sinoff, E. K. Festa, W. C. Heindel, and P. J. Snyder, "Change in retinal structural anatomy during the preclinical stage of Alzheimer's disease," *Alzheimer's & Dementia: Diagnosis, Assessment & Disease Monitoring*, vol. 10, no. 1, pp. 196–209, 2018.

[42] A. López-de-Eguileta, C. Lage, S. López-García et al., "Ganglion cell layer thinning in prodromal Alzheimer's disease defined by amyloid PET," *Alzheimer's & Dementia: Translational Research & Clinical Interventions*, vol. 5, no. 1, pp. 570–578, 2019.

Hindawi
Behavioural Neurology
Volume 2020, Article ID 8438602, 11 pages
https://doi.org/10.1155/2020/8438602

Review Article

Abnormal Homocysteine Metabolism: An Insight of Alzheimer's Disease from DNA Methylation

Tingting Pi, Bo Liu, and Jingshan Shi

Department of Pharmacology and the Key Laboratory of Basic Pharmacology of Ministry of Education, Zunyi Medical University, Zunyi 563000, China

Correspondence should be addressed to Jingshan Shi; zmcshijs@163.com

Received 24 May 2020; Accepted 30 July 2020; Published 8 September 2020

Academic Editor: Horacio Soto

Alzheimer's disease (AD) is a chronic neurodegenerative disease in the central nervous system that has complex pathogenesis in the elderly. The current review focuses on the epigenetic mechanisms of AD, according to the latest findings. One of the best-characterized chromatin modifications in epigenetic mechanisms is DNA methylation. Highly replicable data shows that AD occurrence is often accompanied by methylation level changes of the AD-related gene. Homocysteine (Hcy) is not only an intermediate product of one-carbon metabolism but also an important independent risk factor of AD; it can affect the cognitive function of the brain by changing the one-carbon metabolism and interfering with the DNA methylation process, resulting in cerebrovascular disease. In general, Hcy may be an environmental factor that affects AD via the DNA methylation pathway with a series of changes in AD-related substance. This review will concentrate on the relation between DNA methylation and Hcy and try to figure out their rule in the pathophysiology of AD.

1. Introduction

The increasing number of dementia patients in recent years is a serious problem, of which Alzheimer's disease (AD) is the most common type that accounts for an estimated 70% of dementia cases [1]. Data suggest that the prevalence of AD in people over 65 years old is approximately 10-30% and the estimated incidence is 1-3% [2]. Moreover, approximately 9.5 million people suffer from AD in China, accounting for an estimated 20% of the world in 2015 [3].

AD is a chronic neurodegenerative disease, which manifests as progressive memory loss and cognitive impairment [4, 5]. Senile plaques (SP) formed by extracellular amyloid-β (Aβ) peptide deposition and neurofibrillary tangles (NFTs) formed by excessive phosphorylation of intracellular tau protein constitute the hallmarks of AD [6, 7], which is also accompanied by the massive loss of neurons and synapses, as well as brain structural and functional abnormalities [8–10]. DNA methylation is an important part of epigenetics and is becoming a very attractive subject for researchers because it can shed light on unknown aspects of complex disease pathophysiology like AD. In addition, homocysteine (Hcy) is an environmental factor that seems related to AD through DNA methylation pathways.

2. Mechanisms

2.1. Alzheimer's Disease. Currently, the interaction of various factors such as genetics and environment affects the etiology and pathophysiological changes of AD [11, 12]. Multiple hypotheses are related to the pathogenesis of AD, such as the amyloid cascade hypothesis [13–15], tau protein hypothesis [16–18], cholinergic hypothesis [19], lipid metabolism disorder hypothesis [20], neuroinflammation hypothesis [21], and oxidative stress hypothesis [22], among which the amyloid cascade hypothesis and tau protein hypothesis provide the predominantly theoretical construct for AD.

The amyloid cascade hypothesis indicates that the β-amyloid precursor protein (APP) generates Aβ peptide under the cleavage of β-secretase and γ-secretase, which eventually forms SP [23]. Previous studies have found that excessive Aβ accumulated will cause synaptic damage, glial

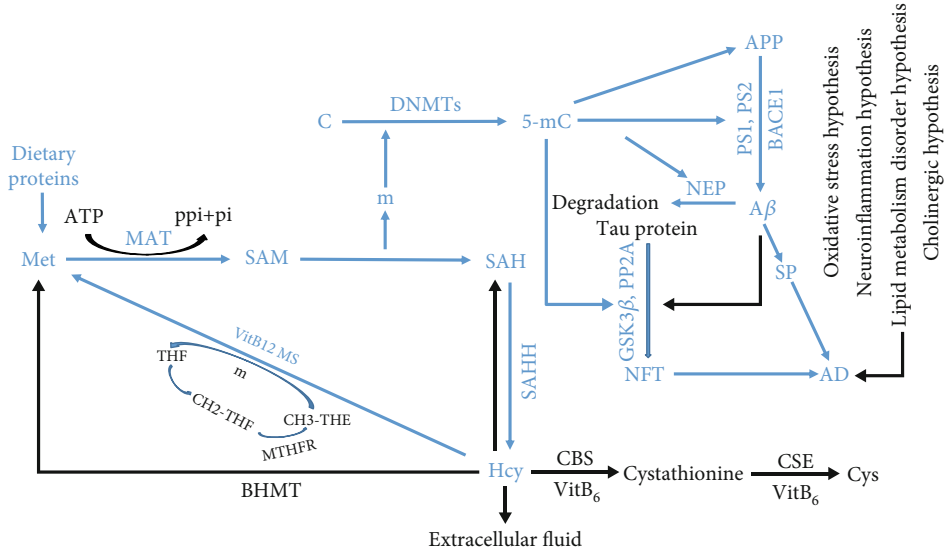

Figure 1: The mechanism of AD, DNA methylation and Hcy interaction. 5-mC: 5-methylcytosine; AD: Alzheimer's disease; Aβ: amyloid-β; APP: β-amyloid precursor protein; ATP: adenosine triphosphate; BACE1: β-secretase-1; BHMT: betaine-homocysteine methyltransferase; C: cytosine; CBS: cystathionine β synthase; CSE: cystathionine γ-lyase; Cys: cysteine; DMG: dimethylglycine; GSK3β: glycogen synthase kinase 3β; Hcy: homocysteine; m: methyl; MAT: methionine adenosyltransferase; Met: methionine; MTHFR: methylenetetrahydrofolate reductase; MS: methionine synthase; NFT: neurofibrillary tangle; NEP: neprilysin; PP2A: protein phosphatase 2A; PS1: presenilin-1; PS2: presenilin-2; SAH: S-adenosine homocysteine; SAHH: S-adenosine homocysteine hydrolase; SAM: S-adenosine methionine; SP: senile plaques; THF: tetrahydrofolate.

cell overactivation [24], and inflammatory reaction [25, 26], followed by SP formation (Figure 1) [27]. A series of landmark studies states that the role of targeting Aβ peptide in the treatment of AD will delay the progression of the disease [28, 29] by inhibiting monomer aggregation and preventing the formation of toxic species [30]. Zhai et al.'s [31] study revealed that the structural origin of β-sheet and plaque deposition, therefore, blocking and inhibiting the transmission of Aβ from the source, may effectively inhibit Aβ deposition, which may be an important method to prevent the formation of AD.

Phosphate-containing tau protein is part of the essential components of the cytoskeleton. In normal brain cells, a single tau molecule with 2 to 3 phosphate groups is related to the stability of microtubules and the axon transport of nerve cells [32]. Abnormal hyperphosphorylation of tau protein and intraneural aggregation are hallmark features of the early development of AD-related neurofibrillary pathology. The binding capacity of hyperphosphorylated tau protein and tubulin is reduced, paired helical filaments (PHFs) aggregated; while its conversion and clearance ability are reduced, formed NFTs are the early markers of AD [33–35]. The degree of tau protein phosphorylation is the consequence of the interaction of various protein kinases (PK) and protein phosphatases (PP) in the brain (Figure 1) [36–38]. The dysregulation of PP and PK activities reduces the binding capacity and stability of tau protein to microtubules, which result in neuronal dysfunction and neurodegeneration, and further to functional defects [39–41]. A notable exception study is that tau-specific site phosphorylation protects the brain in the early stages of AD by inhibiting Aβ toxicity [42]. The hyperphosphorylation of tau is considered independent of Aβ, but the final spread of tau throughout the neocortex is driven by Aβ [7]. AD is the interaction of multiple factors and mechanisms that exert multiple effects at different stages of disease progression, which is not possible to ascribe changes in one factor. It is debatable whether the existing hypothesis fully explains to the pathogenesis of AD. Therefore, it needs further exploration to identify.

2.2. Homocysteine. In 1933, Vincent du Vigneaud isolated a sulfur-containing nonprotein amino acid called Hcy from bladder stones. Methionine (Met) is metabolized to S-adenosine methionine (SAM) under the action of methionine adenosyltransferase (*MAT*). SAM is one of the major methyl donors that can be converted to S-adenosine homocysteine (SAH), a methyl removed in this process, which is involved in epigenetic modifications under the action of methyltransferase [43]. SAH removes adenosine by S-adenosine homocysteine hydrolase (SAHH) to form Hcy [44], substances well associated with the methionine cycle and energy metabolism (Figure 1) [45, 46]. A clinical trial suggests that oral Met load increased plasma Hcy from 12.8 $\pm$1.8 to 33.3 $\pm$ 3.4 micromol·L (-1) at 4 h [47]. Consequently, excessive Met can elevate the level of Hcy, which finally results in hyperhomocysteinemia (HHcy) [48, 49].

Subsequently predominant metabolism of Hcy occurs via three pathways (Figure 1): (1) Met cycle—under the action of methionine synthase, tetrahydrofolate metabolism provides a methyl group, and Hcy is remethylated to Met with assistance of vitamin B12 (VitB12) [50, 51]; (2) transsulfuration pathway—with vitamin B6 (VitB6) as a coenzyme, Hcy and serine are condensed into cystathionine under the catalysis of cystathionine β synthase (CBS), followed by cystathionine

catalyzed by γ-cystathionine lyase to produce cysteine, which is oxidized to sulfate after a series of enzyme catalysis and excreted through the urine in the form of inorganic salts [52]; and (3) direct release into the extracellular fluid—excessive Hcy is thought to be released from the intracellular fluid to the extracellular fluid through the difference in internal and external concentrations and then exported to the systemic circulation to prevent its intracellular accumulation [53–55]. VitB6, VitB12, and folic acid are the main metabolic pathways of Hcy in the methylation cycle and transsulfuration pathway, the lack of which leads to the production of HHcy. Hence, the production and metabolism balance of Hcy is essential for maintaining the body's homeostasis. Genetic factors, nutritional factors, estrogen levels, and age all affect the Hcy plasma level [56–58]. Several recent fundamental discoveries highlight important pathological roles of HHcy in many diseases [59–62]. Studies suggest that HHcy induced hypertension by promoting TLR-4-driven chronic vascular inflammation and mitochondria-mediated cell death [63]. Moreover, HHcy aggravates atherosclerosis with elevated oxidative stress and reduced S-nitrosylation level of redox-sensitive protein residues in the vasculature [64], which also as a metabolic disorder parameter is independently associated with the severity of coronary heart disease [65]. Elevated plasma total Hcy level is associated with an increased risk of neurodegenerative disease [66].

2.3. DNA Methylation. Epigenetics is the study of genetic changes in gene expression that is not caused by the DNA sequence changes [67]. Among them, DNA methylation is one of the best-characterized epigenetic modification, which exerts an important role in maintaining cell function, genetic imprinting, and gene expression [68, 69]. DNA methylation occurs in cytosine-phosphate-guanine (CPG) fundamental sequence with catalyzing of DNA methyltransferase enzymes (DNMTs). Specific bases in the DNA sequence and cofactor proteins are jointly involved in maintaining and regulating the methylation pattern [70–72]. DNA methylation needs a series of DNMTs [73], such as maintenance methyltransferase DNMT1 and de novo methyltransferases DNMT3a and DNMT3b [74–77]. DNMT1 maintains the continuous methylation status of DNA, which is responsible for repeated methylation during cell division [78], and DNMT3a and DNMT3b methylate DNA strands that have not been methylated, which is responsible for de novo synthesis of DNA methylation [79].

In the genome, methylated CpG sites account for approximately 70% of human genes [80]. CpG sites are located in the first exon region, gene promoter region, or intron region and regulate the expression of downstream genes [81], where the covalent bonding of the methyl group with the 5th carbon atom of cytosine is considered to be the most stable epigenetic marker [82].

3. DNA Methylation in Alzheimer's Disease

Epigenetics studies have found an association between DNA methylation and AD [83], which is involved in the progression of the neurodegenerative disease [84]. The earliest accumulation of Aβ reduces the overall level of 5-hydroxymethylcytosine in vitro [85], resulting in DNA hypomethylation, and affects the pathological progress of AD [86]. Furthermore, DNA methylation is associated with Aβ and NFTs [87]. PS1 is a component of the γ-secretase that will cleave APP to produce various Aβ [88]. Increased expression of APP and induction of hypomethylation of APP and PS1 gene promoters will increase the production of Aβ in BV-2 cells [89]. Moreover, β-secretase-1 (BACE1) is also hypomethylated, which affects Aβ accumulation and accelerates AD pathology [87], as well as significantly reduces DNMT1 expression in cell experiments [90]. In short, the methylation or demethylation of key enzymes will increase Aβ synthesis and reduce Aβ degradation, eventually resulting in the development of AD.

Tau phosphorylation and dephosphorylation reactions are catalyzed by glycogen synthase kinase 3β (GSK3β) and protein phosphatase 2A (PP2A), respectively; GSK3β and PP2A are two major kinds of enzymes that regulate hyperphosphorylated Tau. Sonawane and Chinnathambi's [91] study indicated the upregulation of GSK3β promoter demethylation expression and the downregulation of PP2A promoter methylation in the AD brain, both of which accelerated tau phosphorylation (Figure 1). In addition, the reduced expression of netrin-1-promoter hypermethylation may be related to memory loss [92].

DNA methylation is closely related to AD [93, 94]. Changes in DNA methylation are related to neural differentiation of the hippocampus [95], as well as across multiple brain regions. So far, DNA methylation exerts a central role in amyloid production, fibrogenesis, inflammation, and oxidative pathways. All the above studies suggest that DNA methylation is involved in the AD-related molecular mechanism [96].

4. Homocysteine in Alzheimer's Disease

With increasing age, the risk of AD increases under the interaction of genetic and environmental factors (obesity, smoking, and an unhealthy lifestyle) [97], of which Hcy is a risk factor of AD. Several studies are indicating that high Hcy concentrations cause cognitive dysfunction [98] and might be associated with dementia [99–101].

HHcy may promote dementia through a variety of mechanisms, including cerebral microangiopathy, endothelial dysfunction, oxidative stress, neuronal damage, and Aβ-mediated enhancement of vascular toxicity, neurotoxicity, and apoptosis [102]. The brain of AD patients is accompanied by cerebrovascular disease [103], and studies show a long-term high Hcy diet severely induces microbleeds, which may be the cause of memory deficits [104]. Although elevated Hcy does not induce lipid peroxidation in the whole brain of rats, similar physiological changes in levels are observed in both malondialdehyde (MDA) and superoxide anion (SOA), resulting in oxidative stress [105]. Not only does Hcy can increase the activity of MMP-9 and MMP-2 but also reduce the activity of arginase. Meanwhile, it is accompanied by nitrosative stress reaction that destroys the integrity of the blood-brain barrier (BBB), leading to cerebrovascular

permeability and neurodegeneration [106, 107]. Lin et al.'s [108] study suggests that Hcy can affect nerve cell proliferation and Aβ deposit formation by inducing an increase in intracellular SAH [109–111]. Additionally, DNA damage-related genes are significantly upregulated and trigger oxidative and genotoxic stress [112]. Since high Hcy levels are a metabolic risk factor for neurodegenerative diseases, diet-induced Hcy levels not only increase aggravate Tau neuropathology in H-TAU mice but also affect synaptic integrity, neuroinflammation, and cognition function [113]. Moreover, the AD transgenic mouse model shows that Aβ content in cerebral blood vessels increased significantly, neurons died, and DNA damage of hippocampal neurons further reduce cognitive ability [114]. Excessive deposition of hyperphosphorylated Tau and neuropathy caused by synaptic inactivation lesions are also associated with the elevated Hcy level [115–117].

Hcy level changes AD development by inducing neuronal DNA damage, neuroinflammation, apoptosis, and autophagy abnormalities [117–119]. Genetic variation affects the relevant genes, which advances the age of onset and accelerates cognitive function decline [120, 121].

5. DNA Methylation and Homocysteine in Alzheimer's Disease

Dementia-like symptoms caused by HHcy are related to abnormal methylation and gene expression disorders [122]. One study found that HHcy can reduce the methylation level and increase cell damage by inhibiting the protein expression and enzyme activity of DNMT1, DNMT3A, and DNMT3B in the hippocampal neural stem cells of raw rat [123]. Another study also illustrates that HHcy enhances DNA damage by inducing methyl donor deficiency and disrupting DNA repair, resulting in neuronal cell death [124]. In addition, the upregulation of the 5lo enzyme pathway leads to hypomethylation of 5loDNA and promotes the formation of Aβ [125]. HHcy can decrease the activity of methylenetetrahydrofolate reductase (MTHFR) and tight connexin expression, while SAHH expression, BBB permeability, and oxidative stress are increased with DNA methyltransferase upregulation, resulting in neurodegeneration and synaptic toxicity [126]. Most importantly, the Met cycle and transsulfuration pathway are related to VitB family folic acid [127, 128].

Folic acid is involved in the regulation of one-carbon metabolism and methylation. In addition to this, the active form of folic acid is 5-methyltetrahydrofolate, which is a methyl donor for the remethylation of Hcy. HHcy is elicited by low folic acid, which damages hippocampal neurons and is an important factor of the high incidence of dementia in the elderly [129]. Furthermore, folic acid is not only positively related to the DNA methylation level of the cognitive impairment elderly but also related to the intensity of DNA methylation [130]. MTHFR is involved in folate metabolism, and the high level of Hcy caused by MTHFR deficiency will reduce the expression and methylation level of PP2A and leucine carboxylmethyltransferase 1 (LCMT1), resulting in tau dephosphorylation [131].

HHcy is a risk factor for AD and is also associated with VitB12 deficiency [132]. The accumulation of Hcy induced by VitB deficiency may impair the "methylation potential," resulting in the upregulation of PS1, BACE, and increased Aβ [133, 134]. Several studies have implicated that the plasma Hcy level in the AD group increased while the folate and VitB12 levels decreased [135–138]. Moreover, abnormal Hcy metabolism causes plasma folic acid and VitB12 deficiency [139–142], which in turn affects the methylation level of AD-related genes via participating in AD development [143]. Mice lacking folic acid and VitB diets will have increased Hcy levels, Aβ levels, and tau phosphorylation, which is also accompanied by hypomethylation of the Alox5 promoter [144]. High Hcy-induced SAH increases [123, 124], and the SAM/SAH ratio decreases, both of which are related to the inhibition of methyltransferase [145]. Methylation analysis also further demonstrates the correlation between the SAM/Hcy cycle and DNA methylation, involved in PS1 and BACE1 methylation [141]. SAM is the predominant methyl donor; Scarpa et al. [145] analyzed the effect of SAM administration on the expression of 588 central nervous system genes in nerve cells and showed that among the seven genes treated by SAM, three genes had DNA methylation upregulated and four genes had DNA methylation downregulated [146]. SAM can regulate its products to take part in the methylation status of APP genes, which affects the formation of Aβ [147] by increasing APP and PS1 proteins expression; it can also induce hypomethylation of APP and PS1 gene promoters and increase Aβ production in BV-2 cells [148]. In short, Hcy can change the DNA methylation levels of key metabolic enzymes and cause brain damage [149].

6. Future Directions

Possible mechanisms for Hcy to induce AD are shown in Figure 1; high levels of Met intake produce excessive Hcy in the body which metabolizes through the Met cycle, during which the generated methyl adds to the five-bit carbon atom of the cytosine under the action of DNMTs, causing the methylation levels of the AD-related genes to change. The changes in methylation levels in turn affect the expression of the gene, resulting in the occurrence of AD. At the same time, excess accumulation of Hcy is regeneration to methionine under the action of methionine synthesis enzyme and VitB12, finally producing the Hcy. As a result, high levels of Hcy may induce AD along with changes in methylation levels of AD-related genes.

Unbalanced nutritional intake will not only increase Hcy levels but also affect DNA methylation and gene expression. At present, most researchers focus on the effect of Hcy on AD symptoms, rather than on molecular mechanisms. At the molecular level, studying the regulatory mechanism of Hcy and its metabolites on the expression of related genes in AD patients helps determine the appropriate nutritional requirements. Preventing the increase of the Hcy level caused by the imbalance of nutrition intake can either avoid or arrest the occurrence and aggravation of AD.

As AD progresses, treatment becomes difficult with little effect [150, 151]; the research and development of drugs also consume a lot of manpower and material resources [152]. So far, the main drugs used in AD treatment are donepezil, rivastigmine, galantamine, and memantine, which can only relieve symptoms but can not cure and reverse the development of AD [153–156]. In addition, some drugs must be used in combination to achieve the best therapeutic effect, which is also accompanied by increasing the risk of various adverse reactions [157]. Since 2003, the FDA has not approved a new drug for the treatment of AD [158]. Therefore, early diagnosis and treatment are essential. The current clinical early diagnosis depends on clinical observation, and cognitive testing is the first step to diagnose the complex disease characteristics in AD, which is time-consuming and has limitations. More definite diagnosis requires imaging (MRI or PET scan) or invasive lumbar puncture to measure CSF markers which is expensive. Thus, efficient diagnostic methods and early disease biomarkers are essential for the prevention and treatment of early AD [159].

Several researchers have reported that plasma Hcy levels are usually elevated in patients with AD [160]. HHcy is closely related to cortical atrophy and more severe cognitive decline [161, 162]. The high plasma Hcy concentrations are significantly associated with mild cognitive impairment (MCI) and AD, which is more strongly correlated with AD patients as compared to patients with MCI [163]. A meta-analysis included 34 studies with 9397 subjects and demonstrated a causal link between plasma total Hcy and the risk factor of AD [164]. More than 40% of patients with AD are associated with a high Hcy level in the plasma, which is associated with a more rapid neural atrophy than those with normal levels of Hcy [165]. Moreover, HHcy levels can predict a cognitive decline in healthy elderly patients [166, 167]. Therefore, HHcy also has the potential to predict AD, and preventing Hcy-induced neurotoxicity may become a novel strategy for AD prevention and treatment.

DNA methylation alteration in the hippocampus of AD patients occurs in specific regulatory regions that are critical to neurodifferentiation; this supports the idea that hippocampus neurogenesis may play a role in AD through epigenetic mechanisms [168]. The current findings suggest that the epigenetic modulation of DNA is vulnerable to the state of neurodegenerative diseases [169]. Moreover, brain DNA methylation is associated with AD pathology in multiple AD loci, and the results further prove that the destruction of DNA methylation is involved in the pathological process of AD [170]. Many researches have shown that DNA methylation is a useful marker for screening individuals at the risk of AD [171]. Therefore, AD-related gene methylation levels are a convenient and useful biomarker for AD diagnosing [172–174].

Proper nutrition not only changes Hcy levels but also prevents the development of AD and reduces cognitive impairment. Hcy levels may develop into AD biomarkers for diagnosis; moreover, factors that affect Hcy's production and metabolism not only increase Hcy levels but also affect DNA methylation levels of AD-related genes. Studying the mechanisms of DNA methylation in AD can help to explore the etiology and pathogenesis of AD, which can also be a very useful tool for researchers to identify AD biomarkers and even play an important role in early screening of patients in the future. Meanwhile, effective measures to reduce Hcy levels and DNA methylation will provide new ideas for the prevention and treatment of AD.

Data Availability

No data were used to support this study.

Conflicts of Interest

The authors declare that there is no conflict of interest regarding the publication of this paper.

Authors' Contributions

Tingting Pi wrote the paper and Jing-Shan Shi reviewed drafts of the paper.

Acknowledgments

This work was supported by the Shijingshan's Tutor Studio of Pharmacology [GZS-2016(07)] and Funds for the Construction of National First Class Pharmacy Discipline [GESR (2017-85)].

References

[1] A. García-Blanco, M. Baquero, M. Vento, E. Gil, L. Bataller, and C. Cháfer-Pericás, "Potential oxidative stress biomarkers of mild cognitive impairment due to Alzheimer disease," *Journal of the Neurological Sciences*, vol. 373, no. 3, pp. 295–302, 2017.

[2] C. L. Masters, R. Bateman, K. Blennow, C. C. Rowe, R. A. Sperling, and J. L. Cummings, "Alzheimer's disease," *Nature reviews. Disease Primers*, vol. 1, no. 1, pp. 50–56, 2015.

[3] A. Yee, Avalon Genomics (HK) Limited, H. K. Shatin et al., "Alzheimer's disease: insights for risk evaluation and prevention in the Chinese population and the need for a comprehensive programme in Hong Kong/China," *Hong Kong Medical Journal*, vol. 24, no. 5, pp. 492–500, 2018.

[4] C. A. Lane, J. Hardy, and J. M. Schott, "Alzheimer's disease," *European Journal of Neurology*, vol. 25, no. 1, pp. 59–70, 2018.

[5] M. R. Minter, J. M. Taylor, and P. J. Crack, "The contribution of neuroinflammation to amyloid toxicity in Alzheimer's disease," *Journal of Neurochemistry*, vol. 136, no. 3, pp. 457–474, 2016.

[6] A. R. Morgan, S. Touchard, C. Leckey et al., "Inflammatory biomarkers in Alzheimer's disease plasma," *Alzheimer's & Dementia*, vol. 15, no. 6, pp. 776–787, 2019.

[7] R. van der Kant, L. S. B. Goldstein, and R. Ossenkoppele, "Amyloid-β-independent regulators of tau pathology in Alzheimer disease," *Nature Reviews Neuroscience*, vol. 21, no. 1, pp. 21–35, 2020.

[8] M. Taga, T. Minett, J. Classey et al., "Metaflammasome components in the human brain: a role in dementia with Alzheimer's pathology?," *Brain Pathology*, vol. 27, no. 3, pp. 266–275, 2017.

[9] M. P. Mattson, "Pathways towards and away from Alzheimer's disease," *Nature*, vol. 430, no. 7000, pp. 631–639, 2004.

[10] N. Musi, J. M. Valentine, K. R. Sickora et al., "Tau protein aggregation is associated with cellular senescence in the brain," *Aging Cell*, vol. 17, no. 6, article e12840, 2018.

[11] V. Hachinski, "Dementia: paradigm shifting into high gear," *Alzheimer's & Dementia*, vol. 15, no. 7, pp. 985–994, 2019.

[12] C. Madore, Z. Yin, J. Leibowitz, and O. Butovsky, "Microglia, Lifestyle Stress, and Neurodegeneration," *Immunity*, vol. 52, no. 2, pp. 222–240, 2020.

[13] K. Herrup, "The case for rejecting the amyloid cascade hypothesis," *Nature Neuroscience*, vol. 18, no. 6, pp. 794–799, 2015.

[14] B. De Strooper and E. Karran, "The cellular phase of Alzheimer's disease," *Cell*, vol. 164, no. 4, pp. 603–615, 2016.

[15] J. A. Hardy and G. A. Higgins, "Alzheimer's disease: the amyloid cascade hypothesis," *Science*, vol. 256, no. 5054, pp. 184-185, 1992.

[16] B. Eftekharzadeh, J. G. Daigle, L. E. Kapinos et al., "Tau protein disrupts nucleocytoplasmic transport in Alzheimer's disease," *Neuron*, vol. 99, no. 5, pp. 925–940.e7, 2018.

[17] G. S. Gibbons, V. M. Y. Lee, and J. Q. Trojanowski, "Mechanisms of cell-to-cell transmission of pathological tau: a review," *JAMA Neurology*, vol. 76, no. 1, pp. 101–108, 2019.

[18] S. Wegmann, R. E. Bennett, L. Delorme et al., "Experimental evidence for the age dependence of tau protein spread in the brain," *Science Advances*, vol. 5, no. 6, p. eaaw6404, 2019.

[19] R. Bartus, R. Dean, B. Beer, and A. Lippa, "The cholinergic hypothesis of geriatric memory dysfunction," *Science*, vol. 217, no. 4558, pp. 408–414, 1982.

[20] D. L. Sparks, S. W. Scheff, J. C. Hunsaker III, H. Liu, T. Landers, and D. R. Gross, "Induction of Alzheimer-like β-Amyloid Immunoreactivity in the Brains of Rabbits with Dietary Cholesterol," *Experimental Neurology*, vol. 126, no. 1, pp. 88–94, 1994.

[21] Y. Zhou, Y. Su, B. Li et al., "Nonsteroidal anti-inflammatory drugs can lower amyloidogenic $A\beta_{42}$ by inhibiting Rho," *Science*, vol. 302, no. 5648, pp. 1215–1217, 2003.

[22] S. A. Farr, J. L. Ripley, R. Sultana et al., "Antisense oligonucleotide against GSK-3β in brain of SAMP8 mice improves learning and memory and decreases oxidative stress: involvement of transcription factor Nrf2 and implications for Alzheimer disease," *Free Radical Biology & Medicine*, vol. 67, pp. 387–395, 2014.

[23] C.-C. Tan, J.-T. Yu, M.-S. Tan, T. Jiang, X.-C. Zhu, and L. Tan, "Autophagy in aging and neurodegenerative diseases: implications for pathogenesis and therapy," *Neurobiology of Aging*, vol. 35, no. 5, pp. 941–957, 2014.

[24] A. M. Arranz and B. De Strooper, "The role of astroglia in Alzheimer's disease: pathophysiology and clinical implications," *Lancet Neurology*, vol. 18, no. 4, pp. 406–414, 2019.

[25] E. E. Tuppo and H. R. Arias, "The role of inflammation in Alzheimer's disease," *The International Journal of Biochemistry & Cell Biology*, vol. 37, no. 2, pp. 289–305, 2005.

[26] B. M. Bettcher, S. C. Johnson, R. Fitch et al., "Cerebrospinal fluid and plasma levels of inflammation differentially relate to CNS markers of Alzheimer's disease pathology and neuronal damage," *Journal of Alzheimer's Disease*, vol. 62, no. 1, pp. 385–397, 2018.

[27] M. Awasthi, S. Singh, V. P. Pandey, and U. N. Dwivedi, "Alzheimer's disease: An overview of amyloid beta dependent pathogenesis and its therapeutic implications along with *in silico* approaches emphasizing the role of natural products," *Journal of the Neurological Sciences*, vol. 361, pp. 256–271, 2016.

[28] J. Sevigny, P. Chiao, T. Bussière et al., "The antibody aducanumab reduces Aβ plaques in Alzheimer's disease," *Nature*, vol. 537, no. 7618, pp. 50–56, 2016.

[29] P. D. Wes, F. A. Sayed, F. Bard, and L. Gan, "Targeting microglia for the treatment of Alzheimer's disease," *Glia*, vol. 64, no. 10, pp. 1710–1732, 2016.

[30] J. Steffen, M. Krohn, K. Paarmann et al., "Revisiting rodent models: Octodon degus as Alzheimer's disease model?," *Acta Neuropathologica Communications*, vol. 4, no. 1, p. 91, 2016.

[31] L. Zhai, Y. Otani, and T. Ohwada, "Uncovering the networks of topological neighborhoods in β-strand and amyloid β-sheet structures," *Scientific Reports*, vol. 9, no. 1, p. 10737, 2019.

[32] F. P. Chong, K. Y. Ng, R. Y. Koh, and S. M. Chye, "Tau proteins and tauopathies in Alzheimer's disease," *Cellular and Molecular Neurobiology*, vol. 38, no. 5, pp. 965–980, 2018.

[33] U. Rüb, K. Stratmann, H. Heinsen, K. Seidel, M. Bouzrou, and H. W. Korf, "Alzheimer's disease: characterization of the brain sites of the initial tau cytoskeletal pathology will improve the success of novel immunological anti-tau treatment approaches," *Journal of Alzheimer's Disease*, vol. 57, no. 3, pp. 683–696, 2017.

[34] J. Horvath, P. R. Burkhard, F. R. Herrmann, C. Bouras, and E. Kövari, "Neuropathology of parkinsonism in patients with pure Alzheimer's disease," *Journal of Alzheimer's Disease*, vol. 39, no. 1, pp. 115–120, 2014.

[35] M. del Carmen Cárdenas-Aguayo, L. Gómez-Virgilio, S. DeRosa, and M. A. Meraz-Ríos, "The role of tau oligomers in the onset of Alzheimer's disease neuropathology," *ACS Chemical Neuroscience*, vol. 5, no. 12, pp. 1178–1191, 2014.

[36] R. H. Ma, Y. Zhang, X. Y. Hong, J. F. Zhang, J. Z. Wang, and G. P. Liu, "Role of microtubule-associated protein tau phosphorylation in Alzheimer's disease," *Journal of Huazhong University of Science and Technology [Medical Sciences]*, vol. 37, no. 3, pp. 307–312, 2017.

[37] C. Yang, X. Li, W. Gao et al., "Cornel iridoid glycoside inhibits tau hyperphosphorylation via regulating cross-talk between GSK-3β and PP2A signaling," *Frontiers in Pharmacology*, vol. 9, 2018.

[38] V. Theendakara, D. E. Bredesen, and R. V. Rao, "Downregulation of protein phosphatase 2A by apolipoprotein E: implications for Alzheimer's disease," *Molecular and Cellular Neurosciences*, vol. 83, pp. 83–91, 2017.

[39] A. J. Moszczynski, W. Yang, R. Hammond, L. C. Ang, and M. J. Strong, "Threonine^{175}, a novel pathological phosphorylation site on tau protein linked to multiple tauopathies," *Acta Neuropathologica Communications*, vol. 5, no. 1, p. 6, 2017.

[40] A. Bejanin, D. R. Schonhaut, R. La Joie et al., "Tau pathology and neurodegeneration contribute to cognitive impairment in Alzheimer's disease," *Brain*, vol. 140, no. 12, pp. 3286–3300, 2017.

[41] Z. He, J. L. Guo, J. D. McBride et al., "Amyloid-β plaques enhance Alzheimer's brain tau-seeded pathologies by facilitating neuritic plaque tau aggregation," *Nature Medicine*, vol. 24, no. 1, pp. 29–38, 2018.

[42] A. Ittner, S. W. Chua, J. Bertz et al., "Site-specific phosphorylation of tau inhibits amyloid-β toxicity in Alzheimer's mice," *Science*, vol. 354, no. 6314, pp. 904–908, 2016.

[43] S. Friso, S. W. Choi, D. Girelli et al., "A common mutation in the 5,10-methylenetetrahydrofolate reductase gene affects genomic DNA methylation through an interaction with folate status," *Proceedings of the National Academy of Sciences of the United States of America*, vol. 99, no. 8, pp. 5606–5611, 2002.

[44] S. J. Mentch and J. W. Locasale, "One-carbon metabolism and epigenetics: understanding the specificity," *Annals of the New York Academy of Sciences*, vol. 1363, no. 1, pp. 91–98, 2016.

[45] H. Jakubowski, "Homocysteine editing, thioester chemistry, coenzyme A, and the origin of coded peptide synthesis †," *Life*, vol. 7, no. 1, p. 6, 2017.

[46] S. Tian, J. Han, R. Huang et al., "Increased plasma homocysteine level is associated with executive dysfunction in type 2 diabetic patients with mild cognitive impairment," *Journal of Alzheimer's Disease*, vol. 58, no. 4, pp. 1163–1173, 2017.

[47] P. R. Mandaviya, L. Stolk, and S. G. Heil, "Homocysteine and DNA methylation: a review of animal and human literature," *Molecular Genetics and Metabolism*, vol. 113, no. 4, pp. 243–252, 2014.

[48] A. Coppola, C. Astarita, E. Liguori et al., "Impairment of coronary circulation by acute hyperhomocysteinaemia and reversal by antioxidant vitamins," *Journal of Internal Medicine*, vol. 256, no. 5, pp. 398–405, 2004.

[49] F. Nappo, N. de Rosa, R. Marfella et al., "Impairment of endothelial functions by acute hyperhomocysteinemia and reversal by antioxidant vitamins," *JAMA*, vol. 281, no. 22, pp. 2113–2118, 1999.

[50] M. F. Bellamy, I. F. W. McDowell, M. W. Ramsey et al., "Hyperhomocysteinemia after an oral methionine load acutely impairs endothelial function in healthy adults," *Circulation*, vol. 98, no. 18, pp. 1848–1852, 1998.

[51] M. Visram, M. Radulovic, S. Steiner et al., "Homocysteine regulates fatty acid and lipid metabolism in yeast," *The Journal of Biological Chemistry*, vol. 293, no. 15, pp. 5544–5555, 2018.

[52] H. Škovierová, E. Vidomanová, S. Mahmood et al., "The molecular and cellular effect of homocysteine metabolism imbalance on human Health," *International Journal of Molecular Sciences*, vol. 17, no. 10, p. 1733, 2016.

[53] K. L. Schalinske and A. L. Smazal, "Homocysteine imbalance: a pathological metabolic marker," *Advances in Nutrition*, vol. 3, no. 6, pp. 755–762, 2012.

[54] L. Hannibal and H. J. Blom, "Homocysteine and disease: causal associations or epiphenomenons?," *Molecular Aspects of Medicine*, vol. 53, pp. 36–42, 2017.

[55] V. Genoud, P. G. Quintana, S. Gionco, A. Baldessari, and I. Quintana, "Structural changes of fibrinogen molecule mediated by the N-homocysteinylation reaction," *Journal of Thrombosis and Thrombolysis*, vol. 45, no. 1, pp. 66–76, 2018.

[56] P. M. Ueland, H. Refsum, S. P. Stabler, M. R. Malinow, A. Andersson, and R. H. Allen, "Total homocysteine in plasma or serum: methods and clinical applications," *Clinical Chemistry*, vol. 39, no. 9, pp. 1764–1779, 1993.

[57] R. Velazquez, E. Ferreira, W. Winslow et al., "Maternal choline supplementation ameliorates Alzheimer's disease pathology by reducing brain homocysteine levels across multiple generations," *Molecular Psychiatry*, vol. 10, 2019.

[58] A. Kalani, P. K. Kamat, S. Givvimani et al., "Nutri-epigenetics ameliorates blood-brain barrier damage and neurodegeneration in hyperhomocysteinemia: role of folic acid," *Journal of Molecular Neuroscience*, vol. 52, no. 2, pp. 202–215, 2014.

[59] P. Tessari, D. Cecchet, M. Vettore, A. Coracina, L. Puricelli, and E. Kiwanuka, "Decreased homocysteine trans-sulfuration in hypertension with hyperhomocysteinemia: relationship with insulin resistance," *The Journal of Clinical Endocrinology and Metabolism*, vol. 103, no. 1, pp. 56–63, 2018.

[60] G. J. Weber, S. Pushpakumar, S. C. Tyagi, and U. Sen, "Homocysteine and hydrogen sulfide in epigenetic, metabolic and microbiota related renovascular hypertension," *Pharmacological Research*, vol. 113, Part A, pp. 300–312, 2016.

[61] L. Miao, G. X. Deng, R. X. Yin et al., "No causal effects of plasma homocysteine levels on the risk of coronary heart disease or acute myocardial infarction: a Mendelian randomization study„" *European Journal of Preventive Cardiology*, 2019.

[62] K. S. McCully, "Homocysteine metabolism, atherosclerosis, and diseases of aging," *Comprehensive Physiology*, vol. 6, no. 1, pp. 471–505, 2015.

[63] A. D. Smith and H. Refsum, "Homocysteine, B vitamins, and cognitive impairment," *Annual Review of Nutrition*, vol. 36, no. 1, pp. 211–239, 2016.

[64] A. Familtseva, P. Chaturvedi, A. Kalani et al., "Toll-like receptor 4 mutation suppresses hyperhomocysteinemia-induced hypertension," *American Journal of Physiology-Cell Physiology*, vol. 311, no. 4, pp. C596–C606, 2016.

[65] J. Li, Y. Zhang, Y. Zhang et al., "GSNOR modulates hyperhomocysteinemia-induced T cell activation and atherosclerosis by switching Akt S-nitrosylation to phosphorylation," *Redox Biology*, vol. 17, pp. 386–399, 2018.

[66] C. Montecinos-Oliva, M. S. Arrázola, C. Jara, C. Tapia-Rojas, and N. C. Inestrosa, "Hormetic-like effects of L-homocysteine on synaptic structure, function, and Aβ aggregation," *Pharmaceuticals*, vol. 13, no. 2, p. 24, 2020.

[67] W. Reik and G. Kelsey, "Cellular memory erased in human embryos," *Nature*, vol. 511, no. 7511, pp. 540-541, 2014.

[68] L. A. Wakeling, L. J. Ions, S. M. Escolme et al., "SIRT1 affects DNA methylation of polycomb group protein target genes, a hotspot of the epigenetic shift observed in ageing," *Human Genomics*, vol. 9, no. 1, p. 14, 2015.

[69] J. Zhong, G. Agha, and A. A. Baccarelli, "The role of DNA methylation in cardiovascular risk and disease: methodological aspects, study design, and data analysis for epidemiological studies," *Circulation Research*, vol. 118, no. 1, pp. 119–131, 2016.

[70] O. Castillo-Aguilera, P. Depreux, L. Halby, P. Arimondo, and L. Goossens, "DNA methylation targeting: the DNMT/HMT crosstalk challenge," *Biomolecules*, vol. 7, no. 4, p. 3, 2017.

[71] A. Jeltsch and R. Z. Jurkowska, "Allosteric control of mammalian DNA methyltransferases - a new regulatory paradigm," *Nucleic Acids Research*, vol. 44, no. 18, pp. 8556–8575, 2016.

[72] J. R. Edwards, O. Yarychkivska, M. Boulard, and T. H. Bestor, "DNA methylation and DNA methyltransferases," *Epigenetics & Chromatin*, vol. 10, no. 1, p. 23, 2017.

[73] A. Bansal and S. E. Pinney, "DNA methylation and its role in the pathogenesis of diabetes," *Pediatric Diabetes*, vol. 18, no. 3, pp. 167–177, 2017.

[74] Y. T. Tsai, C. M. Chang, J. Y. Wang et al., "Function of DNA methyltransferase 3a in lead (Pb(2+))-induced cyclooxygenase-2 gene," *Environmental Toxicology*, vol. 30, no. 9, pp. 1024–1032, 2015.

[75] D. Álvarez-Errico, R. Vento-Tormo, and E. Ballestar, "Genetic and epigenetic determinants in autoinflammatory diseases," *Frontiers in Immunology*, vol. 8, p. 318, 2017.

[76] R. Yang, Z. Zheng, Q. Chen et al., "The developmental regulator PKL is required to maintain correct DNA methylation patterns at RNA-directed DNA methylation loci," *Genome Biology*, vol. 18, no. 1, p. 103, 2017.

[77] C. M. Hedrich, K. Mäbert, T. Rauen, and G. C. Tsokos, "DNA methylation in systemic lupus erythematosus," *Epigenomics*, vol. 9, no. 4, pp. 505–525, 2017.

[78] A. Jeltsch, J. Broche, and P. Bashtrykov, "Molecular processes connecting DNA methylation patterns with DNA methyltransferases and histone modifications in mammalian genomes," *Genes*, vol. 9, no. 11, p. 566, 2018.

[79] B. Chatterjee, M. H. Lin, C. C. Chen et al., "DNA Demethylation by DNMT3A and DNMT3B *in vitro* and of Methylated Episomal DNA in Transiently Transfected Cells," *Biochimica et Biophysica Acta (BBA) - Gene Regulatory Mechanisms*, vol. 1861, no. 11, pp. 1048–1061, 2018.

[80] P. A. Jones, "Functions of DNA methylation: islands, start sites, gene bodies and beyond," *Nature Reviews Genetics*, vol. 13, no. 7, pp. 484–492, 2012.

[81] B. Liu, J. Song, J. Luan et al., "Promoter methylation status of tumor suppressor genes and inhibition of expression of DNA methyltransferase 1 in non-small cell lung cancer," *Experimental Biology and Medicine*, vol. 241, no. 14, pp. 1531–1539, 2016.

[82] M. Kim and J. Costello, "DNA methylation: an epigenetic mark of cellular memory," *Experimental & Molecular Medicine*, vol. 49, no. 4, p. e322, 2017.

[83] J. Xu, G. He, J. Zhu et al., "Prenatal nutritional deficiency reprogrammed postnatal gene expression in mammal brains: implications for schizophrenia," *International Journal of Neuropsychopharmacology*, vol. 18, no. 4, 2015.

[84] V. Nicolia, M. Lucarelli, and A. Fuso, "Environment, epigenetics and neurodegeneration: focus on nutrition in Alzheimer's disease," *Experimental Gerontology*, vol. 68, pp. 8–12, 2015.

[85] L. Shu, W. Sun, L. Li et al., "Genome-wide alteration of 5-hydroxymenthylcytosine in a mouse model of Alzheimer's disease," *BMC Genomics*, vol. 17, no. 1, 2016.

[86] S. Do Carmo, C. E. Hanzel, M. L. Jacobs et al., "Rescue of Early *bace-1* and Global DNA Demethylation by S-Adenosylmethionine Reduces Amyloid Pathology and Improves Cognition in an Alzheimer 's Model," *Scientific Reports*, vol. 6, no. 1, article 34051, 2016.

[87] A. Iwata, K. Nagata, H. Hatsuta et al., "Altered CpG methylation in sporadic Alzheimer's disease is associated with APP and MAPT dysregulation," *Human Molecular Genetics*, vol. 23, no. 3, pp. 648–656, 2014.

[88] B. De Strooper, T. Iwatsubo, and M. S. Wolfe, "Presenilins and γ-secretase: structure, function, and role in Alzheimer disease," *Cold Spring Harbor Perspectives in Medicine*, vol. 2, article a006304, no. 1, 2012.

[89] H. C. Lin, H. M. Hsieh, Y. H. Chen, and M. L. Hu, "*S* -Adenosylhomocysteine increases β-amyloid formation in BV-2 microglial cells by increased expressions of β-amyloid precursor protein and presenilin 1 and by hypomethylation of these gene promoters," *Neurotoxicology*, vol. 30, no. 4, pp. 622–627, 2009.

[90] W. Li, M. Jiang, S. Zhao et al., "Folic acid inhibits amyloid β-peptide production through modulating DNA methyltransferase activity in N2a-APP cells," *International Journal of Molecular Sciences*, vol. 16, no. 10, pp. 25002–25013, 2015.

[91] S. K. Sonawane and S. Chinnathambi, "Prion-like propagation of post-translationally modified tau in Alzheimer's disease: a hypothesis," *Journal of Molecular Neuroscience*, vol. 65, no. 4, pp. 480–490, 2018.

[92] M. Nuru, N. Muradashvili, A. Kalani, D. Lominadze, and N. Tyagi, "High methionine, low folate and low vitamin B6/B12 (HM-LF-LV) diet causes neurodegeneration and subsequent short-term memory loss," *Metabolic Brain Disease*, vol. 33, no. 6, pp. 1923–1934, 2018.

[93] S. A. Semick, R. A. Bharadwaj, L. Collado-Torres et al., "Integrated DNA methylation and gene expression profiling across multiple brain regions implicate novel genes in Alzheimer's disease," *Acta Neuropathologica*, vol. 137, no. 4, pp. 557–569, 2019.

[94] R. G. Smith, E. Hannon, P. L. De Jager et al., "Elevated DNA methylation across a 48-kb region spanning theHOXAgene cluster is associated with Alzheimer's disease neuropathology," *Alzheimer's & Dementia*, vol. 14, no. 12, pp. 1580–1588, 2018.

[95] M. Altuna, A. Urdánoz-Casado, J. S.-R. de Gordoa et al., "DNA methylation signature of human hippocampus in Alzheimer's disease is linked to neurogenesis," *Clinical Epigenetics*, vol. 11, no. 1, p. 91, 2019.

[96] V. Nicolia, M. Lucarelli, and A. Fuso, "Environment, epigenetics and neurodegeneration: focus on nutrition in Alzheimer's disease," *Experimental Gerontology*, vol. 68, pp. 8–12, 2015.

[97] Q. Hu, W. Teng, J. Li, F. Hao, and N. Wang, "Homocysteine and Alzheimer's disease: evidence for a causal link from Mendelian randomization," *Journal of Alzheimer's Disease*, vol. 52, no. 2, pp. 747–756, 2016.

[98] K. Nazef, M. Khelil, H. Chelouti et al., "Hyperhomocysteinemia is a risk factor for Alzheimer's disease in an Algerian population," *Archives of Medical Research*, vol. 45, no. 3, pp. 247–250, 2014.

[99] M. Sharma, M. Tiwari, and R. K. Tiwari, "Hyperhomocysteinemia: impact on neurodegenerative diseases," *Basic & Clinical Pharmacology & Toxicology*, vol. 117, no. 5, pp. 287–296, 2015.

[100] E. Grossi, A. Stoccoro, P. Tannorella, L. Migliore, and F. Coppedè, "Artificial neural networks link one-carbon metabolism to gene-promoter methylation in Alzheimer's disease," *Journal of Alzheimer's Disease*, vol. 53, no. 4, pp. 1517–1522, 2016.

[101] E. Setién-Suero, M. Suárez-Pinilla, P. Suárez-Pinilla, B. Crespo-Facorro, and R. Ayesa-Arriola, "Homocysteine and cognition: a systematic review of 111 studies," *Neuroscience and Biobehavioral Reviews*, vol. 69, pp. 280–298, 2016.

[102] S. Love and J. S. Miners, "Cerebrovascular disease in ageing and Alzheimer's disease," *Acta Neuropathologica*, vol. 131, no. 5, pp. 645–658, 2016.

[103] M. Pirchl, C. Ullrich, and C. Humpel, "Differential effects of short- and long-term hyperhomocysteinaemia on cholinergic neurons, spatial memory and microbleedings in vivo in rats,"

The European Journal of Neuroscience, vol. 32, no. 9, pp. 1516–1527, 2010.

[104] A. Ataie, M. Sabetkasaei, A. Haghparast, A. H. Moghaddam, R. Ataee, and S. N. Moghaddam, "Curcumin exerts neuroprotective effects against homocysteine intracerebroventricular injection-induced cognitive impairment and oxidative stress in rat brain," *Journal of Medicinal Food*, vol. 13, no. 4, pp. 821–826, 2010.

[105] N. Nath, H. K. Prasad, and M. Kumar, "Cerebroprotective effects of hydrogen sulfide in homocysteine-induced neurovascular permeability: involvement of oxidative stress, arginase, and matrix metalloproteinase-9," *Journal of Cellular Physiology*, vol. 234, no. 3, pp. 3007–3019, 2018.

[106] S. Love and J. S. Miners, "Cerebrovascular disease in ageing and Alzheimer's disease," *Acta Neuropathologica*, vol. 131, no. 5, pp. 645–658, 2016.

[107] P. K. Kamat, P. Kyles, A. Kalani, and N. Tyagi, "Hydrogen sulfide ameliorates homocysteine-induced Alzheimer's disease-like pathology, blood-brain barrier disruption, and synaptic disorder," *Molecular Neurobiology*, vol. 53, no. 4, pp. 2451–2467, 2016.

[108] N. Lin, S. Qin, S. Luo, S. Cui, G. Huang, and X. Zhang, "Homocysteine induces cytotoxicity and proliferation inhibition in neural stem cells via DNA methylation in vitro," *The FEBS Journal*, vol. 281, no. 8, pp. 2088–2096, 2014.

[109] A. R. Collins, "Measuring oxidative damage to DNA and its repair with the comet assay," *Biochimica et Biophysica Acta (BBA) - Gene Regulatory Mechanisms*, vol. 1840, no. 2, pp. 794–800, 2014.

[110] J. G. Li, C. Barrero, S. Gupta, W. D. Kruger, S. Merali, and D. Praticò, "Homocysteine modulates 5-lipoxygenase expression level via DNA methylation," *Aging Cell*, vol. 16, no. 2, pp. 273–280, 2017.

[111] A. Di Meco, J.-G. Li, and D. Praticò, "Dissecting the role of 5-lipoxygenase in the homocysteine-induced Alzheimer's disease pathology," *Journal of Alzheimer's Disease*, G. Perry, J. Avila, M. Tabaton, and X. Zhu, Eds., vol. 62, no. 3, pp. 1337–1344, 2018.

[112] M. Currò, A. Gugliandolo, C. Gangemi, R. Risitano, R. Ientile, and D. Caccamo, "Toxic effects of mildly elevated homocysteine concentrations in neuronal-like cells," *Neurochemical Research*, vol. 39, no. 8, pp. 1485–1495, 2014.

[113] A. Di Meco, J.-G. Li, C. Barrero, S. Merali, and D. Praticò, "Elevated levels of brain homocysteine directly modulate the pathological phenotype of a mouse model of tauopathy," *Molecular Psychiatry*, vol. 24, no. 11, pp. 1696–1706, 2019.

[114] J. G. Li and D. Praticò, "High levels of homocysteine results in cerebral amyloid angiopathy in mice," *Journal of Alzheimer's Disease*, vol. 43, no. 1, pp. 29–35, 2015.

[115] I. I. Kruman, T. S. Kumaravel, A. Lohani et al., "Folic acid deficiency and homocysteine impair DNA repair in hippocampal neurons and sensitize them to amyloid toxicity in experimental models of Alzheimer's disease," *The Journal of Neuroscience*, vol. 22, no. 5, pp. 1752–1762, 2002.

[116] N. Shirafuji, T. Hamano, S. H. Yen et al., "Homocysteine increases tau phosphorylation, truncation and oligomerization," *International Journal of Molecular Sciences*, vol. 19, no. 3, p. 891, 2018.

[117] H. Negahdar, S. R. Hosseini, H. Parsian et al., "Homocysteine, trace elements and oxidant/antioxidant status in mild cognitively impaired elderly persons: a cross-sectional study," *Romanian Journal of Internal Medicine*, vol. 53, no. 4, pp. 336–342, 2015.

[118] R. Velazquez, E. Ferreira, W. Winslow et al., "Maternal choline supplementation ameliorates Alzheimer's disease pathology by reducing brain homocysteine levels across multiple generations," *Molecular Psychiatry*, 2019.

[119] S. Chaudhury, T. Patel, I. S. Barber et al., "Polygenic risk score in postmortem diagnosed sporadic early-onset Alzheimer's disease," *Neurobiology of Aging*, vol. 62, pp. 244.e1–244.e8, 2018.

[120] J. C. Wang, S. Alinaghi, A. Tafakhori et al., "Genetic screening in two Iranian families with early-onset Alzheimer's disease identified a novel *PSEN1* mutation," *Neurobiology of Aging*, vol. 62, pp. 244.e15–244.e17, 2018.

[121] J. Hara, W. R. Shankle, L. W. Barrentine, and M. V. Curole, "Novel therapy of hyperhomocysteinemia in mild cognitive impairment, Alzheimer's disease, and other dementing disorders," *The Journal of Nutrition, Health & Aging*, vol. 20, no. 8, pp. 825–834, 2016.

[122] M. Halil, M. Cemal Kizilarslanoglu, M. Emin Kuyumcu, Y. Yesil, and A. J. Cruz Jentoft, "Cognitive aspects of frailty: mechanisms behind the link between frailty and cognitive impairment," *The Journal of Nutrition, Health & Aging*, vol. 19, no. 3, pp. 276–283, 2015.

[123] N. Lin, S. Qin, S. Luo, S. Cui, G. Huang, and X. Zhang, "Homocysteine induces cytotoxicity and proliferation inhibition in neural stem cells via DNA methylation in vitro," *The FEBS Journal*, vol. 281, no. 8, pp. 2088–2096, 2014.

[124] M. Mattson, I. Kruman, and W. Duan, "Folic acid and homocysteine in age-related disease," *Ageing Research Reviews*, vol. 1, no. 1, pp. 95–111, 2002.

[125] J. G. Li, C. Barrero, S. Gupta, W. D. Kruger, S. Merali, and D. Praticò, "Homocysteine modulates 5-lipoxygenase expression level via DNA methylation," *Aging Cell*, vol. 16, no. 2, pp. 273–280, 2017.

[126] A. Kalani, P. K. Kamat, S. Givvimani et al., "Nutri-epigenetics ameliorates blood-brain barrier damage and neurodegeneration in hyperhomocysteinemia: role of folic acid," *Journal of Molecular Neuroscience*, vol. 52, no. 2, pp. 202–215, 2014.

[127] L. Hannibal and H. J. Blom, "Homocysteine and disease: causal associations or epiphenomenons?," *Molecular Aspects of Medicine*, vol. 53, pp. 36–42, 2017.

[128] F. Tchantchou, "Homocysteine metabolism and various consequences of folate deficiency," *Journal of Alzheimer's Disease*, vol. 9, no. 4, pp. 421–427, 2006.

[129] J. R. Araújo, F. Martel, N. Borges, J. M. Araújo, and E. Keating, "Folates and aging: role in mild cognitive impairment, dementia and depression," *Ageing Research Reviews*, vol. 22, pp. 9–19, 2015.

[130] M. Bednarska-Makaruk, A. Graban, A. Sobczyńska-Malefora et al., "Homocysteine metabolism and the associations of global DNA methylation with selected gene polymorphisms and nutritional factors in patients with dementia," *Experimental Gerontology*, vol. 81, pp. 83–91, 2016.

[131] J.-M. Sontag, B. Wasek, G. Taleski et al., "Altered protein phosphatase 2A methylation and tau phosphorylation in the young and aged brain of methylenetetrahydrofolate reductase (MTHFR) deficient mice," *Frontiers in Aging Neuroscience*, vol. 6, p. 214, 2014.

[132] K. Nazef, M. Khelil, H. Chelouti et al., "Hyperhomocysteinemia is a risk factor for Alzheimer's disease in an Algerian

population," *Archives of Medical Research*, vol. 45, no. 3, pp. 247–250, 2014.

[133] A. Fuso, R. A. Cavallaro, A. Zampelli et al., "γ-Secretase is differentially modulated by alterations of homocysteine cycle in neuroblastoma and glioblastoma cells," *Journal of Alzheimer's Disease*, vol. 11, no. 3, pp. 275–290, 2007.

[134] A. Fuso, L. Seminara, R. A. Cavallaro, F. D'Anselmi, and S. Scarpa, "S-adenosylmethionine/homocysteine cycle alterations modify DNA methylation status with consequent deregulation of PS1 and BACE and beta-amyloid production," *Molecular and Cellular Neurosciences*, vol. 28, no. 1, pp. 195–204, 2005.

[135] P. K. Kamat, P. Kyles, A. Kalani, and N. Tyagi, "Hydrogen sulfide ameliorates homocysteine-induced Alzheimer's disease-like pathology, blood-brain barrier disruption, and synaptic disorder," *Molecular Neurobiology*, vol. 53, no. 4, pp. 2451–2467, 2016.

[136] N. Janel, P. Alexopoulos, A. Badel et al., "Combined assessment of DYRK1A, BDNF and homocysteine levels as diagnostic marker for Alzheimer's disease," *Translational Psychiatry*, vol. 7, no. 6, article e1154, 2017.

[137] B. K. Yadav, S. Y. Oh, N. K. Kim, and B. S. Shin, "Association of *rs2075575* and *rs9951307* Polymorphisms of AQP-4 Gene with Leukoaraiosis," *Journal of Stroke and Cerebrovascular Diseases*, vol. 23, no. 5, pp. 1199–1206, 2014.

[138] P. Tannorella, A. Stoccoro, G. Tognoni et al., "Methylation analysis of multiple genes in blood DNA of Alzheimer's disease and healthy individuals," *Neuroscience Letters*, vol. 600, pp. 143–147, 2015.

[139] J. G. Li, J. Chu, C. Barrero, S. Merali, and D. Praticò, "Homocysteine exacerbates β-amyloid pathology, tau pathology, and cognitive deficit in a mouse model of Alzheimer disease with plaques and tangles," *Annals of Neurology*, vol. 75, no. 6, pp. 851–863, 2014.

[140] V. Rai, "Folate pathway gene methylenetetrahydrofolate reductase C677T polymorphism and Alzheimer disease risk in Asian population," *Indian Journal of Clinical Biochemistry*, vol. 31, no. 3, pp. 245–252, 2016.

[141] V. Rai, "Methylenetetrahydrofolate reductase (MTHFR) C677T polymorphism and Alzheimer disease risk: a meta-analysis," *Molecular Neurobiology*, vol. 54, no. 2, pp. 1173–1186, 2017.

[142] R. Obeid and W. Herrmann, "Mechanisms of homocysteine neurotoxicity in neurodegenerative diseases with special reference to dementia," *FEBS Letters*, vol. 580, no. 13, pp. 2994–3005, 2006.

[143] E. Grossi, A. Stoccoro, P. Tannorella, L. Migliore, and F. Coppedè, "Artificial neural networks link one-carbon metabolism to gene-promoter methylation in Alzheimer's disease," *Journal of Alzheimer's Disease*, vol. 53, no. 4, pp. 1517–1522, 2016.

[144] J.-G. Li, C. Barrero, S. Merali, and D. Praticò, "Five lipoxygenase hypomethylation mediates the homocysteine effect on Alzheimer's phenotype," *Scientific Reports*, vol. 7, no. 1, article 46002, 2017.

[145] S. Scarpa, R. A. Cavallaro, F. D'Anselmi, and A. Fuso, "Gene silencing through methylation: an epigenetic intervention on Alzheimer disease," *Journal of Alzheimer's Disease*, vol. 9, no. 4, pp. 407–414, 2006.

[146] R. A. Cavallaro, A. Fuso, F. D'Anselmi, L. Seminara, and S. Scarpa, "The effect of S-adenosylmethionine on CNS gene expression studied by cDNA microarray analysis," *Journal of Alzheimer's Disease*, vol. 9, no. 4, pp. 415–419, 2006.

[147] S. Scarpa, A. Fuso, F. D'Anselmi, and R. A. Cavallaro, "Presenilin 1 gene silencing by S-adenosylmethionine: a treatment for Alzheimer disease?," *FEBS Letters*, vol. 541, no. 1-3, pp. 145–148, 2003.

[148] H. C. Lin, H. M. Hsieh, Y. H. Chen, and M. L. Hu, "S-Adenosylhomocysteine increases β-amyloid formation in BV-2 microglial cells by increased expressions of β-amyloid precursor protein and presenilin 1 and by hypomethylation of these gene promoters," *Neurotoxicology*, vol. 30, no. 4, pp. 622–627, 2009.

[149] A. Kalani, P. K. Kamat, S. C. Tyagi, and N. Tyagi, "Synergy of homocysteine, microRNA, and epigenetics: a novel therapeutic approach for stroke," *Molecular Neurobiology*, vol. 48, no. 1, pp. 157–168, 2013.

[150] E. Joe and J. M. Ringman, "Cognitive symptoms of Alzheimer's disease: clinical management and prevention," *BMJ*, vol. 367, article l6217, 2019.

[151] F. Panza, M. Lozupone, A. Bellomo, and B. P. Imbimbo, "Do anti-amyloid-β drugs affect neuropsychiatric status in Alzheimer's disease patients?," *Ageing Research Reviews*, vol. 55, p. 100948, 2019.

[152] M. Knapp, D. King, R. Romeo et al., "Cost-effectiveness of donepezil and memantine in moderate to severe Alzheimer's disease (the DOMINO-AD trial)," *International Journal of Geriatric Psychiatry*, vol. 32, no. 12, pp. 1205–1216, 2017.

[153] J. S. Birks and R. J. Harvey, "Donepezil for dementia due to Alzheimer's disease," *Cochrane Database of Systematic Reviews*, vol. 6, no. 6, article CD001190, 2018.

[154] N. Kandiah, M. C. Pai, V. Senanarong et al., "Rivastigmine: the advantages of dual inhibition of acetylcholinesterase and butyrylcholinesterase and its role in subcortical vascular dementia and Parkinson’s disease dementia," *Clinical Interventions in Aging*, vol. 12, pp. 697–707, 2017.

[155] Z. Wu, L. Zhao, X. Chen, X. Cheng, and Y. Zhang, "Galantamine attenuates amyloid-β deposition and astrocyte activation in APP/PS1 transgenic mice," *Experimental Gerontology*, vol. 72, pp. 244–250, 2015.

[156] S. Matsunaga, T. Kishi, I. Nomura et al., "The efficacy and safety of memantine for the treatment of Alzheimer's disease," *Expert Opinion on Drug Safety*, vol. 17, no. 10, pp. 1053–1061, 2018.

[157] W. J. Deardorff and G. T. Grossberg, "A fixed-dose combination of memantine extended-release and donepezil in the treatment of moderate-to-severe Alzheimer's disease," *Drug Design, Development and Therapy*, vol. Volume 10, pp. 3267–3279, 2016.

[158] J. E. Galvin, "Optimizing diagnosis and management in mild-to-moderate Alzheimer's disease," *Neurodegenerative Disease Management*, vol. 2, no. 3, pp. 291–304, 2012.

[159] Z. Arvanitakis, R. C. Shah, and D. A. Bennett, "Diagnosis and management of dementia: review," *JAMA*, vol. 322, no. 16, pp. 1589–1599, 2019.

[160] S. K. Madsen, P. Rajagopalan, S. H. Joshi, A. W. Toga, P. M. Thompson, and Alzheimer's Disease Neuroimaging Initiative (ADNI), "Higher homocysteine associated with thinner cortical gray matter in 803 participants from the Alzheimer's disease neuroimaging initiative," *Neurobiology of Aging*, vol. 36, no. 1, pp. S203–S210, 2015.

[161] C. W. Huang, W. N. Chang, S. H. Huang et al., "Impact of homocysteine on cortical perfusion and cognitive decline in mild Alzheimer's dementia," *European Journal of Neurology*, vol. 20, no. 8, pp. 1191–1197, 2013.

[162] M. C. Tu, C. W. Huang, and N. C. Chen, "Hyperhomocysteinemia in Alzheimer dementia patients and cognitive decline after 6 months follow-up period," *Acta Neurologica Taiwanica*, vol. 19, no. 3, pp. 168–177, 2010.

[163] F. Ma, T. Wu, J. Zhao et al., "Plasma homocysteine and serum folate and vitamin B_{12} levels in mild cognitive impairment and Alzheimer's disease: a case-control study," *Nutrients*, vol. 9, no. 7, p. 725, 2017.

[164] Q. Hu, W. Teng, J. Li, F. Hao, and N. Wang, "Homocysteine and Alzheimer's disease: evidence for a causal link from Mendelian randomization," *Journal of Alzheimer's Disease*, vol. 52, no. 2, pp. 747–756, 2016.

[165] P. K. Kamat, P. Kyles, A. Kalani, and N. Tyagi, "Hydrogen sulfide ameliorates homocysteine-induced Alzheimer's disease-like pathology, blood-brain barrier disruption, and synaptic disorder," *Molecular Neurobiology*, vol. 53, no. 4, pp. 2451–2467, 2016.

[166] A. McCaddon, P. Hudson, G. Davies, A. Hughes, J. H. H. Williams, and C. Wilkinson, "Homocysteine and cognitive decline in healthy elderly," *Dementia and Geriatric Cognitive Disorders*, vol. 12, no. 5, pp. 309–313, 2001.

[167] A. McCaddon and B. Regland, "Homocysteine and cognition - No longer a hypothesis?," *Medical Hypotheses*, vol. 66, no. 3, pp. 682-683, 2006.

[168] M. Altuna, A. Urdánoz-Casado, J. Sánchez-Ruiz de Gordoa et al., "DNA methylation signature of human hippocampus in Alzheimer's disease is linked to neurogenesis," *Clinical Epigenetics*, vol. 11, no. 1, p. 91, 2019.

[169] M. Blanch, J. L. Mosquera, B. Ansoleaga, I. Ferrer, and M. Barrachina, "Altered mitochondrial DNA methylation pattern in Alzheimer disease-related pathology and in Parkinson disease," *The American Journal of Pathology*, vol. 186, no. 2, pp. 385–397, 2016.

[170] L. Yu, L. B. Chibnik, G. P. Srivastava et al., "Association of brain DNA methylation in SORL1, ABCA7, HLA-DRB5, SLC24A4, and BIN1 With pathological diagnosis of Alzheimer disease," *JAMA Neurology*, vol. 72, no. 1, pp. 15–24, 2015.

[171] A. Di Francesco, B. Arosio, A. Falconi et al., "Global changes in DNA methylation in Alzheimer's disease peripheral blood mononuclear cells," *Brain, Behavior, and Immunity*, vol. 45, pp. 139–144, 2015.

[172] A. Sliwinska, P. Sitarek, M. Toma et al., "Decreased expression level of BER genes in Alzheimer's disease patients is not derivative of their DNA methylation status," *Progress in Neuro-Psychopharmacology & Biological Psychiatry*, vol. 79, article Part B, pp. 311–316, 2017.

[173] N. Kobayashi, S. Shinagawa, T. Nagata et al., "Usefulness of DNA methylation levels in COASY and SPINT1 gene promoter regions as biomarkers in diagnosis of Alzheimer's disease and amnestic mild cognitive impairment," *PLoS One*, vol. 11, no. 12, article e0168816, 2016.

[174] N. Kobayashi, S. Shinagawa, T. Nagata et al., "Development of biomarkers based on DNA methylation in the NCAPH2/LMF2 promoter region for diagnosis of Alzheimer's disease and amnesic mild cognitive impairment," *PLoS One*, vol. 11, no. 1, article e0146449, 2016.

Hindawi
Behavioural Neurology
Volume 2020, Article ID 2825037, 9 pages
https://doi.org/10.1155/2020/2825037

Research Article

A Novel Metabolic Connectome Method to Predict Progression to Mild Cognitive Impairment

Min Wang,[1] Zhuangzhi Yan,[1] Shu-yun Xiao,[2] Chuantao Zuo,[3] and Jiehui Jiang[1,4]

[1]*Institute of Biomedical Engineering, School of Communication and Information Engineering, Shanghai University, Shanghai, China*
[2]*Department of Brain and Mental Disease, Shanghai Hospital of Traditional Chinese Medicine, Shanghai, China*
[3]*PET Center, Huashan Hospital, Fudan University, Shanghai, China*
[4]*Shanghai Institute for Advanced Communication and Data Science, Shanghai University, Shanghai, China*

Correspondence should be addressed to Zhuangzhi Yan; zzyan@shu.edu.cn and Shu-yun Xiao; lindaxsy@163.com

Received 16 June 2020; Revised 17 July 2020; Accepted 10 August 2020; Published 18 August 2020

Academic Editor: Muh-Shi Lin

Objective. Glucose-based positron emission tomography (PET) imaging has been widely used to predict the progression of mild cognitive impairment (MCI) into Alzheimer's disease (AD) clinically. However, existing discriminant methods are unsubtle to reveal pathophysiological changes. Therefore, we present a novel metabolic connectome-based predictive modeling to predict progression from MCI to AD accurately. *Methods*. In this study, we acquired fluorodeoxyglucose PET images and clinical assessments from 420 MCI patients with 36 months follow-up. Individual metabolic network based on connectome analysis was constructed, and the metabolic connectivity in this network was extracted as predictive features. Three different classification strategies were implemented to interrogate the predictive performance. To verify the effectivity of selected features, specific brain regions associated with MCI conversion were identified based on these features and compared with prior knowledge. *Results*. As a result, 4005 connectome features were obtained, and 153 in which were selected as efficient features. Our proposed feature extraction method had achieved 85.2% accuracy for MCI conversion prediction (sensitivity: 88.1%; specificity: 81.2%; and AUC: 0.933). The discriminative brain regions associated with MCI conversion were mainly located in the precentral gyrus, precuneus, lingual, and inferior frontal gyrus. *Conclusion*. Overall, the results suggest that our proposed individual metabolic connectome method has great potential to predict whether MCI patients will progress to AD. The metabolic connectome may help to identify brain metabolic dysfunction and build a clinically applicable biomarker to predict the MCI progression.

1. Introduction

Alzheimer's disease (AD) is a neurodegenerative brain disease and the most common cause of dementia, affecting millions of individuals worldwide [1]. In the intermediate stage between healthy aging and AD, one had developed cognitive deficits that can be diagnosed as mild cognitive impairment (MCI) [2]. Yet MCI disease is very complex, manifesting in clinical and neuropathological heterogeneity. The development of MCI is so labile that some remain in stable stage for many years after diagnosis and even revert to normal cognition. Early diagnosis of whether MCI patients will progress into AD is a daunting challenge.

Currently, most diagnosis studies on MCI conversion are using neuroimaging to acquire the features among MCI groups and then consider these features as biomarkers to predict MCI progression. As a frequently used neuroimaging technique in clinics, ^{18}F-fluorodeoxyglucose (FDG) positron emission tomography (PET) imaging has been employed to detect the progression from MCI to AD [3]. For instance, clinical studies have revealed that FDG-PET could capture the information of resting-state regional cerebral glucose metabolic rate and predicted progression from MCI to AD, and it is mainly due to FDG uptake is reduced in abnormal high cerebrospinal fluid amyloid-β concentrations [4–6]. Recently, as the studies for FDG-PET imaging has advanced, there are various predictive modeling that has been proposed. Previously, some studies had used voxel-wise or region-of-interest- (ROI-) wise quantitative metabolic measures to predict MCI patient's progress into AD [7–9].

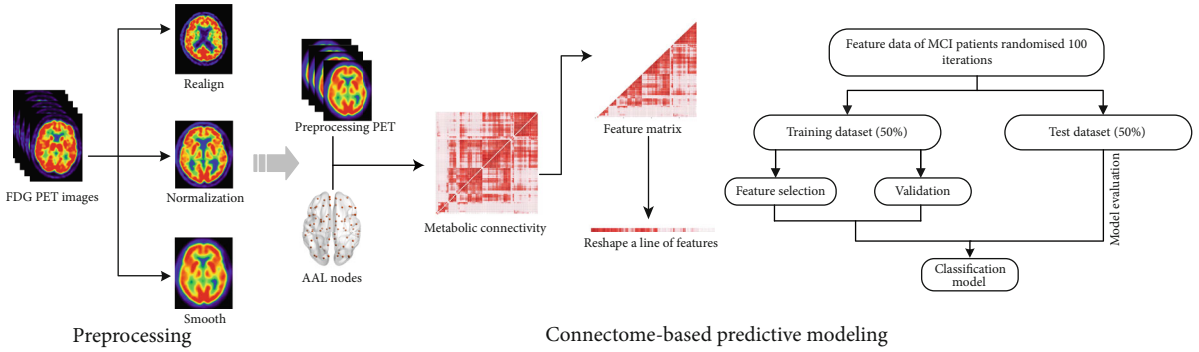

Figure 1: The overall framework of the proposed metabolic connectome-based predictive modeling (CPM) approach in this study.

However, the subtle difference between stable MCI and progression MCI causes it difficult to diagnose and require exquisite predictive modeling. Besides, some studies have explored the application of deep learning methods, such as convolutional neural network (CNN) and deep Boltzmann machine (DBM) [10–12]. Nonetheless, deep learning methods face the challenge that limited sample of FDG-PET images and inaccessible biomarkers could hardly reveal the neuropathological changes associated with MCI conversion. Specifically, a previous study evaluated different predictive models on the same FDG-PET images for reproducible evaluation among MCI patients, and the results showed that the accuracy of classification range between 67% and 83% [13]. Thus, the development of new predictive modeling is necessary to assist diagnosis in clinical assessments and provide higher performance to predict MCI progression.

Connectome-based predictive modeling (CPM) is a novel data-driven protocol for developing predictive models of brain-behavior relationships, which has addressed challenges in brain neurodegenerative disease [14, 15]. Brain connectivity characterizes by different brain regions and the relationship between paired regions and discloses the dynamic communication by neuronal activity. The brain network based on FDG-PET images is an exciting new opportunity to understand the neurological disorders and has been proved adept at analyzing the abnormalities in AD patients [16–18]. As a result, CPM has the potential to provide a novel predictive model for MCI conversion.

The aim of this study is therefore to combine CPM with glucose metabolic imaging to identify discriminative features for accurately classifying whether MCI patients will progress to AD. Specifically, we have two secondary aims: (1) verify whether CPM can be used as a novel feature extraction method in FDG-PET images and (2) evaluate the predictive performance of our proposed metabolic CPM in MCI groups.

2. Materials and Methods

2.1. Motivation. The goal of this study is to develop a predictive model to capture predictive individual differences in MCI patients using CPM and FDG-PET imaging. We hypothesize that the combination of CPM and glucose metabolic imaging may identify the subtle brain metabolic dysfunction and use this information to obtain remarkable diagnosis performance. The framework of our proposed approach is summarized in Figure 1.

2.2. Participants and Imaging Protocols. The ^{18}F-FDG-PET data used in this study were obtained from the Alzheimer's Disease Neuroimaging Initiative (ADNI) database (http://adni.loni.usc.edu). The primary goal of ADNI has been to test whether serial magnetic resonance imaging (MRI), positron emission tomography (PET), other biological markers, and clinical and neuropsychological assessments can be combined to measure the progression of mild cognitive impairment (MCI) and early Alzheimer's disease (AD). The institutional review board of ADNI approved all aspects of this study, and each participant has given written informed consent to undergo PET scanning of a long-term observational study.

This study acquired 420 MCI participants with FDG-PET scanning from ADNI-1, ADNI-2, and ADNI-GO database. The participant group was comprised of 242 stable MCI (sMCI) subjects and 178 progressive MCI (pMCI) subjects, and the images were used to establish a predictive model and test the validity of the model. The detailed eligibility criteria for all participants included the following: all participants underwent FDG-PET scanning and clinical cognitive evaluations at baseline visit and were followed during at least 36 months; stable MCI participants were diagnosed of MCI at baseline visit and did not progress to AD within 36 months of follow-up; and progressive MCI participants were diagnosed of MCI at baseline visit and progressed to AD within 36 months of follow-up. The demographic and clinical characteristics of all participants are summarized in Table 1.

Resting-state FDG-PET images at baseline visits were acquired and the detailed acquisition process could be found in the online information of ADNI. All participants were scanned using ^{18}F-fluorodeoxyglucose (FDG) positron emission tomography (PET). There were 218 dynamic 3D images with six 5 min frames acquired 30 min after injection of 185 $\pm$ 18.5 MBq FDG. Besides, 202 participants were scanned with a static 30-minute acquisition.

2.3. Preprocessing. We preprocessed the brain FDG-PET images using the Statistical Parametric Mapping software (SPM12; Wellcome Department of Imaging Neuroscience,

Table 1: Demographic information of all participants.

Group	sMCI ($n = 242$)	pMCI ($n = 178$)	P value
Sex (M/F)	136/106	102/76	0.89[a]
Age (year)	71.6 ± 7.82	73.7 ± 6.91	0.004[b]
Education (year)	15.9 ± 2.67	16.1 ± 2.65	0.496[c]
MMSE	28.2 ± 1.64	27.1 ± 1.80	<0.001[b]
CDRSB	1 (0.5,1.5)	1.5 (1, 2.5)	<0.001[c]
ADAS11	8.4 ± 3.4	13.0 ± 4.6	<0.001[b]
ADAS13	13.5 ± 5.5	21.0 ± 6.2	<0.001[b]
Conversion time (month)	\	20.6 ± 10.3	\
APOE $\varepsilon 4$ positive rate	44.6%	68.5%	<0.001[a]

Data are given as mean ± standard deviation. P^a: the chi-square test; P^b: the two-sample t-test; P^c: the Wilcoxon rank-sum test. MMSE: Mini-Mental State Examination; CDRSB: Clinical Dementia Rating Sum of Boxes; ADAS11: The Alzheimer's Disease Assessment Scale with 11 tasks; ADAS13: The Alzheimer's Disease Assessment Scale with 13 tasks; APOE $\varepsilon 4$ positive rate: positive or negative for the presence of at least one $\varepsilon 4$ allele.

Institute of Neurology, London, UK) implemented in MATLAB (MathWorks Inc., Sherborn, MA). We realigned a time-series of FDG-PET images to generate a stable FDG-PET image. PET images were then spatially normalized into the Montreal Neurological Institute (MNI) brain space with linear and nonlinear 3D transformations. The normalized PET images were smoothed by a Gaussian filter of 8 mm full width at half maximum (FWHM) over a 3D space to blur individual variations in gyral anatomy and to increase signal to noise ratio for statistical analysis. Each PET image was intensity normalized to the global mean brain uptake to avoid individual uptake differences. For further analysis, the whole brain images were divided into 90 regions-of-interest (ROIs) defined by the automated anatomical labeling (AAL) atlas [19].

2.4. Metabolic Connectome Analysis. To acquire individual metabolic network from the FDG-PET image, we employed an individual-level graphical approach for metabolic connectivity, namely the Kullback-Leibler Divergence Similarity Estimation (KLSE) [20]. The globally normalized metabolic activity in ROIs was used to generate a glucose metabolic network for each participant. Firstly, the 90 cortical and subcortical ROIs derived by AAL were defined as network nodes. Then, for estimating the metabolic connectivity (metabolic correlations) between network nodes, we applied relative entropy into the spatial dimension, where the FDG-PET signal in ROIs reflected afferent synaptic activity and probability distribution between these ROIs denote interneuronal information transfer. The closer the relative entropy was to zero, the stronger metabolic connectivity between two random ROIs.

The detailed mathematical derivation of metabolic connectivity included the following three steps (see Figure 2). Firstly, we estimated the probability density function (PDF) of a random brain region (ROI) using a nonparametric way, namely the kernel density estimation (KDE). The estimation of kernel width was using a solve-the-equation bandwidth. Given the sample array quantifying the metabolic intensity of each voxel with ROI, we estimated the characteristic function as

$$\widehat{\varphi}(\mathrm{t}) = \left(\frac{1}{n}\sum_{j=1}^{n} e^{itx_j}\right). \quad (1)$$

In this study, we had chosen the Gaussian function as a damping function to circumvent the question of diverging integral. After the damping function has been chosen, the Fourier transform formula may be applied, and the density estimation can be derived. Secondly, we assessed the metabolic correlation using the relative entropy between ROIs, which was estimated from the symmetric Kullback-Leibler (KL) divergence. The similarity of pairwise probability density functions (PDFs) was measured as given in the below mathematical equation:

$$D_{KL}(P\|Q) = \int_X \left(P(x)\log\frac{P(x)}{Q(x)} + Q(x)\log\frac{Q(x)}{P(x)}\right)dx. \quad (2)$$

in which P and Q represent the probability density functions PDFs of voxel intensities in pairwise ROIs. Lastly, t4he normalized similarity of these ROIs was acquired by KL divergence using the following representation:

$$KLS(P\|Q) = \exp\left(-D_{KL}(P\|Q)\right). \quad (3)$$

Thus, a metabolic correlation matrix (90×90, region × region, 90 is the number of ROI) for each participant was obtained by the magnitude of KL-based similarity (KLS), where the correlation matrix elements represented the metabolic connectivity between pairwise nodes. Thus, we had constructed a metabolic network for each subject by AAL template (nodes) and KLSE algorithm (metabolic connectivity).

2.5. Predictive Modeling Analysis. For the metabolic network of each participant, a feature vector was obtained by extracting the lower triangular elements of correlation matrix. Each participant could acquire 4005 ($90 \times 89/2$) features which defined as the metabolic connectivity between ROIs. The feature vectors then underwent predictive modeling analysis to discriminate sMCI and pMCI groups. To evaluate our proposed metabolic CPM approach fairly and minimize the influence factors, we employed three different classifiers, that are support vector machine (SVM), logistic regression (LR) model, and random forest (RF). Meanwhile, we also performed the Hosmer-Lemeshow goodness of fit test for the LR model.

To avoid the sampling variability of training and test datasets and obtain more stable estimates of predictive performance, we implemented the randomized cross-validation strategy. The detailed cross-validation procedures include two main steps. Firstly, all MCI participants were randomly partitioned into training dataset (50%, training the model) and test dataset (50%, test

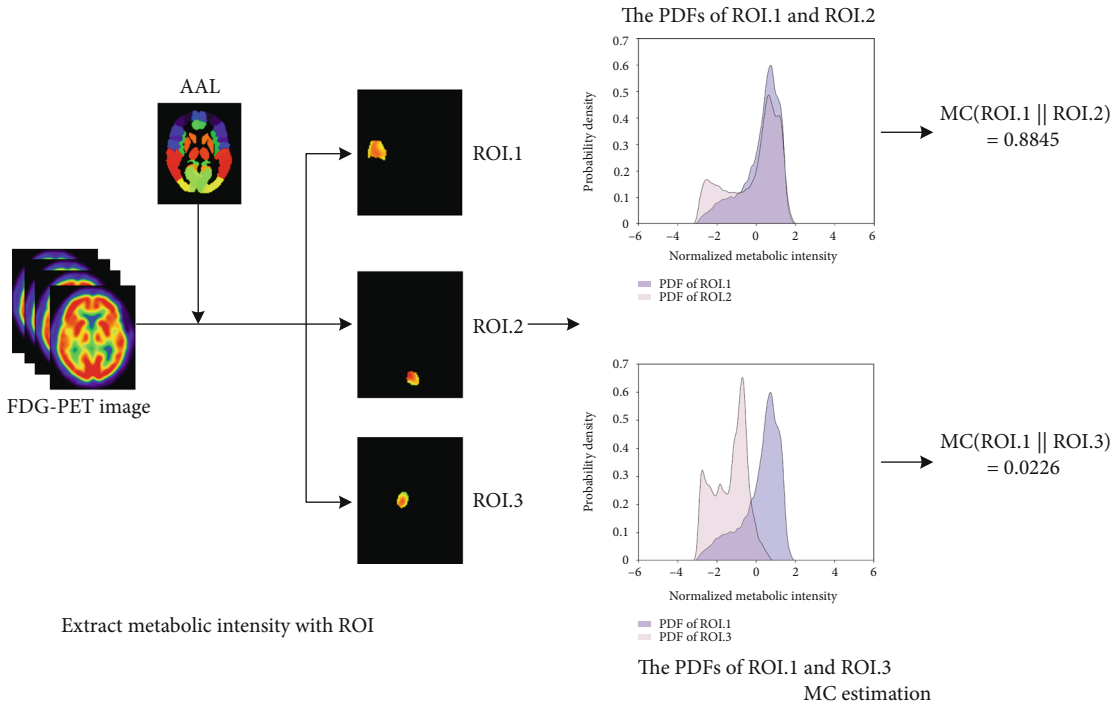

Figure 2: The framework for the estimation of metabolic connectivity (MC) between pairwise regions from individual FDG-PET image. Firstly, the FDG-PET image was divided into 90 ROIs, and the metabolic intensity values of voxels with random ROI were extracted. Then, kernel density estimation was employed to estimate the probability density function (PDF) of each ROI. Lastly, the KLSE algorithm was implemented to measure the metabolic correlation by the similarity among PDFs.

classification performance) for multiple times (100 iterations). Secondly, we implemented 10-fold cross-validation in the training dataset for hyperparameter optimization. In each random sampling of the training dataset, sparse regression least absolute shrinkage and selection operator (LASSO) approach was adopted to reduce the redundant features and to select the feature subset with higher discriminability [21]. The fitting models were built using those selected features. The predictive performance of models was evaluated by accuracy, sensitivity, specificity, the receiver-operating-characteristic curve, and the relevant area under the curve (AUC). The random split procedure was repeated for 100 iterations, and the mean and standard deviation of classification indicators were reported. SVM with linear kernel, L1-penalized LR model, random forest, and following receiver-operating-characteristic curve analysis and accuracy measurements were performed using the LIBSVM 3.23 toolbox and Statistics and Machine Learning Toolbox implemented in MATLAB.

2.6. Comparative Experiment. To further evaluate the performance of our proposed approach, two previous predictive methods in FDG-PET imaging were applied to the same predictive tasks: (1) the conventional feature quantification approach was performed based on mean metabolic uptakes in brain regions, and the FDG uptake values were regarded as features; (2) the spatial covariance analysis was performed on the training dataset to acquire a metabolic AD conversion-related pattern (ADCRP) topography, in which each voxel value represented the predictive weights [22]. The ADCRP expressions of each FDG-PET images were obtained by the Z-transformed score and regarded as the input features of the model. The comparative experiments underwent the same process procedures with the above metabolic connectivity.

2.7. Structural Brain Regions Associated with Effective Features. To verify the effectiveness of our proposed method, we further identified the structural brain regions associated with effective features. Firstly, part connectome features were considered efficient and discriminative features after undergoing the above feature select procedures. Then, the correlation matrix was generated which included only selected connectome features, and the weights of 90 brain regions were derived by column-summing the entries. In this case, the higher weight of regions implied that the region had more discriminative connectivity incident upon it. Lastly, we normalized the region weights by Z-score and sorted by the sign of the corresponding region weights. We obtained the structural brain regions associated with effective features by the criteria: Z-scored weight of region was greater than +1.0. These brain regions were considered relevant to AD progression [23].

3. Result

3.1. Clinical Characteristics. Clinical and demographic characteristics are reported in Table 1. The result of the age ($P = 0.004$) and the APOE $\varepsilon 4$ positive rate ($P < 0.001$)

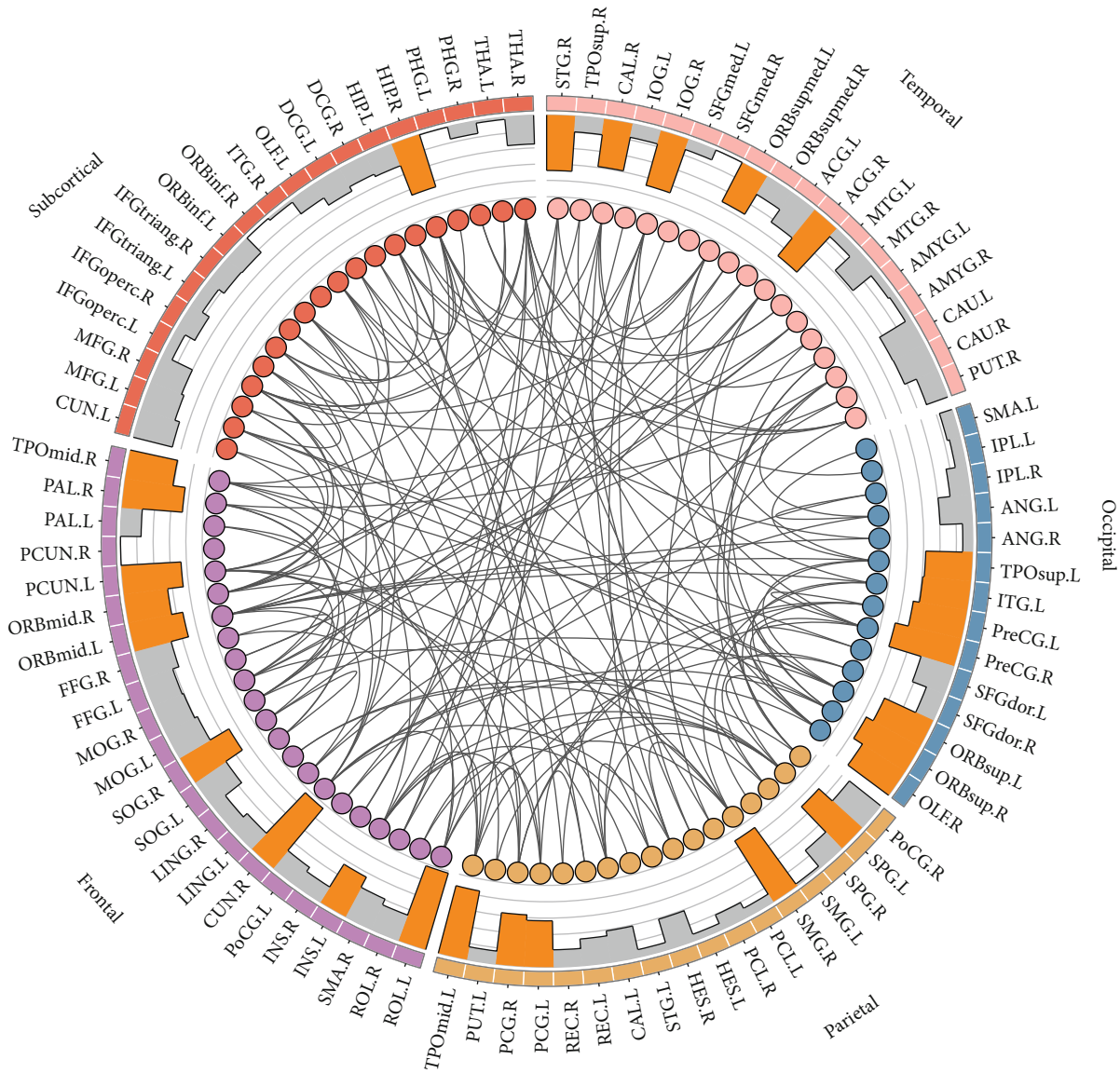

Figure 3: The brain metabolic connectivity associated with MCI conversion. The nodes in the circle represent 90 brain regions (ROIs). The different colors of nodes on the circle represent different anatomical classifications of brain regions (purple: frontal, orange: parietal, blue: occipital, pink: temporal, and red: subcortical). The black lines within nodes represent functional connectivity between ROIs selected with sufficient discriminative ability and associated with AD progression. The yellow histogram bars represent the hubs with more metabolic connectivity and the grey bars with little discriminative ability.

showed significant changes between sMCI and pMCI groups. The cognitive assessments in the pMCI subjects tended to decrease than that in the sMCI subjects (Mini-Mental State Examination (MMSE), $P < 0.001$; Clinical Dementia Rating Sum of Boxes (CDRSB), $P < 0.001$; The Alzheimer's Disease Assessment Scale with 11 tasks (ADAS11), $P < 0.001$; and The Alzheimer's Disease Assessment Scale with 13 tasks (ADAS 13), $P < 0.001$). There were no significant differences in sex ($P = 0.89$) or education level ($P = 0.496$).

3.2. Predictive Modeling Analysis. The 4005 functional connectivities drawn from the KLSE algorithm were the input features for predictive analysis. In the randomized cross-validations in 100 iterations, 153 metabolic connectivities were selected. Figure 3 shows the brain metabolic connectivity associated with MCI conversion. The hubs were defined as the network nodes that had more quantitatively selected features. These hubs were highlighted to be associated with MCI conversion and mainly located in the brain regions including the precentral gyrus, precuneus, lingual, and inferior frontal gyrus.

We compared the predictive performances of different feature extraction methods: (1) ROI uptake; (2) MCI pattern; and (3) metabolic CPM. Table 2 shows the results of different methods using three classifiers, and the best results for MCI groups diagnosis were achieved by the selected features from connectome with SVM classifier. The corresponding accuracy, sensitivity, specificity, and AUC values were 85.2%,

Table 2: Predictive performance of different methods among MCI groups.

Classifier	Predictive method	Accuracy (%)	Sensitivity (%)	Specificity (%)	AUC
SVM	ROI uptake	74.8 ± 2.41	82.2 ± 1.72	66.7 ± 2.51	0.829 ± 0.035
	MCI pattern	76.7 ± 2.48	83.7 ± 4.46	67.1 ± 6.29	0.831 ± 0.026
	Connectome	85.2 ± 2.34	88.1 ± 3.17	81.2 ± 4.28	0.933 ± 0.014
LR model	ROI uptake	72.4 ± 2.73	81.1 ± 5.99	60.7 ± 4.83	0.748 ± 0.037
	MCI pattern	74.8 ± 4.36	82.3 ± 2.49	66.8 ± 5.91	0.829 ± 0.036
	Connectome	82.3 ± 3.29	80.9 ± 3.14	84.3 ± 6.64	0.867 ± 0.043
Random forest	ROI uptake	70.8 ± 4.73	81.1 ± 3.75	59.3 ± 6.23	0.725 ± 0.045
	MCI pattern	73.1 ± 4.02	85.4 ± 2.86	61.4 ± 8.84	0.787 ± 0.032
	Connectome	76.2 ± 3.19	87.6 ± 2.99	62.9 ± 7.48	0.807 ± 0.031

The predictive performance of MCI participants was not involved in the training dataset.

88.1%, 81.2%, and 0.933, respectively. Moreover, the CPM method achieved the lowest false-positive rate (18.8 ± 4.28%, 15.7 ± 6.64%, and 37.1 ± 7.48%) and false-negative rate (11.9 ± 3.17%, 19.1 ± 3.14%, and 12.4 ± 2.99 %) in the three classifiers, respectively (Table 3). The receiver-operating-characteristic curves showed a high ability to diagnose MCI groups for metabolic CPM method (AUC, 0.933) but the lower discriminative ability for MCI pattern (AUC, 0.829) and ROI uptake (AUC, 0.831). The result of LR model showed that the information in the metabolic data has been extracted effectively and the goodness of the model fitting is high ($X^2 = 7.25$, $P = 0.51$). Besides, the SVM classifier had better diagnostic ability than other classifiers (LR and RF) for the prediction of MCI conversion.

Table 3: Predictive performance of different methods among MCI groups.

Classifier	Method	FPR	FNR
SVM	ROI uptake	33.3 ± 2.51	17.8 ± 1.72
	MCI pattern	32.9 ± 6.29	16.3 ± 4.46
	Connectome	18.8 ± 4.28	11.9 ± 3.17
LR model	ROI uptake	39.3 ± 4.83	18.9 ± 5.99
	MCI pattern	33.2 ± 5.91	17.7 ± 2.49
	Connectome	15.7 ± 6.64	19.1 ± 3.14
Random forest	ROI uptake	40.7 ± 6.23	18.9 ± 3.75
	MCI pattern	38.6 ± 8.84	14.6 ± 2.86
	Connectome	37.1 ± 7.48	12.4 ± 2.99

3.3. Discriminative Brain Regions Associated with MCI Conversion. We applied the concept of hubs into the brain regions associated with the progression from MCI to AD (Table 4). The result of hubs showed that some regions had more discriminative connectivity, including the precentral gyrus, precuneus, lingual gyrus, inferior temporal gyrus, and inferior frontal gyrus (Figures 4(a)–4(c)). When the PET images of pMCI participants were compared with sMCI participant's images, we observed significant hypometabolism in the precuneus, posterior cingulate, superior temporal gyrus, inferior frontal gyrus, etc. The result of metabolic CPM was implied that the hubs were statistically related to the conversion from MCI to AD.

Table 4: The information of brain regions associated with MCI conversion.

Brain labels	Region	MNI coordinate (mm)		
		X	*Y*	*Z*
1	Precentral gyrus (left)	-38.65	-5.68	50.94
11	Inferior frontal gyrus (left)	-48.43	12.73	19.02
48	Lingual gyrus (right)	16.29	-66.93	-3.87
67	Precuneus (left)	9.98	-56.05	43.77
89	Inferior temporal gyrus (left)	-49.77	28.05	-23.17

4. Discussion

The accurate and sensitive diagnosis of MCI conversion is a paramount challenge to guide MCI patients for suitable clinical treatments as soon as possible. To address the challenge, in this study, we develop an efficiently metabolic CPM approach to diagnose whether MCI patients will progress to AD using metabolic images (^{18}F-FDG-PET). The performance of our approach suggests that the metabolic connectivity derived by connectome analysis could be used for MCI conversion diagnosis and obtain excellent accuracy compared to other predictive models.

To further reveal the accuracy of our method, we compared the results between previous similar predictive methods and our proposed method, as shown in Table 5 [24–29]. Although the sample sizes and methodology of these studies are not identical, our proposed CPM method has better predictive performances with a large sample size. Maybe because of the deficiency of unbalanced sample sizes, the false-positive rates (FPR) and false-negative rates (FNR) of other methods are significantly higher than that of the

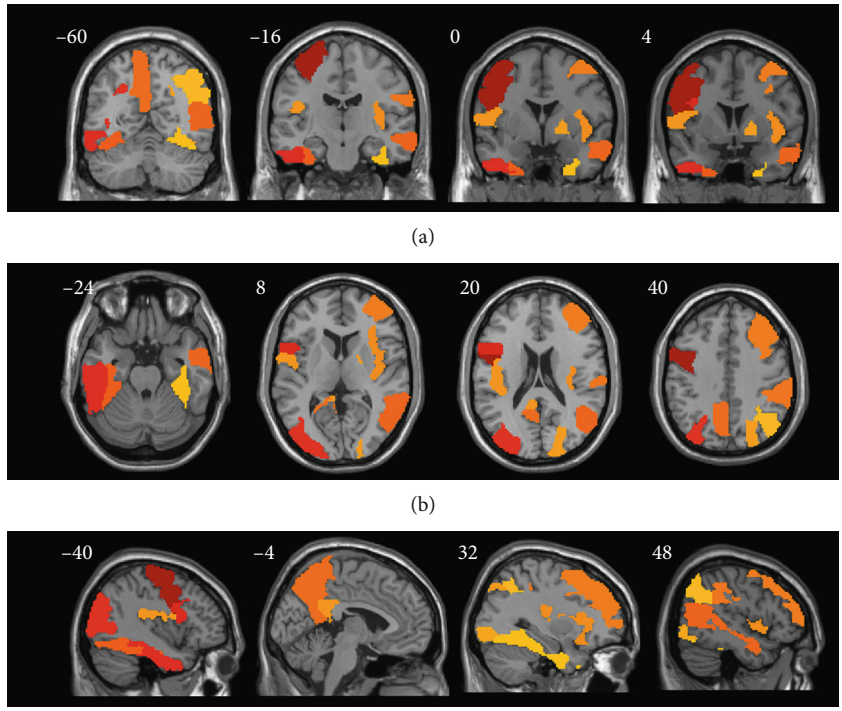

Figure 4: Topographic representations of connectome approach. The hubs regions were acquired from the training dataset using the LASSO approach in 100 iterations and were associated with the conversion from MCI to AD. The overlays are depicted in neurological coronal (a), transverse (b), and sagittal (c) orientations, respectively. Coordinates are displayed in MNI standard space.

Table 5: The predictive performance of the different methods in MCI conversion study.

Reference	Method	Conversion time (month)	sMCI (*n*)	pMCI (*n*)	Accuracy (%)	Sensitivity (%)	Specificity (%)	AUC
Young et al.	Gaussian process	36	96	47	65.0	66.0	64.6	0.767
Liu et al.	Independent component analysis and Cox model	36	108	126	68.8	57.1	82.4	0.736
Lange et al.	SPM *t*-test	36	77	31	/	/	/	0.832
Kengo et al.	Logistic regression	24	47	41	83	70	90	/
Lu et al.	Deep neural network	36	409	217	81.5	78.2	82.5	/
Pagani et al.	Independent components analysis	60	27	95	83.5	83.2	85.2	0.894
Proposed	Metabolic CPM	36	242	178	85.2	88.1	86.4	0.933

results of our CPM model. Besides, previous studies summarize the MCI conversion approaches and propose a classification framework for reproducible and objective experiments using the ADNI database and other publicly available databases [13, 30]. The results show that the accuracy of these previous methods is ranging between 62% and 81% and the mean accuracy is 74%, and the reproducibility of these methods is not great. Meanwhile, our CPM method underwent a rigorous evaluation strategy to verify its feasibility and reproducibility. This method could capture more detailed and straightforward metabolic information within paired regions which performed as good as or better than many existing approaches. Thus, we believe that our metabolic CPM approach is more effective in predicting MCI conversion.

As an effective tool in the brain neuroscience field, CPM in AD has been pursued to develop an efficient biomarker for early diagnosis [14]. From the perspective of methodology, it is worth noting that the CPM approach is a generalizable model that takes brain connectivity data as input and generates predictions of MCI progression in novel subjects. In the neurodegenerative progress of AD, the brain changes involve the interaction of many brain regions rather than isolated regions, and neuronal degeneration is associated with cognitive deterioration. The between-region metabolic activities are impaired in MCI patients who are converting to AD. Thus, the most relevant indicator is the identification of corresponding brain regions and their connectivity. The brain network can delineate the full metabolic connectome and the connectivity dynamics of brain metabolism, and these

findings provide opportunities to develop more accurate predictive models. The progressive disintegration of MCI patients is disclosed by the metabolic network. Therefore, the model based on selected connectivity has excellent diagnostic utility and reveals local brain pathologies.

From the results of connectome analysis, the metabolic connectivity abnormalities in MCI patients who converted to AD are mainly located in the precentral gyrus, precuneus, lingual, and inferior frontal gyrus. These brain regions are hubs of metabolic connectivity corresponding to synaptic disconnection. Metabolic connectivity in these regions decreases in progressive MCI patients compared to that in stable MCI patients. Previous MCI conversion investigation had shown the metabolic AD conversion-related pattern (ADCRP) which was characterized by relative decreases in temporoparietal, frontal, posterior cingulate, and precuneus cortex between sMCI and pMCI patients, and these results agreed with our experimental findings [22]. The voxel-wise two-sample t-test SPM analysis also found a highly similar metabolic difference which verified the pathophysiologic significance of regions that derived our approach [7, 31]. This result also indicates that our proposed metabolic CPM is an effective biomarker for MCI progression prediction.

5. Conclusion

In this study, we have proposed an innovative metabolic CPM method based on FDG-PET imaging, which can accurately diagnose whether the patients with MCI will eventually progress to AD. The experiment results suggest that metabolic connectivity can identify the metabolic abnormalities features and abnormal brain regions associated with MCI conversion. Our proposed metabolic CPM approach may be a potential tool with other clinical information to develop biomarkers for predicting the conversion of MCI patients.

Data Availability

The PET imaging data used to support the findings of this study may be released upon application to the ADNI database (http://adni.loni.usc.edu/).

Conflicts of Interest

The authors declare that they have no conflicts of interest.

Acknowledgments

This study was supported in part by the National Key Research and Development Program of China under Grant No. 2018YFC1707704. Data collection and sharing for this project was funded by the Alzheimer's Disease Neuroimaging Initiative (ADNI) (National Institutes of Health Grant U01 AG024904) and DOD ADNI (Department of Defense award number W81XWH-12-2-0012). ADNI is funded by the National Institute on Aging, the National Institute of Biomedical Imaging and Bioengineering, and through generous contributions from the following: AbbVie, Alzheimer's Association; Alzheimer's Drug Discovery Foundation; Araclon Biotech; BioClinica, Inc; Biogen; Bristol-Myers Squibb Company; CereSpir, Inc; Cogstate; Eisai Inc; Elan Pharmaceuticals, Inc; Eli Lilly and Company; EuroImmun; F. Hoffmann-La Roche Ltd and its affiliated company Genentech, Inc; Fujirebio; GE Healthcare; IXICO Ltd; Janssen Alzheimer Immunotherapy Research & Development, LLC; Johnson & Johnson Pharmaceutical Research & Development LLC; Lumosity; Lundbeck; Merck & Co., Inc; Meso Scale Diagnostics, LLC; NeuroRx Research; Neurotrack Technologies; Novartis Pharmaceuticals Corporation; Pfizer Inc; Piramal Imaging; Servier; Takeda Pharmaceutical Company; and Transition Therapeutics. The Canadian Institutes of Health Research is providing funds to support ADNI clinical sites in Canada. Private sector contributions are facilitated by the Foundation for the National Institutes of Health (https://www.fnih.org). The grantee organization is the Northern California Institute for Research and Education, and the study is coordinated by the Alzheimer's Therapeutic Research Institute at the University of Southern California. ADNI data are disseminated by the Laboratory for Neuro Imaging at the University of Southern California.

References

[1] Alzheimer's Association, "2019 Alzheimer's disease facts and figures," *Alzheimer's & Dementia*, vol. 15, no. 3, pp. 321–387, 2019.

[2] B. Dubois, H. Hampel, H. H. Feldman et al., "Preclinical Alzheimer's disease: definition, natural history, and diagnostic criteria," *Alzheimer's & Dementia*, vol. 12, no. 3, pp. 292–323, 2016.

[3] B. Olsson, R. Lautner, U. Andreasson et al., "Csf and blood biomarkers for the diagnosis of Alzheimer's disease: a systematic review and meta-analysis," *The Lancet Neurology*, vol. 15, no. 7, pp. 673–684, 2016.

[4] K. Ong, V. L. Villemagne, A. Bahar-Fuchs et al., "^{18}F-florbetaben Aβ imaging in mild cognitive impairment," *Alzheimer's Research & Therapy*, vol. 5, no. 1, 2013.

[5] L. F. Kalheim, P. Selnes, A. Bjørnerud, C. Coello, K. Vegge, and T. Fladby, "Amyloid dysmetabolism relates to reduced glucose uptake in white matter hyperintensities," *Frontiers in Neurology*, vol. 7, 2016.

[6] C. Cabral, P. M. Morgado, D. C. Costa, M. Silveira, and For the Alzheimer's Disease Neuroimaging Initiative, "Predicting conversion from mci to ad with FDG-PET brain images at different prodromal stages," *Computers in Biology and Medicine*, vol. 58, pp. 101–109, 2015.

[7] M. Pagani, F. Nobili, S. Morbelli et al., "Early identification of mci converting to ad: a FDG PET study," *European Journal of Nuclear Medicine and Molecular Imaging*, vol. 44, no. 12, pp. 2042–2052, 2017.

[8] H. Zhou, J. Jiang, J. Lu et al., "Dual-model radiomic biomarkers predict development of mild cognitive impairment progression to Alzheimer's disease," *Frontiers in Neuroscience*, vol. 12, 2019.

[9] F. Carbonell, A. Charil, A. P. Zijdenbos, A. C. Evans, B. J. Bedell, and for the Alzheimer's Disease Neuroimaging Initiative, "Hierarchical multivariate covariance analysis of metabolic connectivity," *Journal of Cerebral Blood Flow & Metabolism*, vol. 34, no. 12, pp. 1936–1943, 2014.

[10] M. Liu, D. Cheng, W. Yan, and Alzheimer's Disease Neuroimaging Initiative, "Classification of Alzheimer's disease by combination of convolutional and recurrent neural networks using FDG-PET images," *Frontiers in Neuroinformatics*, vol. 12, 2018.

[11] H. I. Suk, S. W. Lee, D. Shen, and Alzheimer's Disease Neuroimaging Initiative, "Hierarchical feature representation and multimodal fusion with deep learning for ad/mci diagnosis," *NeuroImage*, vol. 101, pp. 569–582, 2014.

[12] H. Choi and K. H. Jin, "Predicting cognitive decline with deep learning of brain metabolism and amyloid imaging," *Behavioural Brain Research*, vol. 344, pp. 103–109, 2018.

[13] N. Smailagic, L. Lafortune, S. Kelly, C. Hyde, and C. Brayne, "^{18}F-FDG PET for Prediction of Conversion to Alzheimer's Disease Dementia in People with Mild Cognitive Impairment: An Updated Systematic Review of Test Accuracy," *Journal of Alzheimer's Disease*, vol. 64, no. 4, pp. 1175–1194, 2018.

[14] X. Shen, E. S. Finn, D. Scheinost et al., "Using connectome-based predictive modeling to predict individual behavior from brain connectivity," *Nature Protocols*, vol. 12, no. 3, pp. 506–518, 2017.

[15] C. J. Stam, "Modern network science of neurological disorders," *Nature Reviews. Neuroscience*, vol. 15, no. 10, pp. 683–695, 2014.

[16] M. N. Hallquist and F. G. Hillary, "Graph theory approaches to functional network organization in brain disorders: a critique for a brave new small-world," *Network Neuroscience*, vol. 3, no. 1, pp. 1–26, 2019.

[17] T. Yan, W. Wang, L. Yang, K. Chen, R. Chen, and Y. Han, "Rich club disturbances of the human connectome from subjective cognitive decline to Alzheimer's disease," *Theranostics*, vol. 8, no. 12, pp. 3237–3255, 2018.

[18] W. Jagust, "Imaging the evolution and pathophysiology of Alzheimer disease," *Nature Reviews Neuroscience*, vol. 19, no. 11, pp. 687–700, 2018.

[19] N. Tzourio-Mazoyer, B. Landeau, D. Papathanassiou et al., "Automated anatomical labeling of activations in spm using a macroscopic anatomical parcellation of the mni mri single-subject brain," *NeuroImage*, vol. 15, no. 1, pp. 273–289, 2002.

[20] M. Wang, Alzheimer's Disease Neuroimaging Initiative, J. Jiang et al., "Individual brain metabolic connectome indicator based on Kullback-Leibler divergence similarity estimation predicts progression from mild cognitive impairment to Alzheimer's dementia," *European Journal of Nuclear Medicine and Molecular Imaging*, 2020.

[21] B. M. Tijms, P. Series, D. J. Willshaw, and S. M. Lawrie, "Similarity-based extraction of individual networks from gray matter MRI scans," *Cerebral Cortex*, vol. 22, no. 7, pp. 1530–1541, 2012.

[22] G. Blazhenets, Y. Ma, A. Sörensen et al., "Principal component analysis of brain metabolism predicts development of Alzheimer's dementia," *Journal of Nuclear Medicine*, vol. 60, no. 6, pp. 837–843, 2019.

[23] R. L. Buckner, J. Sepulcre, T. Talukdar et al., "Cortical hubs revealed by intrinsic functional connectivity: mapping, assessment of stability, and relation to Alzheimer's disease," *The Journal of Neuroscience*, vol. 29, no. 6, pp. 1860–1873, 2009.

[24] J. Young, M. Modat, M. J. Cardoso et al., "Accurate multimodal probabilistic prediction of conversion to Alzheimer's disease in patients with mild cognitive impairment," *NeuroImage: Clinical*, vol. 2, pp. 735–745, 2013.

[25] K. Liu, K. Chen, L. Yao, and X. Guo, "Prediction of mild cognitive impairment conversion using a combination of independent component analysis and the Cox model," *Frontiers in Human Neuroscience*, vol. 11, 2017.

[26] C. Lange, P. Suppa, L. Frings, W. Brenner, L. Spies, and R. Buchert, "Optimization of statistical single subject analysis of brain FDG PET for the prognosis of mild cognitive impairment-to-Alzheimer's disease conversion," *Journal of Alzheimer's Disease*, vol. 49, no. 4, pp. 945–959, 2016.

[27] K. Ito, H. Fukuyama, M. Senda et al., "Prediction of outcomes in mild cognitive impairment by using 18f-FDG-PET: a multicenter study," *Journal of Alzheimer's Disease*, vol. 45, no. 2, pp. 543–552, 2015.

[28] D. Lu, Alzheimer's Disease Neuroimaging Initiative, K. Popuri, G. W. Ding, R. Balachandar, and M. F. Beg, "Multimodal and multiscale deep neural networks for the early diagnosis of Alzheimer's disease using structural mr and FDG-PET images," *Scientific Reports*, vol. 8, no. 1, 2018.

[29] M. Pagani, A. Giuliani, J. Öberg et al., "Progressive Disintegration of Brain Networking from Normal Aging to Alzheimer Disease: Analysis of Independent Components of ^{18}F-FDG PET Data," *Journal of Nuclear Medicine*, vol. 58, no. 7, pp. 1132–1139, 2017.

[30] J. Samper-González, N. Burgos, S. Bottani et al., "Reproducible evaluation of classification methods in Alzheimer's disease: framework and application to mri and pet data," *NeuroImage*, vol. 183, pp. 504–521, 2018.

[31] R. C. Petersen, E. S. Lundt, T. M. Therneau et al., "Predicting progression to mild cognitive impairment," *Annals of Neurology*, vol. 85, no. 1, pp. 155–160, 2019.